AN ABSTRACT OF THE DISSERTATION OF

Eric C. Brown for the degree of Doctor of Philosophy in Chemistry presented on October 31, 2002. Title: Rhenium-Catalyzed Oxygen-Atom Transfer Reactions: Mechanism and Applications.

Redacted for privacy

Abstract Approved: _____
Kevin P. Gable

In situ reduction of hydrido-*tris*-(3,5-dimethylpyrazolyl)borato(trioxo) rhenium(V) with triphenylphosphine or triethylphosphite leads to a reactive rhenium(V) species that catalytically deoxygenates epoxides at 75-105°C. The reaction is stereospecific, except for *trans*- and *cis*-butene oxide which formed minor amounts of the opposite isomer. A variety of different functional groups were tolerated and even epoxides that reacted slowly could be pushed to greater than 95 % conversion given extended time and/or higher temperature. The absence of clustering processes shows how the choice of ligand can have a major influence on the design of the catalytic cycle.

The rhenium(V) species formed from reduction of $Tp'ReO_3$ was identified as $Tp'Re(O)(OH)_2$. $Tp'Re(O)(OH)_2$ reacted with ethanol and HCl to form ethoxide and hydroxo chloride complexes, respectively. In addition, $Tp'Re(O)(OH)_2$ was an excellent catalytic and stoichiometric reagent for the deoxygenation of epoxides

and sulfoxides. Loss of water from $Tp'Re(O)(OH)_2$ to form the catalytically active species $Tp'ReO_2$ was shown to be a necessary preequilibrium process.

The kinetic behavior of the catalytic system is complex. First-order behavior in $[Re]_T$, zero-order dependence in $[PPh_3]$ and saturation behavior for epoxide were observed. The reversible formation of a coordinated epoxide complex was proposed to explain the saturation behavior. The epoxide complex was shown experimentally and computationally to engage in two separate reactions: ring expansion to form a *syn*-diolate complex, and direct fragmentation to alkene and trioxide. A steady-state concentration of diolate is eventually reached explaining a "burst" of alkene production prior to generation of a pseudo-zero-order catalytic system. The diolate formed is the *syn*-isomer, which is the kinetically formed product. Direct epoxide fragmentation is the primary source of alkene. This process was determined to be four times faster than ring expansion for *cis*-stilbene oxide.

The synthesis and characterization of a tethered-epoxide Cp* rhenium trioxide complex has been achieved. Reduction of this complex leads to an unsaturated rhenium(V) species that is immediately complexed by the tethered epoxide. Experimental data and molecular mechanics modeling support intramolecular coordination of the epoxide to the rhenium center. These results confirm that the coordinate epoxide is a viable intermediate in rhenium-catalyzed epoxide deoxygenations.

# Rhenium-Catalyzed Oxygen-Atom Transfer Reactions: Mechanism and Applications

by
Eric C. Brown

A DISSERTATION

submitted to

Oregon State University

in partial fulfillment of
the requirements for the
degree of

Doctor of Philosophy

Presented October 31, 2002
Commencement June 2003

Doctor of Philosophy dissertation of Eric C. Brown presented on October 31, 2002.

APPROVED:

Redacted for privacy

Major Professor, representing Chemistry

Redacted for privacy

Head of Department of Chemistry

Redacted for privacy

Dean of Graduate School

I understand that my dissertation will become part of the permanent collection of Oregon State University libraries. My signature below authorizes release of my dissertation to any reader upon request.

Redacted for privacy

Eric C. Brown, Author

# ACKNOWLEDGMENTS

I would like to sincerely thank Prof. Kevin Gable for all his assistance, guidance and encouragement as an advisor throughout my career here at Oregon State University. I would also like to thank my committee members Prof. James White, Prof. Max Deinzer, Prof. Douglas Keszler and Prof. Janet Tate for their support. My collegues Fedor Zhuravlev, Kriangsak Khownium, Scott Allen and Pitak Chuawong provided me great aid and friendship. I also owe much gratitude to the OSU Chemistry Department for financial support through teaching assistantships. Finally, I would like to thank my friends and family for their friendship and support.

TABLE OF CONTENTS

TABLE OF CONTENTS (Continued)

TABLE OF CONTENTS (Continued)

Page

TABLE OF CONTENTS (Continued)

LIST OF FIGURES

LIST OF FIGURES (Continued)

LIST OF TABLES

LIST OF APPENDIX TABLES

*This is dedicated to my wife, Amy Pence Brown and my parents, Garry and Urania Brown.*

# Rhenium-Catalyzed Oxygen-Atom Transfer Reactions: Mechanism and Applications

## Chapter 1: Background and Significance

### 1.1 Metal-Mediated Oxygen-Atom Transfer Reactions

The transfer of oxygen atoms between a metal center and substrate is a reaction that holds both academic and industrial importance. Transition metal complexes play an essential role in the stoichiometric and catalytic oxidation of organic compounds as well as roles in biological processes. Examples of metal-mediated O-atom transfer reactions include epoxidation and *cis*-dihydroxylation of olefins. Furthermore, evidence exists to support the involvement of O-atom transfer reactions in biological systems such as cytochrome P-450[1] and molybdenum hydroxylase enzymes[2].

Numerous obstacles exist for the oxidation of organic compounds. These include the kinetic inertness of varies chemical oxidants, the thermodynamic preference for overoxidation, and the challenge to control chemoselectivity, stereoselectivity, and regioselectivity. Metal complexes offer a variety of solutions to these challenges. First, they can overcome the kinetic obstacle by providing alternative pathways with lower Gibbs free energies of activation. For example, reactions of organic compounds with dioxygen in its ground state (triplet) are spin

forbidden (Woodward-Hoffman rules), but this barrier may be overcome by forming oxo or peroxo metal complexes. Second, modification of the properties of the metal complex can have an effect on selectivity. Simple changes in steric bulk can influence regiochemistry, changes in electronic structure can influence chemoselectivity and a chiral structure can influence stereochemistry.

Despite the interest in O-atom transfer reactions, the mechanistic understanding of metal-catalyzed oxidations is often limited. A complex combination of mechanisms exists in many cases, making structural identification of intermediates and determination of rate constants associated with individual reaction steps difficult to determine. Unfortunately, the rational design of new reagents or enantioselective versions of existing reagents requires an adequate understanding of mechanism.

Catalytic O-atom transfer reactions can be described by equations (1) and (2). The oxygen atom donor (**XO**), such as $O_2$, $H_2O_2$, PhIO, $Me_2SO$, epoxides or amine *N*-oxides, donates an oxygen atom to the transition metal complex, **M**, forming either an oxo- or peroxometal complex, **MO**. The oxo- or peroxometal complex can either transfer the newly acquired oxygen atom back to **X** or it can transfer the oxygen atom to the oxygen atom acceptor **Y**. The most common oxygen atom acceptors are olefins, sulfides, tertiary phosphines and phosphites.

$$XO + M \rightleftharpoons MO + X \qquad (1)$$

$$MO + Y \rightleftharpoons YO + M \qquad (2)$$

## 1.2 Electronic Structure of Metal Terminal Oxo Complexes

Two general types of metal complexes are involved in O-atom transfer reactions: (i) peroxide/peroxo complexes and (ii) terminal oxo complexes. Group IV and V metals form active epoxidation reagents as peroxo/peroxide transition metal complexes. Conversely, group VI-VIII metals more often form oxo metal complexes with multiple bonds. As a general rule, the formation of terminal oxo metal complexes seems to be most favorable along a diagonal from vanadium to osmium.[3]

High oxidation state metal oxo compounds, such as $OsO_4$[4], $SeO_2$[5], $RuO_4$[6] and $MnO_2$[7], catalyze a variety of O-atom transfer reactions. Their ability to selectively oxidize organic compounds under mild conditions has made them some of the more commonly used reagents in organic synthesis. The nature of the oxo metal bond can best be described by examining the possible resonance structures and valence bond diagrams (Figure 1). Oxo metal compounds can exist with bond orders ranging from three to as low as one. Overall, the terminal oxo metal bond consists of a $\sigma$ bond along with one or two $\pi$ bonds. If the oxo metal bond is designated as lying along the $z$-axis, $d_\pi$-$p_\pi$ overlap occurs between the $d_{xz}$ and $p_x$ orbitals and/or the $d_{yz}$ and $p_y$ orbitals. The metal must be an excellent $\pi$-acceptor and be in a high oxidation state ($\geq$ 4+) with no more than four $d$ electrons. Low $d$ electron counts are required since configurations $d^{0\text{-}4}$ contain vacant or half-filled $d$

orbitals available for bonding with the filled ligand *p* orbitals. As a result, no stable M=O groups are known for transition metals right of the iron triad.

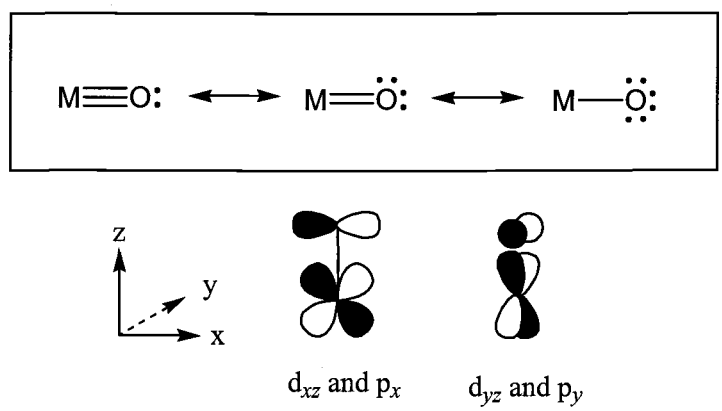


Figure 1.1 Resonance structures and valence bond diagrams.

The partial molecular orbital diagram for an octahedral complex with one oxo metal bond is shown in Figure 1.2.[3] The diagram illustrates the effect of π-bonding on the relative energies of orbitals found in the $t_{2g}$ set. As a result of the $d_z^2$ and $d_{x^2-y^2}$ orbitals pointing directly at the ligands, the five metal *d* orbitals are split into an $e_g$ set ($d_z^2$, $d_{x^2-y^2}$) and $t_{2g}$ set ($d_{xz}$, $d_{yz}$, $d_{xy}$). The doubly degenerate $e_g$ set consists of $\sigma^*$ character, while the triply degenerate $t_{2g}$ set is considered primarily nonbonding. The addition of an oxo group lowers the symmetry to $C_{4v}$ and the degeneracies among the $e_g$ and $t_{2g}$ sets are lost. The $d_{xz}$ and $d_{yz}$ orbitals, which possess the correct symmetry to interact with the $p_x$ and $p_y$ orbitals on oxygen, further split the $t_{2g}$ set into a nonbonding orbital and a doubly degenerate $\pi^*$ orbital.

In addition, the higher electronegativity of oxygen places the π orbitals of the oxo ligand at lower energy than the metal *d* orbitals.

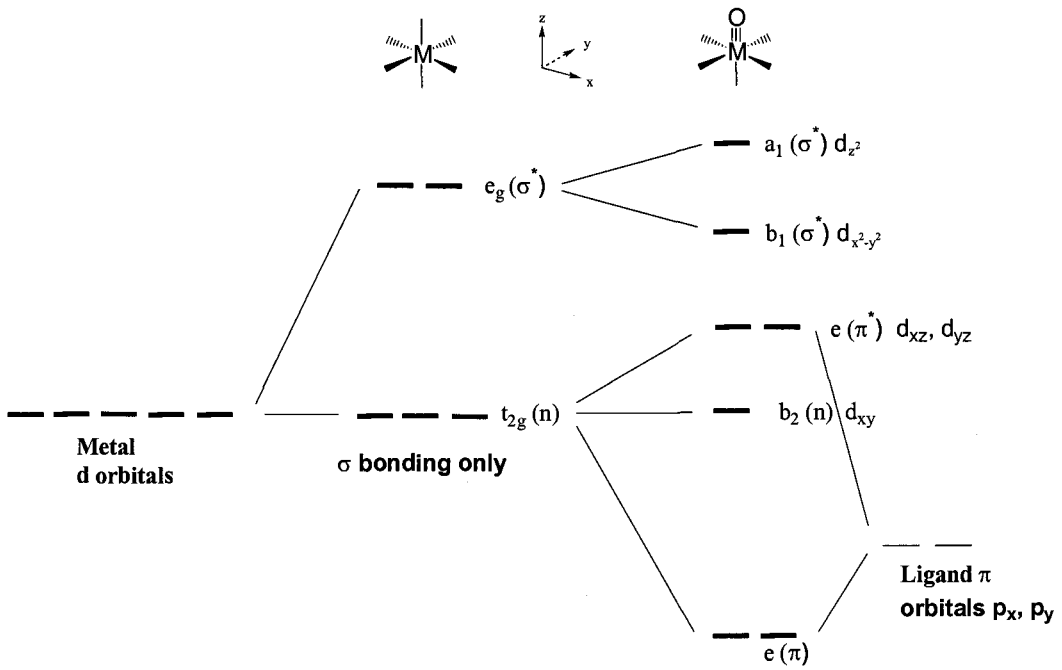


Figure 1.2 Partial molecular orbital diagram of octahedral complex.

The consequences of the bonding model on reactivity can be described by frontier molecular orbital theory (Figure 1.3). Typically for metal oxides the LUMO is localized on the metal, which is subject to attack and coordination by nucleophiles (pathway A).[8] This implies polarization of the oxo group towards oxygen as indicated by the dipolar resonance form on the left. However, the oxo ligand is expected to become more electrophilic as the metal oxo π* orbital drops in

energy and attains more oxygen character.[9] An electrophilic oxo group is necessary to explain migrations of σ-bonded aryl groups from rhenium to oxygen in $[(HBpz_3)ReO_2Ph]OTf$.[9] In this case, the dipolar resonance form on the right is a more adequate representation and is commonly referred to as an "oxene". A concerted oxene or oxenoid mechanism has been invoked to explain alkane hydroxylation by cytochrome P-450[10] and epoxidations mediated by oxo metal complexes[11]. The oxene insertion involves electrophilic attack, similar to a carbene, on the carbon-hydrogen bond of the alkane or carbon-carbon π-bond of the alkene.

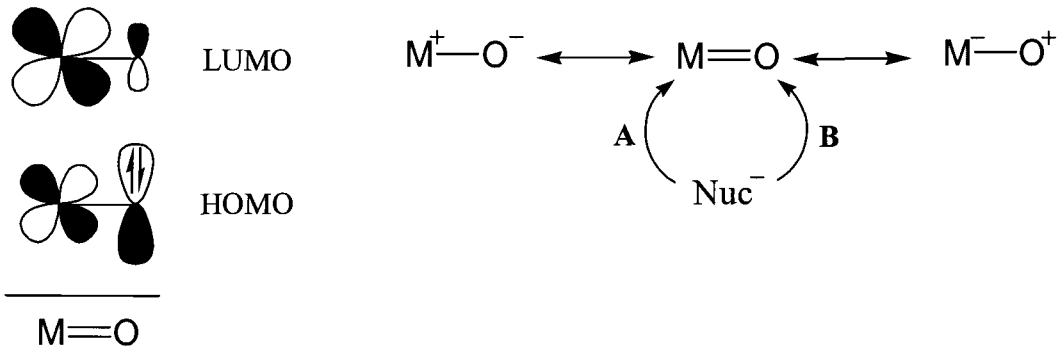


Figure 1.3 Dipolar resonance structures and molecular orbitals.

## 1.3 C-O Bond Forming Reactions Mediated By Oxo Metal Complexes

The transition metal, its oxidation state and ligand environment all have a major effect upon oxygen atom transfer reactivity. Consequently, countless

possibilities exist for the rational design of more efficient and selective oxidizing agents. Two exceptional examples of how ligand design led to efficient catalysis are Sharpless asymmetric *cis*-dihydroxylation (AD)[12] and Jacobsen-Katsuki asymmetric epoxidation[13] of olefins. Both processes use high oxidation state oxo metal complexes to catalyze the reaction and chiral ligands to induce asymmetry in the product. These reactions are appealing since they allow the formation of two chiral carbons simultaneously from an achiral alkene. They are also extremely good catalytic reactions; high turnovers, fast rates and mild conditions are typically observed.

The osmium-catalyzed asymmetric dihydroxylation reaction is one of the more elegant and reliable reactions for 1,2-functionalization of alkenes.[4] The hydroxylations can be highly enantioselective (> 90% ee) in the presence of chiral ligands. The cinchona alkaloids dihydroquinine (DHQ) and dihydroquinidine (DHQD) are the most developed ligands and have led to considerable increases in enantioselectivities. However, the most effective ligands are the dimeric derivatives formed by linking the cinchona alkaloids to heterocyclic spacers ($(DHQ)_2$-PHAL; Figure 1.4 A).[14] Besides inducing high enantioselectivity, the ligands accelerate the reaction by stabilizing the transition state through aromatic stacking interactions.[15] Numerous stoichiometric oxidants have been successfully used, but $K_3Fe(CN)_6$ results in greater enantioselectivity.[16] A by-product-free preparation using molecular oxygen as the stoichiometric oxidant has also recently been published.[17]

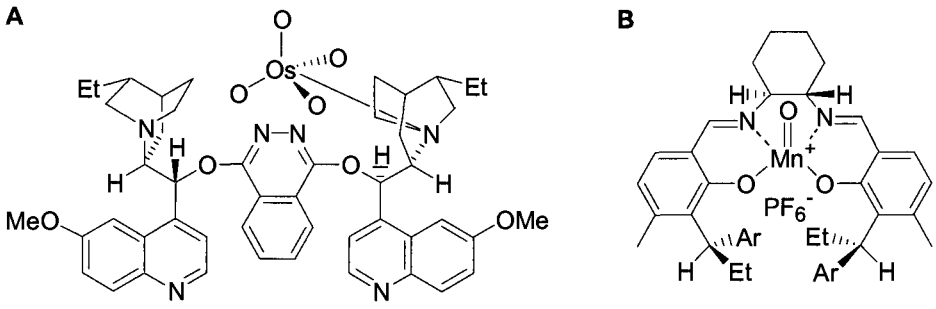


Figure 1.4 Structures of (A) Sharpless asymmetric dihydroxylation catalyst and (B) Jacobsen-Suzuki asymmetric epoxidation catalyst.

A variety of chiral manganese(III) salens have been shown to be efficient catalysts for the asymmetric epoxidation of unfunctionalized olefins. The catalysts are used in combination with a stoichiometric amount of oxidant, and evidence exists to support a Mn(V) oxo species as the active oxidant (Figure 1.3B). Examples of stoichiometric oxidants successfully used include NaOCl[18], idosylarenes[19] and amine *N*-oxides[20]. Epoxidations with chiral Mn(III) salen complexes afforded high enantioselectivites with a wide range of different substituted olefins. For example, asymmetric epoxidation of *cis-B*-methylstyrene by commercial bleach (NaOCl) afforded (*R,S*)-*cis-B*-methylstyrene oxide in 87% yield and 82% ee. Several other appealing features exist for using chiral Mn(III) salen catalysts for asymmetric epoxidations. The reactions can be run in air, purification of solvents is unnecessary, the reagents are inexpensive, and the workup procedure is simple. Overall, epoxidations using Jacobsen's catalyst give yields of up to 97% with asymmetric induction as high as 98% ee.

## 1.4 C-O Bond Cleavage Mediated By Oxo Metal Complexes

Metal mediated cleavage of C-O bonds with concomitant formation of a M=O bond can also have practical applications. An excellent example is the use of high oxidation state oxo metal catalysts to convert carbohydrates into other useful chemicals.[21] Since most fuels and organic chemicals come from dwindling fossil fuel supplies, the development of a process that converts renewable biomass into raw materials is desirable. Biomass is the most abundant and renewable resource; unfortunately, carbohydrates are often too oxygen-rich to be of any direct value without extensive elaboration. Selective removal of oxygen can retain stereocenters while reducing structural complexity. In addition, the product resulting from oxygen removal, for example an olefin, can be further functionalized. Another possible application of high oxidation state oxo metal complexes is the removal of various organosulfur compounds present in petroleum and natural gas feedstocks. Since sulfur is isoelectronic with oxygen, similiar nonoxidative processes might be applicable to sulfur containing substrates.

The development of a catalytic process to deoxydehydrate diols and polyols to alkenes and allylic alcohols was published[21a] shortly after reports of alkene extrusion from rhenium(VII) diolate complexes at elevated temperatures.[22] Scheme 1.1 illustrates the catalytic cycle responsible for converting vicinal diols to alkenes. The catalytic cycle involves in situ reduction of $Cp^*ReO_3$ ($Cp^* = C_5Me_5$) with phosphines, cyclocondensation with the diol and cycloreversion of the

corresponding rhenium diolate complex to give alkene. Cycloreversion also regenerates $Cp^*ReO_3$, which is then returned back into the catalytic cycle. Unfortunately, catalyst deactivation prevented efficient catalysis. Low turnover numbers ranging from 1 to 60 were obtained. Catalyst deactivation was attributed to over-reduction of the Re(V) complex by phosphine to an inactive Re(III) species. However, the true identity of the Re(III) species has remained elusive.

Scheme 1.1

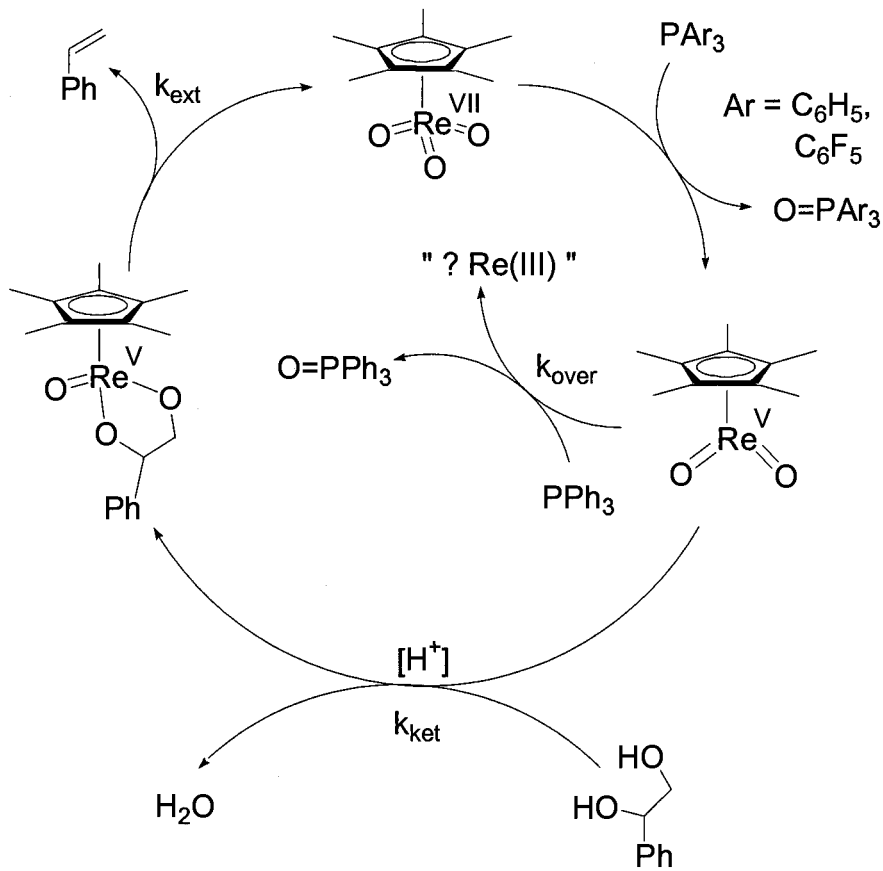

Reactions run in coordinating solvents, such as tetrahydrofuran (THF) or *N*-methyl-2-pyrrolidinone (NMP) were unsuccessful compared to reactions run in chlorobenzene. It was soon realized catalyst deactivation was a function of the partitioning of $Cp^*ReO_2$ to form Cp*ReO(diolate) ($k_{ket}$) and over-reduction ($k_{over}$) to form the inactive species. The partition coefficient was determined experimentally to be $k_{ket}/k_{over} = 60$ for benzene-$d_6$ and $k_{ket}/k_{over} = 2$ for THF-$d_8$. The addition of *p*-toluenesulfonic acid in THF as a cocatalyst resulted in efficient catalysis by accelerating the formation of diolate compared to over-reduction. Catalytic deoxygenation of the protected alditol **1** to the *trans*-alkene was achieved in 86% yield (Scheme 1.2A), while the unprotected alditol **2** yielded the fully deoxygenated product butadiene in 80% yield (Scheme 1.2 B).

Scheme 1.2

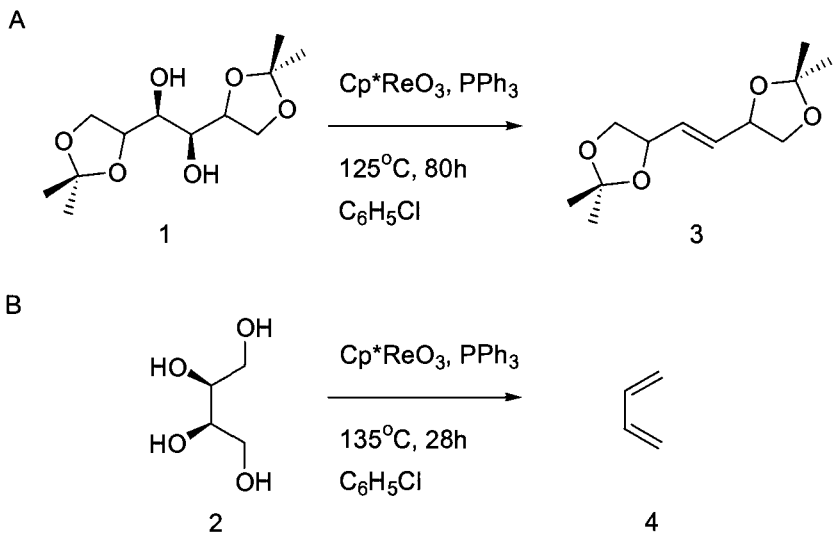

## 1.5 MTO Catalyzed Epoxidation of Alkenes

An interesting periodic trend is observed for epoxidation and dihydroxylation of olefins. Early-transition metal ions such as titanium[23], vanadium[24] and chromium[25] are excellent epoxidation reagents, while permanganate[26], ruthenium tetraoxide[27] and osmium tetraoxide[4] preferentially dihydroxylate olefins. Rhenium, which is located in Group VII, is positioned nicely in the middle of the transition series. Rhenium oxo compounds ($LReO_3$) exhibit a range of reactivity patterns that mimic both dihydroxylation and epoxidation reactivity as a function of L. When L = $CH_3$, epoxidation of alkenes occurs with hydrogen peroxide.[28] When L = Cp* (Cp* = $C_5Me_5$), a metallodioxylate is formed from strained alkenes.[29] Therefore, rhenium oxo compounds offer a useful model for probing both epoxidation and dihydroxylation mechanisms.

Methyltrioxorhenium (MTO) has been successfully used to catalytically activate hydrogen peroxide toward a number of useful transformations. Some of these include the oxidation of alkynes[30], phosphines[31], sulfides[32], halides[33] and, more importantly, alkenes[28]. MTO activates hydrogen peroxide through the formation of mono- and bis-peroxorhenium compounds (Scheme 1.3).[34] Each has been detected by $^1H$ and $^{13}C$ NMR and by UV. In addition, the structure of the diglyme adduct of the bis-peroxo complex was confirmed by X-ray crystallography.[35]

Scheme 1.3

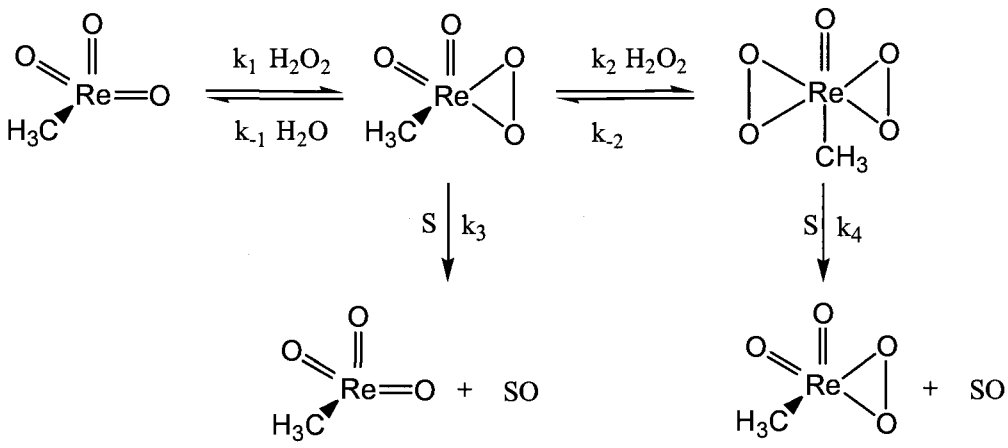


There are two possible catalytic cycles for the oxidation of substrates (S) (Scheme 1.3). First, at high hydrogen peroxide concentrations the equilibrium is shifted to the right and only the bis-peroxorhenium compound builds up to an appreciable concentration. Conversely, at low concentrations of hydrogen peroxide, a second catalytic cycle can operate where the mono-peroxo complex is responsible for the oxidations.

Scheme 1.4

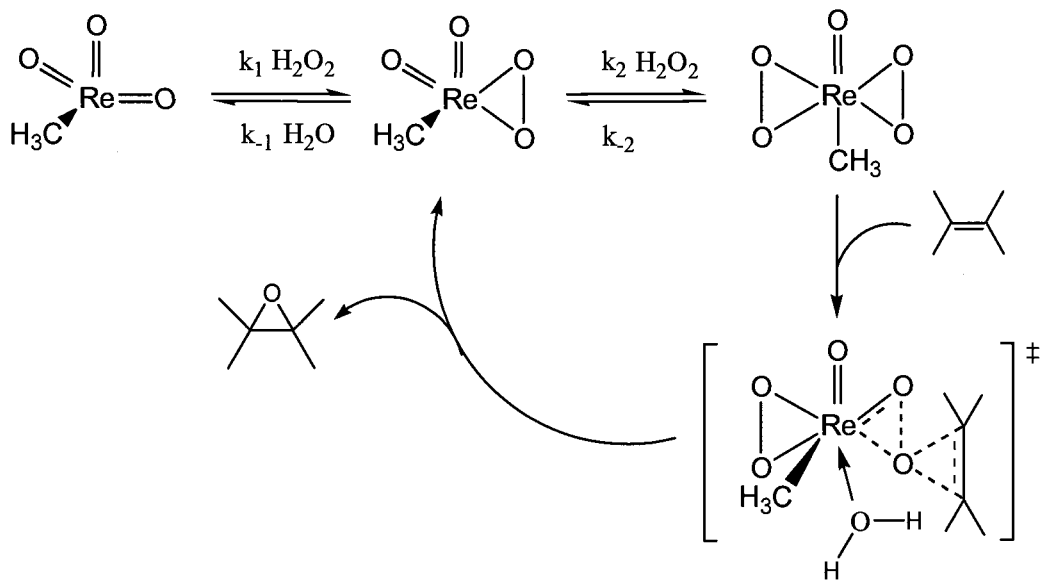


Epoxidations catalyzed by MTO are stereospecific and allow oxidation of the alkene without overoxidation. Since MTO is soluble in both aqueous and organic solvents, epoxides are obtained as products in acetonitrile and 1,2-diols are formed from catalytic ring opening of the epoxide in aqueous media.[28a] The epoxidation mechanism is proposed to occur via direct O-atom transfer mechanism (Scheme 1.4).[36] The mechanism involves nucleophilic attack of the electron-rich olefin on the electrophilic peroxy oxygen. Concerted transfer of oxygen and subsequent reaction with $H_2O_2$ regenerates the $\eta^2$-peroxy complex to continue the catalytic cycle. The driving force for these reactions is the strength of the Re=O bond. Both the mono and bis-peroxo compounds regenerate the Re=O bond after O-atom transfer. Labeling studies have been performed to verify that the oxygen

transferred to the substrate comes from the $\eta^2$-peroxide and not from the terminal oxo group.[37]

The formation of rhenium(VII) diolates has also been observed. Two routes were shown to account for diolate formation: refluxing MTO with diol,[38] and refluxing MTO with epoxides (Scheme 1.5).[39] The formation of rhenium(VII) diolates reduces the catalytic turnover in the epoxidation reaction when the supply of hydrogen peroxide becomes exhausted.

Scheme 1.5

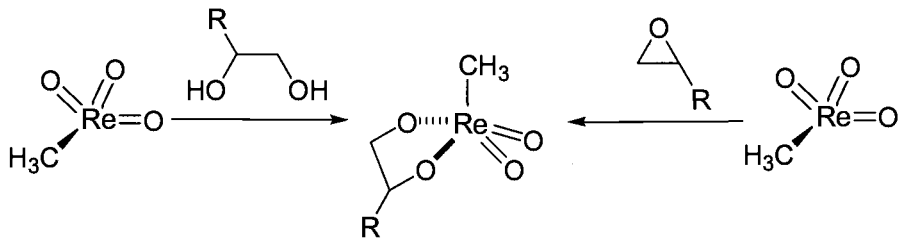


## 1.6 Atom-Transfer Reactions Catalyzed by MTO

MTO is also involved in other oxygen atom transfer processes. MTO catalyzes the transfer of oxygen from molecular oxygen, epoxides, sulfoxides, aromatic tertiary amine oxides, triphenylarsine oxide and triphenylstilbene oxide to the oxygen acceptor triphenylphosphine or hydrophosphorous acid.[40] By analogy to the mechanism reported above for $Cp^*ReO_3$ catalyzed deoxydehydrations, a

rhenium(V) intermediate $CH_3ReO_2$ (MDO) or $CH_3Re(O)_2 \cdot OPPh_3$ results from the reduction of MTO by phosphines (Scheme 1.6). Once formed, the rhenium(V) intermediate reacts with the oxygen containing substrate (S-O) (pathway B), depending on the presence of molecular oxygen. If the reduction is done in the presence of molecular oxygen (pathway A), phosphine oxides and MTO are produced. The mono $\eta^2$-peroxorhenium complex, which is one of two intermediates involved in MTO catalyzed epoxidation of olefins (See Scheme 1.3), is the likely intermediate formed from MDO and $O_2$. However, detecting the peroxo intermediate is difficult since the conditions used to generate MDO will also reduce the $\eta^2$-peroxorhenium complex.

Scheme 1.6

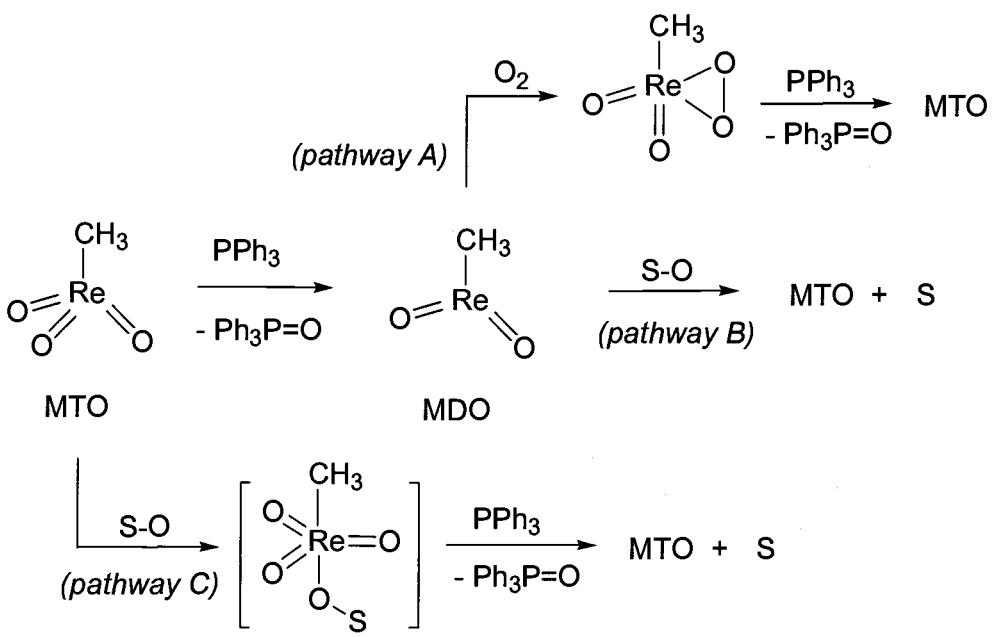

The second possible mechanistic explanation is prior coordination of the oxygen containing substrate (S-O) to MTO, followed by abstraction of oxygen by triphenylphosphine and regeneration of the catalyst (pathway C, see Scheme 1.6). Since the rhenium center is extremely electron deficient in MTO, prior coordination of the substrate to MTO is quite plausible. Support for this alternative mechanism is provided by the observation that rhenium(VII) diolate complexes, which are generated from MTO and epoxide (see Scheme 1.5), react with triphenylphosphine to produce alkene and MTO (Scheme 1.7). Obviously, this mechanistic possibility does not exist for deoxygenations catalyzed by the more electron rich $Cp^*ReO_3$ complex.

Scheme 1.7

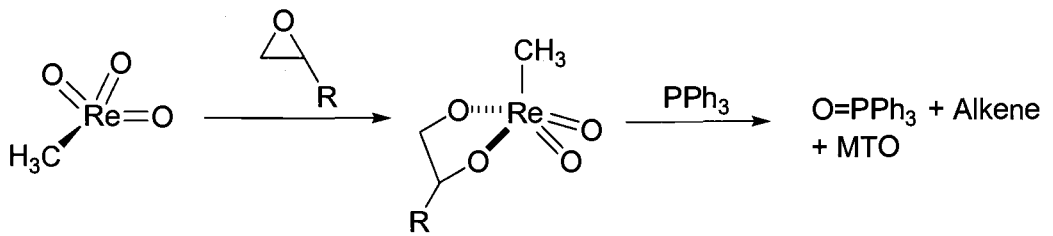


## 1.7 Dihydroxylation of Alkenes by $Cp^*ReO_3$

As previously mentioned, structural modifications in rhenium oxo chemistry have a major impact on molecular reactivity. In MTO (L = $CH_3$), the

ligand can be classified as a strong σ / weak π-donor. When L = Cp*, the ligand is a moderate σ / good π-donor. As a consequence of the different donor properties of the ligands, the reactivity of the two compounds is completely different. MTO reacts with hydrogen peroxide to form rhenium peroxo complexes which epoxidize olefins. Conversely, $Cp^*ReO_3$ does not epoxidize olefins in the presence of hydrogen peroxide. However, it will react with strained alkenes to form rhenium(V) diolate complexes[29] while MTO is unreactive.

Scheme 1.8

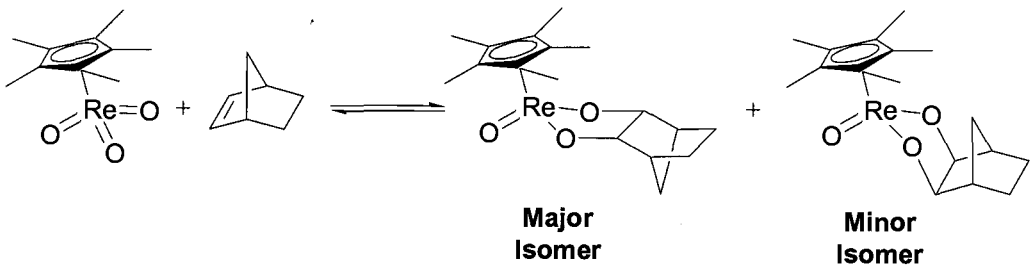


Strained alkenes, such as norbornene, norbornadiene and *trans*-cyclooctene, undergo cycloaddition with $Cp^*ReO_3$ to form an equilibrium mixture of diolate complexes and reactants.[41] In the case of norbornene, the exo, anti isomer was the major product identified along with the exo, syn isomer as the minor product (Scheme 1.8). A strain-induced acceleration was also observed for more strained alkenes. For example, the pseudo-first-order rate constant for alkene oxidation of norbornadiene at 370.4K was $7.20 \times 10^{-5}$ $M^{-1}s^{-1}$, while the rate constant for *trans*-

cyclooctene at 370.4K was 3.92 x $10^{-3}$ $M^{-1}s^{-1}$. Since the total strain energy between the alkene and corresponding alkane is 8.0 kcal/mol for norbornadiene and 9.0 kcal/mol for *trans*-cyclooctene, a larger rate constant for alkene oxidation is observed and expected for *trans*-cyclooctene. In the case of unstrained alkenes, no addition to Cp*$ReO_3$ is observed; cycloreversion of the diolate occurs instead. The results clearly indicate that Cp*$ReO_3$ is at a thermodynamic balance point with respect to diolate formation and diolate cycloreversion.

The double bond strain energy for norbornene was estimated to be 5.7 kcal/mol based on its heat of hydrogenation.[42] In addition, the temperature dependence of the equilibrium constant (K) for norbornene oxidation by Cp*$ReO_3$ gave $\Delta H^o$ = -10.9 kcal/mol and $\Delta S^o$ = -22.8 eu. The $\Delta H^o$ for a disubstituted alkene was determined by subtracting the strain energy from the $\Delta H^o$ for norbornene. Isodemic evalution of methyl substitution gives $\Delta H^o$ for ethylene, which is then used to calculate the $\Delta H_{rxn}$ for Cp*$ReO_3$ + olefin → Diolate. The oxidation of unstrained alkenes with Cp*$ReO_3$ was determined to by thermoneutral or slightly exothermic. Then using C-C, C=C and C-O bond dissociation energies[43], the Re-O π-bond strength was determined to be approximately 50 kcal/mol. Computational studies confirmed that reacting Cp*$ReO_3$ with ethylene is exothermic by 4 kcal/mol.[44] Even though the reaction is slightly exothermic, the oxidation of unstrained alkenes with Cp*$ReO_3$ is disfavored because of the unfavorable change in entropy. The implication of these results is that the Re=O π-bond in Cp*$ReO_3$ is too strong to be an effective dihydroxylation reagent for any but strained alkenes.

## 1.8 Cycloreversion of Rhenium(V) Diolates

The condensation of substituted vicinal diols to a 1:1 mixture of $Cp^*ReO_3$ and $PPh_3$ results in the formation of rhenium(V) diolate complexes.[22,45] The process is accelerated and the yields increased by the addition of one equivalent of *p*-toluenesulfonic acid (PTSA). Furthermore, 4 Å molecular sieves facilitate the process by removing water formed from the condensation reaction.

Rhenium(V) diolates of unstrained alkenes will undergo alkene extrusion at elevated temperatures.[22] Thermal cycloreversion of rhenium diolates is the microscopic reverse of alkene dihydroxylation by metal oxides. The cycloaddition of $OsO_4$ to alkenes, a reaction surrounded by mechanistic controversy, is the quintessential example of a metal reagent adding two oxygen atoms at a carbon-carbon double bond.[4] Particular attention has focused on whether the reaction is concerted ([3+2] mechanism) or whether it proceeds through a stepwise intermediate ([2+2] mechanism). Since $LReO_3$ is isoelectronic with $OsO_4$ and cycloreversion is mechanistically the reverse of cycloaddition, the cycloreversion of rhenium(V) diolates is an excellent probe to investigate cycloaddition of $OsO_4$ to alkenes.

Cycloreversion of rhenium(V) diolates is highly stereospecific and proceeds between 50-120°C.[22] Scheme 1.9 lists several possible mechanisms for this reaction. Since the reaction is stereospecific, mechanisms involving homolytic or heterolytic cleavage of a C-O bond can be immediately excluded. However, this

presumes that any intermediate formed will undergo single bond rotation faster than cleavage of the second C-O bond to form alkene. Further evidence against an ionic and homolytic mechanism is the observation that substituents that would stabilize radical or ionic intermediates by lengthening their lifetime, still resulted in maintained stereospecificity. In addition, an ionic mechanism is unlikely since the rate of diolate cycloreversion was largely unaffected by changes in solvent.[46]

Scheme 1.9

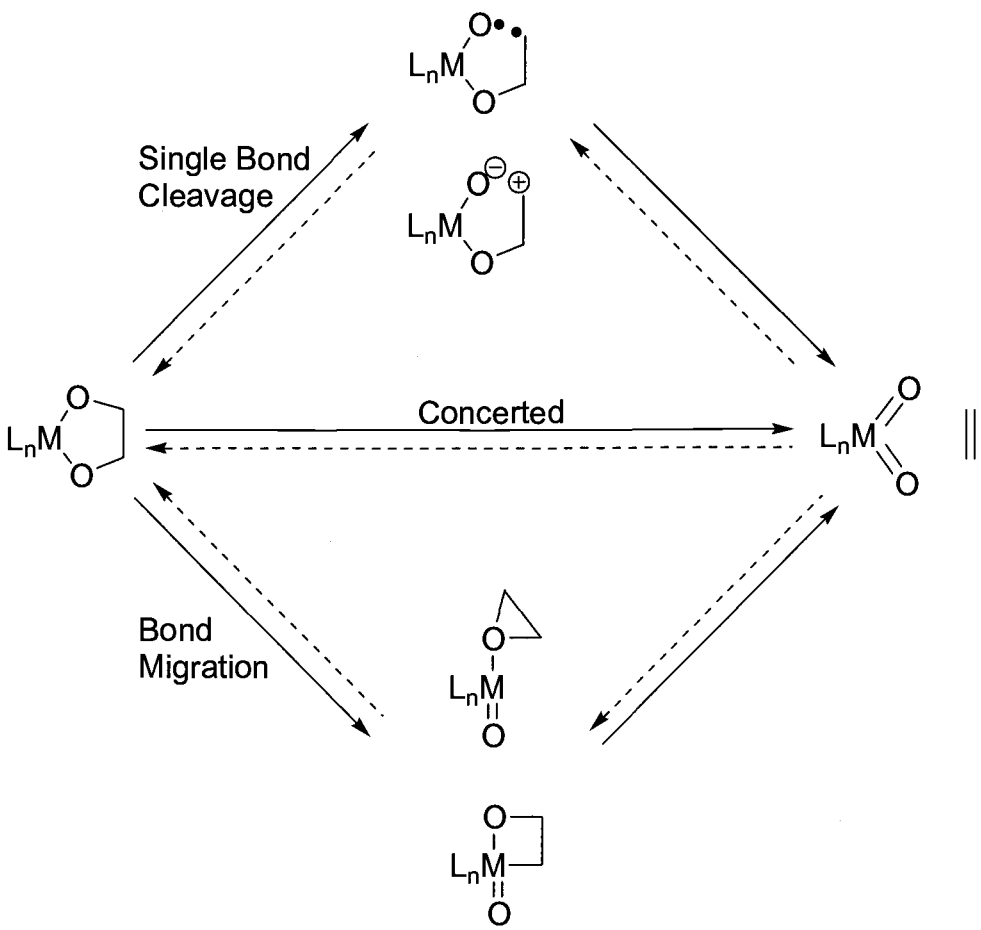

Possible stepwise mechanisms include migration of carbon to rhenium to form a metalloxetane intermediate or migration of carbon to the second diolate oxygen forming a coordinated epoxide intermediate. Each of these intermediates would then undergo a rapid concerted fragmentation to form alkene and $Cp^*ReO_3$. Preliminary experimental evidence supported cleavage of only one of the two C-O bonds in the transition state. Experimental evidence in favor of a stepwise mechanism versus a concerted mechanism include the following: (1) The extrusion of alkenes was independent of strain in the newly formed double bond.[22] (2) A significant secondary kinetic isotope effect was observed, indicating considerable C-O bond cleavage at the transition state.[22] (3) Structure/reactivity studies demonstrated staggered diolate conformations cycloreverted faster than eclipsed diolate conformations.[47]

Activation parameters for alkene oxidation of norbornene, norbornadiene and *trans*-cyclooctene and activation parameters for alkene extrusion of ethylene, 2-butene and bicyclo[2.2.2]oct-2-ene from Cp*Re(O)(OCH(R)CH(R)O) were determined. The activation parameters demonstrated that strain in the alkene had a large effect on the enthalpy of activation ($\Delta H^{\ddagger}$) for alkene oxidation but little or no effect on the enthalpy of activation ($\Delta H^{\ddagger}$) for alkene extrusion.[22] For instance, the $\Delta H^{\ddagger}$ for alkene extrusion was determined to be approximately 30 kcal/mol for each rhenium(V) diolate tested, while a decrease of the $\Delta H^{\ddagger}$ for alkene oxidation from 18 kcal/mol for norbornene (strain = 5.7 kcal/mol) to 12 kcal/mol for *trans*-cyclooctene (strain = 9.0 kcal/mol) resulted with increasing strain in the double

bond. The results clearly indicate the reacting carbon is $sp^3$ hybridized at the transition state. The absence of variation in $\Delta H^{\ddagger}$ for alkene extrusion is consistent with a stepwise mechanism since the hybridization of the reacting carbon does not change going from diolate to either the metalloxetane or coordinated epoxide intermediate (Scheme 1.10). This does, however, assume migration of carbon to form the metalloxetane or migration of carbon to form the coordinated epoxide to be the rate determining step. A concerted pathway, which is the only remaining mechanistic possibility, would be inconsistent since an increase in $\Delta H^{\ddagger}$ for alkene extrusion and a decrease in $\Delta H^{\ddagger}$ for alkene oxidation would be expected.[48]

Scheme 1.10

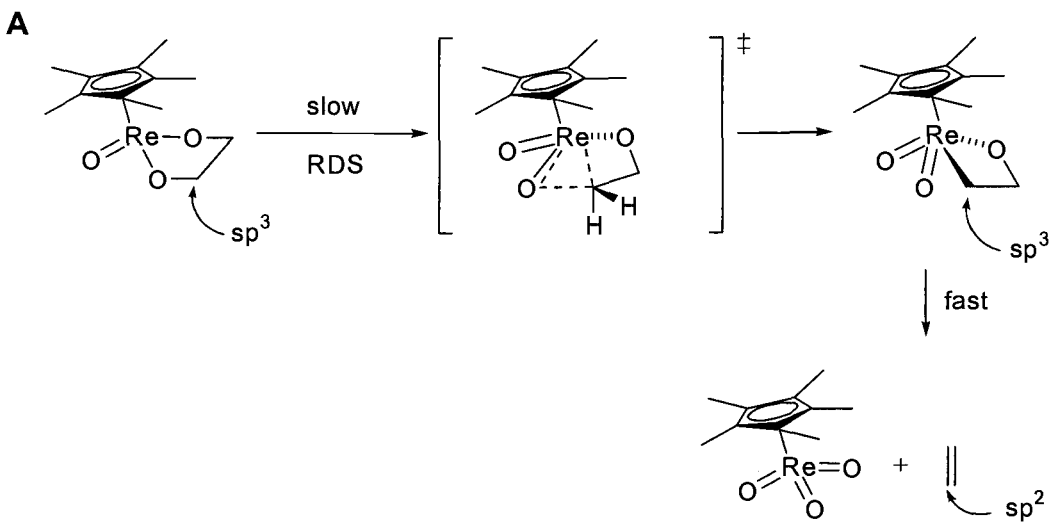

Scheme 1.10 Continued

**B**

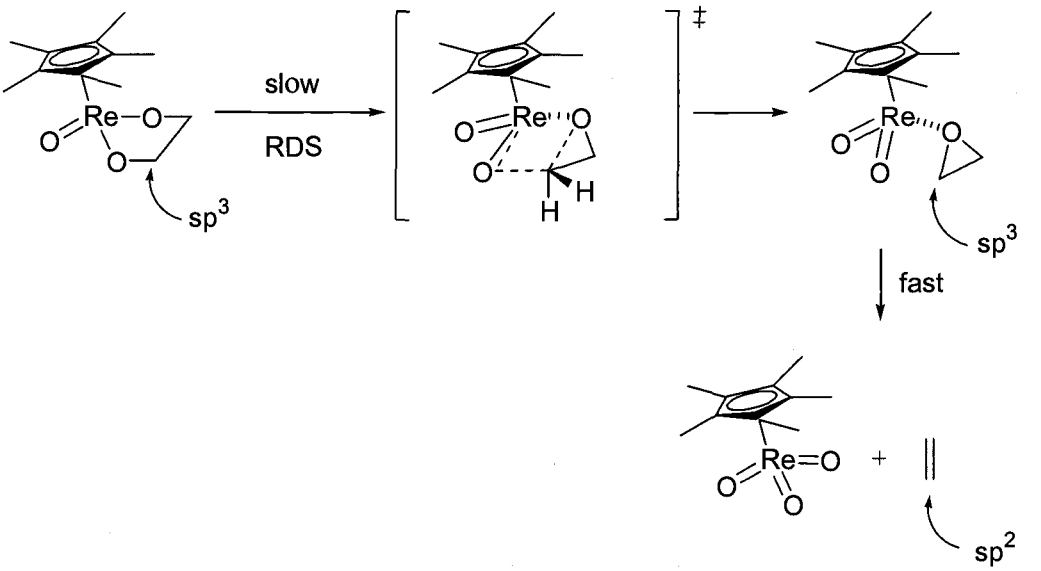


The results from the strain studies can be rationalized for the concerted process if the transition state is very reactant-like. If an early transition state existed one would expect very little rehybridization of the two reacting carbons from $sp^3$ to $sp^2$, which would be consistent with the earlier data. However, the high $\Delta H^{\ddagger}$ values for diolate cycloreversions are inconsistent with an early transition state. Furthermore, a significant secondary deuterium kinetic isotope effect ($k_{H4}/k_{D4}$ = 1.25 ± 0.05 at 100°C) indicated substantial C-O bond cleavage at or before the transition state. An early transition state would result in a low KIE since little rehybridization is occurring.

Conformational studies on rhenium(V) diolates also support a stepwise mechanism.[47] The dihedral angles of various substituted diolates were determined from H-H coupling constants and the Karplus relationship. The study revealed that the reaction rate for alkene extrusion is dependent on the geometry of the diolate ring. The rate is inhibited if the ring is flattened and promoted if the ring is staggered. A concerted pathway would require a flat or eclipsed conformation to ensure proper alignment of the developing $\pi$ bond. The increase in rate with more staggered conformations, coupled with the effect of strain on the $\Delta H^{\ddagger}$ and the significant secondary KIE, suggests a stepwise mechanism is operating in rhenium(V) diolate cycloreversions.

Even though preliminary experimental data argued against a concerted mechanism, recent high-level computational calculations argue that the concerted [3+2] process is energetically favored over formation of a metalloxetane.[44,49] This is the simplest mechanism and is the microscopic reverse of Crigee's concerted [3+2] cycloaddition mechanism proposed for the addition of alkenes to $OsO_4$.[50] Among the findings from these calculations are the following: (1) The activation barrier for the [2+2] process is higher than the barrier for the [3+2] process. For example, the activation energy for [2+2] addition of ethylene to $Cp^*ReO_3$ was calculated to be 168.6 kJ/mol, while the barrier for [3+2] addition was calculated to be 70.3 kJ/mol. (2) The metallaoxetane forms of $ReO_4^-$-$C_2H_4$ and $ClReO_3$-$C_2H_4$ are lower in energy than the metallodioxylates, whereas the metallodioxylates of $OsO_4$-$C_2H_4$ and $CpReO_3$-$C_2H_4$ are more stable than the

corresponding metalloxetanes. (3) $LReO_3$ compounds (L = $O^-$, Cl, Cp) have higher activation barriers for the [3+2] process ($CpReO_3$ = 15.7 kcal/mol, $ClReO_3$ = 24.0 kcal/mol, $ReO_4^-$ = 37 kcal/mol) compared to $OsO_4$ (6.9 kcal/mol).

Numerous studies have shown that primary and secondary kinetic isotope effects (KIE) can be used to determine the mechanism and transition state geometry of organic reactions.[51] The advantage of the experiment compared to other techniques is it imposes the least possible structural change and thus minimizes risk of structurally-induced change of mechanism. The mechanism for enantioselective asymmetric dihydroxylation was resolved experimentally and theoretically by determining the primary and secondary KIEs for the oxidation of *tert*-butylethylene.[52] As previously mentioned, the mechanism for osmium tetraoxide mediated dihydroxylation of olefins has been surrounded by controversy. Mechanistic investigations have focused on two major proposals: (1) A concerted [3+2] cycloaddition that directly forms the cyclic osmate ester, or (2) A [2+2] process involving formation of an osmaoxetane followed by ring expansion to form the cyclic osmate ester. The primary KIEs at the two olefin positions were determined experimentally to be 1.027 and 1.028, while the secondary KIE at the substituted carbon was determined to be 0.906. Theoretical DFT calculations predicted primary KIEs of 1.025 and 1.025 for the [3+2] process and 0.989 and 1.039 for the [2+2] process. The secondary D KIE for the substituted carbon was calculated to be 0.907 for the concerted process and 0.880 for the stepwise process. Since the both carbons show identical primary KIE and the magnitude of the

primary and second KIEs match the theoretical values for the [3+2] process, it was concluded that enantioselective asymmetric dihydroxylations proceed through a concerted [3+2] rate-limiting step.

The method used to determine the primary $^{13}C$ KIEs from natural abundance isotopomers using NMR techniques was developed by Singleton et. al..[53] The methodology is based on the phenomenon that the starting materials will become enriched by isotopically slower-reacting materials as the reaction proceeds to greater conversion. The isotope effects are calculated according to equation (3). $R/R_0$ represents the ratios of isotopically enriched starting material recovered relative to the original starting material. A nonreacting reference position is used to determine the proportion of labeled compounds, compared to unlabeled starting material. $F$ is the fractional conversion of reactants ($0<F<1$). The advantage of this method is at high conversions the $R/R_0$ ratio approaches infinity and the observed KIEs are magnified. In addition, individual KIE's can be determined simultaneously.

$$KIE = \frac{\ln(1-F)}{\ln((1-F)R/R_0)} \qquad (3)$$

Primary and secondary kinetic isotope effects were also used to resolve the mechanistic controversy surrounding the thermal cycloreversion of rhenium(VII) diolates. The cycloreversion of 4-methoxystyrene from the corresponding

Tp'Re(O)(diolato) complex (Tp' = hydrido-*tris*-(3,5-dimethylpyrazolyl)borate) at 103°C was consistent with an asynchronous but concerted transition state.[54] For the concerted [3+2] process, cleavage of both carbon-oxygen bonds occurs at the transition state. As a result, the primary and secondary effects at both positions are expected to be greater than unity (Scheme 1.11). Conversely, the [2+2] process would result in cleavage of only one of the C-O bonds. The [2+2] process would then result in primary and secondary effects to greater than unity at one position and unity at the other position. The primary KIEs resulting from cycloreversion of 4-methoxystyrene were determined to be $k_{12C}/k_{13C}$ = 1.041±0.005 at the α position and 1.013±0.006 at the β position. In addition, the secondary KIEs were $k_H/k_D$ = 1.076±0.005 at the α position and 1.017±0.005 at the β position. The data clearly indicates KIEs greater than unity at both the α and β positions, though only slightly greater than unity at the β position. Since both reacting positions show KIEs greater than unity, the extrusion of 4-methoxystyrene was determined to be an asynchronous concerted mechanism with more bond breaking occurring at the α carbon than the β carbon. The transition-state structure was considered to be quite flexible (physically and electronically), which would account for earlier experimental data that supported a stepwise mechanism.

Scheme 1.11

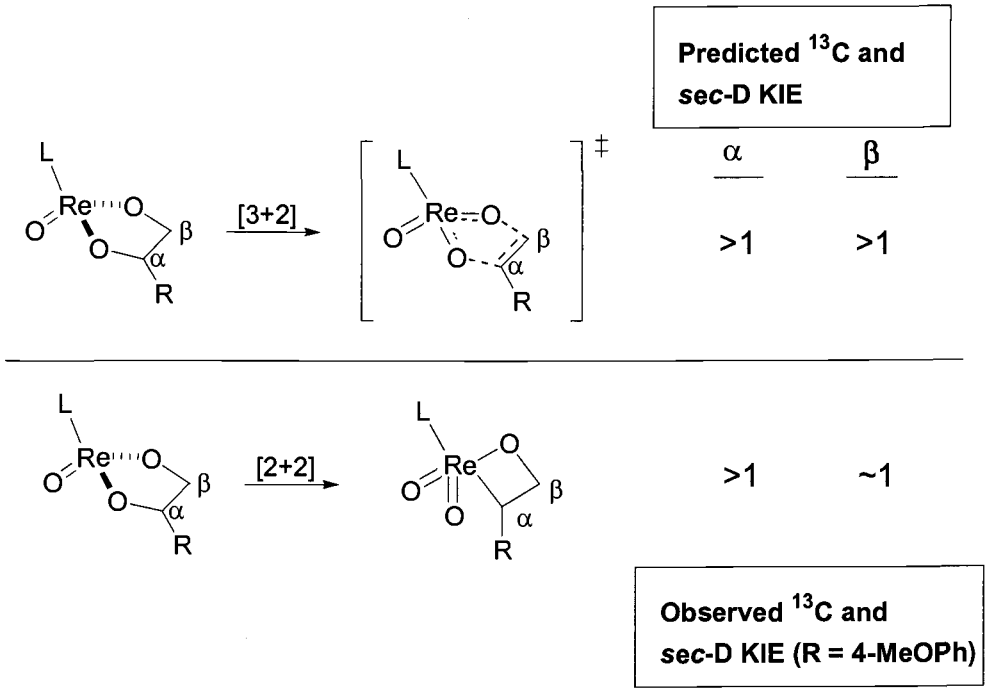


## 1.9 Atom-Transfer Reactions Catalyzed by $Cp^*ReO_3$

The abstraction of an oxo group from $Cp^*ReO_3$ by oxophilic $PPh_3$ results in the formation of the bridging oxo dimer $(Cp^*ReO)_2(\mu\text{-}O)_2$ (Scheme 1.12).[55] Fragmentation of the dimer to the reactive monomer, $Cp^*ReO_2$, was observable by both NMR and UV-vis spectroscopy.[56] At room temperature, a single $^1H$ NMR signal, assigned to the dimer, at δ 1.96 ppm was observed. However, upon

warming, a second signal corresponding to the monomer was observed at δ 1.60 ppm. The dimer / monomer equilibrium constant was calculated to be (6.05±1.29) x $10^{-4}$ M at 366K. Overall, the reaction enthalpy for transfer of oxygen from $Cp^*ReO_3$ to $PPh_3$ is exothermic by about 30 kcal/mol experimentally[57] or 20 kcal/mol calculated.[58] The strength of the Re=O bond was determined to be 117 kcal/mol, while the bond strength of P=O in $O=PPh_3$ is roughly 136 kcal/mol. The difference in bond strengths between the Re=O bond in $Cp^*ReO_3$ and P=O bond in $O=PPh_3$ makes up about ~ 19 kcal/mol of the total 30 kcal/mol exothermicity. The remaining 11 kcal/mol is attributed to formation of the dimer.

Scheme 1.12

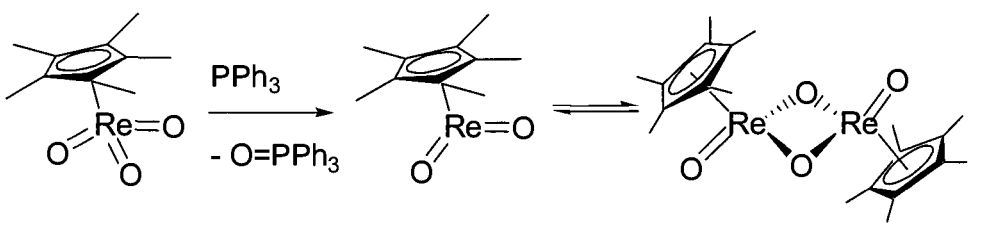


The monomer, $Cp^*ReO_2$, is a 16 $e^-$ $d^2$ cis-dioxo complex that is highly reactive because of competition from the two oxo groups to π bond into a single empty *d* orbital. Besides reacting with vicinal diols to form rhenium(V) diolates, the Re(V) monomer is capable of other oxygen atom abstraction processes. These include the deoxygenation of epoxides, sulfoxides and activation of molecular

oxygen (Scheme 1.13).[56] In addition, the monomer is susceptible to protonation and nucleophilic attack in aqueous hydrochloric acid to generate the dichloro(oxo)($\eta^5$-pentamethylcyclopentadienyl)rhenium(V) complex.[55]

Scheme 1.13

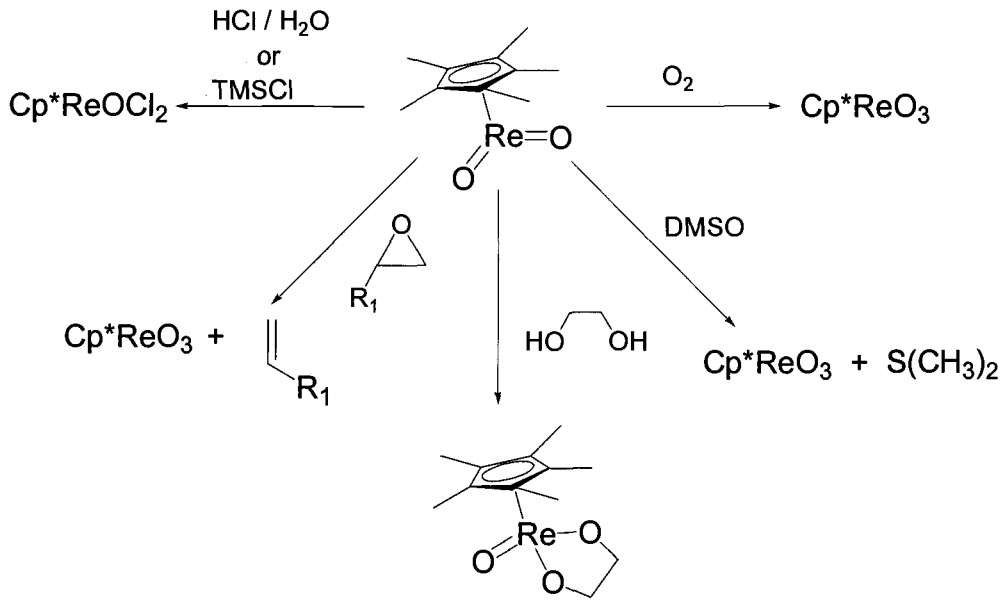


As shown in Scheme 1.6 and 1.13, $LReO_2$ reacts with epoxides producing alkene and $LReO_3$. An initial study with L = Cp* demonstrated $Cp^*ReO_2$, which is in equilibrium with its dimer $[(Cp^*ReO)_2(\mu\text{-}O)_2]$, would react with several epoxides at 50-105°C.[56] The epoxides tested include the following: 1,1-dimethyoxirane, styrene oxide, cyclohexene oxide and (*E*)- and (*Z*)-1,2-dimethyloxirane. The deoxygenation of (*E*)- and (*Z*)-1,2-dimethyloxirane resulted

in retention of configuration and the rate law was determined to be half order in dimer and first order in epoxide (Eq. 4).

$$-d[(Cp^*ReO)_2(\mu\text{-}O)_2]/dt = k_{obs}[epoxide][(Cp^*ReO)_2(\mu\text{-}O)_2]^{1/2} \qquad (4)$$

The development of a process for deoxygenating epoxides using catalytic amounts of rhenium were soon reported after the discovery that $(Cp^*ReO)_2(\mu\text{-}O)_2$ / $Cp^*ReO_2$ deoxygenated epoxides.[60] The catalytic process involves reduction of $Cp^*ReO_3$ with triphenylphosphine to generate $Cp^*ReO_2$ (Scheme 1.14). $Cp^*ReO_2$ then reacts with epoxide to generate alkene and regenerate $Cp^*ReO_3$. Unfortunately, low turnover numbers were observed for each of the epoxides studied. The catalyst deactivation resulted from conproportionation of the reduced and oxidized intermediates to form a novel tetranuclear cluster that was unreactive to epoxides. The structure of the cluster was elucidated by X-ray crystallography and exhibited a unique IR peak at 736 $cm^{-1}$. Not surprisingly, an increase in the concentration of triphenylphospine led to improved conversion from <5% to 50%. An increase in triphenylphospine rapidly reduces any amount of $Cp^*ReO_3$, thus preventing $Cp^*ReO_3$ from conproportionating with $Cp^*ReO_2$. The choice of epoxide was also shown to enhance catalytic turnover. Epoxides with electron-withdrawing substituents, such as 3-fluoropropylene oxide, resulted in larger turnover numbers. Formation of the inactive tetranuclear cluster explains why

catalyst deactivation occurred for the deoxygenation of carbohydrates catalyzed by $Cp^*ReO_3$ (See Scheme 1.1).

Scheme 1.14

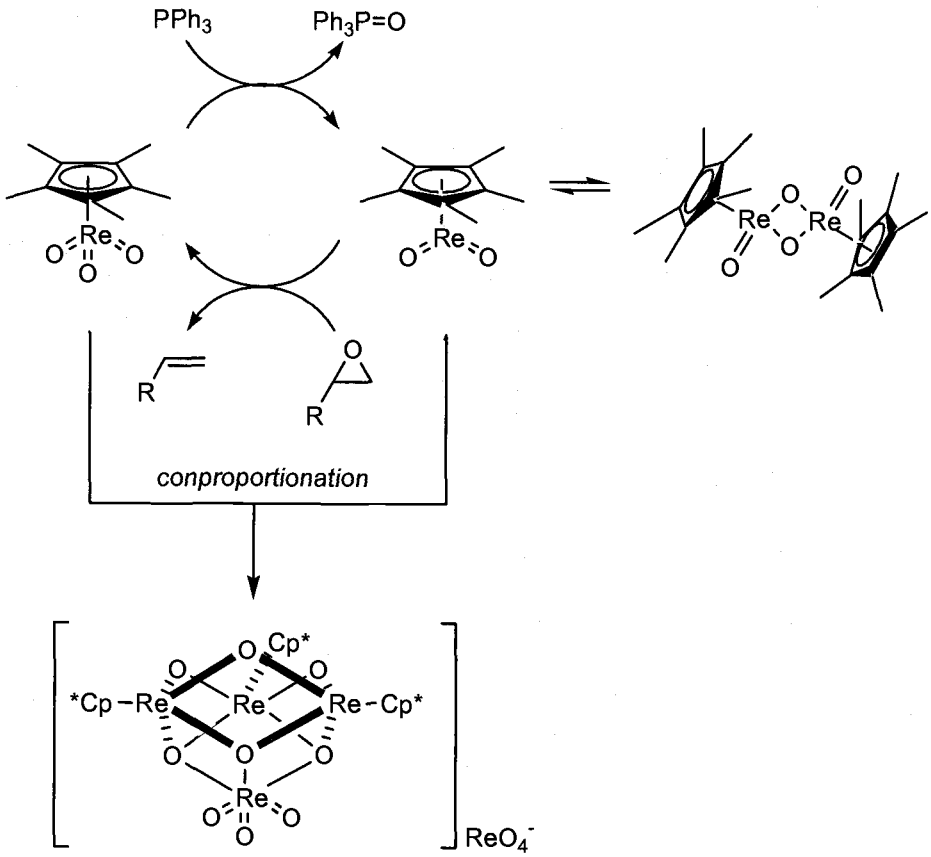


## 1.10 Conclusions

The oxo chemistry of rhenium has expanded dramatically within the last twenty years spurred on by interest in high-valent organometallic oxides.[60] Chapter

1 has focused primarily on MTO and $Cp^*ReO_3$ mediated oxidations and deoxygenations. The advancement of MTO and $Cp^*ReO_3$ mediated C-O bond formation and cleavage has been mainly pioneered by the Herrmann group in Munich, the Espenson group at Iowa State University and the Gable group at Oregon State University. Progress has been made in developing new oxidation reagents and understanding the mechanisms involved in rhenium-mediated organic oxidations. However, several new and old issues remain concerning the question of mechanism in these oxidations.

Some of the questions that this work will address include the following: (1) Does a mechanistic relationship exist relating epoxidation and bishydroxylation processes? This chapter has already shown that rhenium-mediated epoxidations and hydroxylations can be controlled by structure. (2) Can changes in structure allow the isolation of the reactive monomer $LReO_2$ after reduction of $LReO_3$ rather than the bridged oxo compound $[LReO]_2(\mu\text{-}O)_2$. (3) Can efficient catalytic deoxygenation of epoxides occur with simple changes in structure? For example, can changes in structure prevent the formation of clusters? (4) Does a metal-substrate bond exist during the deoxygenation of epoxides or are all the C-O bonds cleaved remotely from the metal? (5) Do the two C-O bonds in the epoxide cleave at the same time or one after the other?

# Chapter 2. Development of a Catalytic O-Atom Transfer System

## 2.1 Epoxidation and De-epoxidation

Epoxides are valuable intermediates in Nature, industry and synthetic organic chemistry. A variety of high oxidation state oxo metal complexes have been successfully used to generate epoxides.[61] In addition, Nature has evolved metal-containing enzymes capable of either alkane hydroxylation, olefin *cis*-dihydroxylation or olefin epoxidation.[62] The high reactivity and ease of introducing additional functionality have made epoxides among the more important and frequently used synthetic intermediates in organic chemistry.

A long standing goal of homogenous catalysis has been the epoxidation of olefins with molecular oxygen. Molecular oxygen is the preferred oxidant since it is cheap, readily available and leaves no by-products. Unfortunately, relatively few examples of catalytic epoxidations using $O_2$ exist. The Shell process for ethylene oxide production is an excellent example of a heterogeneous process which uses molecular oxygen as the stoichiometric oxidant.[63] Silver is used as the catalyst but the identity of the surface oxygen species responsible for the oxidations is still unclear. The reaction is mainly restricted to ethylene as the olefin; low epoxide yields are obtained with different olefins. The production of ethylene glycol resulting from hydrolysis of the epoxide is the desired product.

Scheme 2.1

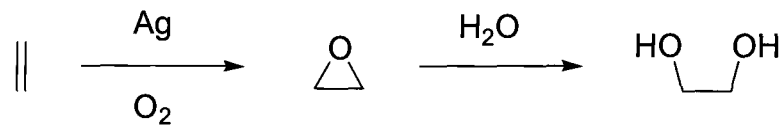


Groves et. al. have shown that ruthenium(II)-porphyrin systems will undergo oxidation with $O_2$, resulting in formation of a dioxoruthenium(VI) complex.[64] Dioxo (tetramesitylporphyrinato)ruthenium(VI), $Ru(TMP)(O)_2$, is a powerful oxidant and was shown to be the active oxidant responsible for oxidations under aerobic conditions. The mechanism is believed to involve initial formation of an oxoruthenium(IV) intermediate, (TMP)RuO, which then disproportionates to $Re(TMP)(THF)_2$ and $Re(TMP)(O)_2$ (Scheme 2.2). The catalytic epoxidations proceed with retention of configuration and cis olefins were 14.5 times more reactive than trans olefins. An asymmetric variation resulted in the enantioselective aerobic oxidation; unfortunately, only moderate to good enantiomeric excess (up to 73% ee for *cis*-β-methylstyrene) was obtained.[65]

Scheme 2.2

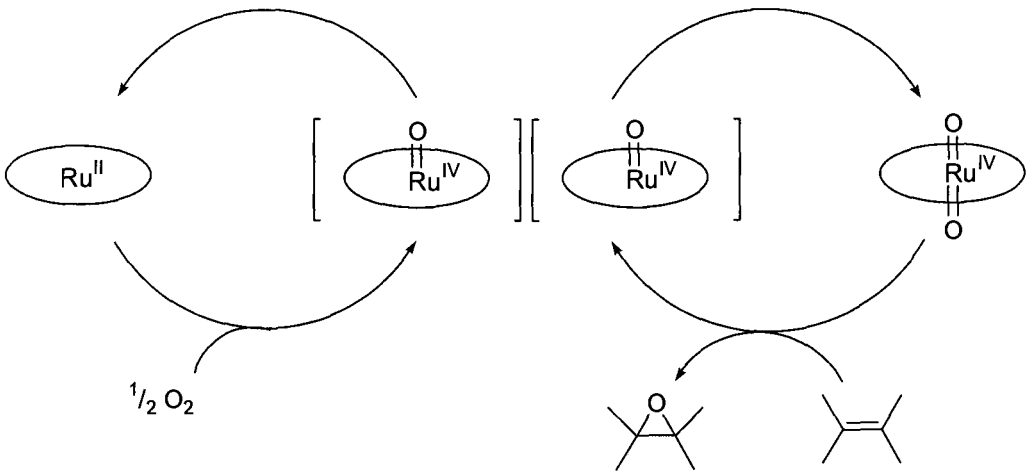


Besides the interest in developing new epoxidation reagents, understanding the mechanism of olefin epoxidation is essential for designing catalysts. For example, asymmetric versions require a detailed understanding of the mechanism to make a predictive model that accounts for the stereochemical result. One powerful method of exploring any mechanism is to study the reverse reaction, which for epoxidation is epoxide deoxygenation (Scheme 2.3). As a result of the principle of microscopic reversibility, one expects that the mechanistic issues observed in C-O cleavage reactions can be applied to C-O bond forming reactions. Therefore, the deoxygenation of epoxides by metal complexes is an area of active research.

Scheme 2.3

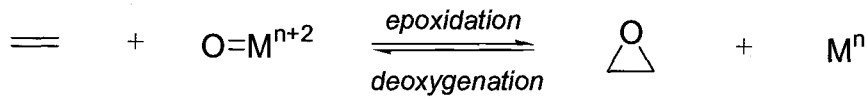


The deoxygenation of epoxides has an assortment of practical applications. As mentioned in Ch. 1, the deoxygenation of renewable biomass feedstocks to more useful materials is a possible application. Procedures exist for converting vicinal diols in carbohydrates into epoxides[66], which can then be deoxygenated. The design of enantioselective regents could allow the kinetic resolution of racemic epoxides.[67] In addition, the deoxygenation of epoxides is an important reaction in organic synthesis since it allows the use of the oxirane ring as a protecting group for alkenes, a means of controlling the geometry of the double bond and a method of simplifying the structure of complex molecules. The synthesis of ryanodine[68], *dl*-$\beta$-Amyrin[69] and the trichothecenes[70] all used a epoxidation / epoxide deoxygenation cycle. Unfortunately, many reagents known to deoxygenate epoxides require multi-step procedures, stoichiometric conditions, harsh reaction conditions, and complicated reagents. The loss of stereochemistry, unknown mechanisms and incompatibility with other functional groups within the substrate also plague many known methods used for epoxide deoxygenation.

Numerous homogeneous reagents are known to deoxygenate epoxides.[71] One of the most powerful oxo acceptors is $WCl_2(PR_3)_3$ (R = $PMe_3$, $PMePh_2$) .[72-74]

The tungsten(II) complex is capable of deoxygenating ketones[72], epoxides[73] and sterically unencumbered phosphine oxides[74]. The reduction of phosphine oxides by the tungsten(II) complex was demonstrated to be thermodynamically favored ($W^{2+}/W^{4+}$=O $\Delta H$ < -74 kcal/mol). However, the reduction of tertiary phosphine oxides, such as O=$PPh_3$, was shown to be kinetically unfavorable because of weak binding of the sterically bulky phosphine oxide to the metal center. Epoxides are readily deoxygenated forming equilibrium mixtures of tungsten(IV) oxo olefin complexes. The tungsten(IV) center is extremely $\pi$-basic and requires $\pi$-backbonding to the olefin to stabilize the olefin complexes.

Another example of a tungsten complex used to convert epoxides to olefins is the generation of low valent tungsten halide derivatives from $WCl_6$ and alkyllithium.[75] In some cases, chlorohydrins are formed as by-products and limited stereoselectivity is observed for acyclic di- and tri-substituted epoxides. Characterization of the catalytic reagents generated and the mechanism of deoxygenation were never determined.

One disadvantage of these systems, aside from not knowing the mechanism involved in $WCl_6$ deoxygenations, is that both require stoichiometric amounts of tungsten. The development of an oxo metal catalyst which can deoxygenate epoxides catalytically would be ideal since stoichiometric amounts of expensive and potentially toxic metal reagents would be unnecessary. Unfortunately, an approach to developing such a process presents several challenges. The properties of the complex must be adjusted, either through structural modifications, choice of

metal or oxidation state, so that O-atom transfer from the substrate to the metal complex is facile. The strength of the metal oxygen bond usually dictates whether O-atom transfer is thermodynamically favored. However, the strength of the metal oxo bond can often be a double edge sword. If the metal oxygen bond strength is too weak then O-atom transfer doesn't occur, but if the metal oxygen bond strength is too strong than the metal oxide is a thermodynamic sink and catalysis is impossible. Therefore, the properties of the metal complex must be balanced so that O-atom transfer from the substrate to the metal complex is favored, but O-atom transfer from the oxo metal complex to the stoichiometric reductant is also possible. $WOCl_4$, which is formed during $WCl_6$ epoxide deoxygenations, contains a very strong metal oxygen bond (BDE = 195 kcal/mol)[76] that is extremely difficult to reduce and would be a poor candidate to develop a catalytic process with.

## 2.2 Ligand Modification of Oxorhenium Complexes

Since the initial attempt to catalytically deoxygenate epoxides failed due to cluster formation, we decided to modify the ligand from pentamethylcyclopentadienyl (Cp*) to hydridotris(3,5-dimethylpyrazolyl)borate (Tp'). Hydridotris(pyrazolyl)borate (Tp) ligands are often considered equivalents to cyclopentadienyl because they serve as anionic six-electron donors. However, electronic and steric differences exist between the two ligands.[77] The Cp ligand is a soft $\pi$ donor and acceptor, while the Tp ligand is a hard nitrogen $\sigma$ donor with

relatively little $\pi$ donor ability. The relative size of the Tp ligand is the primary reason for its use as a Cp equivalent (Figure 2.1). The cone angle for Cp = 150° (R = H), 182° (R = Me) and Tp = 262° (R = H), 276° (R = Me). The large cone angle is often credited for the isolation of Tp analogues of highly reactive Cp compounds.[78]

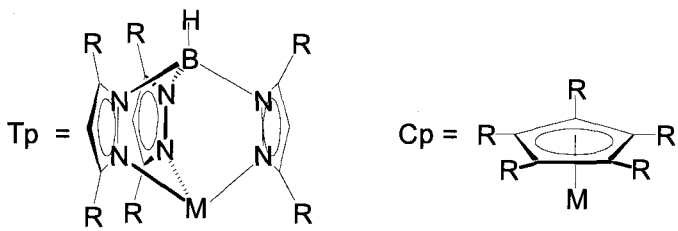


Figure 2.1 Hydridotris(pyrazolyl)borate ligand and cyclopentadienyl ligand.

Poly(pyrazolyl)borate ligands possessing different pyrazolyl ring substituents have found numerous applications in inorganic and organometallic chemistry. Although a variety of poly(pyrazolyl)borate ligands have been synthesized, the most extensively used in chemistry are the tripodal ligands $HB(3,5\text{-}Me_2pz)_3$ (abbreviated Tp'), $HBpz_3$ (abbreviated Tp) and $Bpz_4$ (abbreviated Tk). Rhenium oxo complexes of poly(pyrazolyl)borate ligands have been prepared by a number of groups.[79,80,81,54]

Even though the donor and steric properties between the poly(pyrazolyl)borate ligands and pentamethylcyclopentadienyl ligand are

different, both are involved in similar oxygen atom transfer processes. The reduction of $TpReO_3$ and $TkReO_3$ with triphenylphosphine in THF resulted in the formation $[ReO(\mu\text{-}O)\{B(pz)_4\}]_2$ and $[ReO(\mu\text{-}O)\{HB(pz)_3\}]_2$ respectively.[80b] Mass spectroscopy and $^1H$ NMR spectroscopy were used to verify the assignment. These results are analogous to $Cp^*ReO_3$, which also forms dimeric $[(Cp^*ReO)_2(\mu\text{-}O)_2]$ after reduction with triphenylphosphine (See Ch. 1). The reactivity of the tetrakis(pyrazolyl)borate oxo bridged dimer is shown in Scheme 2.4. Similar to $[(Cp^*ReO)_2(\mu\text{-}O)_2]$, $[ReO(\mu\text{-}O)\{B(pz)_4\}]_2$ reacts with a variety of reagents to form a series of monomeric rhenium(V) compounds.

Scheme 2.4

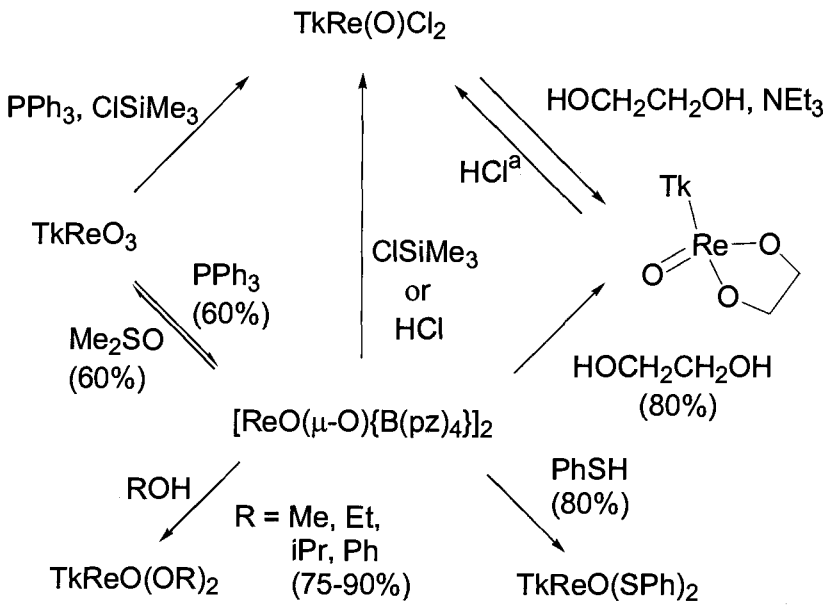


a: ref. 82

Identical kinetic behavior was observed for cycloreversion of hydridotris(3,5-dimethylpyrazolyl)boratorhenium(V) diolates compared to diolate cycloreversions containing the pentamethylcyclopentadienyl ligand.[83] The only difference discerned was higher activation enthalpies by 2-4 kcal/mol, while the entropies of activation and relative reactivity remained the same. In addition, the oxidation of strained alkenes by Tp'$ReO_3$ occurred, indicating cycloreversion and oxidation were close to thermoneutral. Obviously, ligand modification from Cp* to Tp' had a relatively minor effect on the mechanism of diolate cycloreversion.

## 2.3 Catalytic Deoxygenation of Epoxides Mediated by Tp'$ReO_3$

The large cone angle of the Tp' ligand was expected to inhibit cluster formation that killed catalysis using Cp*$ReO_3$ in the epoxide deoxygenation reaction. In addition, the bulkier Tp' ligand was predicted to suppress formation of the dimeric bridged oxo compound $[LReO]_2(\mu\text{-}O)_2$ that resulted from reduction of $LReO_3$ with triphenylphosphine (L = Cp*, Tp or Tk). Since fragmentation of the dimer to the reactive monomer $LReO_2$ was a requirement for oxygen atom transfer,[56] disfavoring dimerization should result in an increase in catalytic turnover by ensuring the catalytically active species remains the predominant species in solution.

Scheme 2.5

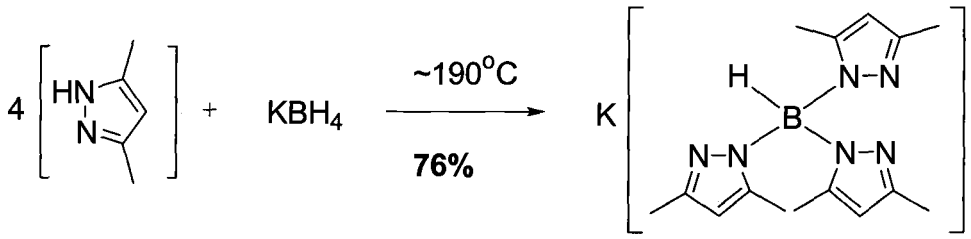


Besides developing an efficient catalytic process of deoxygenating epoxides, the application of the process to organic synthesis is also a goal. One particular disadvantage of many reagents used to deoxygenate epoxides is the complicated synthesis of the reagent. Scheme 2.5 demonstrates the simple one-step process for generating potassium hydridotris(3,5-dimethylpyrazolyl) borate, while Scheme 2.6 shows the easy synthesis of the starting reagent $Tp'ReO_3$. The conditions used to generate KTp' are similar to the conditions reported by Trofimenko et al. for the synthesis of KTp.[84] The generation of $Tp'ReO_3$ requires the initial formation of the mixed anhydride $CF_3CO_2ReO_3$ followed then by the addition of KTp'. $Re_2O_7$ can be used directly, but the mixed anhydride route prevents losing half of the rhenium as perrhenate.[79b] Overall, generation of $Tp'ReO_3$ is a simple process that results in high yields of product.

Scheme 2.6

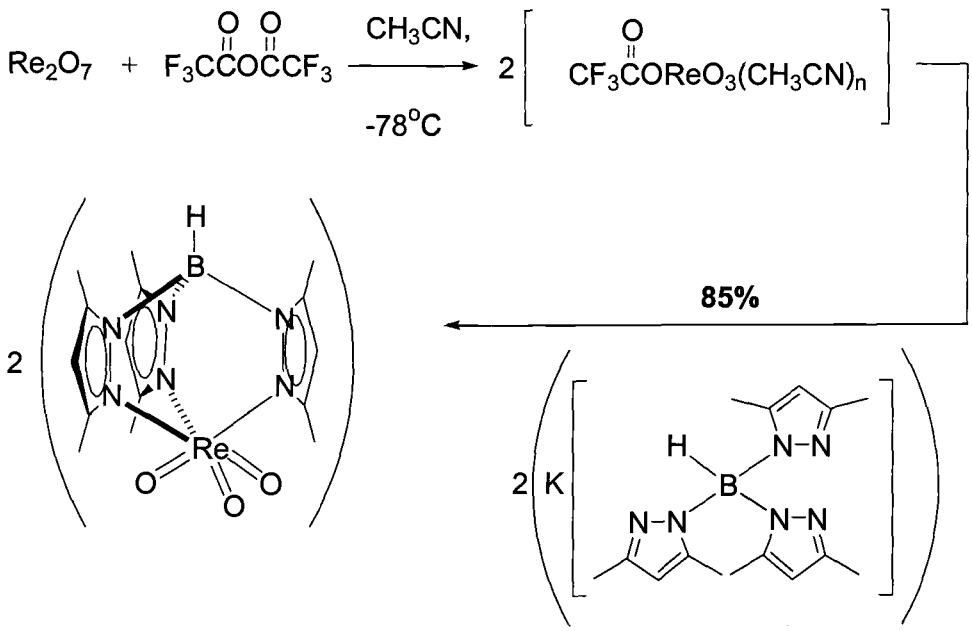


The reaction of 1-5 mole percent of $Tp'ReO_3$ with epoxide and triphenylphosphine (1:1 stoichiometry) in benzene resulted in efficient catalytic epoxide deoxygenation (Scheme 2.7).[85] The reaction conditions involved heating the sample in a tube sealed under vacuum at 75-105°C. The reduced rhenium(V) species $Tp'ReO_2$, analogous to the $Cp^*ReO_3$ species seen in equilibrium with $(Cp^*ReO)_2(\mu\text{-}O)_2$, reacts with epoxides to form alkene and $Tp'ReO_3$. Triethyl phosphite was likewise an excellent stoichiometric reducing agent. Thermodynamically the reaction between epoxides and triphenylphosphine is highly favored ( $\Delta G^\circ \approx$ -55 kcal/mol )[86], but the uncatalyzed reaction requires elevated temperatures (200°C) and results in inversion of configuration.[87] No

alkene formation was observed after heating a sample for 24h at 75°C in the absence of any rhenium compounds. In addition, most reactions catalyzed by $Tp'ReO_3$ were stereospecific with preservation of the relative stereochemistry about the C-C bond of the epoxide. The deoxygenation of *trans*-butene oxide resulted in minor amounts of *cis*-2-butene after the reaction was run to > 95% completion. The deliberate addition of water was shown to inhibit catalytic turnover; predrying the epoxide, internal standard, and triphenylphosphine in $d_6$-benzene over $CaH_2$ enhanced the turnover frequency. Efficient catalysis was also observed in THF, ether and acetonitrile.

Scheme 2.7

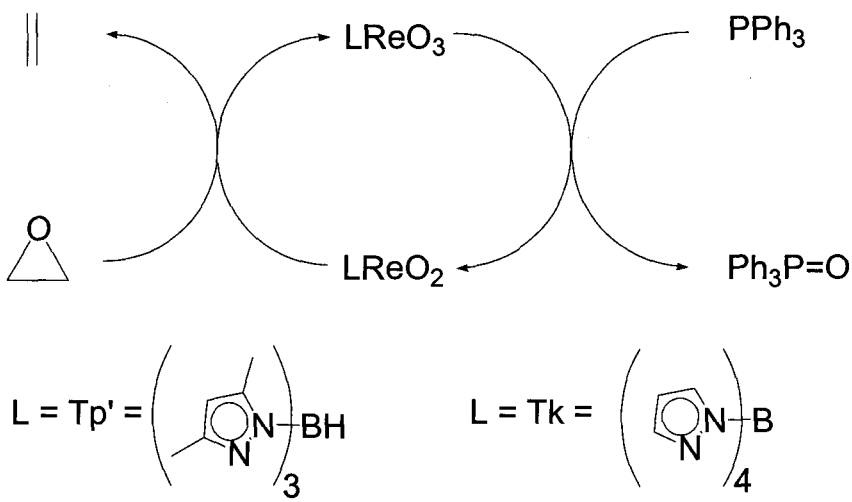


Table 2.1 shows the catalytic deoxygenation of various epoxides using $Tp'ReO_3$ (5 mol %) / $PPh_3$ in benzene-$d_6$. The relative reactivities demonstrate the

effect of electronic and steric structure on the deoxygenation process. Terminal alkenes form faster than internal alkenes and *cis*-alkenes form faster than *trans*-alkenes. More substituted epoxides are deoxygenated less readily, except for isobutylene oxide which deoxygenated faster than propylene oxide. In addition, aryl substituents increase the reaction rate compared to alkyl substituents. Epoxides with electron-withdrawing substituents, such as epoxytrifluoropropane, reacted faster. 7-Oxabicyclo[4.1.0]heptan-2-one was the fastest of all the epoxides tested, resulting in greater than 95% conversion by NMR in less than 25h at 75°C. No evidence of catalyst deactivation occurred compared to the Cp* compound, where conproportionation of the reduced and oxidized intermediates resulted in the formation of an inactive tetranuclear cluster. Furthermore, epoxides which reacted slowly were shown to go to > 95% completion if given enough time. This was demonstrated by heating samples to 105°C for greater than 48h.

Table 2.1 Catalytic deoxygenation of epoxides with $Tp'ReO_3/PPh_3$ in benzene-$d_6$.

2-1

| time, hr | time, secs | temp., °C | Conversion % |
|---|---|---|---|
| 0 | 0 | 75 | 0 |
| 0.5 | 1800 | 75 | <5 |
| 2 | 7200 | 75 | 11 |
| 5 | 18000 | 75 | 19 |
| 25 | 90000 | 75 | 38 |
| 100 | 360000 | 75 | 55 |
| +48 | >172800 | 105 | >95 [a] |

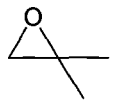

2-2

| time, hr | time, secs | temp., °C | Conversion % |
|---|---|---|---|
| 0 | 0 | 75 | 0 |
| 0.5 | 1800 | 75 | <5 |
| 2 | 7200 | 75 | 13 |
| 5 | 18000 | 75 | 21 |
| 25 | 90000 | 75 | 54 |
| 100 | 360000 | 75 | 82 |
| +48 | >172800 | 105 | >95 [a] |

2-3

| time, hr | time, secs | temp., °C | Conversion % |
|---|---|---|---|
| 0 | 0 | 75 | 0 |
| 0.5 | 1800 | 75 | <5 |
| 2 | 7200 | 75 | <5 |
| 5 | 18000 | 75 | <5 |
| 25 | 90000 | 75 | 23 |
| 100 | 360000 | 75 | 26 |
| >48 | >172800 | 105 | >95 [a] |

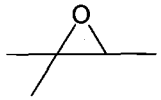

2-4

| time, hr | time, secs | temp., °C | Conversion % |
|---|---|---|---|
| 0 | 0 | 75 | 0 |
| 0.5 | 1800 | 75 | <5 |
| 2 | 7200 | 75 | <5 |
| 5 | 18000 | 75 | <5 |
| 25 | 90000 | 75 | 10 |
| 100 | 360000 | 75 | 16 |
| >48 | >172800 | 105 | >95[a] |

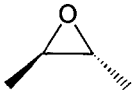

2-5

| time, hr | time, secs | temp., °C | Conversion % |
|---|---|---|---|
| 0 | 0 | 75 | 0 |
| 0.5 | 1800 | 75 | <5 |
| 2 | 7200 | 75 | <5 |
| 5 | 18000 | 75 | <5 |
| 25 | 90000 | 75 | <5 |
| 100 | 360000 | 75 | <5 |
| 220 | 792000 | 75 | <5 |
| 340 | 1224000 | 75 | 14 |
| >48 | >172800 | 105 | >95 [a] |

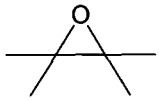

2-6

| time, hr | time, secs | temp., °C | Conversion % |
|---|---|---|---|
| 0 | 0 | 75 | 0 |
| 0.5 | 1800 | 75 | <5 |
| 2 | 7200 | 75 | <5 |
| 5 | 18000 | 75 | <5 |
| 25 | 90000 | 75 | <5 |
| 100 | 360000 | 75 | <5 |
| 220 | 792000 | 75 | <5 |
| 340 | 1224000 | 75 | <5 |

Incompatible

Table 2.1 Continued

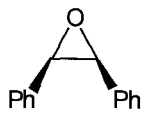


2-7

| time, hr | time, secs | temp., °C | Conversion % |
|---|---|---|---|
| 0 | 0 | 75 | 0 |
| 0.5 | 1800 | 75 | 20 |
| 2 | 7200 | 75 | 23 |
| 5 | 18000 | 75 | 35 |
| 25 | 90000 | 75 | 87 |
| 100 | 360000 | 75 | >95 |

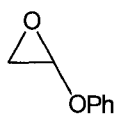


2-8

| time, hr | time, secs | temp., °C | Conversion % |
|---|---|---|---|
| 0 | 0 | 75 | 0 |
| 0.5 | 1800 | 75 | <5 |
| 2 | 7200 | 75 | <5 |
| 5 | 18000 | 75 | <5 |
| 25 | 90000 | 75 | 16 |
| 100 | 360000 | 75 | 33 |
| +48 | >172800 | 105 | >95[a] |

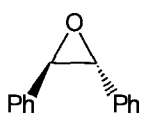


2-9

| time, hr | time, secs | temp., °C | Conversion % |
|---|---|---|---|
| 0 | 0 | 75 | 0 |
| 0.5 | 1800 | 75 | 6 |
| 2 | 7200 | 75 | --- |
| 5 | 18000 | 75 | 9 |
| 25 | 90000 | 75 | 10 |
| 100 | 360000 | 75 | 14 |
| +48 | >172800 | 105 | >95[a] |

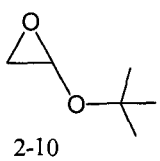


2-10

| time, hr | time, secs | temp., °C | Conversion % |
|---|---|---|---|
| 0 | 0 | 75 | 0 |
| 0.5 | 1800 | 75 | <5 |
| 2 | 7200 | 75 | <5 |
| 5 | 18000 | 75 | <5 |
| 25 | 90000 | 75 | 15 |
| 100 | 360000 | 75 | 38 |
| +48 | >172800 | 105 | >95[a] |

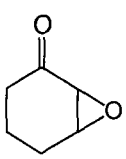


2-11

| time, hr | time, secs | temp., °C | Conversion % |
|---|---|---|---|
| 0 | 0 | 75 | 0 |
| 0.5 | 1800 | 75 | 8 |
| 2 | 7200 | 75 | 32 |
| 5 | 18000 | 75 | 61 |
| 25 | 90000 | 75 | >95 |

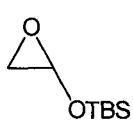


2-12

| time, hr | time, secs | temp., °C | Conversion % |
|---|---|---|---|
| 0 | 0 | 75 | 0 |
| 0.5 | 1800 | 75 | <5 |
| 2 | 7200 | 75 | <5 |
| 5 | 18000 | 75 | <5 |
| 25 | 90000 | 75 | 16 |
| 100 | 360000 | 75 | 39 |
| +48 | >172800 | 105 | >95[a] |

Table 2.1 Continued

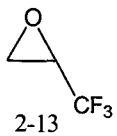

2-13

| time, hr | time, secs | temp., °C | Conversion % |
|---|---|---|---|
| 0 | 0 | 75 | 0 |
| 0.5 | 1800 | 75 | <5 |
| 2 | 7200 | 75 | <5 |
| 5 | 18000 | 75 | 5 |
| 25 | 90000 | 75 | 25 |
| 100 | 360000 | 75 | 63 |
| +48 | >172800 | 105 | >95[a] |

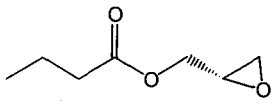

2-14

| time, hr | time, secs | temp., °C | Conversion % |
|---|---|---|---|
| 0 | 0 | 75 | 0 |
| 0.5 | 1800 | 75 | <5 |
| 2 | 7200 | 75 | <5 |
| 5 | 18000 | 75 | <5 |
| 25 | 90000 | 75 | 16 |
| 100 | 360000 | 75 | 39 |
| +48 | >172800 | 105 | >95[a] |

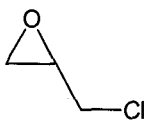

2-15

| time, hr | time, secs | temp., °C | Conversion % |
|---|---|---|---|
| 0 | 0 | 75 | 0 |
| 0.5 | 1800 | 75 | <5 |
| 2 | 7200 | 75 | <5 |
| 5 | 18000 | 75 | <5 |
| 25 | 90000 | 75 | 13 |
| 100 | 360000 | 75 | 29 |
| +48 | >172800 | 105 | >95[a] |

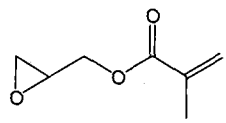

2-16

| time, hr | time, secs | temp., °C | Conversion % |
|---|---|---|---|
| 0 | 0 | 75 | 0 |
| 0.5 | 1800 | 75 | <5 |
| 2 | 7200 | 75 | <5 |
| 5 | 18000 | 75 | <5 |
| 25 | 90000 | 75 | 13 |
| 100 | 360000 | 75 | 30 |
| +48 | >172800 | 105 | >95[a] |

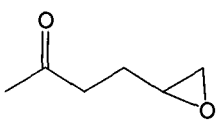

2-17

| time, hr | time, secs | temp., °C | Conversion % |
|---|---|---|---|
| 0 | 0 | 75 | 0 |
| 0.5 | 1800 | 75 | <5 |
| 2 | 7200 | 75 | <5 |
| 5 | 18000 | 75 | <5 |
| 25 | 90000 | 75 | <5 |
| 100 | 360000 | 75 | 6 |
| 196 | 705600 | 75 | 12 |
| 223 | 802800 | 75 | 15 |
| +48 | >172800 | 105 | >95[a] |

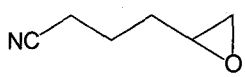

2-18

| time, hr | time, secs | temp., °C | Conversion % |
|---|---|---|---|
| 0 | 0 | 75 | 0 |
| 0.5 | 1800 | 75 | <5 |
| 2 | 7200 | 75 | <5 |
| 5 | 18000 | 75 | <5 |
| 25 | 90000 | 75 | <5 |
| 100 | 360000 | 75 | 18 |
| +48 | >172800 | 105 | >95[a] |

Table 2.1 Continued

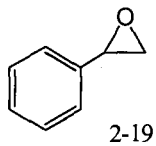

2-19

| time, hr | time, secs | temp., °C | Conversion % |
|---|---|---|---|
| 0 | 0 | 75 | 0 |
| 3 | 10800 | 75 | 29 |
| 28 | 100800 | 75 | 32 |
| 122 | 439200 | 75 | 41 |
| 579 | 2084400 | 75 | 73 |

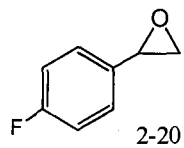

2-20

| time, hr | time, secs | temp., °C | Conversion % |
|---|---|---|---|
| 0 | 0 | 75 | 0 |
| 3 | 10800 | 75 | 39 |
| 22 | 79200 | 75 | 42 |
| 107 | 360000 | 75 | 52 |
| 654 | 2354400 | 75 | >95 |

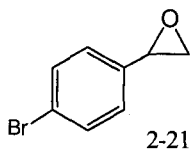

2-21

| time, hr | time, secs | temp., °C | Conversion % |
|---|---|---|---|
| 0 | 0 | 75 | 0 |
| 1.5 | 5400 | 75 | 33 |
| 23.5 | 84600 | 75 | 36 |
| 121.5 | 437400 | 75 | 49 |
| 586 | 2109600 | 75 | >95 |

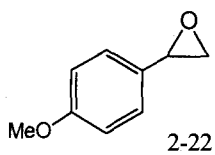

2-22

| time, hr | time, secs | temp., °C | Conversion % |
|---|---|---|---|
| 0 | 0 | 75 | 0 |
| 3.5 | 12600 | 75 | 29 |
| 31.5 | 113400 | 75 | 39 |
| 124.5 | 448200 | 75 | 55 |

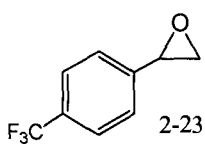

2-23

| time, hr | time, secs | temp., °C | Conversion % |
|---|---|---|---|
| 0 | 0 | 75 | 0 |
| 2.5 | 9000 | 75 | 39 |
| 21 | 75600 | 75 | 48 |
| 112.5 | 405000 | 75 | 67 |
| 303 | 1090800 | 75 | >95 |

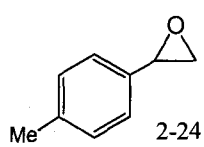

2-24

| time, hr | time, secs | temp., °C | Conversion % |
|---|---|---|---|
| 0 | 0 | 75 | 0 |
| 3.5 | 12600 | 75 | 30 |
| 31.5 | 113400 | 75 | 38 |
| 124.5 | 448200 | 75 | 48 |

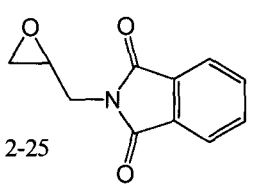

2-25

| time, hr | time, secs | temp., °C | Conversion % |
|---|---|---|---|
| 0 | 0 | 75 | 0 |
| 0.5 | 1800 | 75 | 9 |
| 2 | 7200 | 75 | 9 |
| 5 | 18000 | 75 | 11 |
| 25 | 90000 | 75 | 16 |
| 100 | 360000 | 75 | 28 |
| +48 | >172800 | 105 | >95[a] |

a = Samples were heated for at least 100 h at 75°C before being heated for at least +48 h at 105°C.

## 2.4 Functional Group Interference and Tolerance

Functional group interference was observed for some substrates. Nitro groups resulted in catalyst deactivation presumably by reoxidizing the reduced rhenium(V) species back to $Tp'ReO_3$. Hydroxyl-containing epoxides were also not tolerated, but protecting the alcohol as the *tert*-butyldimethylsilyl ether (**2-12**) resulted in efficient catalysis (see Table 2.1). Surprisingly, 2,3-dimethyl-butene oxide failed to be deoxygenated, indicating the point at which steric interactions prevent catalysis. However, a variety of functional groups were tolerated. Epoxides with pendant ethers (**2-8** and **2-10**) and silyl ethers (**2-12**) were easily deoxygenated with conversions ranging from 33-39% after 100h at 75°C. Epoxides containing esters (**2-14** and **2-16**) and halogens (**2-13** and **2-15**) resulted in excellent conversion of deoxygenated product. An increase in turnover frequency was observed for epoxides conjugated with $sp^2$ systems, such as a carbonyl or phenyl group. For example, *cis*-stilbene oxide and 7-oxabicyclo[4.1.0]heptan-2-one were the most readily deoxygenated epoxides. Even nitrile substituted epoxides (**2-18**) were readily deoxygenated. 5,6-Epoxy-2-hexanone was eventually deoxygenated, but required a longer reaction time. Possible coordination of the carbonyl oxygen to an empty coordination site on the metal could be competing with epoxide ligation and would explain the slower rate. Although free amines were not tested, because of expected formation of imido complexes, an epoxide containing the pthalimide group (**2-25**) as a protecting group was easily

deoxygenated. Substituted styrene oxides (**2-20** thru **2-24**) were all compatible and an increase in turnover frequency was observed with both electron-donating and electron-withdrawing substituents.

## 2.5 Differences between $Tp'ReO_3$ and $TkReO_3$

A comparison between tetrakis(pyrazolylborato)rhenium trioxide ($TkReO_3$) and $Tp'ReO_3$ was performed to determine the advantage of using the Tp' ligand (Table 2.2). Catalytic turnover was seen for reactions catalyzed by $TkReO_3$, but the rate is much slower compared to $Tp'ReO_3$ catalyzed reactions. For instance, the deoxygenation of *cis*-stilbene oxide at 105°C was complete (>95%) in 1.5 hrs for $Tp'ReO_3$, while $TkReO_3$ had only deoxygenated 50% after 73 hrs. The low reactivity of $TkReO_3$ is attributed to formation of dimeric $[ReO(\mu\text{-}O)\{B(pz)_4\}]_2$ from the dioxorhenium(V) intermediate (See scheme 2.4).[80b] Fragmentation of the dimer to the reactive dioxorhenium(V) intermediate ($LReO_2$) was shown for $[(Cp^*ReO)_2(\mu\text{-}O)_2]$ to be necessary for O atom transfer.[56] Since the steric bulk measured by cone angle is smaller for the Tk ligand, the dimeric form would be expected to be more stable than the dimeric form of the Tp' derivative. A decrease in rate was expected for $TkReO_3$ since the reactive species ($LReO_2$) is removed from solution because of dimerization. In addition, some trans/cis isomerization of trans-stilbene oxide was observed using the $TkReO_3$ catalyst. Whether a cationic

or radical mechanism or even some adventitious acidic impurities might be responsible for the isomerization was not determined.

Table 2.2 Reaction of epoxides with catalytic $LReO_3/PPh_3$ (L = Tp', Tk).

| Epoxide | Catalyst | Time, hr | Temp.,°C | Alkene Yield, % |
|---|---|---|---|---|
| 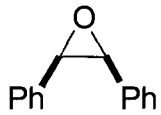 | Tp' | 1.5 | 105 | >95 |
| | Tk | 73 | 105 | 46 |
| 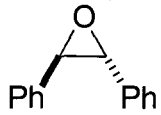 | Tp' | 1.5 | 105 | 18 |
| | Tk | 105 | 105 | tr |
| 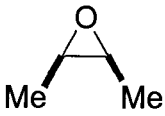 | Tp' | 1.5 | 105 | 63 |
| | Tk | 120 | 105 | tr |
| 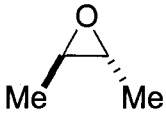 | Tp' | 1.5 | 105 | 12 |
| | Tk | 120 | 105 | 0 |

## 2.6 Preparative Scale

The reaction can easily be run on a preparative scale. 75.0 mg of $Tp'ReO_3$ (0.14 mmol), 884 mg of $PPh_3$ (3.37 mmol) and a magnetic stir bar were added to a 250 mL glass bomb. 30 mL of dry benzene was then vacuum transferred into the bomb, followed by the syringe addition of 0.62 mL of 1,2-epoxydodecane (2.82

mmol). The mixture was stirred under vacuum and heated to 85°C for 86 h. An aliquot was then analyzed by NMR to ensure no epoxide remained. Column chromatography on silica gel gave 447 mg of 1-dodecene (2.7 mmol, 94%). Distillation can also be used for to purify the alkene instead of chromatography though on a 5 mmol scale holdup in the short path apparatus led to a decreased yield (2.6 mmol, 64%). The simple preparative procedure demonstrates the synthetic utility of using $Tp'ReO_3$ to deoxygenate epoxides.

## 2.7 ($Tp'ReO(OH)_2$) versus ($Tp'ReO_2 \cdot H_2O$)

The sterically bulkier Tp' ligand was predicted to suppress formation of the dimeric bridged oxo compound $[LReO]_2(\mu\text{-}O)_2$ that resulted from reduction of $LReO_3$ with triphenylphosphine when L = Cp*, Tp or Tk. Reduction of $Tp'ReO_3$ with triphenylphosphine or triethylphosphite in THF at room temperature resulted in the formation of a green solution over 2-3 days. At elevated temperatures the reduction of $Tp'ReO_3$ is extremely facile and the disappearance of insoluble $Tp'ReO_3$ is complete in a couple of hours. Following the reaction in a sealed NMR tube, the formation of $Ph_3P{=}O$ was apparent along with the formation of a $C_s$ symmetrical rhenium species. Purification of this $C_s$ rhenium species was achieved by two methods: (1) column chromatography on silica gel using nitrogen purged 1% acetone in dichloromethane; and (2) using polymer supported $PPh_3$ followed by filtration and precipitation of the product using hexanes under $N_2$ or Ar. Both

procedures led to the isolation of an air sensitive baby blue powder. The $^1$H NMR spectrum matched the signals previously observed in the crude mixture. Initially, we believed we had isolated the monomer, Tp'$ReO_2$, which would also exhibit $C_s$ symmetry. However, closer examination of the $^1$H NMR showed, in addition to the signals corresponding to the Tp' ligand, a 2-H singlet at 12.8ppm (Figure 2.2). This signal disappeared upon exchange with $D_2O$. Furthermore, the addition of < 0.5 equivalents of $D_2O$ resulted in a second signal 15Hz upfield. In the IR spectrum, a strong oxo stretch at 966 $cm^{-1}$ (compared to 908 $cm^{-1}$ for Tp'$ReO_3$) and a broad O-H stretch at 3335 $cm^{-1}$ was observed. The increase in frequency for the oxo stretch demonstrates how competition of the oxo groups to $\pi$ bond into the empty *d* orbitals weakens each of the Re=O bonds. Removal of an oxo group reduces competition and increases the Re=O bond strength. The oxo stretch for the deuterated species resulting from complete exchange with $D_2O$ is shifted to a higher frequency at 970 $cm^{-1}$. The substitution of deuterium should increase the frequency of the oxo stretch since deuterium will be less likely to H-bond therefore strengthening the rhenium-oxo bond. The FAB mass spectrum shows a major peak at m/z = 516 and a smaller but possibly significant peak at m/z = 533. The weak peak at m/z = 533 (Tp'$^{187}ReO_2$ + $H_2O$) is believed to be the molecular ion peak, while the major peak at m/z = 516 (Tp'$ReO_2$) results from loss of water.

Figure 2.2 $^{1}H$ NMR spectrum in $CD_2Cl_2$ of ($Tp'ReO(OH)_2$) or ($Tp'ReO_2 \bullet H_2O$).

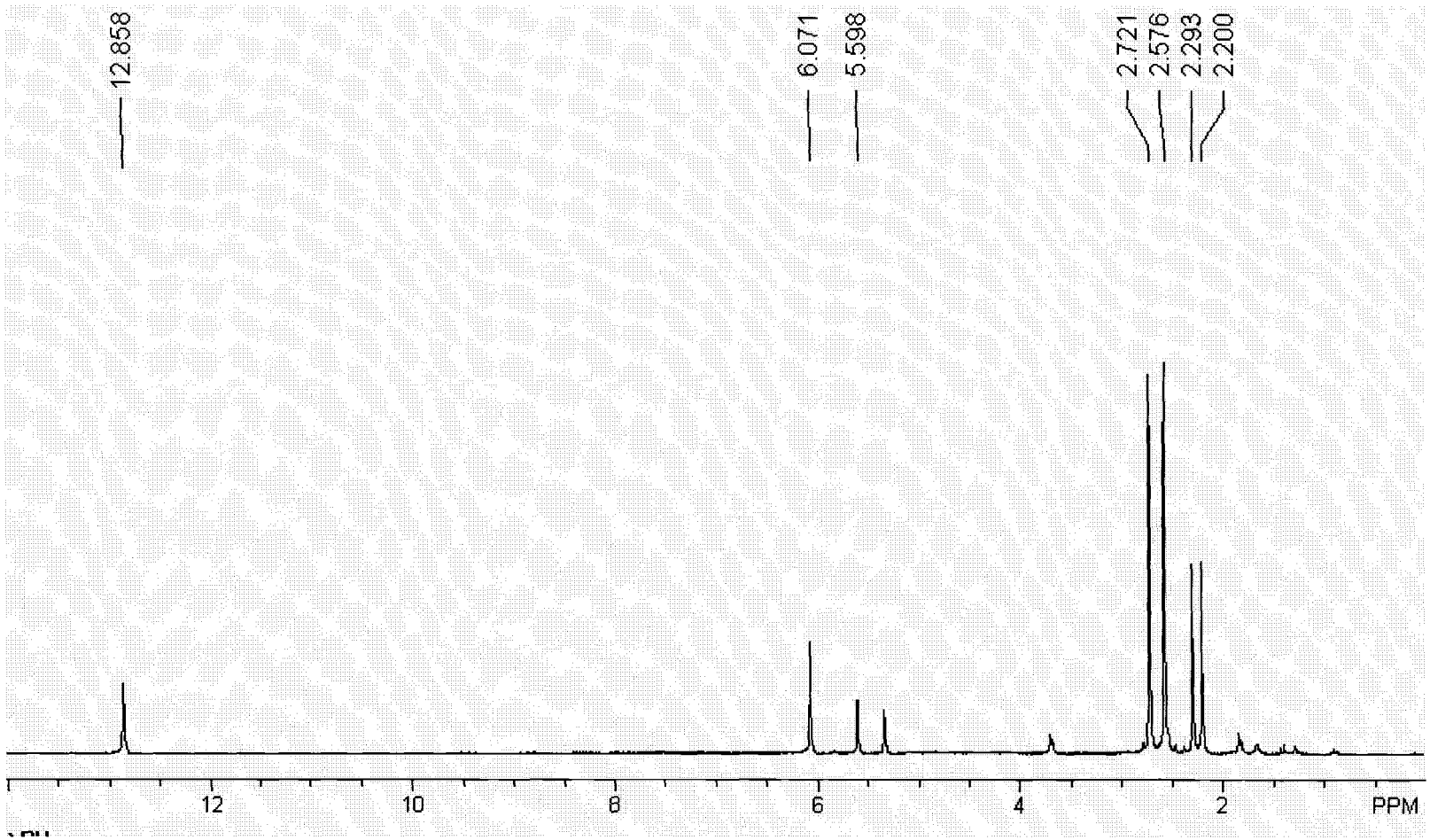

These results led us to propose the compound was either an oxo bis-hydroxide ($Tp'ReO(OH)_2$) or the hydrate of the monomeric dioxo complex ($Tp'ReO_2 \cdot H_2O$) (Figure 2.3). Both isomers would be consistent with the spectroscopic data presented. However, the magnitude of the 15Hz upfield shift that resulted after the addition of < 0.5 equivalents of $D_2O$ was originally believed to be evidence supporting the hydrate structure. The rationale comes from the fact that only two bonds separate hydrogen and deuterium in the hydrate complex compared to four bonds in the oxo bis-hydroxide complex. Therefore, the large value observed would be more consistent with the hydrate structure. However, if H-bonding occurred between one hydroxyl hydrogen to the second hydroxyl group containing the deuteride then a 15 Hz shift can be rationalized for the oxo bis-hydroxide complex (See below for evidence of H-bonding). Further experiments that were performed but resulted in inconclusive results include cooling the sample to -83°C and heating the sample to 50°C. If the compound were the hydrate then cooling the sample would slow down, at least on the NMR time scale, the rapid interconversion of H-bonding occurring between the two terminal oxo groups and the hydrogens found on the coordinated water molecule. Conversely, if the compound were the oxo bis-hydroxide complex, then collapse of symmetry from $C_s$ to $C_{3V}$ would be expected upon heating since proton exchange should be rapid at elevated temperatures. Unfortunately, no dynamic behavior (coalescence of signals) was observed upon heating or cooling the compound. Even though H-D exchange is rapid, as evident by the immediate disappearance of the signal at 12.8

ppm following the addition of $D_2O$, the compound is also not acidic indicating substantial H-bonding within the complex. For example, addition of bases such as pyridine and *N,N,N',N'*-tetramethyl-1,8-naphthalenediamine had no effect on the $^1H$ NMR spectra.

The source of the water that adds to $Tp'ReO_2$ has remained elusive; all reagents and solvents were rigorously dried before use. One possible source could be $Tp'ReO_3$ which requires a water rinse to remove ionic by-products formed during its synthesis (see Scheme 2.6). Retention of water by $Tp'ReO_3$ is quite possible; efforts to removal the water of hydration by heating $Tp'ReO_3$ to > 150°C overnight under vacuum (0.01 mbar) did not prevent the formation of either the hydrate or oxo bis-hydroxide. Attempts to physically (azeotropic distillation) or chemically (N,N'-diisopropyldicarbodimide, $CaH_2$) dehydrate the hydrate or oxo bis-hydroxide led to decomposition.

There is however evidence in favor of the oxo bis-hydroxide complex. The following evidence supports the rhenium(V) compound to be $Tp'Re(O)(OH)_2$: (1) A similarity between the visible spectrum ($\lambda_{max}$ = 606 nm) of the rhenium(V) compound to other $Tp'Re(O)(alkoxide)_2$ compounds exists. (2) Hydrolysis of the oxodichloride $Tp'Re(O)Cl_2$ with $H_2O$ and triethylamine to form $Tp'Re(O)(OH)_2$ is analogous to bisalkoxide $LRe(O)(OR)_2$ formation from alcohols and triethylamine. (3) Computational modeling predicts the oxo bis-hydroxide is 13 kcal/mol more stable then the hydrate.[85] (4) The chemical behavior of the rhenium(V) compound towards ethanol and chlorinated solvents.

An independent synthesis of the rhenium(V) compound was performed starting from $Tp'ReO_3$ (Scheme 2.8). Treatment of the trixoxo complex with ethylene glycol and triphenylphosphine under acidic conditions yielded the ethane diolate $Tp'Re(O)(OCH_2CH_2O)$. The rhenium(V) diolate was then cleaved using HCl and triethylamine giving the oxodichloride $Tp'Re(O)Cl_2$. Refluxing $(HBpz_3)Re(O)Cl_2$ with an alcohol and triethylamine in acetonitrile had already been shown to replace the chlorides with alkoxide ligands, giving bisalkoxide complexes $(HBpz_3)Re(O)(OR)_2$ (R = Me, Et, $^{i}Pr$, $^{n}Bu$, $CH_2Ph$).[88] The replacement of water for the alcohol resulted in a compound identical to that formed by phosphine reduction of $Tp'ReO_3$. One might predict based on the reactivity of alcohols and the products formed that reaction with water would form a compound analogous in structure. Therefore, the oxo bis-hydroxide would be the most reasonable structure.

Scheme 2.8

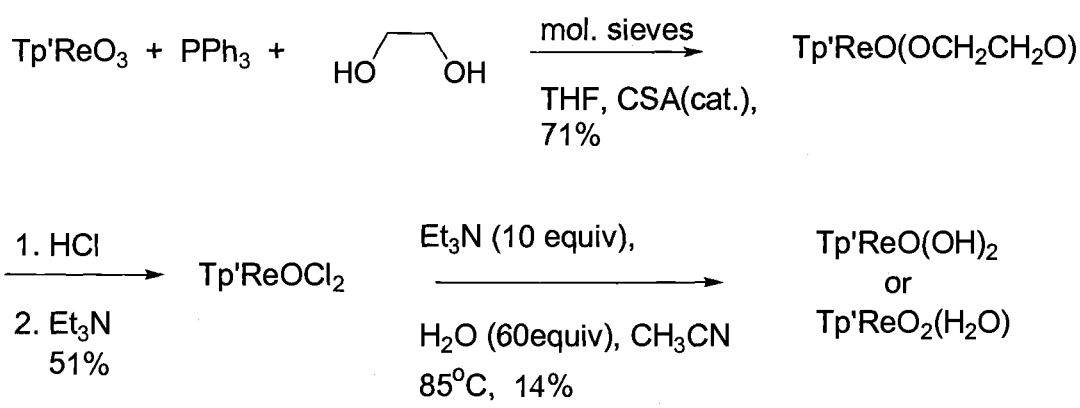

High level computational modeling of $Tp'Re(O)(OH)_2$ and $Tp'Re(O)_2(H_2O)$ were performed at the B3LYP/LACVP** level to determine which isomer was the species generated by phosphine reduction of $Tp'ReO_3$.[85] Both compounds converged to reasonable ground state structures and were determined to be true minima on the potential energy surface by the absence of an imaginary frequency. The energies and structures calculated for $Tp'Re(O)(OH)_2$ and $Tp'Re(O)_2(H_2O)$ are in Figure 2.3 along with the dioxo complex $Tp'ReO_2$. A comparison between the nonmethylated Tp ligand and the Tp' ligand was made to determine if the methyls had an electronic or steric impact on the relative energies of the two compounds. Structurally the two compounds were similar when comparing Tp versus Tp' and only small differences in energies were observed. Overall, the oxo bis-hydroxide is lower in energy by 13 kcal/mol (14.5 kcal/mol after zero point energy corrections) than the hydrate for the Tp' containing complexes. Both structures contain some H-bonding to either the terminal oxo ligands in the hydrate or to the second hydroxyl group in the oxo bis-hydroxide. As previously mentioned, H-bonding of one hydroxyl group to the other hydroxyl oxygen can account for the large 15 Hz isotopic NMR shift if the rhenium(V) compound is the oxo bis-hydroxide.

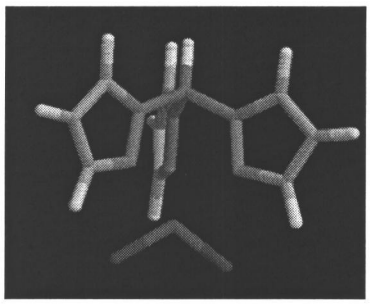

E (L = Tp): -932.0253 H

E (L = Tp'): -1167.9573 H

E H2O: -76.4197 H

Erel = 0 (Tp and Tp')

E (L = Tp): -1008.4781 H

E (L = Tp'): -1244.4151 H

Erel: -20.8 (-23.0)* kcal/mol (Tp)
-23.9 (-19.2)* kcal/mol (Tp')

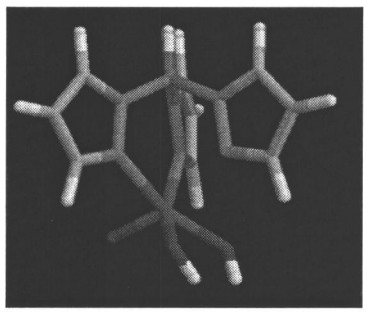

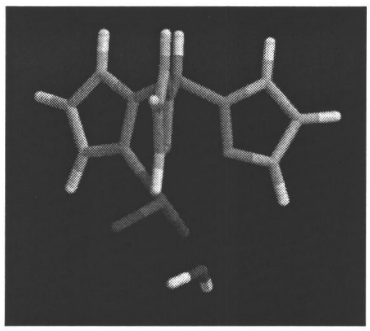

E (L = Tp): -1008.4561 H

E (L = Tp'): -1244.3929 H

Erel: -6.9 (-20.0)* kcal/mol (Tp)
-10.0 (-4.7)* kcal/mol (Tp')

Figure 2.3 Optimized structures and energies of Tp'$ReO_2$, Tp'Re(O)$(OH)_2$ and Tp'$ReO_2(H_2O)$.

The final piece of evidence supporting the oxo bis-hydroxide is the chemical reactivity of the complex in different solvents. The reduction of Tp'$ReO_3$ with phosphines in chlorinated solvents yielded Tp'Re(O)(OH)Cl.[89] Tp'Re(O)(OH)Cl is a known compound and is readily identified in the $^1$H NMR spectrum by its $C_1$-symmetry and by a deuterium-exchangeable signal at 16.53 ppm attributed to the hydroxyl hydrogen (Scheme 2.9). The IR spectrum shows a weak

O-H absorption at 3448 $cm^{-1}$, a B-H stretch at 2546 $cm^{-1}$ and a characteristic Re=O band at 971 $cm^{-1}$. The exact form of the chloride source is still unknown but may be HCl resulting from photodecomposition of the chlorinated solvent. The deliberate addition of HCl during the reduction of the trioxo complex in THF led to exclusive formation of the hydroxo chloride complex in 71% yield. NMR samples containing the oxo bis-hydroxide complex in chlorinated solvents were also slowly converted to the hydoxo chloride complex over time. Hydroxylic solvents, such as ethanol and methanol, resulted in hydroxo alkoxide complexes Tp'Re(O)(OH)(OR) (R = Me, Et) after chromatography (Scheme 2.9). Both were identified by $^{1}H$ NMR but Tp'ReO(OH)(OEt) was further characterized by IR, mass spectroscopy and $^{13}C$ NMR. The $^{1}H$ NMR spectrum of Tp'ReO(OH)(OEt) exhibits a diagnostic $C_1$-symmetrical pattern for the Tp' signals as well as a diagnostic signal corresponding to the diastereotopic $CH_2$ protons of the ethoxy ligand. The FAB mass spectrum for Tp'ReO(OH)(OEt) shows a major peak at m/z = 516 ($Tp'ReO_2$) and a weak peak at m/z = 562 ($Tp'ReO_2$ + EtOH). The purification of the ethoxide complex was extremely difficult for a variety of reasons. First, Tp'ReO(OH)(OEt), similar to $Tp'Re(O)(OH)_2$, will oxidize to the trioxide on exposure to air. Second, equilibrium amounts of $Tp'Re(O)(OH)_2$ always form if any adventitious water is present. For example, small amounts of oxo bis-hydroxide would always coelute with the ethoxide complex during chromatography. Third, a large excess of ethanol would result in the formation of the bis-ethoxide complex[80b] which would coelute with the ethoxide complex. Overall, formation of the ethoxide complex

and hydroxyl chloride complex are more consistent with the oxo bis-hydroxide structure than with the hydrate. Relatively few examples of hydrated rhenium oxo complexes are known,[90] compared to the large number of reported alkoxide and hydroxo rhenium complexes.[45,88-89,91]

Scheme 2.9

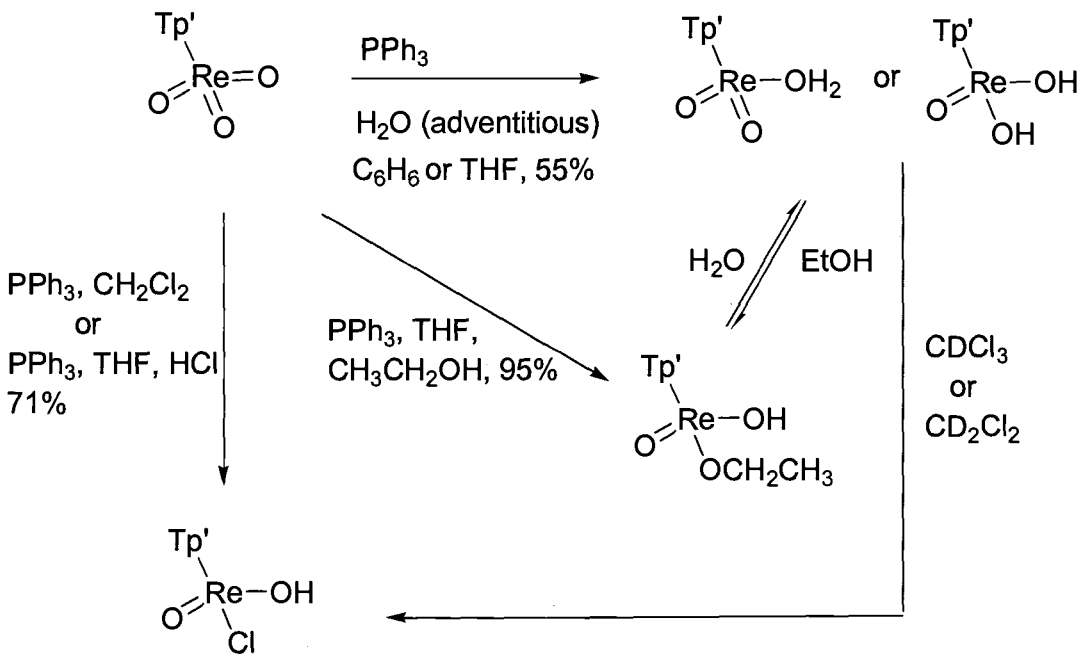


Tp'Re(O)(OH)$_2$ and Tp'ReO(OH)(OEt) were both equally effective catalysts for epoxide deoxygenation. The pseudo-zero order rate constants for *cis*-stilbene oxide deoxygenation at 75°C were $k_{obs}$ = 1.45 x $10^{-6}$ M/s for Tp'Re(O)(OH)$_2$ and $k_{obs}$ = 1.26 x $10^{-6}$ M/s for Tp'ReO(OH)(OEt) (Figure 2.4). Both catalysts were shown to deoxygenate *cis*-stilbene oxide to > 95% conversion in less than 35hrs at

75°C. Tp'Re(O)(OH)Cl was a poor catalyst for deoxygenation of epoxides; only 14% conversion of *cis*-stilbene oxide to *cis*-stilbene was observed after 45 hrs at 75°C. These results confirm that loss of water, ethanol or HCl to form the reactive dioxo $Tp'ReO_2$ is a necessary preequilibrium process for O atom transfer (Scheme 2.10). Consistent with loss of water being a necessary preequilibrium process was that water was determined to inhibit catalytic turnover. The deliberate addition of 10 μL of $H_2O$ decreased the turnover frequency by almost half.

Scheme 2.10

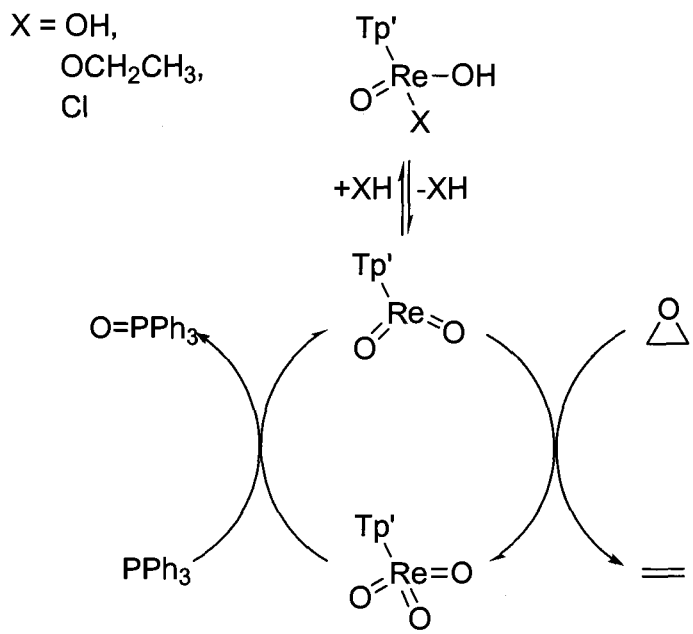

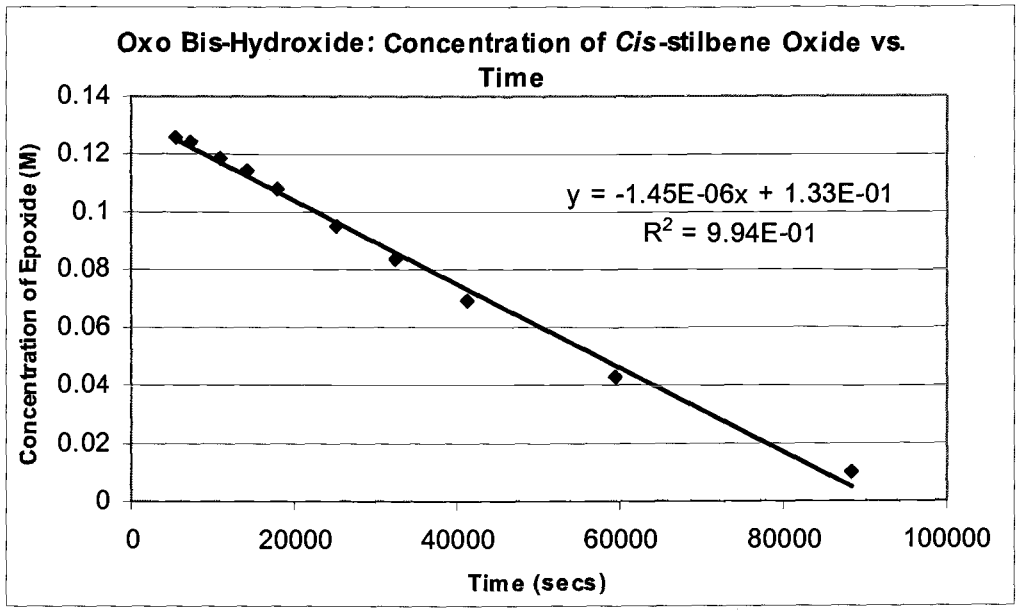


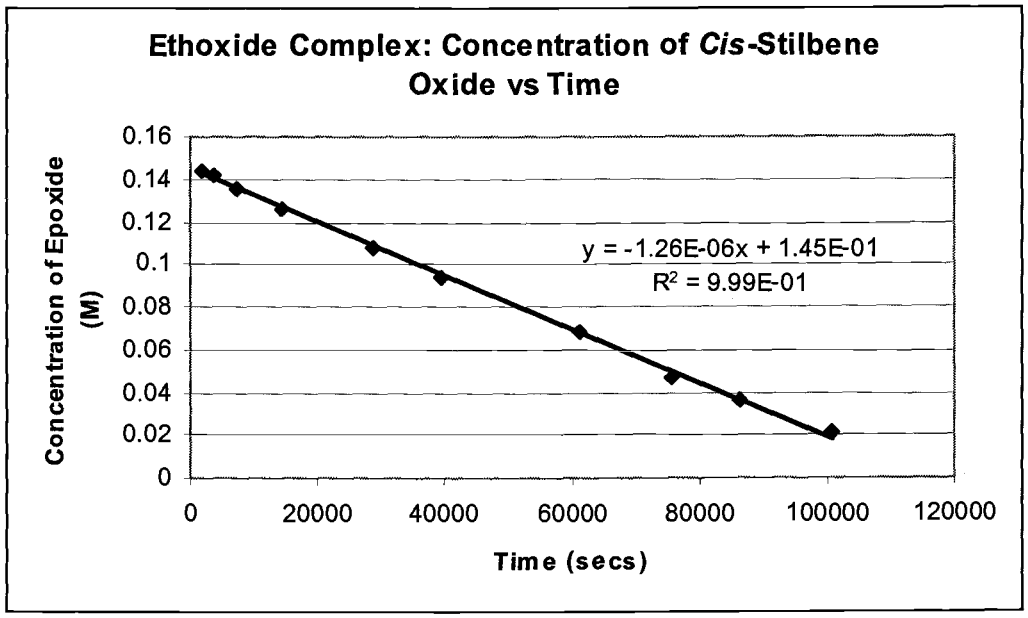


Figure 2.4 Concentration of epoxide versus time plots for Tp'Re(O)$(OH)_2$ and Tp'Re(O)(OH)(OEt).

## 2.8 Stoichiometric Deoxygenations

The chemical reactivity of the oxo bis-hydroxide complex is very similar to $[(L^*ReO)_2(\mu\text{-}O)_2]$ (L = $Cp^*$, Tp, Tk) .[55,56,80b] Besides catalytically deoxygenating epoxides, it also deoxygenates sulfoxides and reacts with vicinal diols to form diolate complexes (Scheme 2.11). The oxo bis-hydroxide complex is also effective at stoichiometric deoxygenations of epoxides. Similar to the catalytic reactions involving in-situ reduction of $Tp'ReO_3$, the stoichiometric reactions resulted in stereospecific formation of alkenes. Stoichiometric reactions were run at 105°C in $d_3$-acetonitrile sealed in a NMR tube under vacuum. *Cis*-alkenes form faster than *trans*-alkenes and aryl groups enhance the reactions compared to alkyl groups. The relative order of reactivity is *cis*-stilbene oxide > *trans*-stilbene oxide > styrene oxide > *cis*-butene oxide > *trans*-butene oxide. Oddly enough, the placement of *cis*-butene oxide and *trans*-stilbene oxide have switched compared to the catalytic process. The reaction is difficult to push to completion because a build up of water, which is a by-product of the stoichiometric reaction, drives the equilibrium towards the oxo bis-hydroxide rather than the reactive dioxo complex. Once again, hydroxyl and nitro containing epoxides interfered with catalysis.

Scheme 2.11

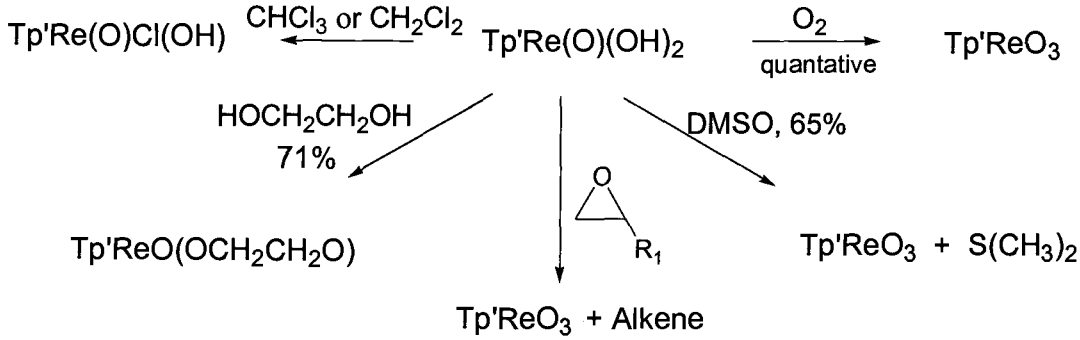


## 2.9 Conclusions

In situ reduction of $Tp'ReO_3$ with triphenylphosphine or triethylphosphite leads to a reactive rhenium(V) species that catalytically deoxygenates epoxides at 75-105°C. The reaction is stereospecific, except for *trans*- and *cis*-butene oxide which formed minor amounts of the opposite isomer. A variety of different functional groups were tolerated and epoxides that reacted slowly could be pushed to greater than 95% conversion. The reaction can also be run effectively on a preparative scale indicating the synthetic utility of the reaction. Furthermore, the absence of clustering processes shows how simple changes in the choice of ligand can have a major influence on the design of the catalytic cycle. Changing the ligand also suppressed formation of dimeric $[LReO]_2(\mu\text{-}O)_2$ which is generated during the reduction of $LReO_3$. Formation of the dimer was shown to be a detriment to catalysis by comparing reactions catalyzed by $TkReO_3$ and $Tp'ReO_3$.

The rhenium(V) species formed from reduction of $Tp'ReO_3$ was identified as $Tp'Re(O)(OH)_2$. $Tp'Re(O)(OH)_2$ reacted with ethanol and HCl to form ethoxide and hydroxo chloride complexes. In addition, $Tp'Re(O)(OH)_2$ was an excellent catalytic and stoichiometric reagent for the deoxygenation of epoxides and sulfoxides. Loss of water from $Tp'Re(O)(OH)_2$ to form the catalytically active species $Tp'ReO_2$ was shown to be a necessary preequilibrium process. Chapter 3 will explore the kinetics and mechanism of this catalytic process.

# Ch. 3. Kinetics and Mechanism of Rhenium-Catalyzed Epoxide Deoxygenations

## 3.1 Introduction

The mechanism of oxygen-atom transfer from high-valent oxo metal complexes to organic substrates and its microscopic reverse, the formation of oxo metal complexes from deoxygenation of organic substrates is a very active topic and continues to be debated.[45-50,52] The mechanism of olefin epoxidation and de-epoxidation is no exception to controversy.[25,71] Numerous oxo metal reagents have been used to effect epoxidations and epoxide deoxygenations and a number of mechanisms have been proposed. Numerous mechanisms have also been proposed for rhenium catalyzed deoxygenations of diols and epoxides.[21-22,39-40,56-58,85]

## 3.2 Mechanism of Mn(salen)-Catalyzed Olefin Epoxidations

In Chapter 1, the Jacobsen-Suzuki asymmetric epoxidation was introduced as an excellent example of how rational design of a catalyst can result in efficient asymmetric catalysis. Jacobsen's Mn(III) salen complex is the most efficient catalyst available for the enantioselective epoxidation of unfunctionalized alkenes.[92] Although the oxo Mn(V) salen compound has never been isolated and characterized, similar oxo species with different metal centers are known. The

difficulty with isolating the oxo Mn(V) species is a problem common to many oxidation catalysts: the rate-determining step of the catalytic cycle is formation of the oxo complex. This explains why the reactions are independent of olefin concentration.[93] A kinetic study revealed the reactions followed Michaelis-Menten kinetics; unfortunately, the kinetics can not provide any information about processes occurring after the rate-determining step. Stereospecific epoxidation was achieved with *trans*-olefins, while conjugated *cis*-olefins produced high yields of conjugated *cis*-epoxides with minor amounts of the corresponding trans isomer.[94] The observed mixture of *cis* and *trans* epoxides immediately argued against a concerted pathway (pathway A) but supported a radical pathway (pathway B) as the simplest mechanism consistent with the data.[95]

However, Katsuki et al. discovered that Mn-salen catalyzed asymmetric epoxidation of certain olefins, such as dihydronaphthalene and styrene, showed a non-linear relationship between temperature and enantioselectivity.[96] Scharf et al. had previously demonstrated that a non-linear relationship between temperature and enantioselectivity could indicate reversible formation of an intermediate that irreversibly forms product or another intermediate.[97] The manganaoxetane (pathway C) was proposed as the intermediate that was reversibly formed, which can then irreversibly undergo ring opening to a radical intermediate.

Metalloxetanes have been previously proposed as intermediates, as first proposed by Sharpless et al. for chromyl chloride oxidation of olefins,[25] to explain observations (see below) that the other mechanisms neglect. An initial reversible

step would argue against the radical process since the reverse reaction from the radical intermediate back to alkene must be extremely slow to avoid isomerization. No isomerization of the starting alkene was detected. However, a extremely slow step would disagree with the nonlinearity of the temperature versus enantioselectivity study.

Scheme 3.1

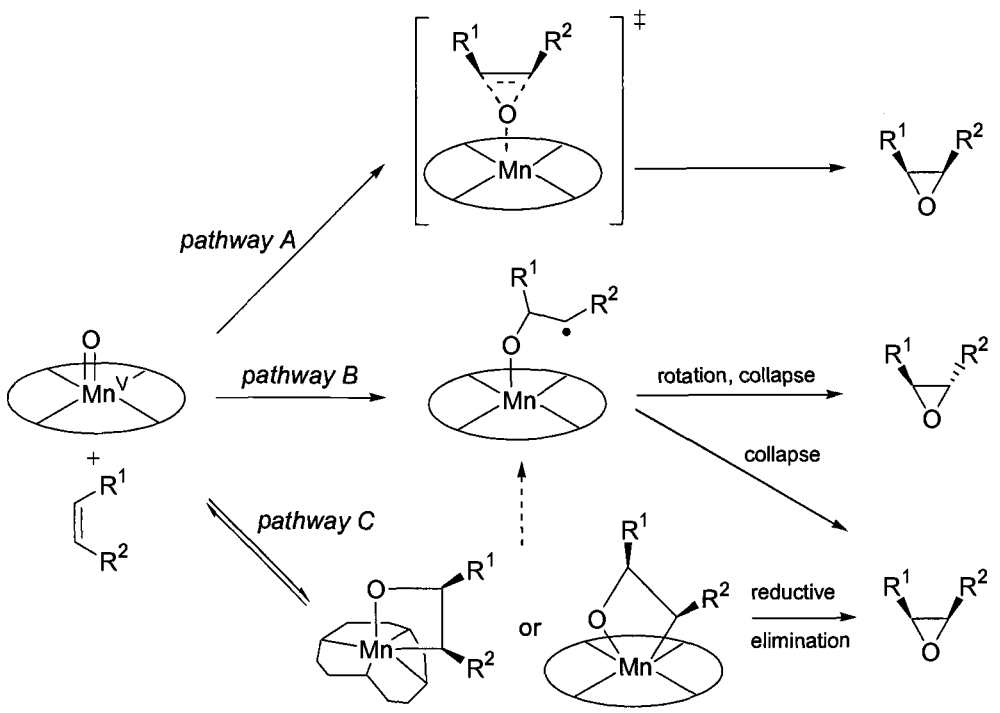


Another particular issue that the radical mechanism failed to answer was how high enantioselectivities could be obtained if the salen ligand was flat. Norrby et al. proposed a mechanism involving reversible formation a metalloxetane

followed by irreversible routes to epoxide (Scheme 3.1, pathway C).[99] Two irreversible routes were proposed to account for the observed cis/trans mixture: (1) Reductive elimination from the oxetane to yield *cis* epoxide, and (2) homolytic cleavage of the carbon-manganese bond, followed by C-C bond rotation and collapse of the intermediate to the *trans* epoxide. In order to account for the high enantioselectivities, it was proposed that puckering of the salen ligand could occur if a metalloxetane intermediate was invoked thus creating a chiral pocket. MacroModel/MM3 calculations were performed on the two diastereotopic metalloxetanes indicating the preference for formation of one diastereotopic metalloxetane over the other. The results from the calculations agreed with the experimental observations.

Additional evidence supporting the metalloxetane mechanism was obtained from phenyl cyclopropane radical probe experiments (Scheme 3.2).[99] The authors investigated the catalytic epoxidation of substituted styrenes **1a-c** to determine if any ring-opened products would form. If the mechanism proceeds through a radical intermediate then ring opened products should be observed. Conversely, if the metalloxetane forms the epoxide by reductive elimination then the cyclopropane unit will remain untouched. Both **1a** and **1b** exclusively formed **3a** and **3b** (100% yield of epoxide) without any traces of the ring-opened product. Conversely, reaction with **1c** resulted in significant amounts of cyclopropane ring opened product. The experimental data indicated that a radical pathway, whether direct (pathway B) or by homolytic cleavage of the metalloxetane, operated for *Z*

alkenes (**1c**), while the mechanism for *E* alkenes (**1b**) argued against a direct radical pathway. The metalloxetane pathway can account for isomerization of *Z* alkenes. The metalloxetane formed from the *Z* alkene can either reductively eliminate to form the *cis* epoxide or the *Z* alkene can relieve steric crowding between the two (*Z*) substituents by homolysis of the Mn-C bond. The relief of steric crowding would be much less for *E* alkenes and explains why products originating from homolytic cleavage are not observed. The direct radical pathway can not account for the survival of the radical probes observed for **1a** and **1b**.

Scheme 3.2

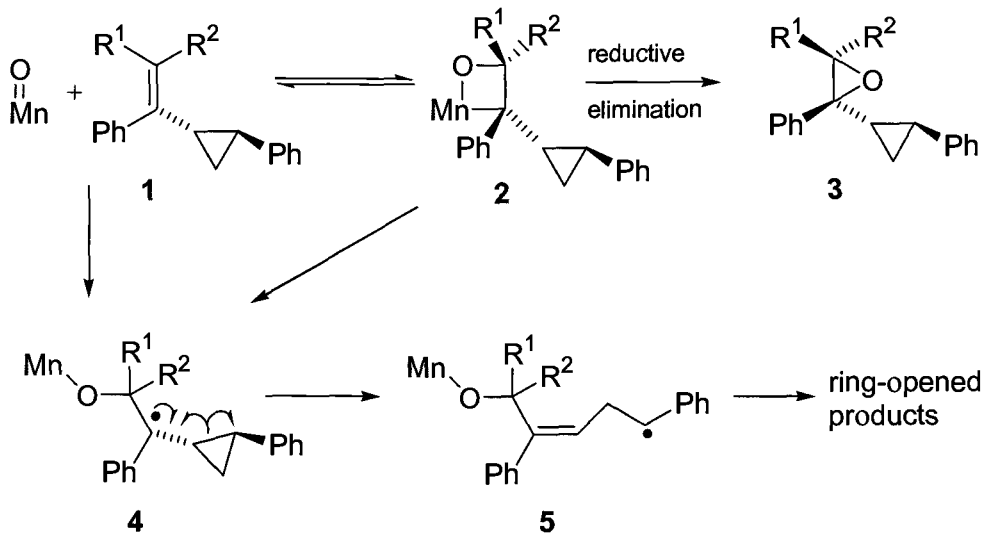


a: $R^1 = R^2 = H$; b: $R^1 = H$, $R^2 = Me$; c: $R^1 = Me$, $R^2 = H$

### 3.3 Mechanism of Chromyl Chloride Oxidation of Olefins

A series of complex mechanisms have been proposed to explain the variety of products formed from the oxidation of alkenes by chromyl chloride.[25,100] Chromyl chloride is unique compared to other transition metal oxo complexes, such as $OsO_4$ and $KMnO_4$, which form diols when reacted with olefins. Chromyl chloride oxidation of olefins generates predominately epoxides and chlorohydrins along with minor amounts of vicinal dichlorides.[100] Three different mechanisms have been proposed to explain the products formed: (1) Direct addition of olefins to one of the oxygen atoms in a single step, (2) [2+2] cycloaddition of olefin to the oxo group on chromium, and (3) [3+2] cycloaddition of olefin to two oxo groups on chromium. The mechanism was initially believed to involve direct addition of olefin to one of the oxygen atoms.[100a] However, Sharpless et al. in 1977 proposed the involvement of a chromaoxetane to account for the variety of products formed (Scheme 3.3).[25] The argument was based on the hypothesis that attack of a nucleophilic alkene should occur at the electrophilic metal center rather than on the oxygen end of the oxo group. A comparison was made to carbonyls of ketones and aldehydes, which are polarized towards oxygen and react with nucleophiles exclusively at the carbonyl carbon.

Scheme 3.3

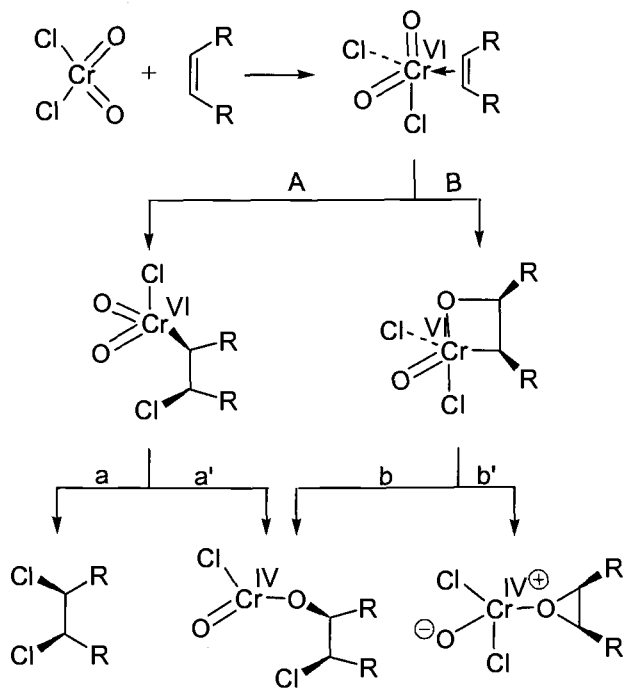


The reaction was proposed to start with pre-coordination of the nucleophilic olefin to the electron deficient Cr(VI) center to form a chromyl chloride-alkene π complex (Scheme 3.3). Competition between pathways **A** and **B** occured, which accounts for the formation of epoxide and vicinal dichloride. Both pathways could account for the formation of chlorohydrin and both occur with retention of configuration resulting in overall *cis* addition. *Cis* addition was observed experimentally. Unfortunately, the chromaoxetane was never observed or isolated. A computational study by Rappé et al. using the generalized valence bond method supported the metalloxetane mechanism.[101] Formation of the chromaoxetane was

exothermic by 14 kcal/mol, while reductive elimination of ethylene oxide was further downhill by 21 kcal/mol. Overall, the calculations predicted oxygen transfer through the chromaoxetane intermediate to be favored by 35 kcal/mol.

Even though the metalloxetane mechanism appeared to support the data, the direct addition of olefin to one of the oxo groups and [3+2] cycloaddition of olefin to two of the oxo groups could also not be excluded. The calculations by Rappe et al.[101] were eventually discredited due to limitations in methodology and because the authors were unable to optimize the structures of the different species involved. However, high level density functional theory (DFT) calculations were applied to the reaction between chromyl chloride and ethylene (Scheme 3.4).[102] The authors examined each of the three mechanisms and were able to determine the reaction energies and activation barriers for each pathway. DFT theory predicted that formation of epoxide occurred through the [3+2] addition pathway. The activation barriers for TS4 (TS = transition state) and TS5 were calculated to be 14.0 kcal/mol and 32.4 kcal/mol respectively. The activation barriers for the two-step [2+2] addition were much higher than the [3+2] process; TS1 and TS2 were calculated to be 27.1 kcal/mol and 46.9 kcal/mol. The direct addition pathway resulted in an activation barrier of 30 kcal/mol for TS3. Formation of chlorohydrins and dichlorides were also shown to proceed via a [3+2] addition rather than a [2+2] process. The driving force for this reaction is the formation of a chromium-oxo triple bond.

Scheme 3.4

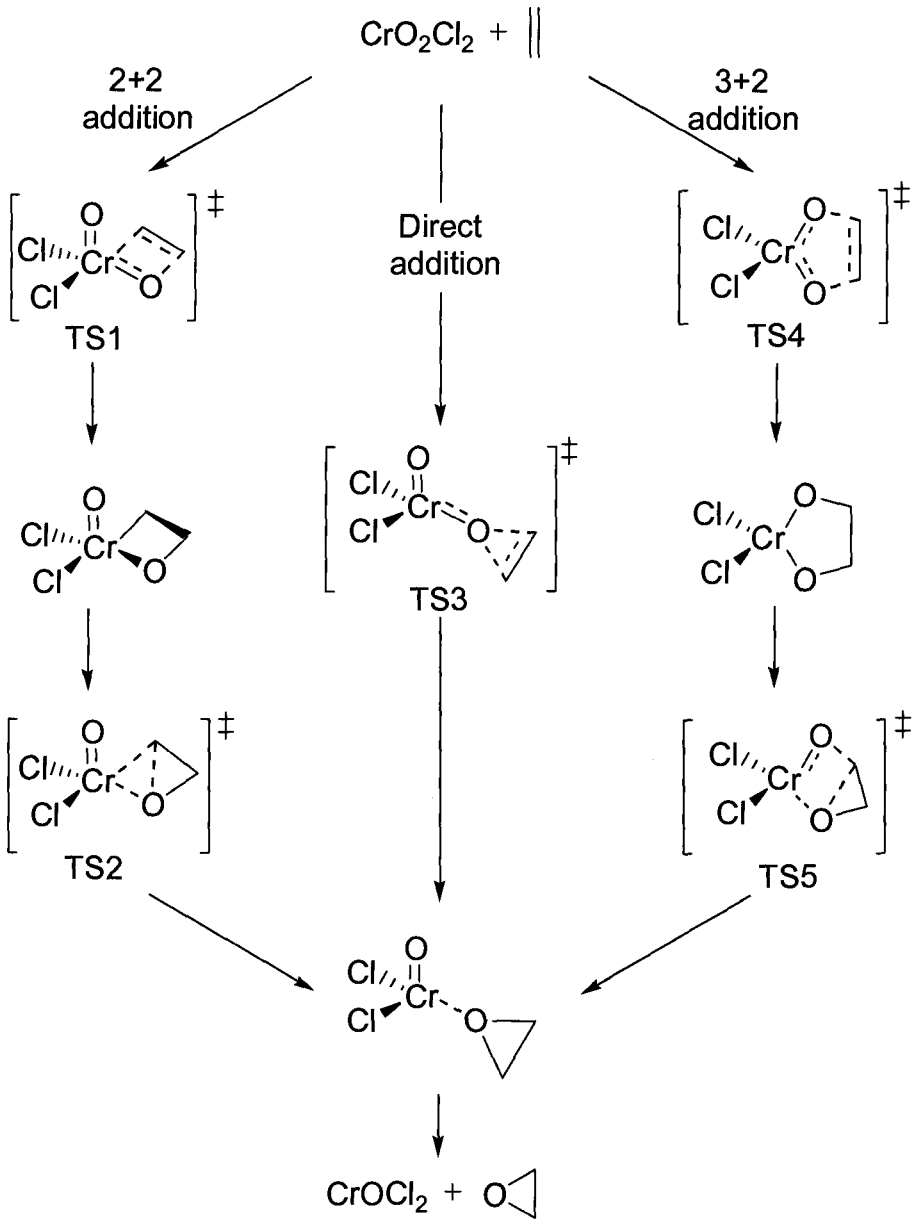
CrO2Cl2 +
2+2 addition
Direct addition
3+2 addition
TS1
TS2
TS3
TS4
TS5
CrOCl2 +

### 3.4 Mechanism of $WCl_2(PR_3)_4$ Catalyzed De-Epoxidations

Based on the principle of microscopic reversibility, the same mechanistic possibilities proposed for epoxidation would be expected for epoxide deoxygenations. $WCl_2(PMePh_2)_4$ and $WCl_2(CH_2{=}CH_2)_2(PMePh_2)_2$, which were introduced in Chapter 2 as efficient reagents for de-epoxidations, were determined to deoxygenate epoxides through a concerted mechanism.[103] Epoxides are readily deoxygenated, forming equilibrium mixtures of tungsten(IV) oxo olefin complexes. The rate was insensitive to the concentration of epoxide but was inhibited by added ethylene. Competition between the epoxide and olefin for the empty coordination site slows the rate later in the reaction as more olefin is produced. The deoxygenations were stereospecific but deoxygenation of *cis*-butene oxide resulted in minor amounts of *trans*-2-butene (9%). Surprisingly, neither the starting epoxide nor the product alkene was isomerized under the conditions employed. More substituted epoxides were deoxygenated less readily, while para-substituted styrene oxides resulted in an enhanced turnover frequency. Reaction of ethylene-$d_4$ oxide with $WCl_2(CH_2{=}CH_2)_2(PMePh_2)_2$ resulted in de-epoxidation. However, the olefin bound to $WCl_2(O)(CH_2{=}CH_2)L_2$ (L = $PMePh_2$) after the reaction is the same olefin bound to $WCl_2(CH_2{=}CH_2)_2L_2$ before the reaction. No exchange of $CD_2{=}CD_2$ for $CH_2{=}CH_2$ has occurred (Scheme 3.5).

Scheme 3.5

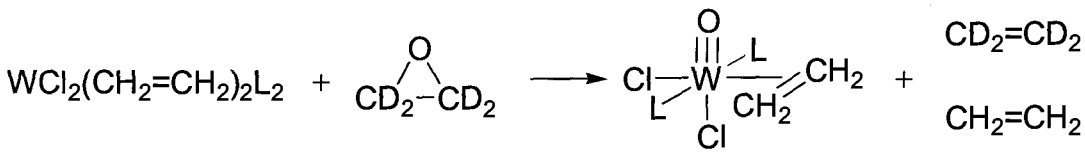

The [2+2] process can immediately be excluded since the reaction with ethylene-$d_4$ oxide is inconsistent with a mechanism proceeding through a metalloxetane intermediate. Rearrangement of the metalloxetane produces a tungsten(IV) oxo olefin complex which is extremely $\pi$-basic and would immediately bind with $CD_2=CD_2$ before it could dissociate. Since partial loss of stereochemistry resulted, a carbocation or radical mechanism might appear to be favored. The carbocation mechanism was excluded since a Hammett study showed very little charge buildup at the transition state. The radical process was excluded since the reactivities of ethylene, isobutylene and tetramethylethylene oxides are roughly 100:10:1 ($k_{Me4}/k_{Me2} = k_{Me2}/k_{H4}$), which is evidence for a concerted mechanism. The [3+2] process is consistent with all the data but the partial loss of stereochemistry observed for *cis*-2-butene oxide. However, loss of stereochemistry may result from a second mechanistic pathway, which makes only a minor contribution. A computational study by Jorgensen et al. supported the [3+2] concerted mechanism as well.[104]

## 3.5 Developing a Mechanism for Rhenium-Catalyzed De-epoxidations

In Chapter 2 we developed an efficient catalytic process capable of deoxygenating epoxides. There are several possible mechanisms for this type of transformation as demonstrated by the preceeding sections. The mechanistic proposal for our system which was developed in Chapter 2 is shown in Scheme 3.6. At this point, the proposal is rather simplified with only three rhenium species involved in the catalytic cycle. The disappearance of insoluble $Tp'ReO_3$ and the immediate formation of a blue or green colored solution suggested that reduction of $Tp'ReO_3$ to form $Tp'ReO_2$ was extremely rapid. Conversely, O-atom transfer from the epoxide to reactive $Tp'ReO_2$ was expected to be the rate-determining step of the catalytic cycle. The equilibrium between $Tp'ReO_2$ and $Tp'Re(O)(OH)_2$ becomes important under hydrous conditions; the deliberate addition of 10 μL of $H_2O$ decreased the turnover frequency by half. Under these conditions, the resting state for the catalyst was determined to be the oxo bis-hydroxide complex as evident by $^1H$ NMR. Formation of $Tp'Re(O)(OH)_2$ effectively removes the amount of catalytically active $Tp'ReO_2$ thus reducing the reaction rate.

Scheme 3.6

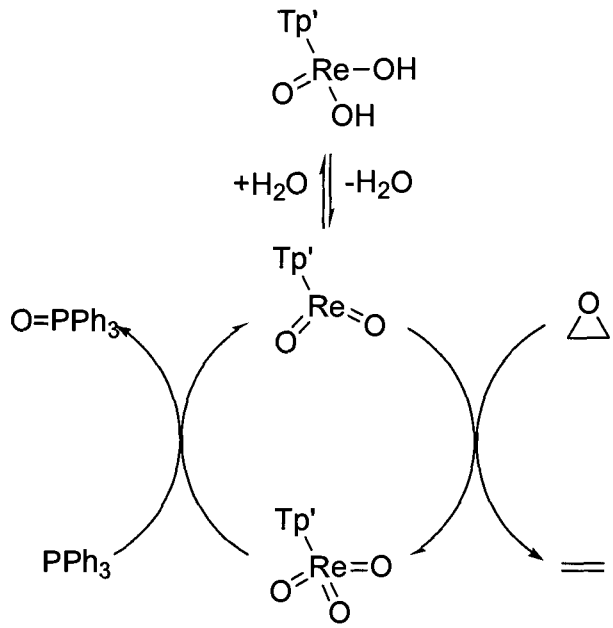


### 3.6 Possible Mechanisms for Rhenium-Catalyzed De-epoxidations

A number of possible mechanisms can be proposed for the O-atom transfer step from epoxide to Tp'$ReO_2$ (Scheme 3.7). The simplest possibility is concerted fragmentation of the epoxide (pathway A). Other possibilities include mechanisms involving C-O bond homolysis (pathway B) to form a diradical intermediate and C-O bond heterolysis (pathway C) to form a zwitterionic intermediate. Possible step-wise mechanisms include oxidative addition of the epoxide to form a metalloxetane intermediate (pathway D) followed by a retro-[2+2] cycloreversion and formation of a rhenium(V) diolate (pathway E) followed by a retro-[3+2] cycloreversion.

Scheme 3.7 also includes possible equilibrium formation of a coordinated epoxide, but direct O-atom transfer without formation a coordinated epoxide intermediate is also possible.

Scheme 3.7

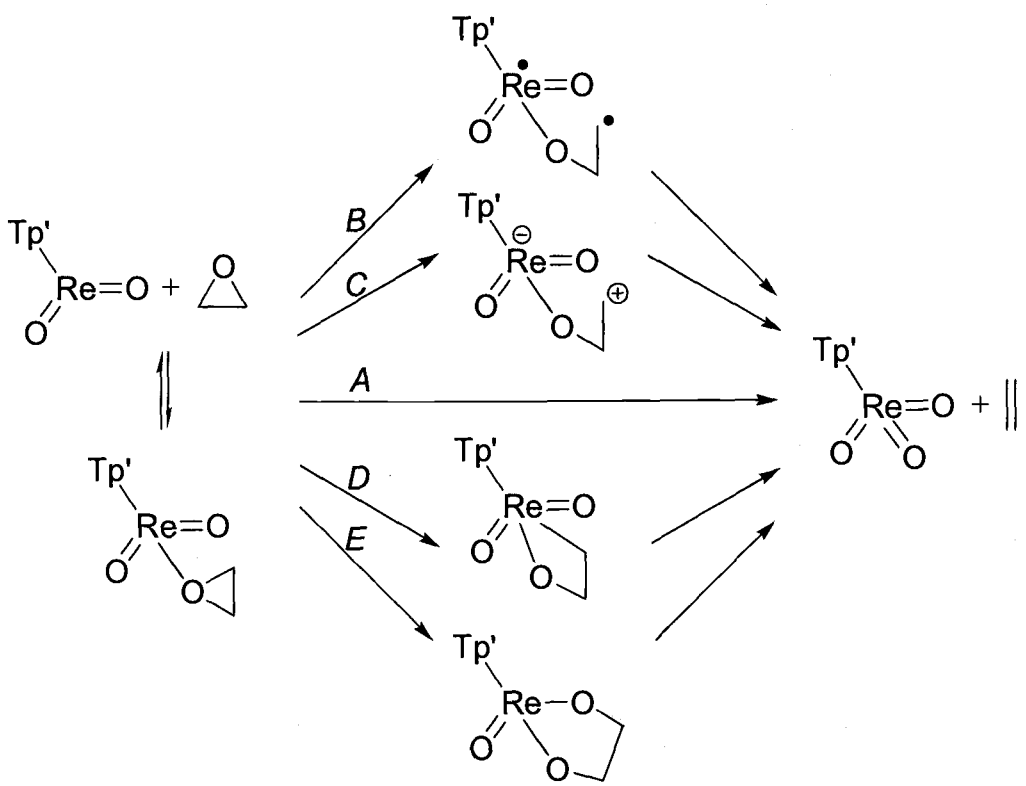


The reactivity study presented in Chapter 2 offers preliminary clues into the mechanism(s) operating in rhenium-catalyzed epoxide deoxygenations. Retention of configuration is the major tool used to determine if a radical or polar mechanism is operating. Any intermediate in which the C-O bond of the epoxide is broken

would be expected to undergo single bond rotation (low-energy process usually costing $\leq$ 5 kcal/mol) rather than collapse to form alkene. Both the radical and ionic mechanisms are unlikely, since predominant retention of configuration was observed for most substrates. However, loss of stereochemistry with *cis*- and *trans*-butene oxide was observed. The deoxygenation of *cis*-butene oxide yielded roughly 88% *cis*- and 12% *trans*-butene oxide. Conversely, *trans*-butene oxide gave 33% *cis*- and 77% *trans*-butene oxide. Partial loss of stereochemistry could occur through a second mechanistic pathway (see Section 3.20). No significant solvent dependence was observed, as shown in Table 3.1. The minor decrease in turnover number for the coordinating solvent acetonitrile-$d_3$ is attributed to solvent ligation rather than a solvent effect resulting from a polar mechanism (the magnitude of the change is too small).

Table 3.1 Solvent effects on deoxygenation of *cis*-stilbene oxide at 75.3°C.

| Solvent | $k_{obs}$ (M/s) |
|---|---|
| benzene-$d_6$ | $1.4 \times 10^{-6}$ |
| benzene-$d_6$ + 3.77 μL ether (0.036mmol) | $1.5 \times 10^{-6}$ |
| benzene-$d_6$ + 0.94 μL acetonitrile (0.018mmol) | $1.6 \times 10^{-6}$ |
| acetonitrile-$d_3$ | $1.0 \times 10^{-6}$ |

From the reactivity study, either the concerted pathway or one of the two organometallic pathways is necessary to explain the retention of stereochemistry. A concerted mechanism would be consistent with the electronic effects observed with increasing aryl and alkyl substitution of the epoxide. Increasing the alkyl substitution of the epoxide was shown to slow the rate of reaction, while increasing the number of aryl groups increased the rate. On the other hand, the electronic effects observed are inconsistent with a metalloxetane mechanism; the rate of reaction of different epoxides has been suggested to depend more upon steric than electronic effects.[105] The faster reaction of isobutylene oxide than of *cis*- or *trans*-butene oxide supports the metalloxetane mechanism. The formation of the metallocycle from *cis*- and *trans*-butene oxide would be much slower compared to isobutylene oxide because a methyl group would occupy the sterically crowded space next to the metal. Likewise, the lack of reactivity for tetramethylethylene oxide could be argued as proof for a metalloxetane mechanism using the same reasoning.

Ring expansion of the epoxide to form a rhenium(V) intermediate that undergoes cycloreversion is also thermodynamically possible. The thermodynamics of the ring expansion for $Cp^*ReO_3$ can be calculated using the reaction enthalpy of olefin epoxidation and dihydroxylation calculated by Ziegler (Scheme 3.8).[102] Ring expansion of the epoxide is favored by 37.6 kcal/mol. Furthermore, the observation that cis epoxides were deoxygenated faster than trans epoxides suggests our transition state is similar to the transition states involved in

many metal-catalyzed epoxidations. Cis olefins are normally epoxidized more readily than trans olefins by oxo metal complexes.[94,105,106] Overall, neither the concerted or stepwise processes can be immediately excluded.

Scheme 3.8

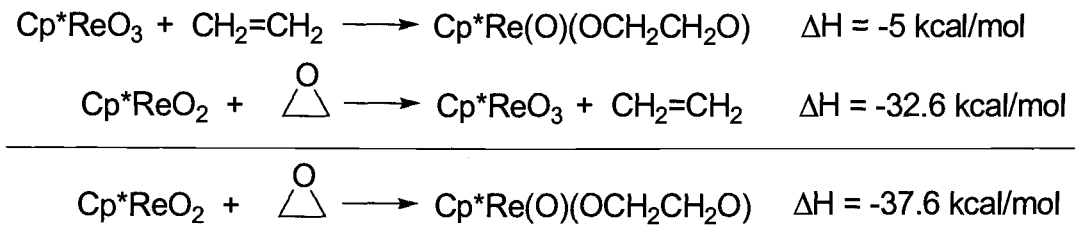


### 3.7 Kinetic Studies

A kinetic study was undertaken to establish the rate law and develop a better understanding of the reaction mechanism. Typical kinetic runs consisted of preparing and drying epoxide solutions containing different concentrations of epoxide, triphenylphosphine and 1,4-di-*tert*-butylbenzene (integration standard) in dry benzene-$d_6$ over $CaH_2$. 0.5 mL aliquots were then added to NMR tubes containing different amounts of $Tp'ReO_3$ and sealed under vacuum. The samples were then heated in thermostated water/ethylene glycol baths and periodically removed and analyzed by $^1H$ NMR. A relaxation delay of 15-30 s was used to ensure accurate integration.

A.

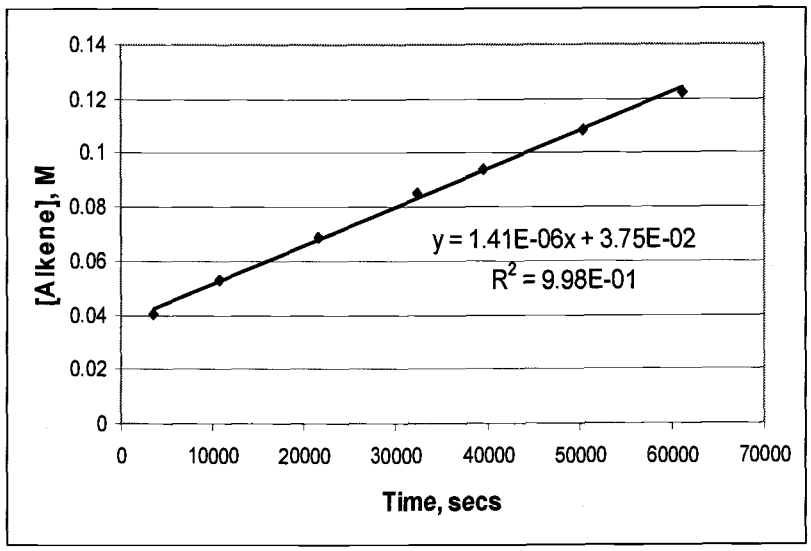


B.

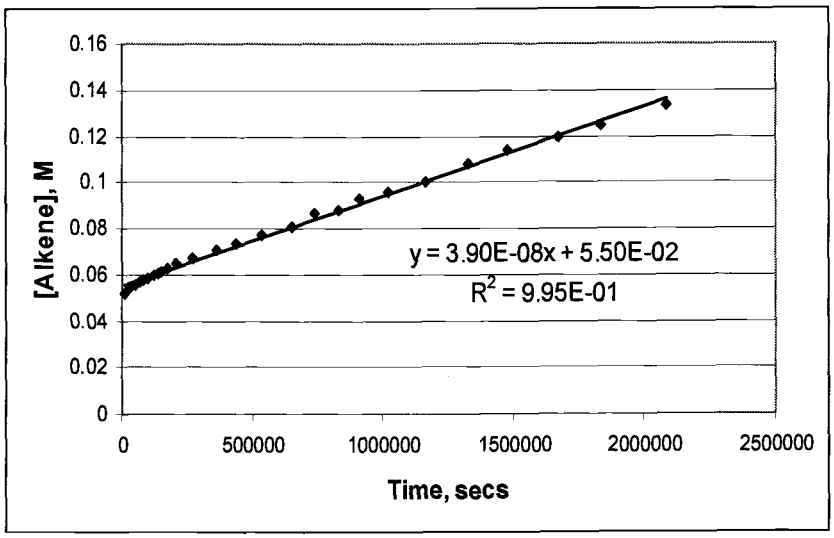


Figure 3.1 Concentration of alkene versus time plot for deoxygenation of (A) *cis*-stilbene oxide and (B) styrene oxide.

The kinetic study was carried out with *cis*-stilbene oxide and styrene oxide as substrates. The preliminary kinetic data showed pseudo-zero order behavior for production of alkene (Figure 3.1). Rate measurements were then taken at different concentrations for each reactant to determine the order of the reaction with respect to each reactant. A first-order dependence in $[Re]_T$ was determined (Figure 3.2); doubling the concentration of rhenium from $9.03 \times 10^{-3}$ M (5 mol-%) to $1.81 \times 10^{-2}$ M (10 mol-%) doubled the rate constant $k_{obs}$. Conversely, zero-order behavior in $[PPh_3]$ was observed as indicated by the near zero slope in Figure 3.3. A dependence in [Epoxide] was also determined, but the kinetic study revealed that the reaction rate was dependent on the concentration of epoxide (Scheme 3.4). The plot of velocity versus *cis*-stilbene oxide concentration is shown in Figure 3.2C. At a constant concentration of catalyst, the reaction rate increased with increasing *cis*-stilbene oxide concentration until a maximum velocity was reached. This kinetic behavior is frequently encountered in enzymology and is described by the Michaelis-Menten equation (Scheme 3.9).[107] The enzyme (E) and substrate (S) reversibly bind to form an intermediate enzyme-substrate complex (E•S) whose decomposition into products (P) is rate-controlling. With an excess of substrate ($[S] >> K_m$), the Michaelis-Menten equation is reduced to rate = $k_3[E_o]$ and one obtains a zero-order reaction. Conversely, when $[S] << K_m$ then the [S] term disappears from the denominator and the rate = $(k_3[E_o]\ [S])/K_m = k'[S]$. This

explains the shape of the velocity versus substrate plot; first-order kinetics is observed at low substrate concentration and zero-order kinetics is observed at high substrate concentration.

Scheme 3.9

$$E + S \underset{k_2}{\overset{k_1}{\rightleftharpoons}} E\bullet S \xrightarrow[\text{rate-determining step}]{k_3} E + P$$

$$\frac{d[P]}{dt} = \frac{k_3\,[E_o]\,[S]}{K_m + [S]} \qquad K_m = (k_3 + k_2)/k_1$$

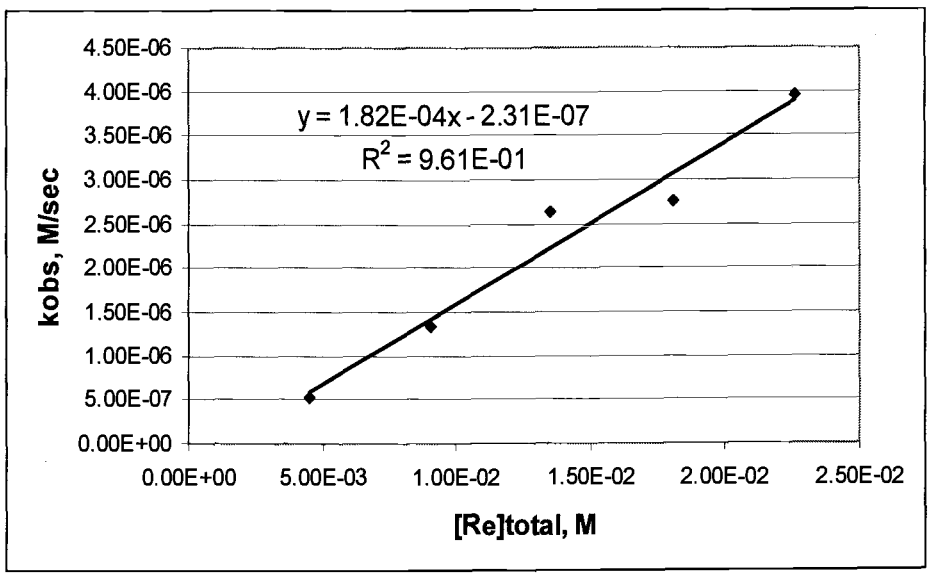


Figure 3.2 Dependence of turnover frequency on initial rhenium concentration.

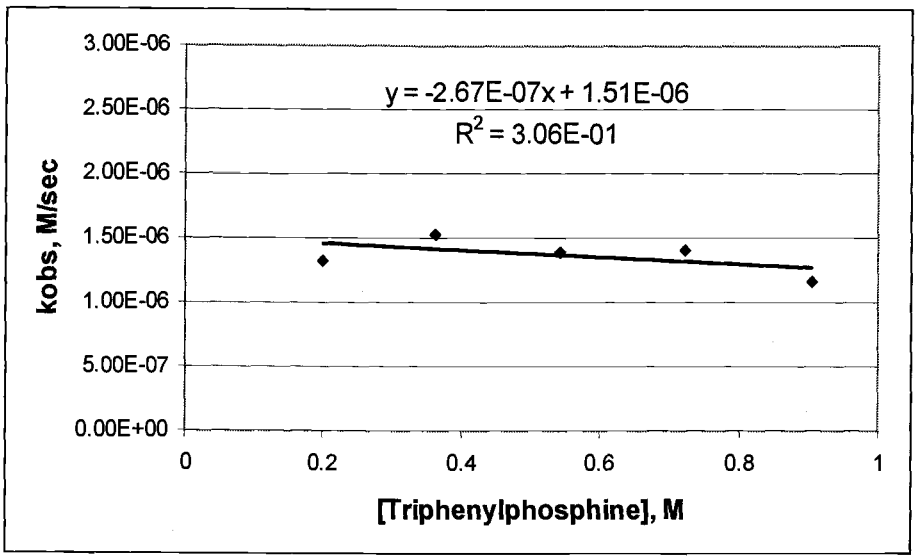


Figure 3.3 Dependence of turnover frequency on initial triphenylphosphine concentration.

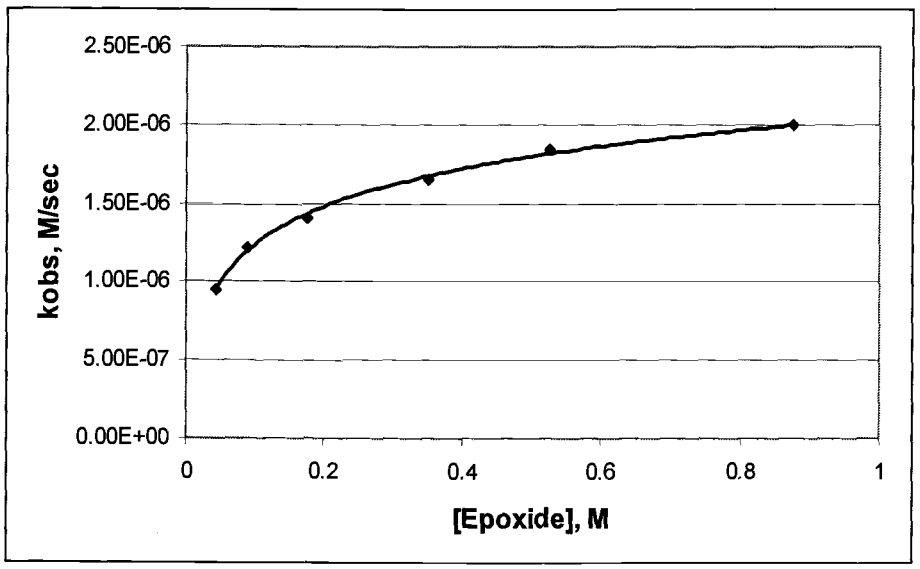


Figure 3.4 Dependence of turnover frequency on initial *cis*-stilbene oxide concentration.

### 3.8 Competition Experiment

In analogy to Scheme 3.9, we propose a mechanism in which the epoxide reversibly binds to $Tp'ReO_2$ forming a coordinated epoxide intermediate. A competition experiment between *cis*-stilbene oxide and styrene oxide as substrates further support the existence of a coordinated epoxide intermediate. A 1:1 mixture of the two substrates along with an integration standard, triphenylphosphine and benzene-$d_6$ were sealed with solid $Tp'ReO_3$ in an NMR tube under vacuum and heated to 75.3°C. Styrene was the major olefin produced after 321 h; 63% of styrene oxide ($k_{obs}$ = 4.7 x $10^{-8}$ M/s) had been converted compared to 5% for *cis*-stilbene oxide ($k_{obs}$ = 5.9 x $10^{-9}$ M/s). Oddly enough, *cis*-stilbene oxide had been shown in separate experiments (see also Chapter 2; Table 2.1) to be deoxygenated more rapidly when it was the sole substrate: the turnover rates for *cis*-stilbene oxide and styrene oxide are 1.41 x $10^{-6}$ M/s (Figure 3.1A) and 3.9 x $10^{-8}$ M/s (Figure 3.1B) respectively. This type of behavior is consistent with a mechanism involving reversible formation of a coordinated epoxide intermediate (Scheme 3.10). Even though *cis*-stilbene oxide is deoxygenated more readily ($k_3 > k_4$; greater relief of steric compression), binding of the epoxide is more favorable for the more electron rich and sterically less hindered styrene oxide ($K_2 > K_1$). As a result, the majority of rhenium is tied up in complex **3-2** preventing **3-1** from building up to an appreciable level.

Scheme 3.10

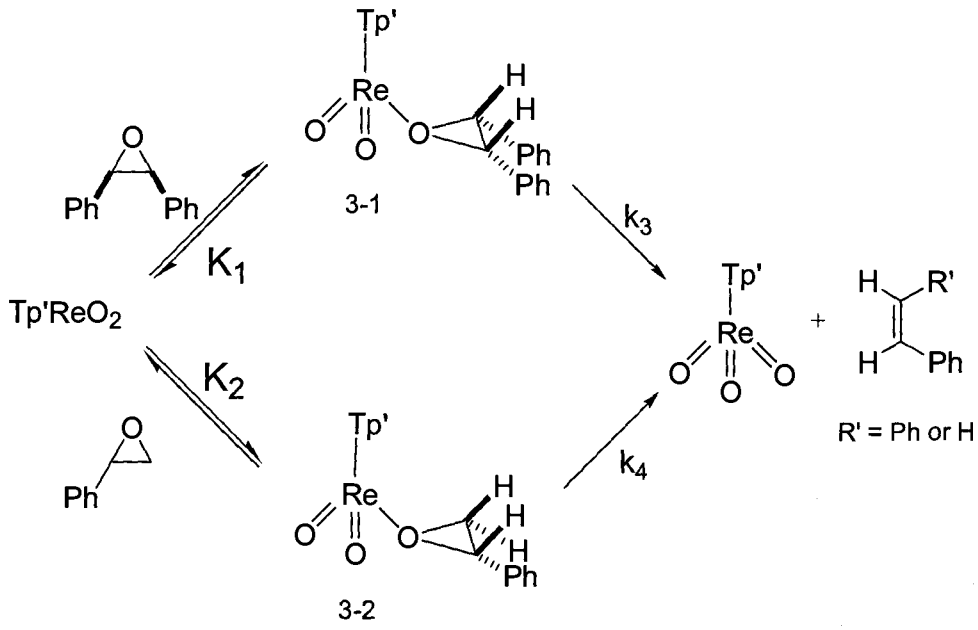


### 3.9 Hammett Study

A linear free energy relationship study was undertaken to gain further insight into the transition state of the rate-determining step. A series of *para*-substituted styrene oxides were synthesized and used as substrates in the Hammett study. A plot of $\ln(k_i/k_h)$ vs $\sigma$[108] is shown in Figure 3.5. In our system a nonlinear Hammett plot was observed depending on the electronic nature of the substituent. Both electron-withdrawing (positive $\sigma$ values) and electron-donating groups (negative $\sigma$ values) enhance the rate versus styrene oxide. Electron donors show a $\rho = -1.28$, while electron-withdrawing groups have a $\rho = +0.52$. A similar concave

deviation is observed with $\sigma^+$ values. An upward V-shaped Hammett plot is indicative of a change in mechanism or of at least two competing pathways.[109] A similar deviation where the curvature occurs at zero has also been observed for rhenium(V) diolate cycloreversions[54] and H/D exchange reactions catalyzed by a molybdocene complex.[110]

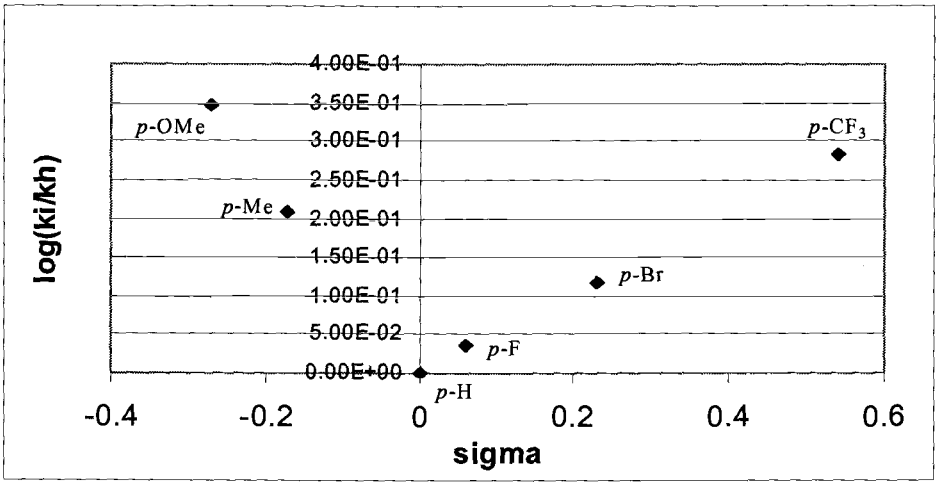


Figure 3.5 Hammet plot for deoxygenation of substituted styrene oxides.

### 3.10 Pseudo-Zero Order Plots

Two important observations required us to reconsider our initial mechanistic model. First, the concentration vs time plots (Figure 3.1) showed that the trend line did not intercept at the origin. Upon following the reaction more closely during the beginning of the deoxygenation process, an initial "burst" of

alkene formation was observed (Figure 3.6). However, a slower steady-state system eventually developed and explained the linear pseudo-zero order portion of the plot. An induction period, resulting from reduction of insoluble $Tp'ReO_3$ by triphenylphosphine, can not explain the "burst" of alkene formation since buildup of active $Tp'ReO_2$ during an induction period would have delayed, not accelerated alkene production.

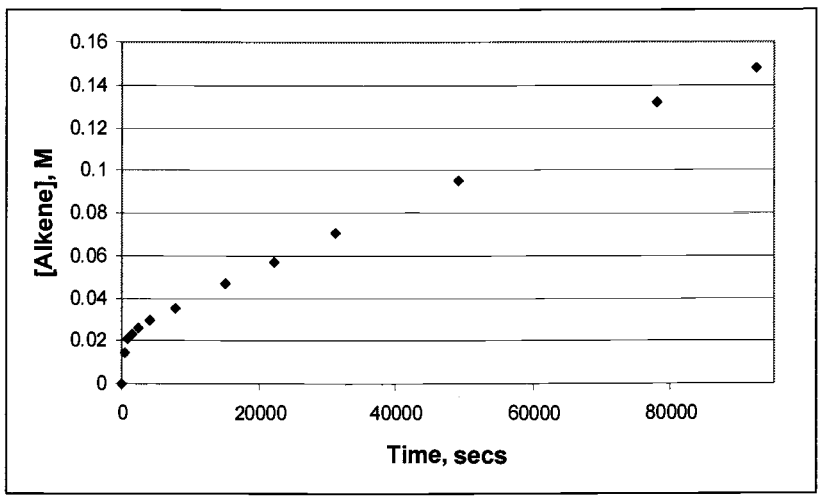


Figure 3.6 Concentration of alkene versus time plot for deoxygenation of *cis*-stilbene oxide.

### 3.11 Catalyst Resting State Species

A second observation was that a reduced Re(V) species could by observed by NMR spectroscopy; the symmetry of the catalyst resting state species changed

with the symmetry of the epoxide. Symmetrical epoxides formed a rhenium species with $C_s$-symmetry and non-symmetrical epoxides formed a species with $C_1$-symmetry. An initial rational was that we were observing the coordination epoxide complex but the absence of epoxide CH proton signals suggested otherwise. The structure was finally determined after the spectrum of the species generated from styrene oxide was matched to the spectrum of the minor isomer in the crude reaction mixture resulting from cyclocondensation of phenylethanediol with $Tp'ReO_3$ and $PPh_3$.[83] The minor isomer formed from the cyclocondensation reaction is the *syn*-monophenyldiolate complex (**3-3**), while the major isomer is *anti*-monophenyldiolate (**3-4**). The syn stereochemistry had already been established for complex **3-3** by a nuclear Overhauser enhancement experiment.[54] The syn stereochemistry for *syn-cis*-diphenyldiolate (**3-5**) was also confirmed by nOe studies. The methyl group on the Tp' ligand that points directly towards the diolate ring provides a useful spectroscopic handle to distinguish between the two diastereoisomers. For **3-5** irradiation of the carbinol-type CH proton at δ 6.70 ppm led to a nuclear Overhauser enhancement of only the ortho phenyl protons at δ 7.33 ppm (Figure 3.7). The pyrazole methyl signal at δ 2.21 ppm was also irradiated and resulted in an enhancement of the pyrazole vinyl signal at δ 5.52 and the ortho phenyl protons at δ 7.33 ppm. The *anti-cis*-diphenyldiolate (**3-5**), which is formed from cyclocondensation of *meso*-hydrobenzoin with $Tp'ReO_3$ and $PPh_3$, was synthesized for comparison. For **3-6** irradiation of the pyrazole methyl led to an enhancement of the pyrazole vinyl signal at 5.56 ppm and the carbinol-type CH

proton at δ 6.64 ppm. Conversely, irradiation at the carbinol-type CH proton led to an enhancement of the pyrazole methyl signal at δ 2.55 ppm and the ortho phenyl protons at δ 7.07 ppm. In addition, the pyrazole methyl of the *syn*-isomer (**3-5**), which sits between the two diolate phenyl rings, undergoes a shift upfield to δ 2.21 ppm compared to δ 2.55 ppm for the *anti*-isomer. This is consistent with the methyl group experiencing anistropy from the diamagnetic ring currents. High resolution mass spectroscopy confirmed that **3-3** and **3-5** had compositions resulting from the addition of epoxide to $Tp'ReO_2$. The IR spectrum for both compounds showed only a single oxo stretch at 957 $cm^{-1}$ for **3-3** and 958 $cm^{-1}$ for **3-5**. The frequency of the Re=O stretch in both compounds resemble that of other diolate complexes (~957 $cm^{-1}$).

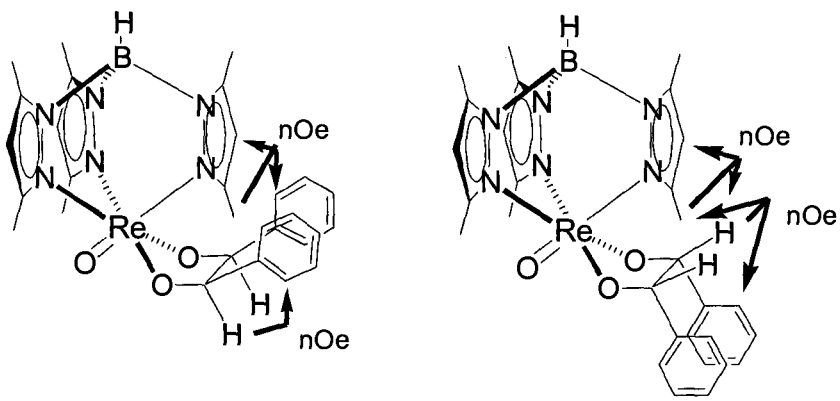


**3-5** Syn-Isomer

**3-6** Anti-Isomer

Figure 3.7 nOe enhancements for **3-5** and **3-6**.

Figure 3.8 nOe spectrum of **3-5**.

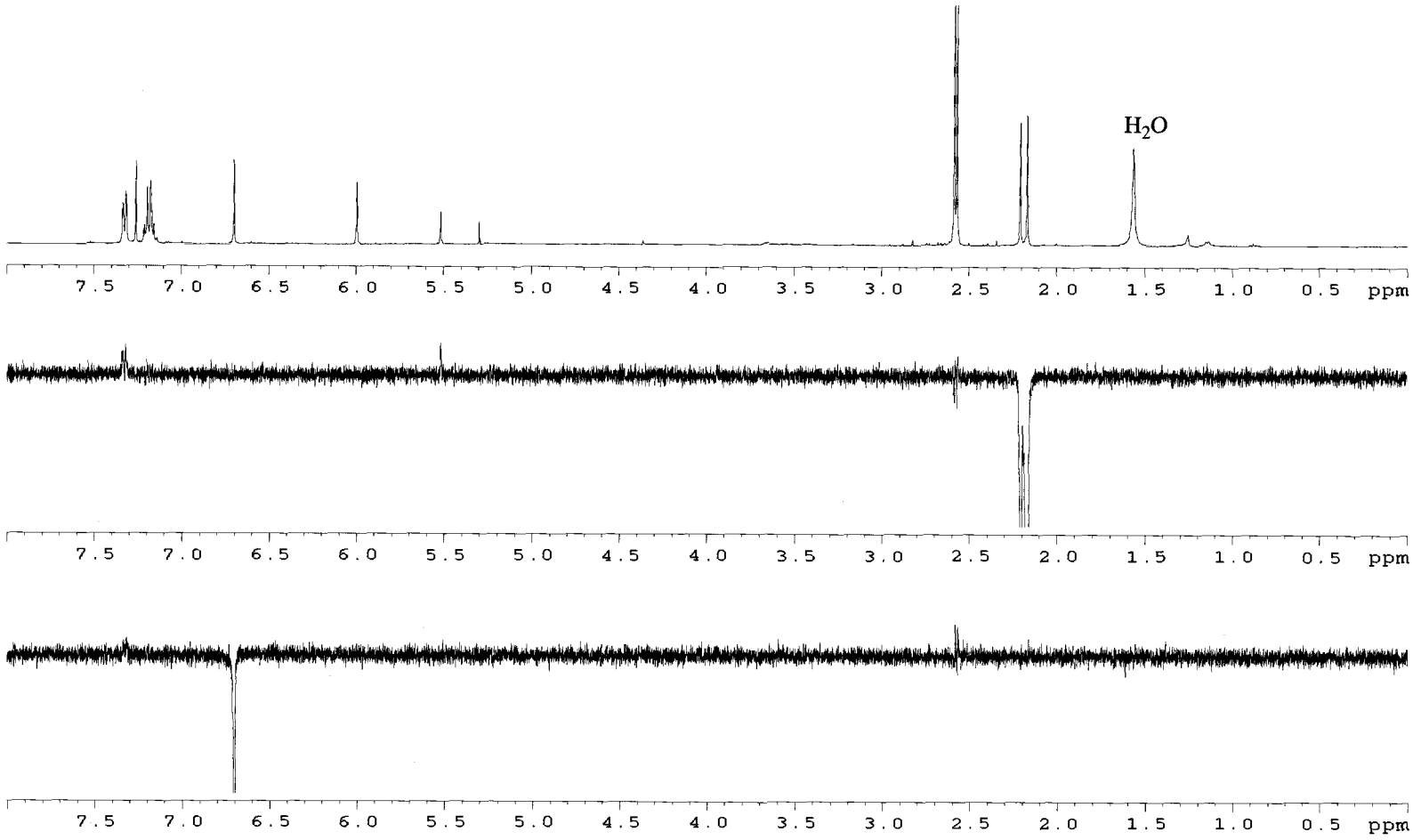

Figure 3.9 nOe spectrum of **3-6**.

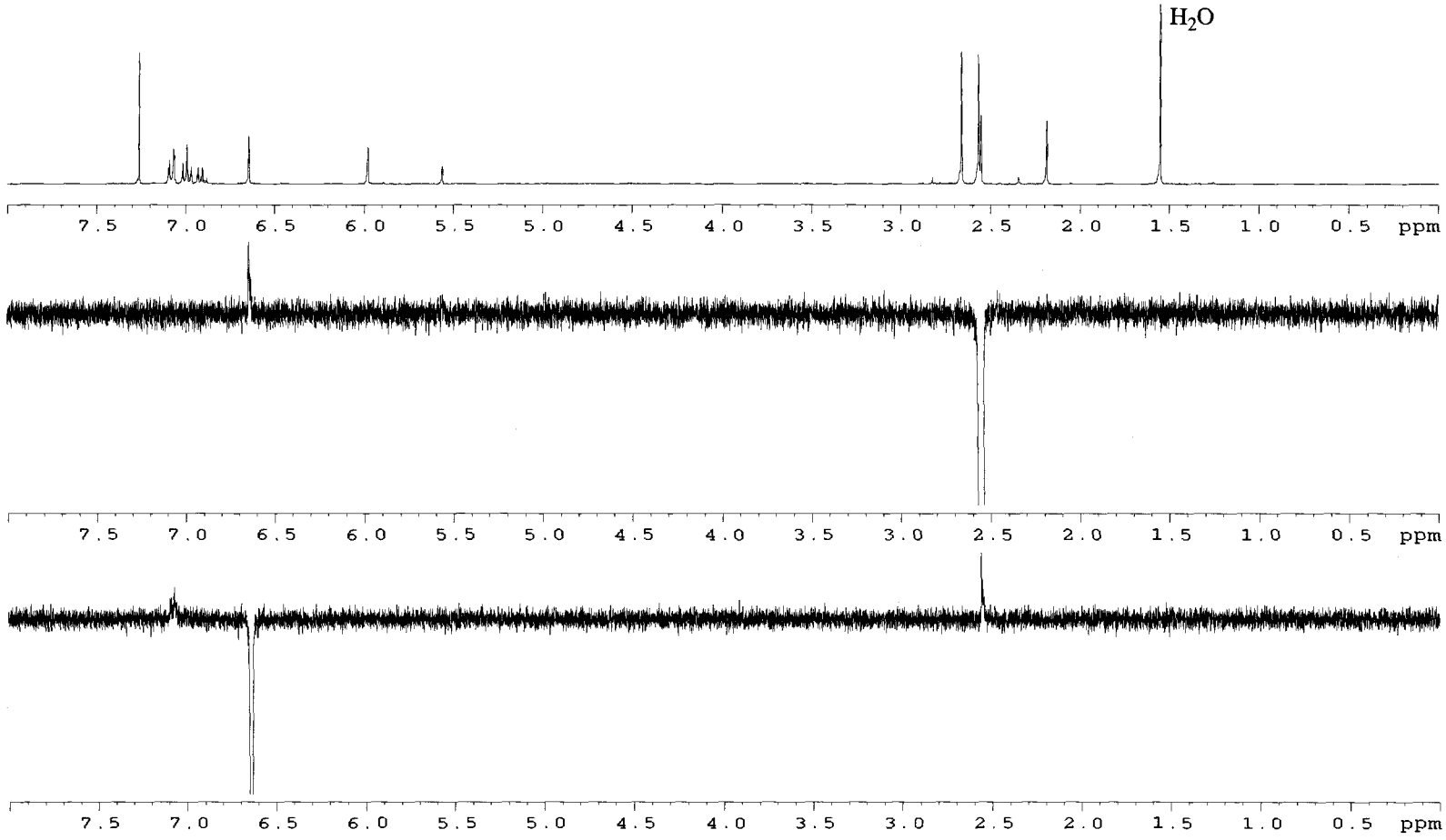

### 3.12 Lewis Acidity of Tp'$ReO_2$

Although ring expansion of an epoxide to form *syn*-Tp'Re(O)(diolate) has never been documented before, MTO ($CH_3ReO_3$) will react with epoxides to form rhenium(VII) diolate complexes as shown in Chapter 1 (Scheme 1.5).[39] MTO is very Lewis acidic and acid-mediated ring opening of the epoxide followed by migration to the adjacent terminal oxo group is a reasonable proposal. However, Tp'$ReO_2$ was shown not to be very electrophilic compared to MTO. For example, incomplete reduction of Lewis acidic MTO by $PPh_3$ forms the metal-coordinated phosphine oxide adduct $CH_3ReO_2$•$OPPh_3$.[111] Reduction of Tp'$ReO_3$ by $PPh_3$ results in the free form of $Ph_3P$=O and Tp'$ReO_2$. This was further demonstrated by measuring the rate of *cis*-stilbene oxide deoxygenation after the deliberate addition of 1 equivalent of $Ph_3P$=O (0.0903 mmol). If a phosphine oxide adduct is formed then the turnover frequency should decrease since $Ph_3P$=O will be competing with epoxide for the empty coordination site on the metal. The turnover frequency was found to be 1.22 x $10^{-6}$ M/s for the reaction with added $Ph_3P$=O compared to 1.4 x $10^{-6}$ M/s for the reaction without added $Ph_3P$=O. The value is well within the 20% experimental error range, which supports the claim that neither phosphines nor phosphine oxides coordinate appreciably to the dioxo complex. Furthermore, the rentention of configuration (>95%) observed for *cis*-stilbene oxide deoxygenations and the lack of solvent effects (see Table 3.1) argue against Lewis acid catalyzed ring opening of the epoxide.

### 3.13 Kinetic vs Thermodynamic Origin

Formation of **3-3** and **3-5** was shown to be kinetic in origin. This was demonstrated by stirring the *syn*, *cis*-diphenyldiolate **3-5** with an excess of 1,2-diphenylethanediol and *p*-toluenesulfonic acid for three days under inert conditions. Exclusive formation of the *anti*-diolate resulted. Conversely, the *anti*-diolate **3-6**, under the same conditions, does not lead to the formation of the *syn*-diolate **3-5**. Computational modeling supports the experiment. Comparison of *syn*, *cis*- and *syn*, *anti*-TpRe(O)(OCH($CH_3$)CH($CH_3$)O) (the nonmethylated ligand is used to simplify the calculations) was undertaken to determine which isomer was thermodynamically favored. The structures were optimized at the B3LYP/LACVP*+ level. A vibrational analysis showed that the calculated structures where true minima (no imaginary frequencies). The *syn*, *anti*-diphenyldiolate was determined to be more favored by 1.23 kcal/mol (Figure 3.10). The two optimized diolate geometries agree with the published X-ray crystal structure reported for TkRe(O)($OCH_2CH_2O$).[112] The difference in energy between the two structures might have been even greater had the modeled reaction included the methylated ligand and the phenyl groups on the diolate ring.

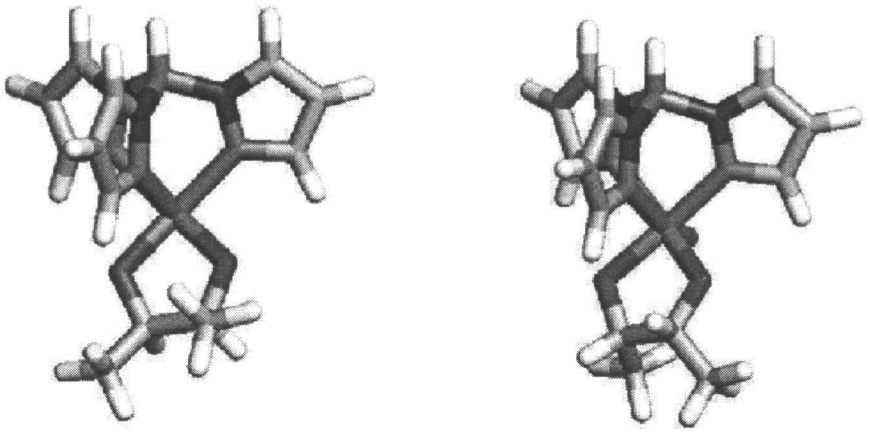

E = -1164.5335 H
$E_{rel}$ = 0 kcal/mol

E = -1164.5349 H
$E_{rel}$ = -0.98 (-1.23) kcal/mol

Figure 3.10 Optimized structures and energies at the B3LYP/LACVP*+ level. Value in parenthesis is ZPE-corrected.

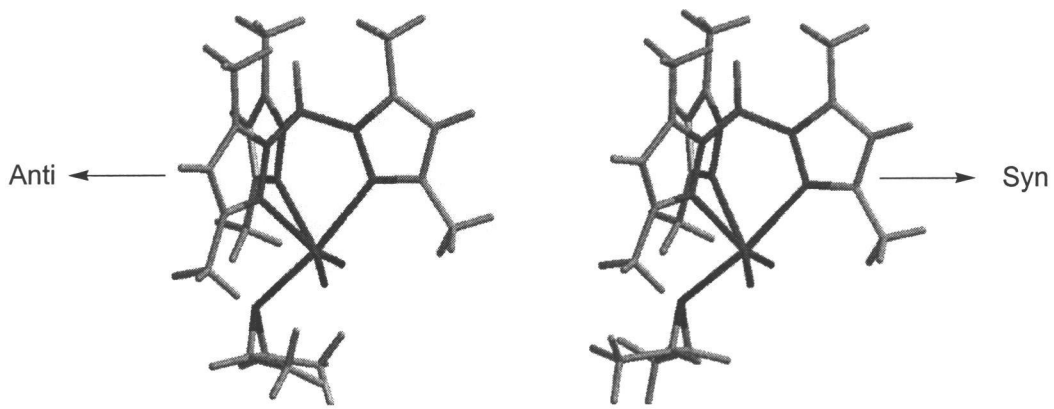


Figure 3.11 Model representation demonstrating how steric factors govern the kinetic preference for the *syn*-diolate.

Kinetic formation of the *syn*-diolate is believed to be driven by steric factors. If the *syn*-diolate proceeds through a coordinated epoxide intermediate and the epoxide binds parallel with the complex, then steric factors will orient the substituents on the epoxide away from the two oxo groups as shown is Figure 3.11. Once the coordinated epoxide is formed, it can undergo ring expansion thus locking the diolate into the *syn* conformation (migration of carbon to oxygen with retention of configuration will fix the stereochemistry, regardless of which carbon migrates). Computational modeling of the *syn*- and *anti*-coordinated epoxide intermediates agree with this model. The *syn*-coordinated epoxide complex converged at the B3LYP/LACVP*+ level. Vibrational analysis confirmed the absence of an imaginary frequency. The optimized structure of the *syn*-epoxide complex is shown in Figure 3.12. The Re-O bond to the epoxide was found to be 2.344 Å and the Re=O bonds were 1.741 Å. The structure that eventually converged for the *anti*-epoxide complex demonstrates how the steric interaction between the substituents on the epoxide and the two oxo groups destabilized the complex more than the energy gained by forming the Re-epoxide interaction.

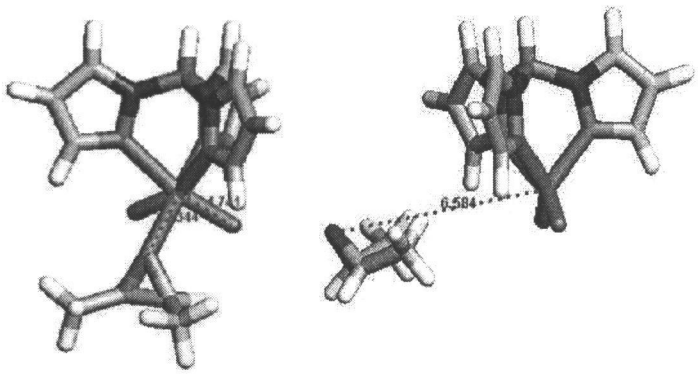

E = -1164.4719H
$E_{rel}$ = - 0.76 kcal/mol

E = -1164.4707H
$E_{rel}$ = 0 kcal/mol

Figure 3.12 Optimized structures at the B3LYP/LACVP*+ level.

### 3.14 Intermediacy of a Rhenium(V) Diolate

Since the *syn*-diolate was determined to be the resting state of the catalyst, a reassessment of the mechanistic model was necessary. The new model (Scheme 3.11) would require cycloreversion of the *syn*-diolate to be the rate-controlling step. Unfortunately, the new model can not account for the saturation behavior since the rate will depend only on the amount of diolate and the rate constant for cycloreversion (formation of the diolate from the epoxide complex is irreversible). Furthermore, the new model does not explain the initial "burst" of alkene production observed in the pseudo-zero order plots. To test the new model, the rate constants for diolate cycloreversion were required for both of the *syn*-diolates.

Diolates **3-3**, **3-5** and **3-6** were dissolved in $C_6D_6$ and sealed in NMR tubes under vacuum. They were heated to 75.3 ± 0.1 °C; the sample tube was periodically removed and the $^1H$ NMR spectrum was recorded. The reactions were first-order to at least four half lives (see Appendix). The reaction rate constants are listed in Table 3.3. The rate constant determined for *anti-cis*-diphenyldiolate **3-6** in benzene-$d_6$ was within experimental error of the extrapolated rate constant for **3-6** taken from prior data measured in toluene-$d_8$. Therefore, the extrapolated rate constant for **3-4** was used rather than repeat the experiment in benzene-$d_6$. Oddly enough, the addition of a second phenyl group switched the relative order of reactivity for *syn*- vs *anti*-diolate cycloreversions. The *syn-cis*-diphenyldiolate **3-5** cycloreverts faster than the *anti-cis*-diphenyldiolate **3-6**, while the *anti*-monophenyldiolate **3-4** cycloreverts faster than the *syn*-monophenyldiolate **3-3**. The greater relief of steric compression for **3-5** can be used to explain this effect.

Scheme 3.11

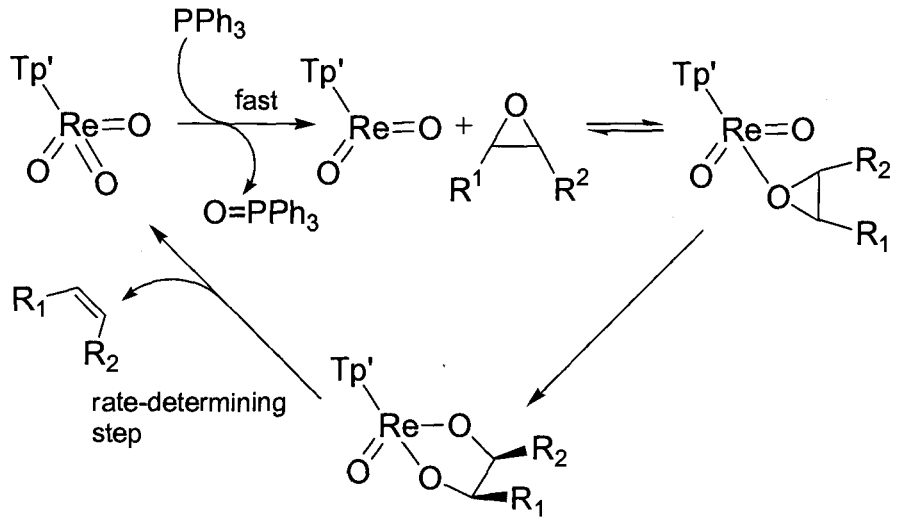


**3-3** $R_1$ = H, $R_2$ = Ph
**3-5** $R_1$ = Ph, $R_2$ = Ph

Table 3.2 Rate constants for cycloreversion at 75.3°C.

| Compound | Measured Rate Constant, $s^{-1a}$ | Extrapolated Rate Constant, $s^{-1b}$ |
|---|---|---|
| **3-3** | $(6.46 \pm 0.20) \times 10^{-7}$ | |
| **3-4** | | $5.88 \times 10^{-6}$ |
| **3-5** | $(6.04 \pm 0.23) \times 10^{-5}$ | |
| **3-6** | $(5.97 \pm 0.35) \times 10^{-6}$ | $6.29 \times 10^{-6}$ |

[a]This work. Uncertainties at 95% confidence levels.
[b]Ref. 83, extrapolated from activation parameters.

### 3.15 Diolates Are Kinetically Incompetent to Explain Reaction Rates

Once the rate constants for cycloreversion were determined, it was now possible to compare the observed reaction rates under catalytic conditions to the calculated rates predicted by Scheme 3.11. The rate of alkene formation should be equal to the concentration of the diolate times the rate constant for cycloreversion. The observed turnover frequency for 0.009 M total rhenium is $1.4 \times 10^{-6}$ M/s for deoxygenation of *cis*-stilbene oxide. If the $d[alkene]/dt = k_{cyclo}[syn\text{-Diolate}]$, then the calculated rate is $4.62 \times 10^{-7}$ M/s. This value is one-third of the observed rate and demonstrates that the mechanism in Scheme 3.11 is incorrect or at least not complete. Similar analysis for the deoxygenation of styrene oxide led to the same conclusion; none of the *syn*-diolates alone are able to account for the observed catalytic rate. Another mechanistic possibility could be a contribution from both the *syn*- and *anti*-diolate complexes as shown in Scheme 3.12. In this case the rate equation is equal to $d[Alkene]/dt = k_{cyclo}[syn\text{-Diolate}] + k'_{cyclo}[anti\text{-Diolate}]$. If we assume that $[Re]_T = [syn\text{-Diolate}]+[anti\text{-Diolate}]$ then we can solve for the relative concentrations of each diolate necessary to obtain the observed rate constant. For styrene oxide the observed turnover frequency for 0.009 M total rhenium was $3.9 \times 10^{-8}$ M/s. To obtain the observed turnover frequency under catalytic conditions, the concentration of the *anti*-diolate ($[anti\text{-Diolate}] = 4.85 \times 10^{-3}$ M) would have to equal the *syn*-diolate concentration ($[syn\text{-Diolate}] = 4.15 \times 10^{-3}$ M). Obviously, this mechanistic model is also incorrect since the only observed rhenium species is the

*syn*-diolate. Therefore, some additional alkene-forming process besides cycloreversion of the *syn*-diolate must by operating.

Scheme 3.12

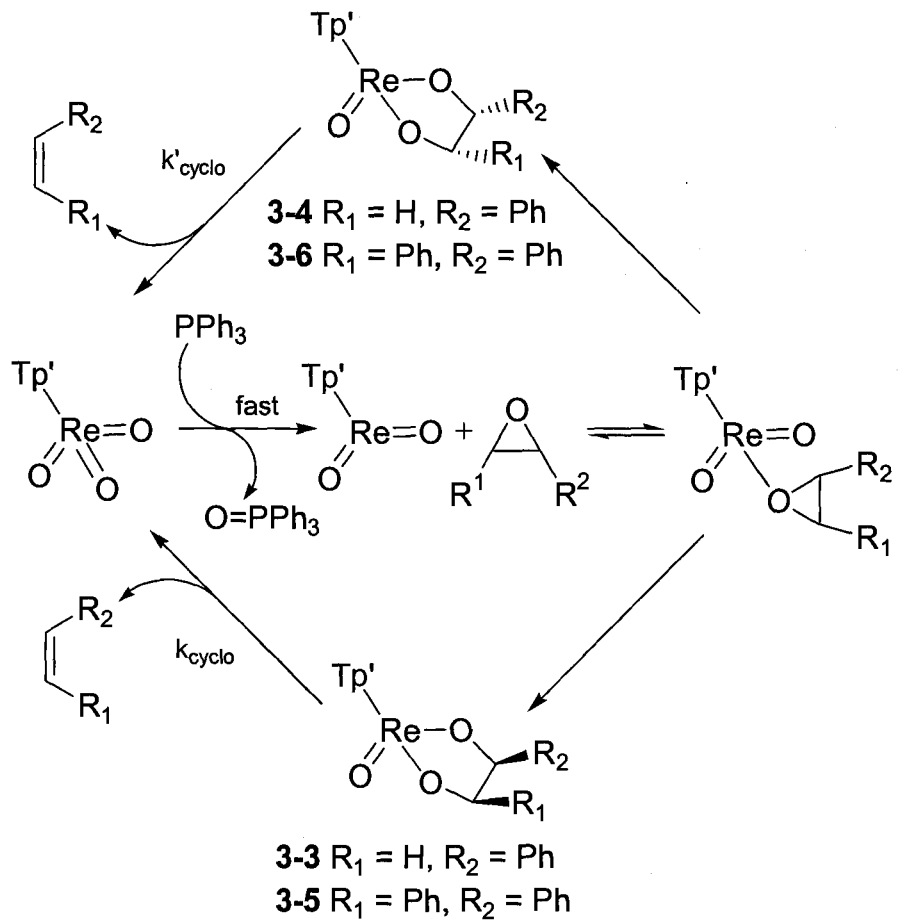

### 3.16 Burst Experiment

Further evidence to support an additional alkene-forming process besides diolate cycloreversion was demonstrated by two burst experiments. First, the ethoxide complex Tp'ReO(OH)(OEt), which was introduced in Chapter 2, was allowed to react with *cis*-stilbene oxide for 30 min at 75°C. Both the formation of *cis*-stilbene and the *syn*-diphenyldiolate **3-5** was observed. Of the 28% of the epoxide converted to alkene only about 5% of the total amount of *syn*-diolate produced could have formed from diolate cycloreversion in that time. Therefore, a ratio between the amount of stilbene produced immediately and the amount of *syn*-diolate produced from ring expansion could be determined. The stilbene/diolate ratio was found to be 3.8. A second experiment using $Tp'ReO_3/PPh_3$ was also performed. In this case, the sample was heated to 75°C for only 15 min. Once again, we know that any alkene formed must have originated from some other process than cycloreversion of the diolate since cycloreversion is slow under these conditions. After six minutes of heating and a 17% conversion of epoxide, the stilbene/diolate ratio was determined to be 4.4. The significance of these results is that the alternative deoxygenation process is about four times faster than ring expansion of the epoxide to form the *syn*-diolate.

### 3.17 Direct Fragmentation of the Coordinated Epoxide

Direct fragmentation of the coordinated epoxide complex is proposed as the alternative alkene-forming process. The new mechanistic model is shown in Scheme 3.13. Fast reduction of $Tp'ReO_3$ with $PPh_3$ generates free $Tp'ReO_2$. In the presence of any adventitious water, $Tp'ReO_2$ can form the oxo bis-hydroxide complex but loss of water is a very facile process. Reaction of $Tp'ReO_2$ with free epoxide generates the coordinated epoxide complex, which can either ring expand to form diolate or undergo direct O-atom transfer. A steady-state distribution of diolate and coordinated epoxide is eventually reached. The new mechanistic proposal can account for a series of important observations.

Scheme 3.13

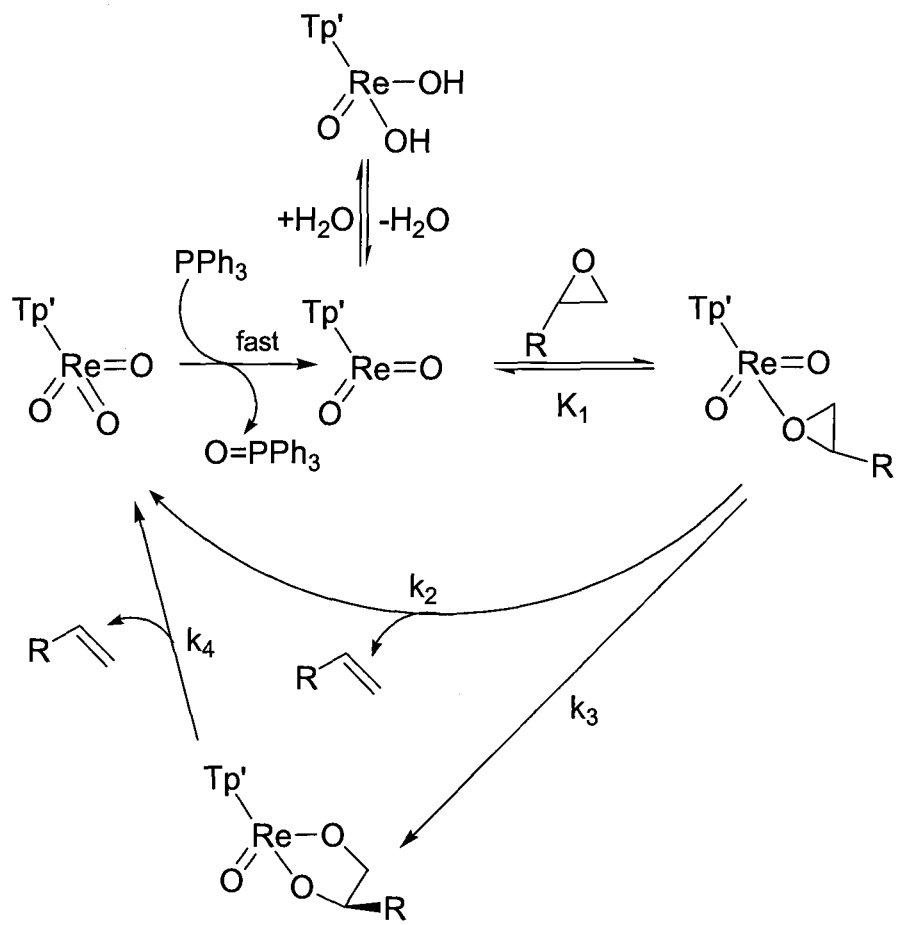


First, the model can adequately account for the "burst" of alkene production observed in the early stages of the reaction. Initial reduction converts all of the rhenium to Tp'$ReO_2$ and coordinated epoxide complex (the ratio of each is dependent on the concentration of epoxide). Since we know from the burst experiments that the ratio of $k_2/k_3$ is roughly 4, then during the early stages of the reaction most of the rhenium exists as coordinated epoxide complex and undergoes

preferential direct fragmentation to alkene and trioxide. At the same time, rhenium is slowly being funneled into the *syn*-diolate, which accumulates. Eventually a steady-state is reached where the rate of diolate cycloreversion is equal to the rate of ring expansion (diolate formation) from the coordinated epoxide complex. This is expressed by the steady-state expression for *syn*-diolate (Eq. 4).

$$k_3[LReO_2\text{-epoxide}] = k_4[\text{diolate}] \quad (4)$$

Since the two product-forming steps are direct fragmentation of the coordinated epoxide complex and cycloreversion of the diolate, then the rate expression is given by Eq. (5).

$$d[\text{Alkene}]/dt = k_2[LReO_2\text{-epoxide}] + k_4[\text{diolate}] \quad (5)$$

Substituting the steady-state expression for [diolate] (Eq. 4) into the rate expression (Eq. 5) we obtain the following reduced rate expression

$$d[\text{Alkene}]/dt = (k_2 + k_3)[LReO_2\text{-epoxide}] \quad (6)$$

The rate expression shows why a first-order dependence of the rate on the concentration of rhenium was observed. The absence of a $[PPh_3]$ term explains the observed zero-order dependence. Furthermore, the rate expression accounts for the

saturation behavior in epoxide. At high epoxide concentrations, free $Tp'ReO_2$ is bound with epoxide and the concentration of the coordinated epoxide complex becomes constant. The [$LReO_2$-epoxide] term can now be substituted by {$[Re]_T$ – [diolate]}. This explains the zero-order behavior at high epoxide concentrations. Conversely, the epoxide complex is in equilibrium with free $Tp'ReO_2$ at low concentrations of epoxide (Eq. 7).

$$k_1[Tp'ReO_2][\text{epoxide}] = k_{-1}[Tp'ReO_2\text{-epoxide}] \quad (7)$$

Substituting the equilibrium expression (Eq. 7) into Eq. (6), we obtain a new rate expression for low epoxide concentrations (Eq. 8). The rate expression contains a first-order term for epoxide concentration and explains why first-order behavior is observed at low concentrations of epoxide.

$$d[\text{Alkene}]/dt = (K_1k_2 + K_1k_3)[Tp'ReO_2][\text{epoxide}] \quad (8)$$

We were also able to confirm the burst experiment results, which showed competitive ring expansion and direct fragmentation, using the derived rate expression (Eq. 6). Under catalytic conditions, *cis*-stilbene oxide was deoxygenated at 75.3°C. The diolate concentration was measured (vs. internal standard) as the reaction progressed and the steady-state concentration of the diolate was determined to be $4.9 \times 10^{-3}$ M (average of 11 measurements over the

course of the reaction) out of a total rhenium concentration of $8.5 \times 10^{-3}$ M ($2.2 \pm 0.5$ mg/0.5 mL based on $Tp'ReO_3$). Since the 0.18 M epoxide signal dominates the $^1H$ NMR spectrum, the other rhenium species ($Tp'ReO_2$-epoxide and $Tp'ReO_2$) could lie below the detection limits. This rationalizes why the *syn*-diolate is the only observed rhenium species ($Tp'ReO_2$ might be paramagnetic and NMR silent, though calculations say it is diamagnetic). The turnover rate for the catalytic deoxygenation of *cis*-stilbene oxide was determined to be $1.4 \times 10^{-6}$ M/s. The final piece of information required is the rate constant $k_4$ for *syn-cis*-diphenyldiolate, which was already determined to be $6.0 \times 10^{-5}$ $s^{-1}$ (Table 3.2). Rearranging Eq. (6) gives

$$k_2[Tp'ReO_2\text{-epoxide}] = \text{rate} - k_4[\text{diolate}] \qquad (9)$$

Dividing Eq. (9) by Eq. (4) gives a $k_2/k_3$ ratio of 3.8. The ratio matches the stilbene/diolate ratio obtained previously, from the burst experiment, when Tp'ReO(OH)(OEt) reacted with *cis*-stilbene oxide. Even though we were successful in using the rate expression and data to confirm the ratio of $k_2/k_3$, attempts to model the concentration vs time plots observed from the catalytic reaction using our data have been unsuccessful. The major limitations are making good estimates for the equilibrium constant, the concentration of the epoxide complex, and the rate constants $k_2$ and $k_3$. Another complication is dissolution of insoluble $Tp'ReO_3$ during the initial reduction by $PPh_3$.

The competition experiment between *cis*-stilbene oxide and styrene oxide is also consistent with the new mechanistic model. The turnover frequency will be determined by three factors: (1) binding of the epoxide, (2) direct fragmentation of the coordinated epoxide complex and (3) ring expansion of the coordinated epoxide. In the presence of another epoxide, competitive binding of the epoxide dictates which epoxide will be deoxygenated more readily by effectively removing the majority of rhenium. However, the model is less successful in describing the V-shaped Hammett plot. The kinetic study already demonstrated there is a fine balanced between ring expansion and direct fragmentation. Both electron-donating and electron-withdrawing substituents could distort the balance so that one process was favored over the other. The other possibility is that the reactions were not run at saturation or that the level of saturation is different for each substituted epoxide. Since the rate of deoxygenation is a composite of all three individual processes, if saturation is not reached then the concentration of [Tp'$ReO_2$-epoxide] will be different for each epoxide tested thus effecting the rate (see Eq. 6).

### 3.18 Eyring Plots

The catalytic deoxygenation of *cis*-stilbene oxide was also carried out at five different temperatures in the range of 65-95°C (Figure 3.13). The enthalpy of activation ($\Delta H^{\ddagger}$) was obtained by plotting the ln(k/T) vs 1/T. This value was then used to calculate the entropy of activation ($\Delta S^{\ddagger}$) using the Eyring equation.[113] The

activation parameters determined were $\Delta H^{\ddagger} = 27.94 \pm 0.9$ kcal/mol and $\Delta S^{\ddagger} = -5.31 \pm 2.56$ cal/(mol K). Surprisingly, the activation parameters are very similar to the activation parameters reported for the cycloreversion of diolates.[83] Cycloreversion of diolates was recently determined to be a concerted process and direct fragmentation might also proceed through a concerted mechanism. The low $\Delta H^{\ddagger}$ is characteristic of a concerted process.[114] The negative entropy of activation would suggest some loss of translation and rotational degrees of freedom in the transition state, but the pre-equilibrium will also effect the thermodynamic properties ($\Delta S^{\ddagger}_{obs} = \Delta S_1^{\circ} + \Delta S_2^{\ddagger}$). The activation parameters for the cycloreversion of *syn*-monophenyldiolate **3-3** were also determined (Figure 3.14). Between 75 and 105°C, $\Delta H^{\ddagger} = 31.8$ kcal/mol and $\Delta S^{\ddagger} = 4.16$ cal/(mol K). The activation parameters are very similar to other diolate cycloreversion, but higher $\Delta H^{\ddagger}$ than for anti. Overall, the activation parameters by themselves offer little mechanistic information without comparison to other substrates.

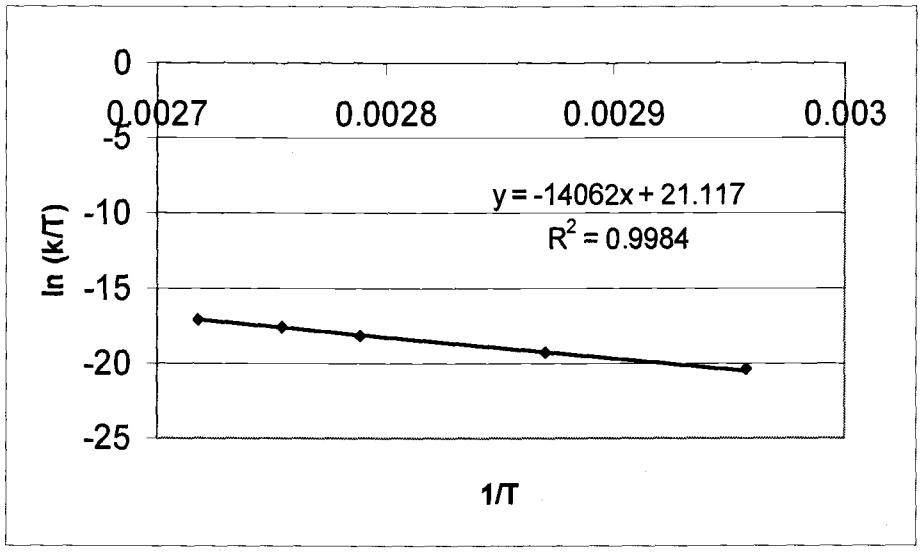


Figure 3.13 Eyring plot for catalytic deoxygenation of *cis*-stilbene oxide.

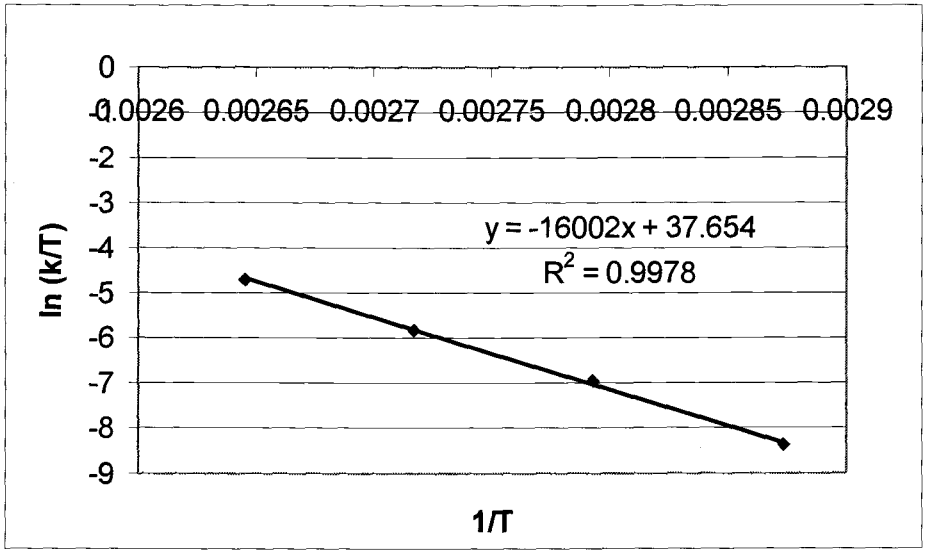


Figure 3.14 Eyring plot for cycloreversion of *syn*-monophenyldiolate **3-3**.

### 3.19 Computational Results

A computational study of the intermediates and transition states in Scheme 3.13 was undertaken at the B3LYP/LACVP*+ level using ethylene oxide as the epoxide and the (nonmethylated) Tp ligand.[115] Table 3.3 lists the calculated energies for the intermediates and transition states. A transition state search yielded two different transition states from the coordinated epoxide complex. One is the direct fragmentation transition state, which is symmetric with respect to cleavage of the C-O bonds and is 13.8 kcal/mol higher than the other transition state. The second transition state is that for ring expansion of epoxide. The structure indicates substantial asymmetry in the cleavage of the C-O bonds. One C-O bond is short (1.578 Å, versus 1.455 Å in the epoxide complex) and the other is extremely long (1.944 Å). Migration to the terminal oxo is evident, but little bond development has occurred (C-O = 3.241 Å). The structure would be consistent with a transition state containing carbocationic character (see below). The transition state structures for both processes are shown in Figure 3.15.

The relative transition state energies argue against direct fragmentation being the faster of the two processes; yet, experimentally it has been determined that direct fragmentation is 4 times faster than ring expansion. The source of the discrepancy is probably a result of the two simplifications used to minimize the computational cost. The first is the use of ethylene oxide as the epoxide. The absence of the phenyl groups will have a major effect on the energies of the

transition states. Second, the steric impact of the ligand methyl groups on the transition state energies is ignored by using the nonmethylated ligand. However, the results do demonstrate that two transition states are accessible from the coordinated epoxide complex, which is consistent with the mechanistic model in Scheme 3.13.

Table 3.3 Calculated energies for species in Scheme 3.13.

| Compound | E, Hartree[a] | ZPE[b] | $E_{rel}$[c] | $E_{rel}$, corrected[d] |
|---|---|---|---|---|
| $TpReO_2$ | -932.0351 | 141.6 | --- | --- |
| $CH_2CH_2O$ | -153.7952 | 34.8 | --- | --- |
| $TpRe(OCH_2CH_2)$ | -1085.8290 | 181.9 | +0.82 | +6.4 |
| $TpRe(O)(OCH_2CH_2O)$ | -1085.8995 | 181.9 | -43.4 | -37.5 |
| TS1: $TpReO_2\cdot\cdot OCH_2CH_2O$ (coordination of epoxide) | -1085.8280 | 186.8 | +1.44 | +11.9 |
| TS2: $TpReO_2O\cdots CH_2CH_2$ (symmetric C-O cleavage) | -1085.7938 | 186.8 | +22.9 | +33.3 |
| TS3: $TpReO_2OCH_2CH_2$ (asymmetric C-O cleavage) | -1085.8018 | 177.9 | +17.9 | +19.5 |

[a]B3LYP/LACVP*+

[b]kcal/mol

[c]kcal/mol, $TpReO_2 + CH_2CH_2O$ = 0 kcal/mol

[d]Erel + ZPE, $TpReO_2 + CH_2CH_2O$ = 0 kcal/mol

A.

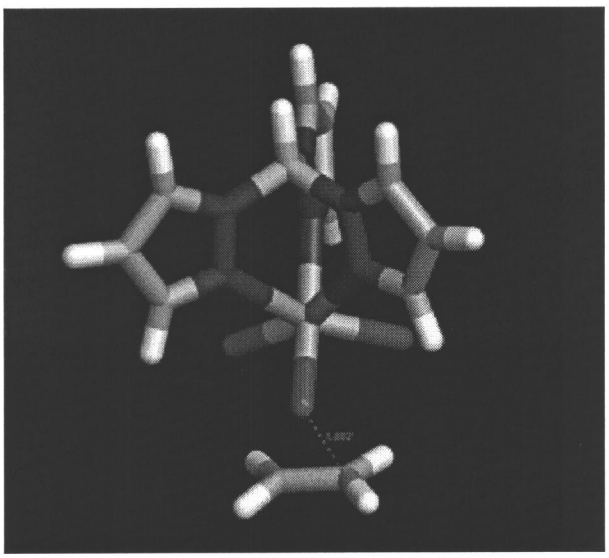

C-O 1.833 Å,
C-C 1.398 Å,
Re-O 1.946 Å,
Re=O 1.735 Å

B.

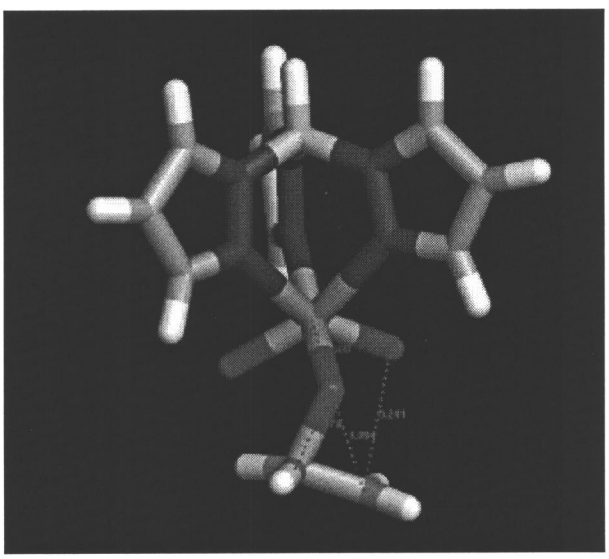

C-O 1.482, 1.992 Å;
C-O(=Re) 3.397 Å;
Re=O 1.729, 1739 Å;
Re-O 2.001 Å

Figure 3.15 Optimized transition state structures for (A) concerted fragmentation and (B) ring expansion.

### 3.20 Possible Carbocation Intermediate Involved in Ring Expansion

The transition state structure for ring expansion shows possible carbocationic character, which would be consistent in explaining why deoxygenation of *cis*- and *trans*-butene oxide was not completely stereospecific. A possible mechanism would be reversible formation of a carbocation intermediate, which can undergo bond rotation resulting in loss of stereochemistry (Scheme 3.14). The observation of minor amounts of cis-butene oxide in the $^{1}$H NMR during the deoxygenation of *trans*-butene oxide indicated that isomerization was occurring to the epoxide rather than the alkene. The observation supports reversible formation of a carbocation intermediate. The activation barrier from the carbocationic intermediate to the diolate is probably much larger for the butene oxides than the stilbene oxides; therefore, the carbocation intermediate for the butene oxides waits around longer and undergoes isomerization.

Scheme 3.14

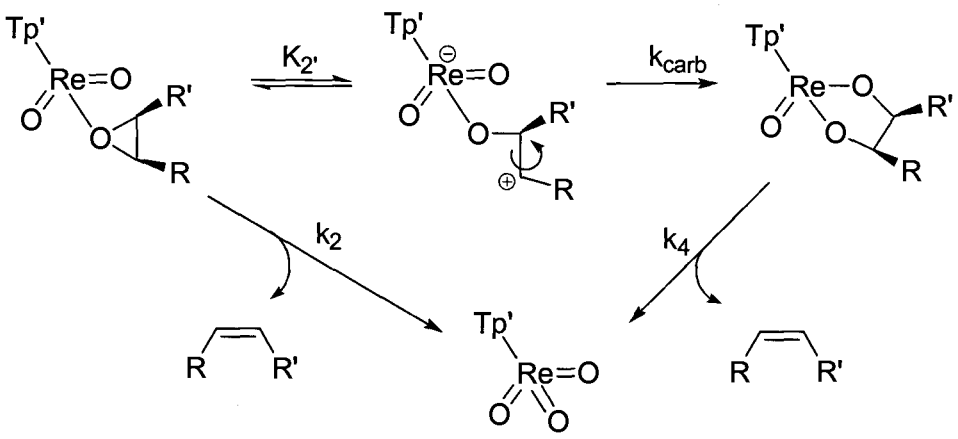


### 3.21 Experimental Evidence Supporting Direct O-atom Transfer

Reaction of $Tp'ReO_3/PPh_3$ and ethylene sulfide at room temperature led to the formation of Tp' rhenium ethanedithiolate (**3-14**) in a 30% yield.[116] Similar to epoxide deoxygenations, ring expansion and direct fragmentation are two possible mechanisms that can lead to the observed product (Scheme 3.15). However, mono- and dithiodiolate complexes were shown to be thermally stable (no cycloreversion to alkene) for more than a week at 120°C.[117] Since **3-10** is unable to cyclorevert to **3-11**, then direct fragmentation from the episulfide complex **3-9** to **3-11** must be occurring. This process is analogous to what it is observed in our catalytic system.

Scheme 3.15

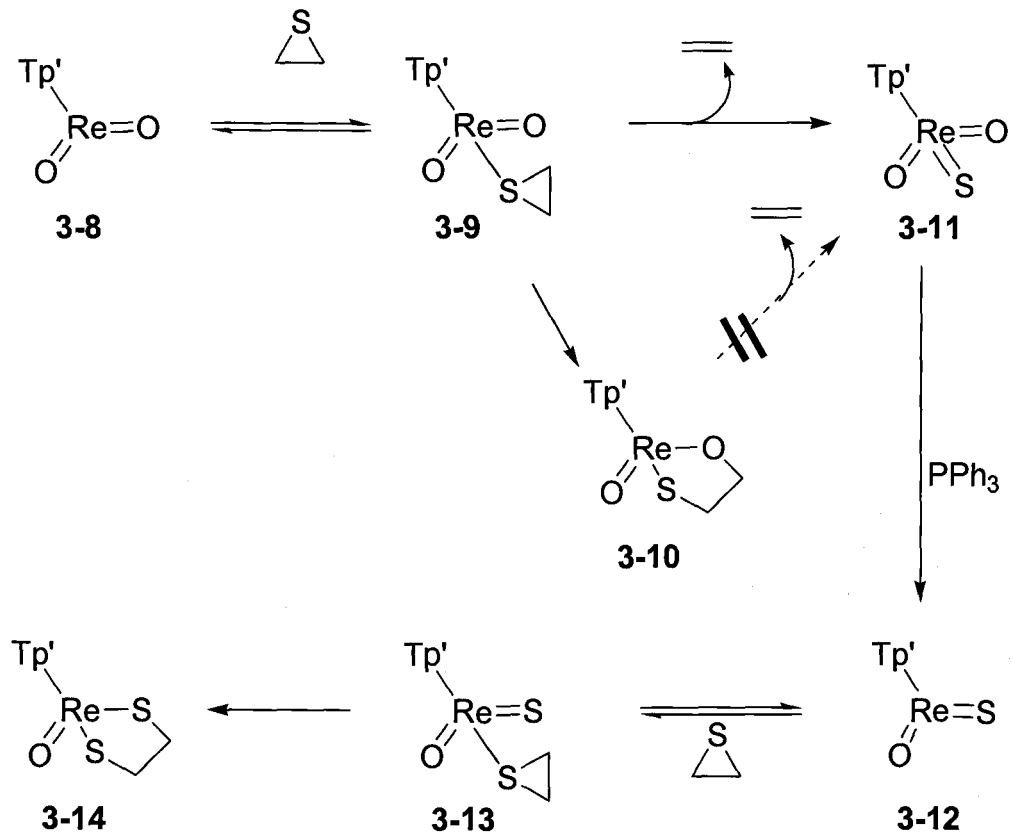


## 3.22 Conclusions

The reduction of $Tp'ReO_3$ with phosphines or phosphites generates a rhenium(V) species that is capable of deoxygenating epoxides in a catalytic fashion. The kinetic behavior of the catalytic system is complex and a V-shaped Hammett plot indicates a change in mechanism or competing processes. First-order behavior in $[Re]_T$, zero-order dependence in $[PPh_3]$ and saturation kinetics for

epoxide were observed. This type of saturation behavior is typical for Michaelis-Menten kinetics which proceeds through reversible formation of an enzyme-substrate intermediate. In analogy, the reversible formation of a coordinated epoxide complex was proposed to explain the saturation kinetics. Evidence for its existence will be further explored in Chapter 4. The epoxide complex was then shown experimentally and computationally to engage in two separate reactions: ring expansion to form a *syn*-diolate complex, and direct fragmentation to alkene and trioxide. A steady-state concentration of diolate is eventually reached explaining the "burst" of alkene production. The diolate formed is the *syn*-isomer, which is the kinetically formed product. Steric factors between the substitutents on the epoxide and the terminal oxo groups control formation of the *syn*-diolate. Direct fragmentation is the primary source of alkene. The direct fragmentation process was determined to be four times faster than ring expansion for *cis*-stilbene oxide deoxygenations. Computational modeling is consistent with the proposed mechanism.

The significance of these results is that the interaction of an oxo metal complex ($LMO_3$) with an alkene can potentially occur by a competition of an epoxidation pathway and bishydroxylation pathway. $Cp^*ReO_3$ and $Tp'ReO_3$ were shown to add to strained alkenes. The typical mechanism would be concerted [3+2] olefin addition to the two oxo groups, while the other mechanism would be [2+1] addition to a single oxo group to form a coordinated epoxide followed by ring expansion. A similar comparison can be made to alkene addition to $OsO_4$. A

relationship between the two epoxidation and bishydroxylation has been suggested,[118] but experimental evidence before now has argued against such a relationship.

# Chapter 4. Epoxide-Tethered Ligand Complex

## 4.1 Introduction

Polydentate ligands containing two types of inequivalent donors, one tightly bound to the metal center and the second weakly bonded, can stabilize coordinatively unsaturated metal complexes by temporarily blocking the coordination site. Phosphine ligands with tethered functional groups capable of binding to the metal have found numerous applications in homogenous catalysis.[119] Likewise, a cyclopentadienyl ligand containing a tethered olefin has been successfully used to isolate the elusive $d^0$ metal-olefin complex in Ziegler-Natta olefin polymerization reactions.[120] A similar approach of attaching a ligand containing a tethered "semi-labile" functional group to rhenium will be applied to our system.

## 4.2 Objectives of Tethered Epoxide Study

Numerous objectives for constructing a ligand with a tethered functional group exist for our system. First, a ligand containing a pendant functionalized side-chain might allow the direct observation or isolation of possible intermediates involved in rhenium-catalyzed epoxide deoxygenations. For example, the isolation of the proposed coordinated epoxide intermediate could be achieved by tethering an

epoxide to a Tp ligand (Scheme 4.1). This coordinated epoxide intermediate was proposed to explain the saturation kinetics observed with changes in epoxide concentration (Chapter 3), but the epoxide complex was never directly detected. Second, a comparison between the formation of the diolate from the epoxide and formation of the diolate from the alkene would help determine whether the coordinated epoxide was a viable intermediate in diolate cycloreversions. At the outset of this project, it was unclear whether the epoxide-to-diolate conversion was viable; exploring the reactivity of an isolable epoxide complex provides a rigorous test of its potential as a reactive intermediate in several reactions. Other important objectives include determining rate constants for individual steps, understanding how the epoxide binds to the metal and how entropy effects deoxygenations. Gable et al. had previously shown that diolate cycloreversions are thermoneutral and are driven by entropy.[41] Tethering the diolate removes the entropic contribution and prevents cycloreversion. Likewise, intramolecular coordination of an epoxide should be faster and more favored over intermolecular coordination because of entropy.

Scheme 4.1

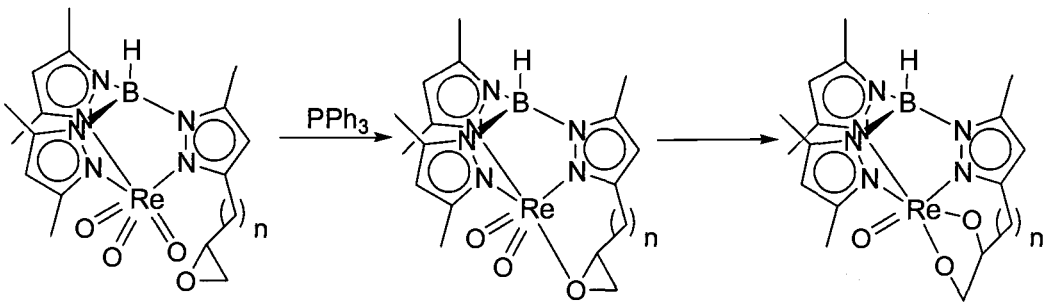


**4-1** **4-2** **4-3**

## 4.3 Epoxide-Tethered Tp Complex

The first obstacle was developing a general approach for the synthesis of the ligand (**4-6**). A general outline of how the ligand would be constructed is shown in Scheme 4.2. The pyrazole containing the tethered alkene would be prepared by alkylation of the disodium salt of acetylacetone, followed by condensation with hydrazine. Potassium dihydrido-*bis*-(3,5-dimethyl-1-pyrazolyl)borate would be generated according to the procedure developed by Trofimenko.[84] Since polypyrazolylborates are formed by thermolysis of the pyrazole with metal borohydrides, temperatures above 190°C would be required. Possible polymerization of the tethered alkene was a major concern.

Scheme 4.2

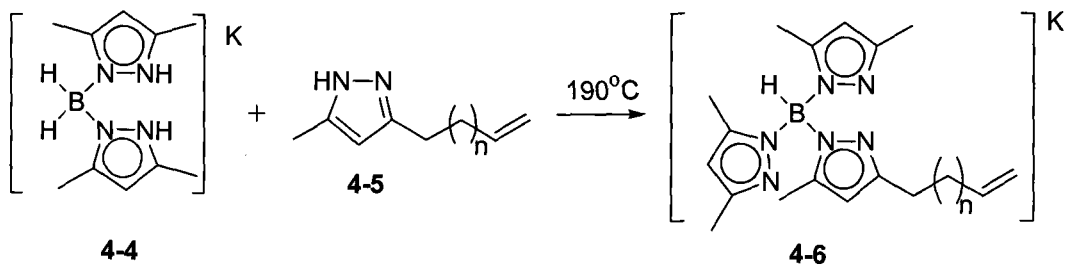


**4-4** **4-5** **4-6**

The length of the tether was also an important consideration. Longer lengths ($n \geq 2$) were expected to allow enough flexibility for epoxide to diolate conversion. Conversely, a shorter tether ($n = 1$) would allow the epoxide to coordinate but would lack enough flexibility to undergo ring expansion to diolate. Since the conversion of the epoxide to the diolate might be extremely rapid, the shorter tether ($n = 2$) offers the best chance of observing the coordinated epoxide complex **4-2**. In addition, the pyrazole with the shorter tether ($n = 2$) is the cheapest to synthesize.

Commercially available anhydrous sodium amide was used to generate the dianion of acetylacetone in liquid ammonia at -78°C.[121] The addition of allyl bromide in ether followed by the evaporation of the liquid ammonia yielded 1-octene-5,7-dione (**4-8**) in 97% yield. The substituted pyrazole was then prepared in a 51% by cyclocondensation of the dione with hydrazine monohydrochloride. The complete sequence is shown in Scheme 4-3.

Scheme 4.3

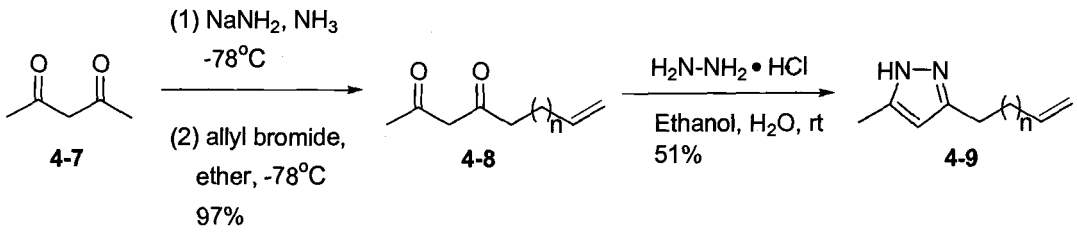


Once the pyrazole was made, potassium dihydrido-*bis*-(3,5-dimethyl-1-pyrazolyl)borate (**4-10**) was prepared in a 67% yield by heating 3,5-dimethylpyrazole with $KBH_4$ to ~ 160°C until hydrogen evolution ceased. The thermolysis of pyrazole **4-9** with potassium dihydrido-*bis*-(3,5-dimethyl-1-pyrazolyl)borate was unsuccessful. Numerous attempts were made under neat conditions and by refluxing the two compounds in toluene and anisole for multiple days. Surprisingly, the only observable product was potassium hydrido-*tris*-(3,5-dimethyl-1-pyrazolyl)borate **4-12** (Scheme 4.4). The remainder of the reaction has not been identified. Scrambling of the pyrazoles by reversible pyrazole group exchange has been reported for other potassium salts.[122] Therefore, a reevaluation of our approach was in order.

Scheme 4.4

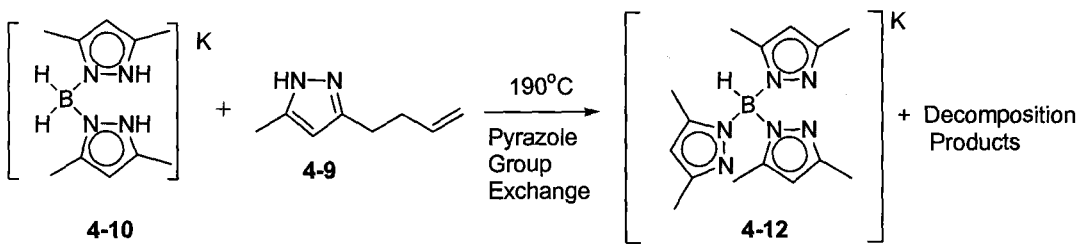


## 4.4 Epoxide-Tethered Cp* Complex

The synthesis of a peralkylated cyclopentadienyl ligand with a 3-butenyl side-chain was chosen as an alternative ligand. It avoids all the problems encountered with the poly(pyrazolyl)borate route, but comparisons to the catalytic process (where L = Tp') are still possible. In addition, more direct comparisons can be made to the less efficient catalytic process that was catalyzed by $Cp^*ReO_3$. Once again, the length of the tether was kept to a minimum (n=2) to ensure possible coordination of the epoxide, yet prevent ring expansion to the diolate.

The synthesis of 1-(3-butenyl)-2,3,4,5-tetramethylcyclopentadiene (**4-13**) has been previously reported.[123] The addition of 2,3,4,5-tetramethylcyclopent-2-enone to a diethyl ether solution of the homoallyl Grignard, followed by the addition of acidic ion-exchange resin Amberlite IR-120® resulted in a 66% yield of **4-13**. **4-13** exists as a mixture of three possible isomers (Scheme 4.5).

Scheme 4.5

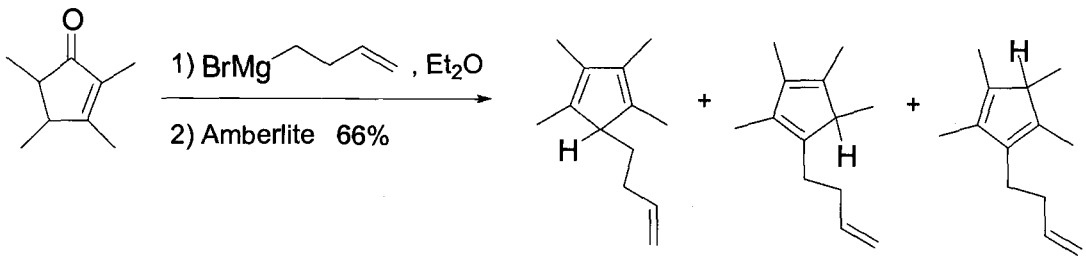


**4-13**

In the case of pentamethylcyclopentadiene, the metal is typically added to the ligand by reaction of $Re_2(CO)_{10}$ with pentamethylcyclopentadiene at 150-210°C.[124] High yields (95%) are generally obtained. The reaction is a dramatic improvement over the other literature procedures[125,126] [$(CO)_5ReCl$ + $Li^+C_5Me_5^-$, 4%; $(CO)_5ReCH_3$ + $C_5Me_5H$; 26%]. Unfortunately, the substitution of **4-13** for pentamethylcyclopentadiene resulted in a low yield (yield = 9%; average of three runs). The addition of the mixed anhydride $CF_3CO_2ReO_3$ to a solution of 1-(3-butenyl)-2,3,4,5-tetramethylcyclopentadienylthallium, which was generated from 1-(3-butenyl)-2,3,4,5-tetramethylcyclopentadiene and thallium(I) ethoxide, resulted in unidentified products. A similar result was observed when $CF_3CO_2ReO_3$ reacted with $(C_5Me_5)Sn(n\text{-}C_4H_9)$.[127] A mismatch of redox potentials between $Cp^*SnBu_3$ and the acyl perrhenate was attributed to the failure.

The procedure which was eventually used is shown is Scheme 4.6. In situ formation of 1-(3-butenyl)-2,3,4,5-tetramethyl cyclopentadienylthallium in

benzene, followed by the addition of rhenium pentacarbonyl bromide produced the tricarbonyl complex **4-15**. The thermodynamic driving force for this reaction is formation of insoluble thallium(I) bromide. The reaction is also low yielding, but is still an improvement over the $Re_2(CO)_{10}$ procedure. Unfortunately, scaling up the reaction to obtain an appreciable amount of product was prohibitive because of the high cost of rhenium pentacarbonyl bromide.

Scheme 4.6

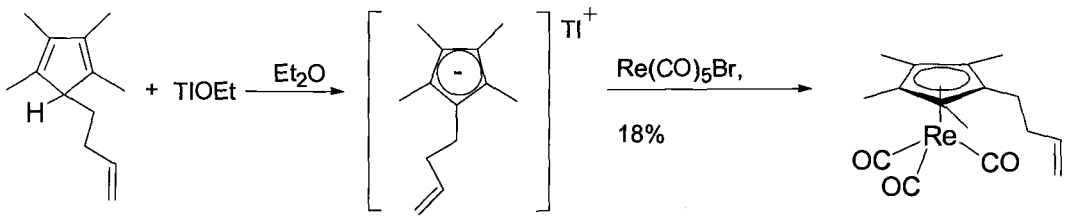


**4-13** **4-14** **4-15**

**4-15** was fully characterized by NMR and IR spectroscopy as well as FAB mass spectroscopy. In the IR spectrum two metal carbonyl stretching frequencies were observed at 2010 and 1918 $cm^{-1}$ and were comparable to the values reported for $(C_5Me_4Et)Re(CO)_3$ ($\nu$ = 2014 and 1923 $cm^{-1}$).[128] The carbonyl stretching frequencies were about 23 $cm^{-1}$ less than those corresponding to $(C_5H_5)Re(CO)_3$ ($\nu$ = 2034 and 1941 $cm^{-1}$).[129] Increasing the alkyl substitution on the ligand increases the electron density on the metal. This increases the amount of π-backbonding from rhenium to the carbon monoxide ligands which in turn lowers the carbon-

oxygen bond order and hence the carbonyl stretching frequency. NMR and IR spectroscopic data clearly indicate that the 3-butenyl substituent of the ligand is not interacting with the rhenium center. Rhenium alkene complexes of the general formula $LRe(CO)_2(\eta^2\text{-alkene})$ show a large up-field shift for the alkene protons in the $^1H$ NMR spectrum.[130]

Oxidative decarbonylation of carbonyl rhenium(I) complexes has been achieved using a variety of oxidizing reagents. The highest yielding procedures are either oxidation of $LRe(CO)_3$ with 100% hydrogen peroxide/MTO[131] or with $Mn_2O_7$.[132] Unfortunately, both procedures risk a possible explosion hazard. Alternative oxidizing reagents, which operate under safer and milder conditions, include ozone[133], $H_2O_2$ [134] and $^t$BuOOH[135]. Unfortunately, the yields are generally $\leq 50\%$. One procedure that has been successfully used in our group to achieve high yields of the desired trioxide is the use of a catalytic amount of $Re_2O_7$ and *bis*-trimethylsilyl peroxide (BTMSP). Sharpless et al. had reported that inorganic rhenium oxides (e.g., $Re_2O_7$, $ReO_3(OH)$ and $ReO_3$) and BTMSP effectively epoxidized olefins.[136] The same conditions were shown to effectively decarbonylate $Cp^*Re(CO)_3$ to the trioxide in a 85% yield.[82] Consequently, $Re_2O_7$/BTMSP was originally used to oxidatively decarbonylate **4-15**. An additional advantage of using the $Re_2O_7$/BTMSP procedure is that epoxidation of the 3-butenyl substituent could also occur saving an additional step later.

A test reaction reaction combining 20mg of **4-15**, 1 mole percent of $Re_2O_7$ and twenty equivalents of BTMSP in $CH_2Cl_2$ at 0°C generated the trioxide complex

**4-16** (no evidence of alkene epoxidation was seen). The IR spectrum showed the disappearance of the CO stretches of **4-15** (2010 and 1918 $cm^{-1}$) and the appearance of new Re=O peaks (909 and 879 $cm^{-1}$). However, attempts to scale up the reaction using $Re_2O_7$/BTMSP were unsuccessful. Eventually the $^tBuOOH$ procedure was used instead.[135] The reproducible decarbonylation of **4-15** by refluxing a benzene solution of $^tBuOOH$ and **4-15** was achieved in a 58% yield (Scheme 4.7). The yield was a 28% improvement compared to the value reported for $Cp^*Re(CO)_3$ decarbonylation (30%).

Scheme 4.7

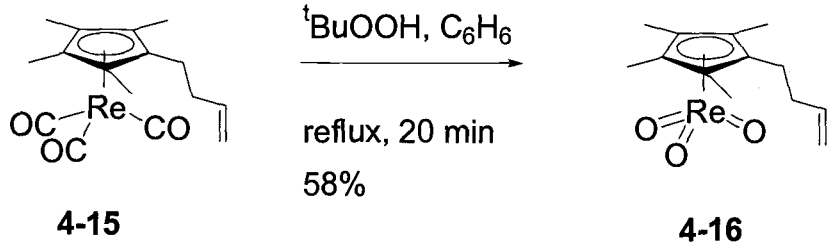


**4-15** **4-16**

Epoxidation of the 3-butenyl side-chain in **4-16** by 3-chloroperoxybenzoic acid (MCPBA) afforded **4-17** in a 46% yield (Scheme 4.8). The compound was moderately oxygen-sensitive and decomposed if concentrated under reduced pressure using a rotary evaporator. The $^1H$ NMR spectrum clearly shows a coupling pattern typical of a mono-substituted epoxide (Figure 4.1), while in the $^{13}C$ NMR spectrum two new signals at $\delta$ 52 and 47 ppm were assigned to the

epoxide carbons. The two diastereotopic methylenic protons at δ 1.29 and 1.12 ppm in the $^1$H NMR spectrum consistently over-integrated (each resonance over-integrated by 1H) because of a broad hump in the baseline. A 2D COSY experiment was performed to show that the two resonances at δ 1.29 and 1.12 ppm belong to the complex **4-17** (Figure 4.2). Correlations were observed with each other and also with the resonances at δ 2.29 and 2.33 ppm. The IR spectrum showed two oxo stretches at 908 and 877 cm$^{-1}$, almost identical to the alkene precursor **4-15**.

Scheme 4.8

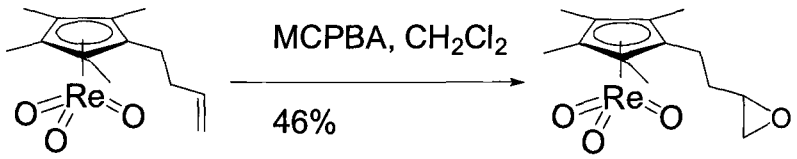


**4-16** **4-17**

Figure 4.1 $^{1}$H NMR spectrum of **4-17** in $C_6D_6$.

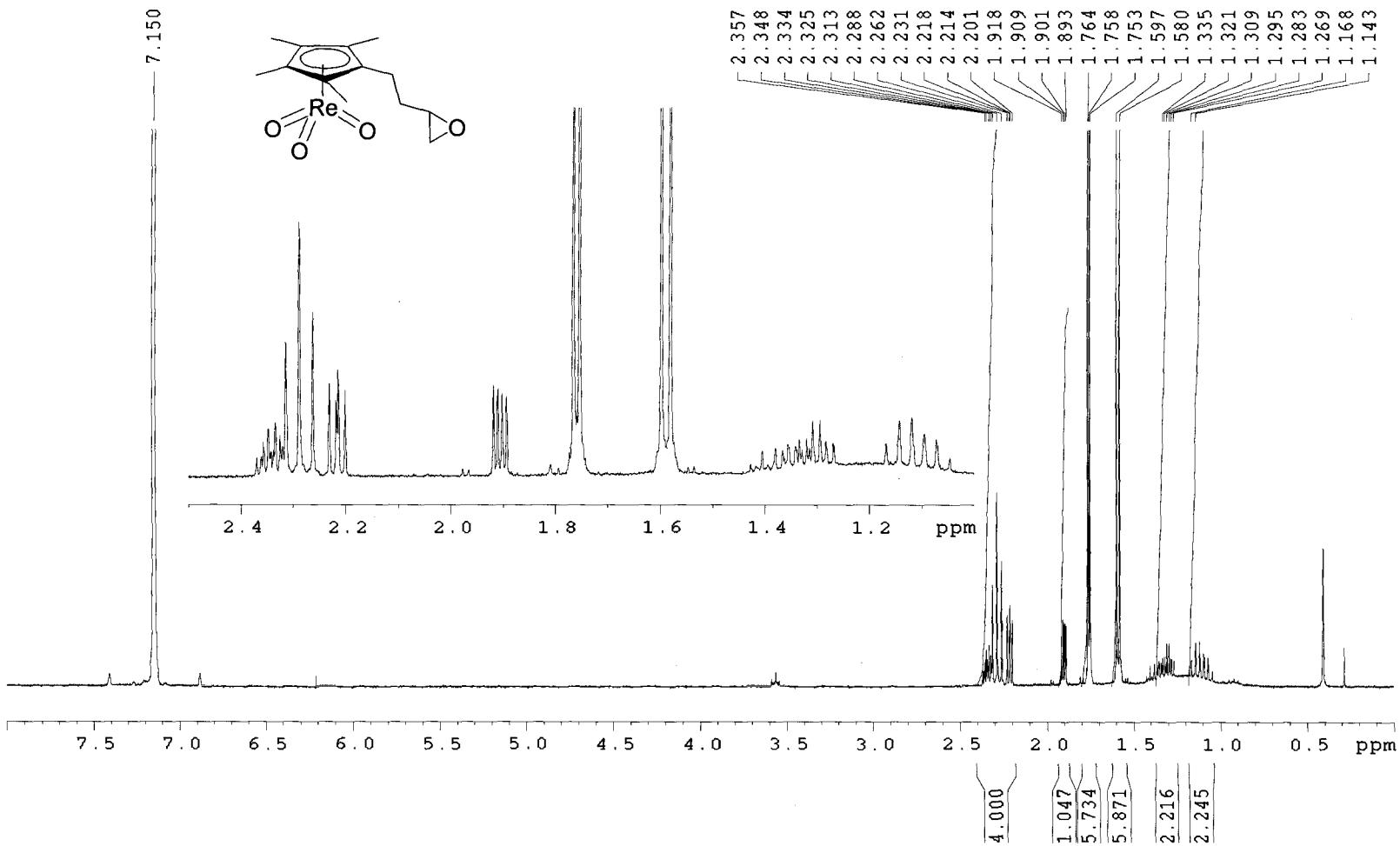

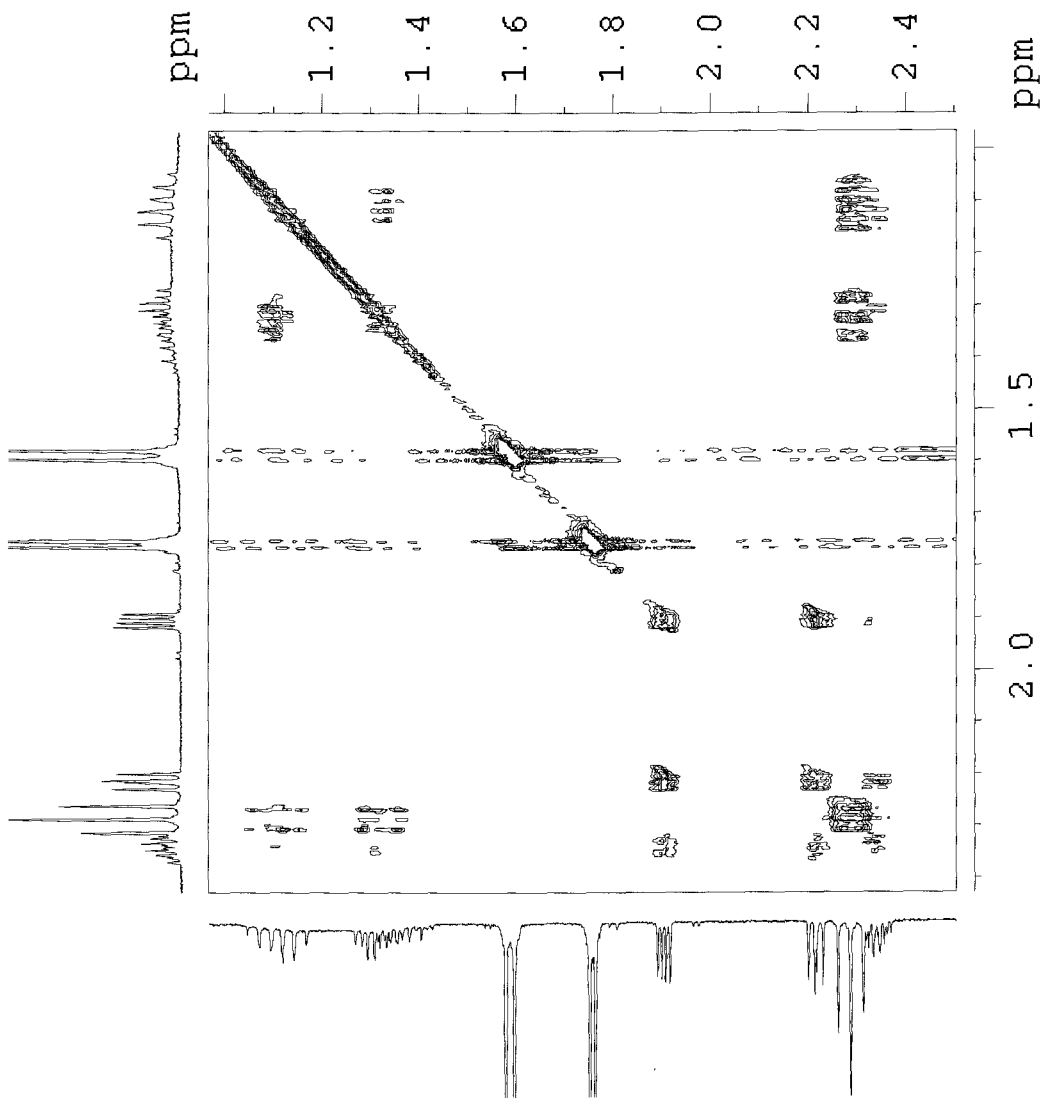


Figure 4.2 COSY spectrum of **4-17** in $C_6D_6$.

## 4.5 Coordinated Epoxide Complex

Reduction of the epoxide derivative **4-17** with triphenylphosphine or polymer supported triphenylphosphine generates the formally 16-electron species **4-18** which is immediately trapped by intramolecular coordination of the epoxide to from complex **4-19** (Scheme 4.9). The coordinated epoxide complex is oxygen-sensitive and could be converted quantitatively to **4-17** by exposing solutions to air for 15hr. Purification of complex **4-19** has so far been unsuccessful; chromatographic separation proved to be unsatisfactory (complex **4-19** failed to elute from the column). The IR spectrum for **4-19** showed only a single Re=O stretch at 932 $cm^{-1}$ (**4-17** shows two oxo stretches at 908 and 877 $cm^{-1}$). The high-frequency oxo stretch in the IR spectra for **4-19** indicates an increase in the rhenium-oxygen bond strength. This would be consistent with a dioxo complex since removal of an oxo group will reduce the competition of the remaining oxo groups to $\pi$-bond into the empty d orbitals. The observation of only one oxo stretch may be a result of the symmetric and asymmetric stretches occurring at similar frequencies (the separation between the two stretches may be small giving the appearance of one oxo stretch) or that one of the stretches is extremely weak (a small stretch is observed at 872 $cm^{-1}$, but isotopic substitution would be required to determine if the stretch was a Re=O stretch). The $^1H$ NMR spectrum reveals that intramolecular coordination of the epoxide has occurred (Figure 4.3). The figure compares the $^1H$ NMR spectra of **4-19** with **4-17**. A significant downfield shift of

the three resonances for the epoxide (δ 2.60, 2.29 and 2.04 ppm) was observed, indicating complexation of the epoxide to the rhenium center. A 2D COSY experiment allowed the assignment of all the signals and verified that one of the epoxide proton resonances lies directly underneath the resonance at δ 2.03 ppm (Figure 4.4). In addition, a change in the coupling pattern is observed for the two diastereotopic methylenic protons closest to the peralkylated cyclopentadienyl ring. In compound **4-17** the side-chain is freely rotating in space and the chemical shifts and coupling constants of the two diastereotopic protons become averaged. This explains the triplet at δ 2.29 ppm which is observed in the $^1$H NMR spectra (Figure 4.1). Conversely, in compound **4-19** the side-chain is locked in one particular confirmation and enhances the non-equivalence of the two diastereotopic methylenic protons closest to the ring. High resolution mass spectroscopy confirms a molecular formula consistent with the compound proposed as **4-19**.

Scheme 4.9

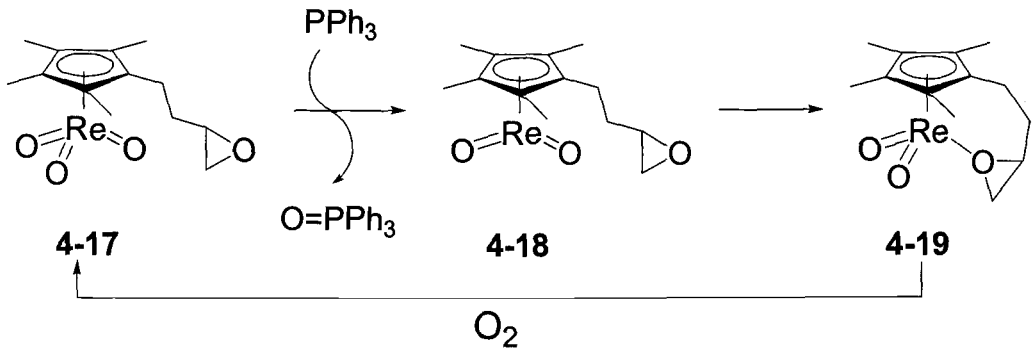

Figure 4.3 $^{1}$H NMR spectrum of **4-17**(top) and **4-19**(bottom) in $C_6D_6$.

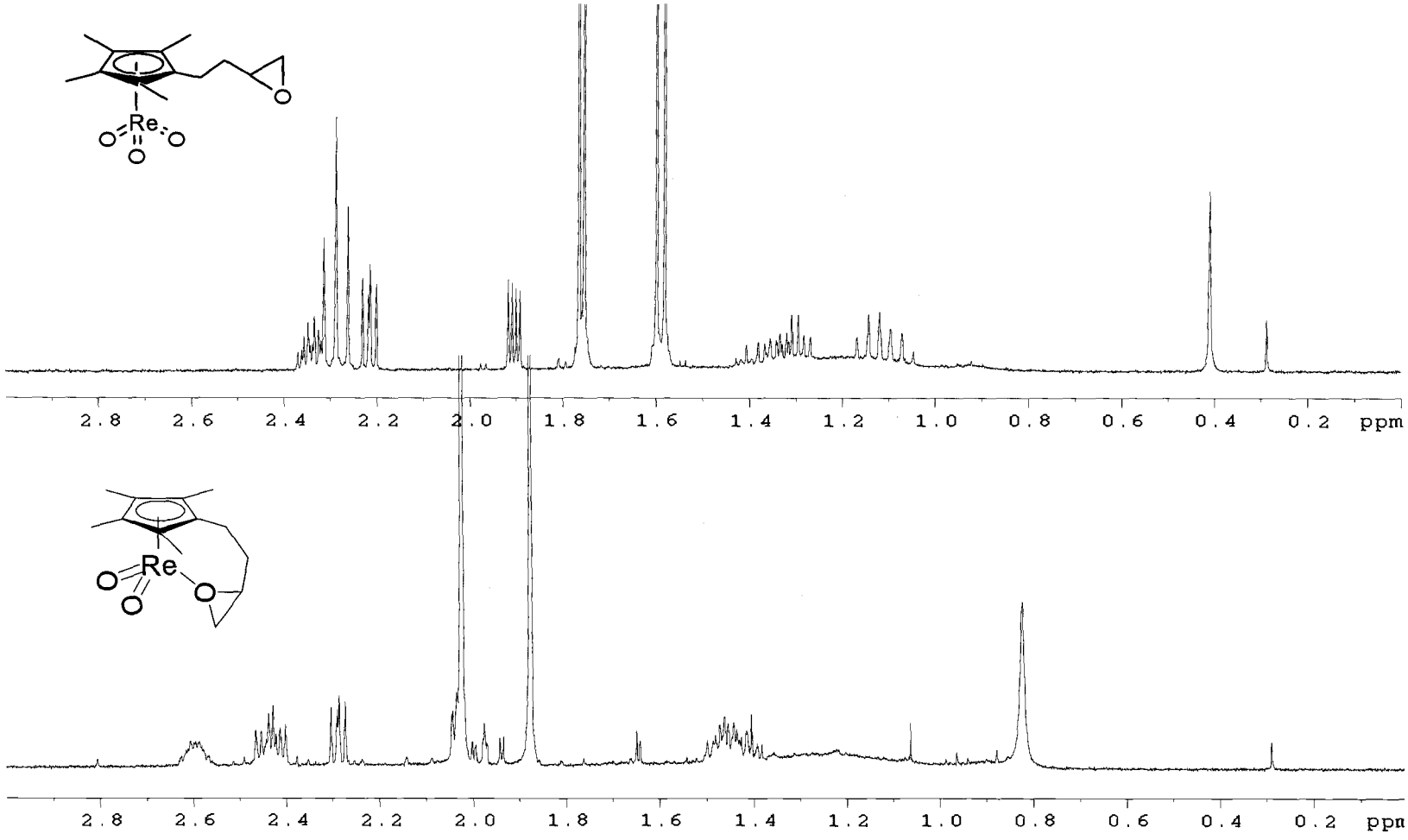

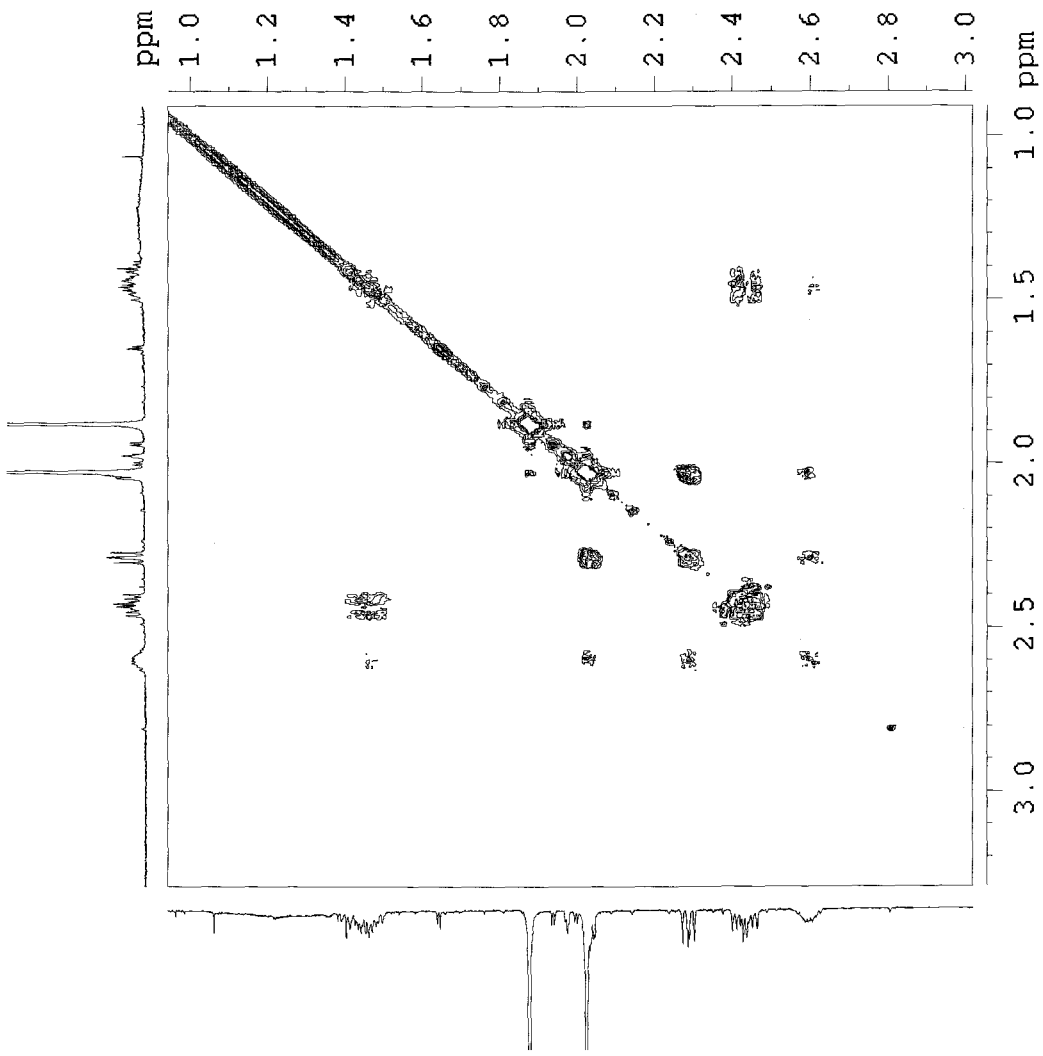


Figure 4.4 COSY spectrum of **4-19** in $C_6D_6$.

## 4.6 nOe and Molecular Mechanics Study

An nOe study in conjunction with molecular mechanics modeling also helped establish that intramolecular coordination of the tethered epoxide to the rhenium center had occurred. Geometry optimization of both **4-18** and **4-19** were performed using Spartan v. 5.0[137] using the MMFF94 force field.[138] The optimized structures of **4-19** and **4-18** are shown in Figure 4.5. Calculated distances are shown as possible nOe interactions with the methyls on the ligand (the precondition for an appreciable nuclear Overhauser effect is that the distance *r* between two nuclei must be small i.e. $\leq$ 2.5 Å).[139] For **4-19** the calculated structure would predict four possible (distances are $\leq$ 2.5 Å) nOe interactions. Conversely, for **4-18** only two nOe interactions would be predicted. The nOe spectrum for **4-19** is shown is Figure 4.6. Irradiation of the signal at δ 1.88 ppm led to an enhancement of four different resonances as predicted from the molecular mechanics modeling. Enhancements occurred for the methyl signal (two $CH_3$ groups actually overlap) at δ 2.03 ppm, for the methylene group closest to the ring at δ 2.44 ppm, for the methylene group alpha to the epoxide at δ 1.45 ppm and for the CH group of the epoxide at δ 2.60 ppm. Had the epoxide been freely rotating in open space then only two nOe interactions would have been observed. This was demonstrated by an nOe study on compound **4-17**. In compound **4-17**, similar to compound **4-18**, the side-chain containing the epoxide is freely rotating in space. Irradiation of the

methyl signal at δ 1.76 ppm led to an enhancement of the two methyl signals at δ ~ 1.58 ppm and the methylene group closest to the ring at δ 2.29 ppm.

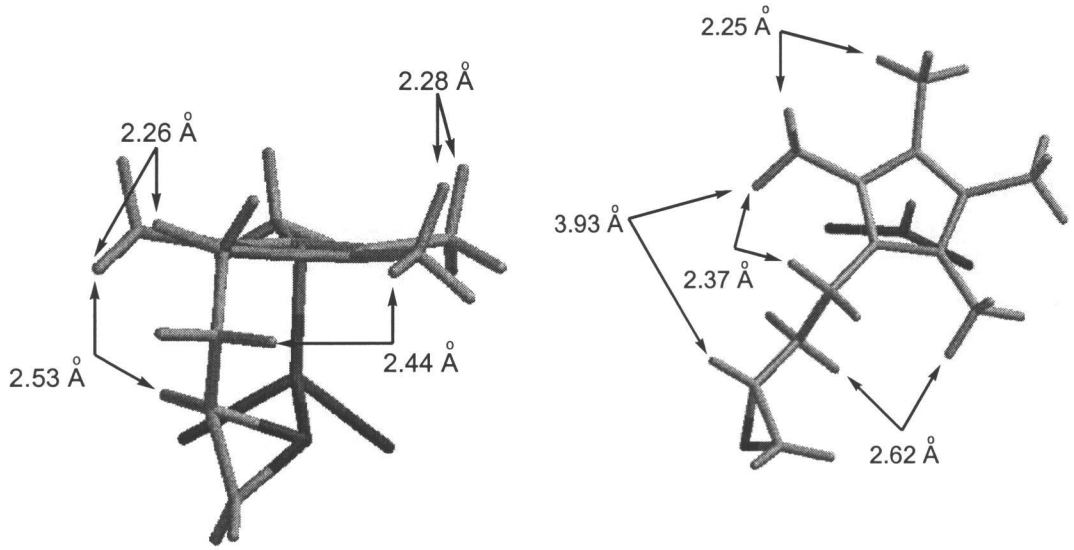


Figure 4.5 Optimized structures for **4-19** (left) and **4-18** (right) along with the distances (Å) separating the indicated nuclei.

Figure 4.6 nOe spectrum of **4-19**.

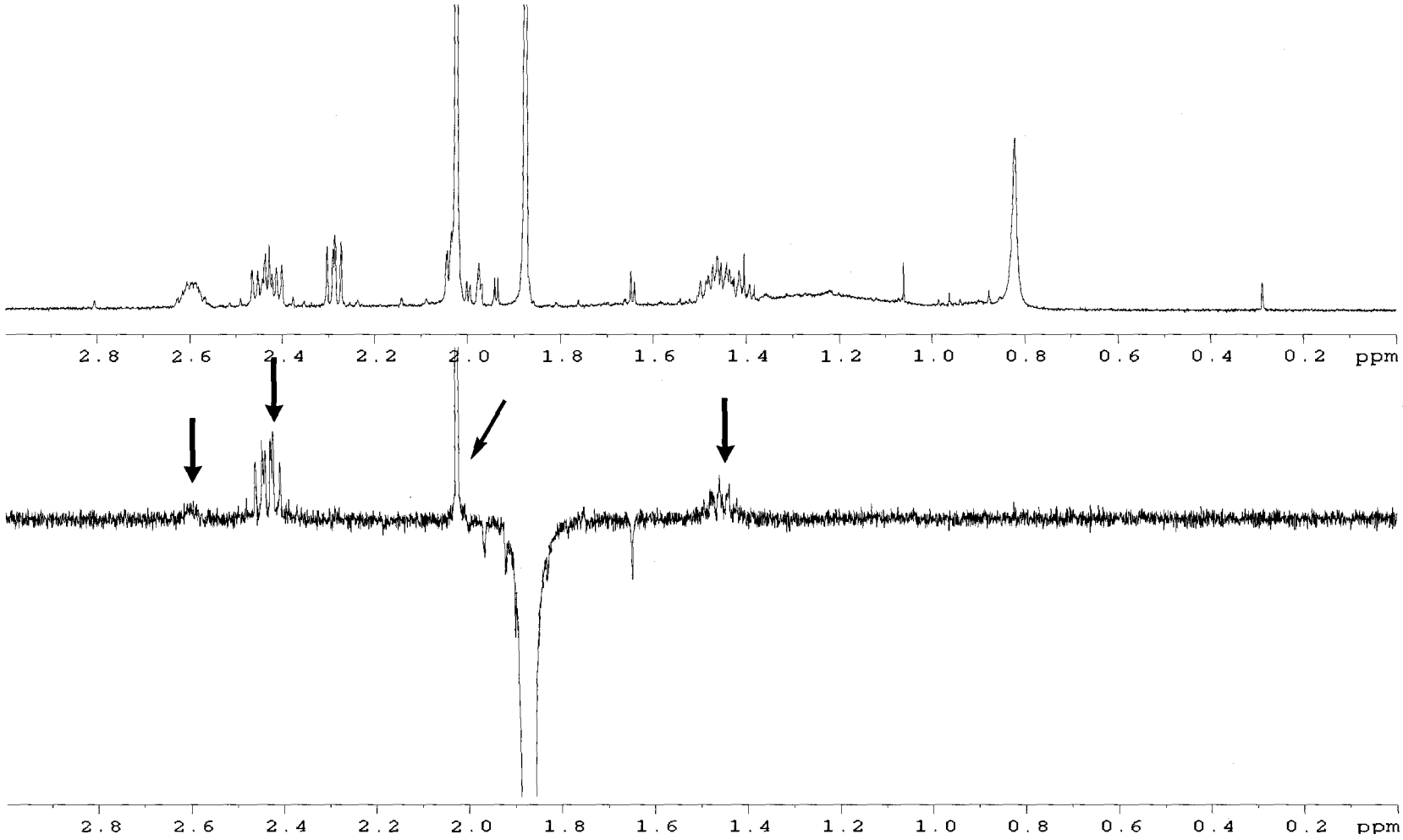

Figure 4.7 nOe spectrum of **4-17**.

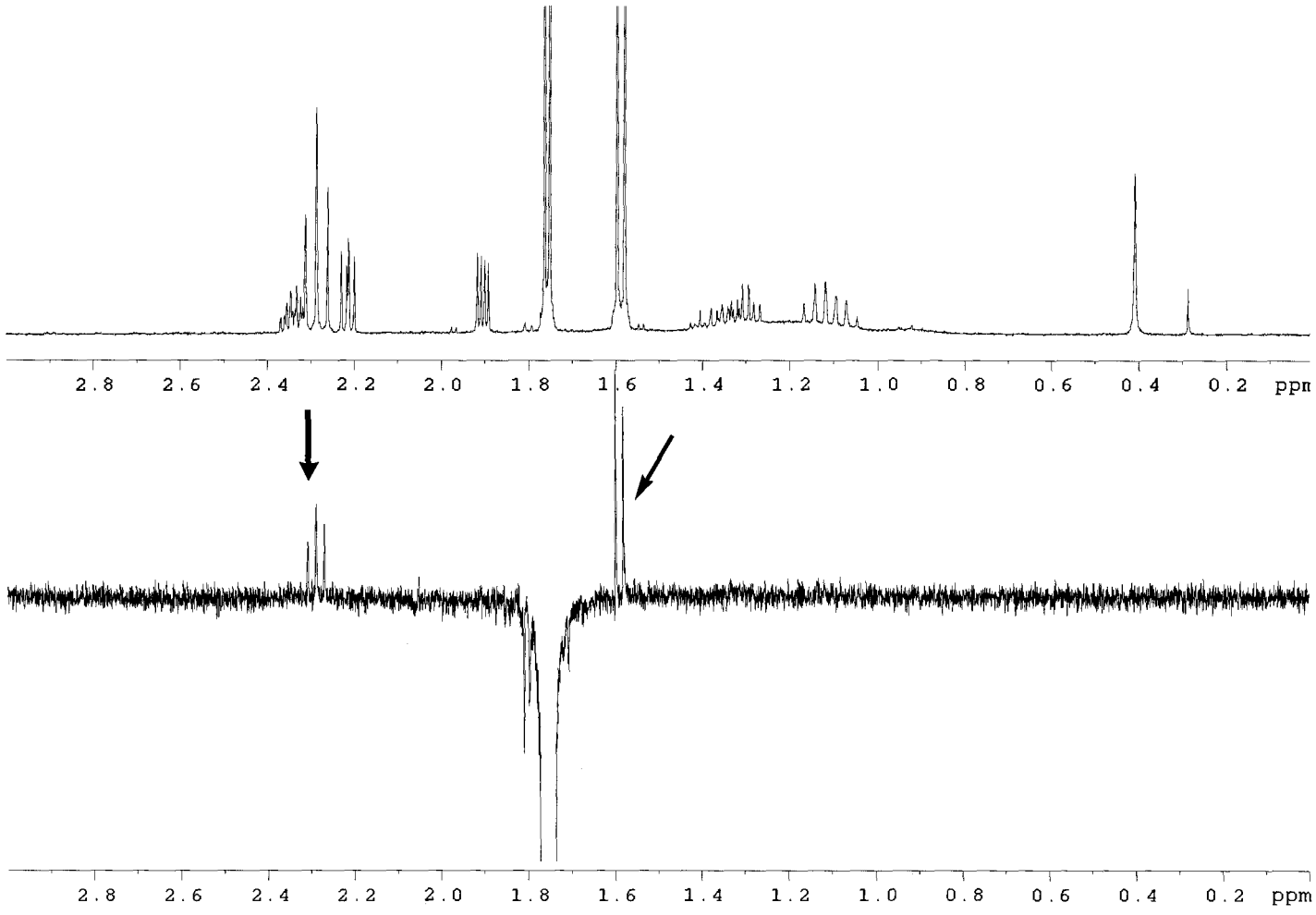

## 4.7 Conclusions

The first objective of this project was to develop a general approach to the synthesis of a epoxide-tethered Tp or Cp* complex. A rhenium(V) complex (**4-17**) containing a peralkylated ligand with a tethered epoxide has been successfully synthesized and characterized. Reduction of this complex with triphenylphosphine generates a reduced $d^2$ rhenium species that is trapped by the tethered epoxide. Preliminary experimental data and molecular mechanics modeling support intramolecular coordination of the epoxide to the rhenium center. A similar rhenium epoxide complex has been implicated in rhenium-catalyzed epoxide deoxygenations. The coordinated epoxide complex is proposed to partition between ring expansion and direct fragmentation to alkene. However, the epoxide complex was never been detected directly. This work confirms that the coordinate epoxide is a viable intermediate. However, the main goal is to study the structures, bonding, reactivity and dynamic properties of different rhenium epoxide complexes that are relevant to catalytic epoxide deoxygenations. This work has provided the initial groundwork but the more interesting chemistry lies ahead. An X-ray crystal structure of **4-19** is needed to absolutely confirm the structure proposed. In addition, rhenium epoxide complexes with longer tethers will need to be synthesized in order to observe the epoxide to diolate conversion.

# Chapter 5. Conclusion

In the course of studying rhenium(V) diolate cycloreversions, $(Cp^*ReO)_2(\mu\text{-}O)_2$ was shown to stereospecifically abstract oxygen from epoxides.[56] The development of a process for deoxygenating epoxides using catalytic amounts of $(Cp^*ReO)_2(\mu\text{-}O)_2$ was developed shortly afterwards.[59] However, comproportionation of $Cp^*ReO_2$ and $Cp^*ReO_3$ produced an unreactive tetranuclear cluster that prevented catalysis. This prompted us to determine if a change in ligand could result in efficient catalysis.

The reaction of epoxide, triphenylphosphine (1:1 stoichiometry) and catalytic amounts of $Tp'ReO_3$ in benzene at elevated temperatures resulted in efficient epoxide deoxygenation. The deoxygenation of *cis*- and *trans*-stilbene oxide was stereospecific, while deoxygenation of *cis*- and *trans*-butene oxide produced minor amounts of the opposite isomer. The relative reactivity of different epoxides demonstrated how the effect of electronic and steric structure affects the deoxygenation process. Terminal epoxides were deoxygenated faster than internal epoxides and *cis*-epoxides reacted faster than *trans*-epoxides. Increasing alkyl substitution resulted in a slower rate. Conversely, an increase in the rate was observed with increasing aryl substitution.

Numerous functional groups were tolerated. A total of twenty-eight different epoxides were tested as possible substrates and only three were incompatible with the catalyst. In addition, deoxygenation of 1,2-epoxydodecane

in a 94% yield was performed on a preparative scale. These two results alone demonstrate the synthetic utility of this reaction. Most reagents known to deoxygenate epoxides require multiple steps, stoichiometric conditions, harsh reaction conditions and complicated reagents. Loss of stereochemistry and incompatibility with other functional groups often occurs as well. Our system is a one-step procedure using catalytic amounts of rhenium run at relatively low temperatures (75-105°C). Furthermore, the catalyst $Tp'ReO_3$ is synthesized in high yields in three simple steps and can be easily scaled up to make gram quantities of catalyst.

Ligand modification was also shown to suppress formation of the dimeric bridged oxo compound $[LReO]_2(\mu\text{-}O)_2$ that resulted from reduction of $LReO_3$ when L = Cp*, Tp and Tk. Instead, reduction of $Tp'ReO_3$ with triphenylphosphine forms a monomeric rhenium(V) species with $C_s$ symmetry. Two possible isomers were proposed but experimental evidence and computational modeling support the formation of $Tp'Re(O)(OH)_2$. The oxo bis-hydroxide complex is extremely reactive and is effective at stoichiometric epoxide deoxygenations. Loss of water to form $Tp'ReO_2$ (species responsible for deoxygenations) was shown to be a necessary preequilibrium process for epoxide deoxygenations. Loss of water is also very facile since Tp'ReO(OH)(OEt) is immediately formed upon contact with ethanol. Both the oxo bis-hydroxide and ethoxide complexes are efficient catalysts for O-atom transfer.

A kinetic study of the catalytic reaction revealed that the reaction is quite complex. The kinetic data showed an initial "burst" of alkene production followed by pseudo-zero order behavior for alkene formation later in the reaction. First-order behavior in $[Re]_T$, zero-order dependence in $[PPh_3]$ and saturation behavior for epoxide were observed. Saturation behavior suggests reversible formation of a catalyst-substrate intermediate whose decomposition is rate-controlling. The intermediate was proposed to be a coordinated epoxide complex, but direct observation of the complex under catalytic conditions has never occurred. Instead, the only rhenium species observed was the *syn*-Tp'Re(O)(diolate) complex, formed by ring expansion of the epoxide. *syn*-Diolate formation was determined experimentally to be kinetic in origin. However, cycloreversion of the *syn*-diolate was unable to account for the observed turnover frequency. Therefore, a second pathway was proposed to account for alkene formation. Direct fragmentation of the coordinated epoxide complex was proposed as the second alkene-forming process. The direct epoxide fragmentation process was determined to be the main source of alkene and was found to be four time faster than ring expansion. A rate law incorporating both pathways was developed and could account for the kinetic behavior. Computational modeling also supports the proposed mechanism.

An epoxide-tethered peralkylated cyclopentadiene complex has also been synthesized in an attempt to observe any possible intermediates involved in rhenium-catalyzed epoxide deoxygenations. Reduction of this complex produces a rhenium(V) species that is immediately trapped by the epoxide attached to the side-

chain. Experimental evidence and molecular mechanics modeling support intramolecular coordination of the epoxide to the rhenium center. This species is analogous to the coordinated epoxide complex proposed in our catalytic system.

The implication of all these results is that oxo metal complexes must be capable of both epoxidation and bishydroxylation processes. Take for example, the chromyl chloride epoxidation mechanism (Scheme 3.4). Three mechanisms were proposed to account for epoxide, chorohydrin and vicinal dichloride formation: (1) Direct addition of olefins to one of the oxygen atoms in a single step, (2) [2+2] cycloaddition of olefin to the oxo group on chromium, and (3) [3+2] cycloaddition of olefin to two oxo groups on chromium. However, none of the proposals took in consideration that maybe multiple pathways might be operating simultaneously. The direct addition and [3+2] cycloaddition pathways are essentially the microscopic reverse of direct epoxide fragmentation and diolate cycloreversion. In fact, it is possible that one pathway gives predominantly epoxides, while the second pathway gives predominantly chlorohydrins and vicinal dichlorides. Numerous other examples exist where two possible pathways might be competing. However, one exciting implication of these results is that it may be possible to favor one pathway over the other by simply changing the steric or electronic nature of the ligand.

# Chapter 6. Experimental

## 6.1 General Methods

All reactions were performed under an inert atmosphere using standard Schlenk and vacuum line techniques[140] and a nitrogen-filled glovebox (Vacuum-Atmospheres Co. HE 493), expect when noted. All solvents were dried, degassed and distilled prior to use. Ether and THF were distilled from Na/benzophenone, hexane and benzene from K/Na alloy, acetonitrile and dichloromethane from $CaH_2$ and dimethyl sulfoxide and toluene from 4 Å molecular sieves. Molecular sieves (4 Å, Fisher) were activated by heating under vacuum (0.01 mbar) at 250°C overnight prior to use. Infrared spectra were run on a Nicolet Magna-IR560. UV-vis spectra were obtained on a Shimadzu UV-2101PC. Samples <5mg were weighed on a calibrated Cahn Model 29 microbalance. Starting reagents were used as purchased from Aldrich or Acros (Fisher) except when noted. All deuterated solvents were purchased from Cambridge Isotopes. Silica gel (32-63 mesh) used for flash column chromatography was purchased from Selecto, Inc.

## 6.2 NMR Measurements

NMR spectra were recorded on either a Brüker DP300 (operating at 300.13 MHz for proton or 75.409 MHz for carbon) or a Brüker DPX400 (operating at

400.134 MHz for proton or 100.614 MHz for carbon). $^{1}H$ chemical shifts are referenced using the residual solvent protons and are reported relative to tetramethylsilane. $^{13}C$ chemical shifts are reported relative to tetramethysilane and are referenced to solvent peaks.

### 6.3 Measurement of Kinetics

Kinetics were followed by measuring $^{1}H$ NMR integrations; a relaxation delay of 15-30 s (>5 $T_1$) per pulse was used in collecting NMR spectra to ensure accurate integration. 1,4-di-*tert*-butylbenzene was used when necessary as an internal integration standard. All epoxide solutions were prepared by mixing epoxide, $PPh_3$ and 1,4-di-*tert*-butylbenzene in the appropriate solvent, then predrying the mixture over $CaH_2$ before adding to solid $Tp'ReO_3$.

A representative example is given for deoxygenation of *cis*-stilbene oxide. *cis*-Stilbene oxide (0.11 g, 0.56 mmol), triphenylphosphine (0.16 g, 0.61 mmol) and 1,4-di-*tert*-butylbenzene (1.61 mg, 0.0085 mmol) was dissolved in 3 mL of $C_6D_6$ and dried over $CaH_2$. A 0.5 mL aliquot was then added to a NMR tube containing $Tp'ReO_3$ (2.41 mg, 0.0045 mmol) and sealed under vacuum. The tube was then submerged and heated to 75.3 ± 0.1°C in a water/ethylene glycol bath. The sample tube was periodically removed and cooled to 25°C and the $^{1}H$ NMR spectrum was recorded. Other kinetic measurements used analogous procedures.

## 6.4 Synthetic Procedures

### Potassium hydrido-*tris*-(3,5-dimethyl-1-pyrazolyl)borate

This was prepared according to Trofimenko.[84] A mixture of 3,5-dimethylpyrazole (11.43 g, 119.0 mmol) and potassium borohydride (1.60 g, 29.66 mmol) were placed into a 100 mL roundbottom equipped with a stirbar and thermometer sidearm. The solids were then heated to 170°C and the mixture was allowed to melt with stirring. Hydrogen begins to evolve and after 30 minutes at 170°C evolution of hydrogen ceases. The melt was then heated to 190-200°C for 2 hours, after which the melt was then cooled to about 150°C and poured into cold toluene. Precipitation of the white product resulted and the mixture was filtered. The product was then washed with toluene and hexane. Yield: 7.18 g (29.7 mmol, 72%). IR (KBr pellet): 2961, 2924, 2437($\upsilon_{BH}$), 1538, 1416, 1349, 1191, 1071, 1024, 813, 776, 761, 724, 666, 653, 640 $cm^{-1}$.

### Hydrido-*tris*-(3,5-dimethyl-1-pyrazolyl)borato(trioxo)rhenium(VII)

This was prepared according to Mayer.[88] 0.91 mL of trifluoroacetic anhydride (6.47 mmol) was added dropwise to a solution containing $Re_2O_7$ (3.13 g, 6.46 mmol) in 30 mL of acetonitrile. A clear pale yellow solution resulted after stirring

for 10 minutes. Potassium hydrido-*tris*-(3,5-dimethyl-1-pyrazolyl)borate (4.35 g, 12.93 mmol) was then added and the solution was allowed to stir for 2 hours. The white solid product was then filtered and washed with hot water and then with hexane. Yield: 6.57 g (12.4 mmol, 96%). $^1$H NMR ($CDCl_3$): δ 5.89 (s, 3H), 2.82 (s, 9H), 2.34 (s, 9H). $^1$H NMR ($C_6D_6$): δ 5.36 (s, 3H), 2.96(s, 9H), 1.93 (s, 9H). IR (KBr pellet): 2928, 2546 ($\upsilon_{BH}$), 1545, 1451, 1416, 1390, 1371, 1213, 1189, 1070, 1049, 938, 907($\upsilon_{ReO}$), 865, 814, 687, 646 cm$^{-1}$.

**Hydrido-*tris*-(3,5-dimethyl-1-pyrazolyl)borato(ethane-1,2-diolato)(oxo) rhenium(V)**

This was prepared according to Gable.[83] Tp'$ReO_3$ (0.51 g, 0.96 mmol), triphenylphosphine (0.51 g, 1.94 mmol), *p*-toluenesulfonic acid monohydrate (2.0 mg, 0.01 mmol), ground molecular sieves (1.0 g), and ethylene glycol (0.30 g, 4.83 mmol) were stirred at room temperature for 24 hours in 50 mL THF. The blue mixture was filtered, and the volatiles removed under reduced pressure. The product was purified by chromatography on silica gel (Scientific Adsorbents Inc., 32-63). A solution of dichloromethane and 1% acetone was used to elute the blue diolate. Removal of solvent left a blue solid. Yield: 0.38 g (0.69 mmol, 71%). $^1$H NMR ($CDCl_3$): δ 5.97 (s, 2H), 5.50 (s, 1H), 5.39 (m, 2H), 5.03 (m, 2H), 2.62 (s, 6H), 2.53 (s, 6H), 2.33 (s, 3H), 2.14 (s, 3H). $^{13}$C NMR ($CDCl_3$): δ 157, 154, 147, 143, 108.0, 107.6, 86, 14.3, 14.3, 12.9, 12.7. IR (KBr): 2910, 2858, 2535 ($\upsilon_{BH}$),

1545, 1452, 1419, 1383, 1203, 1071,1015, 960 ($\upsilon_{ReO}$), 907, 815, 627 $cm^{-1}$. MS (EI): 560.2 [$M^+$].

**Hydrido-*tris*-(3,5-dimethyl-1-pyrazolyl)borato((*cis*-1,2-diphenyl-1,2-diolato)(oxo) rhenium(V)**

This was prepared according to Gable.[83] Tp'$ReO_3$ (0.20 g, 0.38 mmol), polymer-supported triphenylphosphine (0.31 g, 3 mmol/g resin), *p*-toluenesulfonic acid monohydrate (2.0 mg, 0.01 mmol), ground molecular sieves (1.0 g), and *meso*-hydrobenzoin (0.16 g, 7.47 mmol) were stirred at room temperature for 24 hours in 40 mL THF. The blue mixture was filtered, and the volatiles removed under reduced pressure. The product was purified by chromatography on silica gel (Scientific Adsorbents Inc., 32-63). A solution of dichloromethane and 1% of acetone was used to elute the blue diolate. Yield: 0.088 g (0.12 mmol, 33%) $^1H$ NMR ($C_6D_6$): δ 7.38 (d, *J*= 7.68 Hz, 4H), 7.05 (t, *J* = 7.41, 7.41 Hz, 4H), 6.88 (d, *J* = 7.41 Hz, 2H), 6.84 (s, 2H), 5.52 (s, 2H), 5.29 (s, 1H), 2.86 (s, 6H), 2.54 (s, 3H), 2.14 (s, 6H), 1.92 (s, 3H). MS (FAB): 713.2 [$M^+$+1].

**Hydrido-*tris*-(3,5-dimethylpyrazolyl)borato(oxo)rhenium(V) dichloride**

HCl (0.026 g, 0.72 mmol) was added to a solution of Tp'Re(O)($OCH_2CH_2O$) (0.2 g, 0.36 mmol) in 25 mL of THF and stirred for 30 minutes. The solution was then neutralized using triethylamine, filtered and purified by flash column chromatography on silica gel (Scientific Adsorbents Inc., 32-63). Dichloromethane was used to elute the product. Yield: 0.13 g (0.23 mmol, 64%). $^1$H NMR ($CDCl_3$): δ 6.14(s, 2H), 5.72 (s, 1H), 2.98 (s, 6H), 2.70 (s, 6H), 2.39 (s, 3H), 2.25 (s, 3H). $^{13}$C NMR ($CDCl_3$): δ 157.7, 157.6, 148.1, 143.6, 109.4, 108.0, 15.5, 14.9, 12.31, 12.27. IR(KBr): 2930, 2560, 1543, 1449, 1414, 1387, 1363, 1202, 1069, 1044, 973, 863, 814, 791, 690, 644. MS(EI): 570.1 [$M^+$]

**Hydrido-*tris*-(3,5-dimethyl-1-pyrazolyl)borato-*bis*-hydroxy(oxo)rhenium**

Method A: Water (33.9 μL, 1.88 mmol) was added to a solution containing Tp'$ReO_3$ (0.25 g, 0.47 mmol) and polymer-supported triphenylphosphine (0.20 g, 0.61 mmol) in THF (50 mL). The solution was then placed under reduced pressure to ensure the removal of any dissolved oxygen. The colorless solution was allowed to stir for 48 h and over time became dark blue. The solution was then filtered and concentrated under reduced pressure. Treatment of the solution with pentanes resulted in the precipitation of a light blue powder Yield: 1.38 g (2.56 mmol, 55%).

$^1$H NMR ($C_6D_6$): δ 12.97 (br s, 2H), 5.52 (s, 2H), 5.24 (s, 1H), 2.81 (s, 6H), 2.41 (s, 3H), 2.15 (s, 6H), 1.87 (s, 3H). $^1$H NMR ($CD_2Cl_2$): δ 12.8 (br s, 2H), 6.07 (s, 2H), 5.60 (s, 1H), 2.73 (s, 6H), 2.50 (s, 6H), 2.30 (s, 3H), 2.20 (s, 3H). $^{13}$C NMR ($CD_2Cl_2$): δ 156.1, 152.5, 148.1, 143.4, 108.1, 106.7, 14.0, 13.8, 12.6, 12.1. IR (KBr): 3335 ($\upsilon_{OH}$), 2926, 2535 ($\upsilon_{BH}$), 1543, 1450, 1202, 1070, 967 ($\upsilon_{ReO}$), 865, 814, 786, 647 cm$^{-1}$. MS (FAB): *m/e* = 534, 516 ([$Re^{187}$-$H_2O$]$^+$). Exact mass 534.1561, calculated for $C_{15}H_{24}BN_6{}^{187}ReO_3$: 534.1561.

Method B: Tp'$ReOCl_2$ (0.05 g, 0.09 mmol) was placed in a 250 mL thick walled glass bomb equipped with a magnetic stir bar. The vessel was evacuated, and 15 mL of $CH_3CN$ was vacuum transferred into it. Under a flow of argon, $NEt_3$ (0.09 g, 0.86 mmol) and $H_2O$ (0.094 g, 5.22 mmol) was added. The solution was freeze-pump-thaw degassed and heated at 80°C for 24 hrs. The reaction vessel was then opened in the glove box and its contents poured into a 25 mL round bottom attached to a fritted apparatus. The solution was filtered and concentrated under reduced pressure. Treatment of the solution with pentanes resulted in the precipitation of Tp'$ReO(OH)_2$. Yield: 0.0064 g (0.01mmol, 14%).

**Hydrido-*tris*-(3,5-dimethyl-1-pyrazolyl)borato(chloro)(hydroxy)(oxo)rhenium**

Concentrated HCl (30.0 μL, 0.51 mmol) was added to a solution containing Tp'$ReO_3$ (0.13 g, 0.24 mmol) and triphenylphosphine (0.11 g, 0.42 mmol) in THF (20 mL). The solution was then placed under reduced pressure to ensure the removal of any dissolved oxygen. The suspension was allowed to stir for 48 h and over time became dark blue. The solution was evaporated to dryness to yield a blue solid. Column chromatography on silica gel (Scientific Adsorbents Inc, 32-63) with $CH_2Cl_2$ as eluent yielded a deep blue product. Yield: 0.093 g (0.17 mmol, 71%). $^1$H NMR ($CDCl_3$): δ 16.5 (bs, 1H), 6.062 (s, 1H), 6.054 (s, 1H), 5.63 (s, 1H), 2.91 (s, 3H), 2.80 (s, 3H), 2.62 (s, 3H), 2.58 (s, 3H), 2.32 (s, 3H), 2.19 (s, 3H). $^{13}$C NMR ($CDCl_3$): δ 158.1, 157.4, 153.9, 149.0, 147.0, 143.4, 109.1, 108.7, 107.9, 15.3, 15.2, 14.3, 12.81, 12.79, 12.6. IR (KBr): 3448 ($\upsilon_{OH}$), 2929, 2546 ($\upsilon_{BH}$), 1545, 1450, 1419, 1386, 1368, 1204, 1074, 971 ($\upsilon_{ReO}$), 864, 814, 786, 690, 642, 616 cm$^{-1}$. MS (EI): 552.12081 [$M^+$].

**Hydrido-*tris*-(3,5-dimethyl-1-pyrazolyl)borato(ethoxy)(hydroxyl)(oxo)rhenium**

Ethanol (5.0 mL) was added to a solution containing Tp'$ReO_3$ (0.15 g, 0.28 mmol) and polymer-supported triphenylphosphine (0.19 g, 0.56 mmol) in THF (35 mL). The solution was then placed under reduced pressure to ensure the removal of any

dissolved oxygen. The colorless solution was allowed to stir for 72 h and over time became blue. The solution was then filtered and the volatiles were removed in vacuo leaving a blue solid. Yield: 0.15 g (0.27 mmol, 95%). $^{1}$H NMR ($C_6D_6$): δ 13.96 (br s, 1H), 5.86 (m, 1H), 5.58 (s, 1H), 5.50 (s, 1H), 5.38 (m, 1H), 5.31 (s, 1H), 2.92 (s, 3H), 2.63 (s, 3H), 2.49 (s, 3H), 2.18 (s, 3H), 2.16 (s, 3H), 1.90 (s, 3H), 1.60 (t, $J$ = 7.0Hz, 3H). $^{13}$C NMR ($C_6D_6$): δ 156.8, 155.7, 153.8, 147.0, 146.2, 142.3, 108.1, 108.0, 106.9, 77.3, 18.9, 14.3, 14.1, 14.0, 12.4, 12.3, 12.0. IR (KBr): 3335 ($\upsilon_{OH}$), 2924, 2540 ($\upsilon_{BH}$), 1543, 1450, 1203, 1070, 961 ($\upsilon_{ReO}$), 815, 643 cm$^{-1}$.

**Hydrido-*tris*-(3,5-dimethyl-1-pyrazolyl)borato(*syn*-phenyl-1,2-diolato)(oxo) rhenium**

Into a 250 mL thick walled glass bomb equipped with a Teflon valve were placed Tp'$ReO_3$ (0.03g, 0.057 mmol) and a magnetic stir bar. The vessel was evacuated, and 20 mL of dry benzene was vacuum transferred into it. The vessel was then filled with argon and under a flow of argon, 33.8 μL of triethylphosphite (0.28 mmol) and 19.3 μL of styrene oxide (0.17 mmol) was added. The solution was then freeze-pump-thaw degassed and heated at 75°C for 90 minutes. The reaction vessel was opened to the air, its contents were poured into a round-bottom flask, and the volatiles were removed on a rotary evaporator. The product was then purified by chromatography on silica gel (Scientific Adsorbents Inc, 32-63). Initial elution with 1:1 hexane/dichloromethane was used to remove olefin and unreacted

epoxide. Straight dichloromethane was used to elute the blue diolate. The dichloromethane solution was then dried with $MgSO_4$, filtered and the volatiles removed to give a blue powder. Yield: 0.014 g (0.02mmol, 38%). $^1$H NMR ($CDCl_3$): δ 7.71(d, $J$ = 7.50Hz, 2H), 7.43 (t, $J$ = 7.50Hz, 2H), 7.30 (t, $J$ = 7.50Hz, 2H), 6.01 (s, 1H), 5.98 (s, 1H), 5.89 (dd, $J$ = 7.68, 9.70Hz, 1H), 5.82 (dd, $J$ = 7.68, 9.70Hz, 1H), 5.49 (s, 1H), 5.40 (t, $J$ = 9.70Hz, 1H), 2.66 (s, 3H), 2.64 (s, 3H), 2.56 (s, 3H), 2.54 (s, 3H), 2.20(s, 3H), 2.16(s, 3H). $^1$H NMR ($C_6D_6$): δ 7.83 (d, $J$= 7.68Hz, 2H), 7.34 (t, $J$=7.68Hz, 2H), 7.19 (t, 1H), 6.13 (dd, $J$= 7.68, 9.61Hz, 1H), 6.00 (dd, $J$ = 7.68, 9.88 Hz, 1H), 5.59 (m, 3H), 5.10 (s, 1H), 2.83 (s, 3H), 2.81(s, 3H), 2.27 (s, 3H), 2.17 (s, 6H), 1.86 (s, 3H). $^{13}$C NMR ($CDCl_3$): δ 157.7, 157.2, 154.2, 147.9, 147.3, 143.4, 143.1, 128.7, 127.1, 126.4, 108.1, 108.08, 107.5, 98.4, 89.4, 15.7, 14.5, 14.0, 12.93, 12.85, 12.8. IR (KBr): 2925, 2536 ($\upsilon_{BH}$), 1545, 1451, 1420, 1384, 1204, 1071, 957($\upsilon_{ReO}$), 814, 697, 646 cm$^{-1}$. MS (FAB): 637.2 [$M^+$+1].

**Hydrido-*tris*-(3,5-dimethyl-1-pyrazolyl)borato(*syn*,*cis*-1,2-diphenyl-1,2-diolato) (oxo) rhenium**

Into a 250 mL thick walled glass bomb equipped with a Teflon valve were placed Tp'$ReO_3$ (0.03 g, 0.057 mmol), *cis*-stilbene oxide (0.03 g, 0.15 mmol) and a magnetic stir bar. The vessel was evacuated, and 20 mL of dry THF was vacuum transferred into it. The vessel was then filled with argon and under a flow of argon, 67.7 μL of triethylphosphite (0.57 mmol) was added. The solution was then freeze-

pump-thaw degassed and heated at 75°C for 30 minutes. The reaction vessel was opened to the air, its contents were poured into a round-bottom flask, and the volatiles were removed on a rotary evaporator. The product was then purified by chromatography on silica gel (Scientific Adsorbents Inc, 63-200). Initial elution with 2:1 hexane/dichloromethane was used to remove olefin and unreacted epoxide. Straight dichloromethane was used to elute the blue diolate. The dichloromethane solution was then dried with $MgSO_4$, filtered and the volatiles removed to give a blue powder. Yield: 0.0157 g (0.02 mmol, 51%) $^1$H NMR ($C_6D_6$): δ 7.56(d, 4H), 7.10 (m, 6H), 6.93 (s, 2H), 5.58 (s, 2H), 5.21 (s, 1H), 2.76 (s, 6H), 2.31 (s, 3H), 2.18 (s, 6H), 1.92 (s, 3H). $^1$H NMR (300MHz,$CDCl_3$): δ 7.32 (dd, 4H), 7.18 (m, 6H), 6.70 (s, 2H), 6.00 (s, 2H), 5.52 (s, 1H), 2.58 (s, 6H), 2.57 (s, 6H), 2.21 (s, 3H), 2.17 (s, 3H). $^{13}$C NMR ($CDCl_3$): δ 158.0, 155.5, 147.6, 144.3, 142.8, 128.7, 127.7, 126.9, 108.1, 107.2, 99.8, 16.7, 14.2, 13.0, 12.9. IR (KBr): 2926, 2542 ($\upsilon_{BH}$), 1544, 1451, 1383, 1204, 1073, 958($\upsilon_{ReO}$), 943, 723, 698, 669 cm$^{-1}$. MS (FAB): 711.2 [$M^+$-1].

**Preparative Scale: Deoxygenation of 1,2-epoxydodecane**

Chromatography Variant: Into a 250 mL thick walled glass bomb equipped with a Teflon plug were placed Tp'$ReO_3$ (0.08 g, 0.15 mmol), $PPh_3$ (0.88 g, 3.36 mmol) and a magnetic stir bar. The vessel was evacuated, and 30 mL of dry benzene was

vacuum transferred into it. The vessel was then filled with argon and under a flow of argon, 0.62 mL of 1,2-epoxydodecene (2.82 mmol) was added. The solution was then freeze-pump-thaw degassed and heated to 85°C for 86h. The reaction vessel was opened to the air and an aliquot analyzed by NMR showed no remaining epoxide. The contents were then poured into a round-bottom flask and the volatiles were removed on a rotary evaporator. The alkene was then purified by column chromatography on silica gel (Scientific Absorbents Inc., 32-63). Elution with straight hexane, followed by removal of the volatiles gave 1-dodecene. Yield: 447.0 mg (2.70 mmol, 94%).

Distillation Variant: 1,2-epoxydodecane (0.75 g, 4.1 mmol) was dissolved in 60 mL of toluene and dried over $CaH_2$. Tp'$ReO_3$ (110 mg, 0.2 mmol, 0.05 equiv) and $PPh_3$ (1.18 g, 4.5 mmol) were added. The mixture was stirred in a Carius tube under vacuum and heated to 105°C for 72 h. An aliquot analyzed by NMR showed no remaining epoxide; distillation gave 1-dodecene. Yield: 440 mg (2.6 mmol, 64%).

**Burst Experiment with Tp'ReO(OH)(OEt):**

*cis*-Stilbene oxide (0.11 g, 0.56 mmol) , triphenylphosphine (0.16 g, 0.61 mmol) and 1,4-di-*tert*-butylbenzene (1.29 mg, 0.0068 mmol) was dissolved in 3 mL of

$C_6D_6$ and dried over $CaH_2$. A 0.5 mL aliquot was then added to a NMR tube containing Tp'ReO(OH)(OEt) (2.14 mg, 0.0038 mmol) and sealed under vacuum. The tube was then heated to 75°C in a water / ethylene glycol bath. The sample tube was periodically removed and cooled to 25°C and the NMR spectrum was recorded.

**General Procedure for Para-Substituted Styrene Oxide Synthesis:**

30 mL of dry methylene chloride was vacuum transferred into a round-bottom flask containing trimethylsulfonium iodide (4.51 g, 22.0 mmol) and NaH (0.52 g, 22 mmol prewashed with 15 mL of hexane to remove the oil). To the resulting solution was added 1 mL of freshly distilled DMSO and 7.4mmol of the aldehyde. The solution was then cooled in a salt-ice bath and stirred overnight. After the addition of 50 mL of water, the product was extracted with methylene chloride, dried over $MgSO_4$ and the volatiles evaporated. Certain epoxides required additional purification by evaporative distillation.

*p*-Methoxystyrene Oxide: Yield: 0.90 g (6.0 mmol, 82%). $^1H$ NMR ($CDCl_3$): δ7.25-6.85 (m, 4H), 3.81 (dd, J = 2.6, 4.0Hz, 1H), 3.81 (s, 3H), 3.13 (dd, $J$ = 4.0, 5.4 Hz, 1H), 2.81 (dd, $J$ = 2.6, 5.4 Hz, 1H).

*p*-Fluorostyrene Oxide: Yield: 0.43 g (3.1 mmol, 39%). $^1$H NMR ($CDCl_3$): δ 7.27-6.99 (m, 4H), 3.84 (dd, $J$ = 2.5, 4.0 Hz, 1H), 3.13 (dd, $J$ = 4.0, 5.4 Hz, 1H), 2.76 (dd, $J$ = 2.5, 5.4 Hz).

*p*-Methylstyrene Oxide: Yield = 0.30 g (2.2 mmol, 35%). $^1$H NMR ($CDCl_3$): δ 7.26 – 7.17 (m, 4H), 3.85 (dd, $J$ = 2.6, 4.0 Hz, 1H), 3.14 (dd, $J$ = 4.0, 5.5 Hz, 1H), 2.81 (dd, $J$ = 2.6, 5.5Hz, 1H).

*p*-Bromostyrene Oxide: Yield = 0.82 g (4.1 mmol, 76%). $^1$H NMR ($CDCl_3$): δ 7.53 – 7.10 (m, 4H), 3.83 (dd, $J$ = 2.5, 4.0 Hz, 1H), 3.15 (dd, J = 4.1, 5.5 Hz, 1H), 2.75 (dd, $J$ = 2.5, 5.5 Hz, 1H).

*p*-Trifluoromethylstyrene Oxide: Yield: 0.72 g (3.8 mmol, 71%). $^1$H NMR ($CDCl_3$): δ 7.64-7.36 (m, 4H), 3.92 (dd, $J$ = 2.5, 4.0 Hz, 1H), 3.19 (dd, $J$ = 4.1, 5.5Hz, 1H), 2.77 (dd, J = 2.5, 5.5 Hz, 1H).

**Oct-7-ene-2,4-dione**

Sodium amide (16.36 g, 419.5 mmol) was added to a 1L three-necked flask containing 450 mL of liquid ammonia cooled to -78°C in a dry ice-acetone bath while argon was passed through the reaction mixture. 20 mL of acetylacetone (200

mmol) in 80 mL of dry ether was slowly syringed into the reaction vessel. The cooling bath was removed and the solution was stirred for 45 min. 17.4 mL of allylbromide (200 mmol) in 80 mL of ether was then added drop wise over 30 min. The reaction mixture was stirred for 1 hour. 250 mL of ether was added and the ammonia was allowed to evaporate over a 3 hour period. The solution was filtered and the ethereal solution was poured onto ice, followed by 70 mL of cold concentrated hydrochloric acid. The ethereal layer was separated and aqueous layer was extracted three times with ether. The combined ethereal layers was dried with magnesium sulfate and filtered. Removal of the volatiles left a yellow product. Yield: 27.1 g (193.3 mmol, 97%) $^1$H NMR ($CDCl_3$): Mixture of keto/enol forms (1:5); enol: δ 5.78 (m, 1H), 5.48 (s, 1H), 5.0 (m, 2H), 2.34 (m, 4H), 2.02 (s, 3H). IR (KBr): 3081, 2924, 1707, 1618, 1420, 1363, 996, 916, 785 $cm^{-1}$. MS(CI): 140.08 [$M^+$].

**3-(1-Butene)-5-methylpyrazole**

To a solution of 1-octene-5,7-dione (19.2 g, 140 mmol) in 200 mL of ethanol, hydrazine monohydrochloride (9.57 g, 140 mmol) and 30 mL of water was added. After stirring overnight, an aqueous solution containing potassium bicarbonate was added until a neutral pH was obtained. The product was extracted with dichloromethane and dried with magnesium sulfate. Filtration and removal of the

volatiles left the product. Yield: 9.8 g (72.0 mmol, 53%). $^{1}$H NMR ($CDCl_3$): δ 11.82 (s, 1H), 5.87 (s, 1H), 5.86 (m, 1H ), 5.06 (ddd, $J$ = 1.65, 3.43, 17.15 Hz, 1H), 5.00 (ddd, $J$ = 1.37, 3.16, 10.3 Hz, 1H), 2.74 (dd, $J$ = 7.3, 9.2 Hz, 2H), 2.40 (m, 2H), 2.29 (s, 3H). $^{13}$C NMR (75MHz, $CDCl_3$): δ 149.0, 144.4, 138.0, 115.7, 103.6, 33.8, 26.8, 12.5. IR (KBr): 3196, 3135, 3104, 3034, 2979, 2928, 1641, 1582, 1475, 1437, 1029, 1006, 913, 794 $cm^{-1}$. MS (FAB): 137.1 [$M^{+}$+1].

**1-(3-Butenyl)-2,3,4,5-tetramethyl-cyclopentadiene**

This was prepared according to Okuda.[123] 4-Bromo-1-butene (9.7 g, 71.9 mmol) in 30 mL of diethyl ether was added dropwise over 1.5h to a 40 mL diethyl ether solution containing 1.91g (78.7 mmol) of magnesium turnings. The solution was then heated to reflux for 1 h. 2,3,4,5-tetramethylcyclopent-2-enone (9.01 g, 65.2 mmol) was added dropwise. The solution was then refluxed again for 2h, after which 20 mL $H_2O$ and 10g of ice were slowly added. Acidic ion-exchange resin (Amberlite IR-120®) was added with 20 mL of $H_2O$. The mixture was stirred overnight. The solution was filtered and the organic layer was separated from the aqueous layer. The organic layer was then dried with magnesium sulfate and filtered. A yellow oil results after removal of the solvent. Yield: 7.60 g (43.1 mmol, 66%). $^{1}$H NMR ($CDCl_3$): Mixture of three isomers; 5.81 (m), 4.92 (m),

2.39-2.52 (m), 2.29 (m), 2.11 (m), 1.83, 1.81, 1.79, 1.78, 1.03(s), 1.00(s). MS(FAB): 175.15 [$M^+$-1].

**[1-(3-Butenyl)-2,3,4,5-tetramethylcyclopentadienyl]rhenium tricarbonyl**

A three-necked, 250 mL flask is fitted with a magnetic stirring bar and a Dean-Stark condenser. The flask is filled with argon before dry deoxygenated benzene (100 mL) is added. 340 μL of thallium(I) ethoxide (4.8 mmol) is syringed into the solution, followed by the syringe addition of 1-(3-butenyl)-2,3,4,5-tetramethylcyclopentadiene (0.97 g, 5.5 mmol). The solution was heated to reflux for 1 hour and 30 mL of benzene was distilled and removed. $Re(CO)_5Br$ (2.0 g, 4.92 mmol) was then added, during which time the solution was heated to reflux under argon for 25 hours. Filtration and removal of solvent left a dark orange oil. Purification on a silica column (Scientific Adsorbents Inc, 32-63) eluting with methylene chloride yielded analytically pure product. Yield: 0.37 g (0.84 mmol, 18%). $^1$H NMR ($CDCl_3$): δ 5.83 (m, 1H), 5.04 (m, 2H), 2.54 (m, 2H), 2.18 (s, 12H), 2.18(m, 2H). $^1$H NMR ($C_6D_6$): δ 5.57 (m, 1H), 4.90 (m, 2H), 2.24 (dd, 2.24), 1.86 (m, 2H), 1.75 (s, 6H), 1.70 (s, 6H). $^{13}$C NMR ($CDCl_3$): δ 198.3, 137.6, 116.0, 101.7, 99.3, 98.9, 36.5, 25.8, 11.14, 11.12. IR (KBr): 2925, 2855, 2010 ($\upsilon_{CO}$), 1918 ($\upsilon_{CO}$), 1639, 1452, 1377, 909. MS(FAB): 444.09 [$M^+$-2].

**[1-(3-Butenyl)-2,3,4,5-tetramethylcyclopentadienyl]rhenium trioxide**

To a solution containing [1-(3-butenyl)-2,3,4,5-tetramethylcyclopentadienyl] rhenium tricarbonyl (0.058 g, 0.13 mmol) in 10 mL of $C_6H_6$, 156 μL of 5.0 *M tert*-butyl hydroperoxide was added dropwise. The solution was stirred at room temperature for 90 minutes, whereupon the solution was heated to reflux for 20 minutes. The color of the solution turned to a bright yellow, with a small amount of a brown precipitate. After filtration, violates were removed under reduced pressure. The product was then purified by chromatography on silica gel (Scientific Adsorbents Inc, 32-63). $CH_2Cl_2$ with a trace of acetone was used to elute the product. Yield: 0.031 g (0.08 mmol, 58%). $^1$H NMR ($CDCl_3$): δ 5.82 (m, 1H), 5.08 (m, 2H), 2.61 (q, 2H), 2.28 (m, 2H), 2.24 (s, 6H), 2.17 (s, 6H). $^1$H NMR ($C_6D_6$): 5.52 (m, 1H), 4.90 (m, 1H), 4.85 (m, 1H), 2.32 (dd, 2H), 1.89 (m, 2H) 1.76 (s, 6H), 1.61 (s, 6H). $^{13}$C NMR ($CDCl_3$): δ 136.7, 121.59, 121.58, 121.2, 116.8, 33.3, 25.4, 10.86, 10.84. IR (KBr): 2927, 2027, 1919, 1637, 1458, 1381, 1364, 909 ($\upsilon_{Re=O}$), 879 ($\upsilon_{Re=O}$), cm$^{-1}$. MS (EI): 410.1 [M$^+$].

**[1-(3',4'-Epoxy)-2,3,4,5-tetramethylcyclopentadienyl]rhenium trioxide**

To a solution containing [1-(3-butenyl)-2,3,4,5-tetramethylcyclopentadienyl] rhenium trioxide (0.018 g, 0.044mmol) in 15 mL of $C_6H_6$ was added 0.02 g of

MCPBA (0.1 mmol). After stirring overnight at room temperature, the organic layer was then washed successively with potassium hydroxide and water. The product was then purified by chromatography on silica gel (Scientific Adsorbents Inc, 32-63). 1% acetone in methylene chloride solution was used to elute the product. Yield: 0.009 g (0.02 mmol, 46%). $^{1}$H NMR ($C_6D_6$): δ 2.35 (m, 1H), 2.29 (t, $J$ =7.82, 7.82 Hz, 2H), 2.22 (dd, $J$ = 3.84, 4.94 Hz, 1H), 1.97 (dd, $J$ = 2.47, 4.94 Hz, 1H), 1.77 (s, 3H), 1.76 (s, 3H), 1.61 (s, 3H), 1.59 (s, 3H), 1.31 (m, 1H), 1.14 (m, 1H). $^{13}$C NMR ($CDCl_3$): δ 121.6, 121.59, 121.3, 121.2, 121.1, 51.8, 47.3, 32.1, 22.5, 10.9, 10.9, 10.74, 10.76. IR (KBr): 2924, 1459, 1364, 908 ($\upsilon_{Re=O}$), 877 ($\upsilon_{Re=O}$), cm$^{-1}$. MS (EI): 426.1 [M$^{+}$].

**[1-(3',4'-Epoxy)-2,3,4,5-tetramethylcyclopentadienyl]rhenium dioxide**

Polymer-supported triphenylphosphine (0.53 g, 0.16 mmol) was added to a 20 mL round bottom containing [1-(3',4'-epoxy)-2,3,4,5-tetramethylcyclopentadienyl] rhenium trioxide (0.034 g, 0.8 mmol) in 10 mL of benzene at room temperature. The reaction was stirred overnight under a blanket of argon. The solution was filtered and the solvent was removed under reduced pressure to leave a brown solid. $^{1}$H NMR ($C_6D_6$): δ 2.60 (m, 1H), 2.44 (m, 2H), 2.29 (dd, $J$ =3.84, 5.21 Hz, 1H), 2.04 (m, 1H), 2.03 (s, 6H), 1.88 (s, 6H), 1.46 (m, 2H). IR (KBr): 2932, 2854, 1459, 932, 643, 538, 419. MS(EI): 408.1 [M$^{+}$-2].

**2,3-Dimethyl-2,3-epoxybutane**

3-Chloroperoxybenzoic acid (15.63 g, 60.0 mmol) was added in portions to a magnetically stirred two-phase solution of 2,3-dimethyl-2-butene (5.0 g, 59.4 mmol) in $CH_2Cl_2$ (200 mL) and 0.5 *M* aqueous sodium bicarbonate (100 mL). After stirring for 16 hours, the two layers were separated and the organic layer was washed successively with 1N sodium hydroxide and water. Removal of the volatiles under reduced pressure and distillation afforded the product. Yield: 3.4 g (33.9 mmol, 57%). $^1$H NMR ($CDCl_3$): δ 1.28 (s, 12H). $^1$H NMR ($C_6D_6$): δ 1.13 (s, 12H). IR (KBr): 2996, 2928, 1716(C=O), 1411, 1368, 1257, 1169, 912, 836 $cm^{-1}$.

**5,6-Epoxy-2-hexanone**

This was prepared according to Curci.[141] An aqueous solution of potassium peroxomonosulfate (23.5 g, 38.2 mmol) is added dropwise to a mixture of 5-hexen-2-one (1.5 g, 15.3 mmol) and acetone (0.15g, 2.5 mmol) in water at 0°C. 198.9 mmol of acetone should have been used and may be responsible for the low yield. The pH is adjusted to 7.5 and maintained at this value during the reaction by addition of aqueous KOH. The mixture is then acidified to pH 3 using conc. HCl and extracted with $CH_2Cl_2$. The organic layer was then dried ($MgSO_4$) and the

solvent removed in vacuo, affording analytically pure product. Yield: 0.26 g (2.3 mmol, 15%). $^{1}$H NMR ($CDCl_3$): δ 2.78 (m, 1H), 2.57 (t, 1H), 2.43 (t, 1H), 2.31 (m, 1H), 2.00 (s, 3H), 1.77 (m, 1H), 1.50 (m, 1H). $^{13}$C NMR (300MHz): δ 207.8, 51.5, 47.3, 39.6, 30.1, 26.5. IR (KBr): 2996, 2928, 1716(C=O), 1411, 1368, 1257, 1169, 912, 836 $cm^{-1}$. MS (EI): 115.1 [$M^{+}$+1].

**5,6-Epoxyhexanenitrile**

This was prepared according to Griengl.[142] To a mixture of hex-5-enenitrile (0.65g, 6.83mmol) and disodium hydrogen phosphate (1.45 g, 10.24 mmol) in $CH_2Cl_2$ (20 mL), *m*-chloroperbenzoic acid (1.37 g, 6.83 mmol) was added portionwise. The mixture was stirred for 65 h after which the solids were filtered and washed with $CH_2Cl_2$. The supernatants were then washed with an aqueous sodium bicarbonate solution three times and dried ($MgSO_4$). Evaporation and distillation afforded the product. Yield: 0.27 g (2.5 mmol, 36%). $^{1}$H NMR ($CDCl_3$): δ 1.55 (m, 1H), 1.86 (m, 3H), 2.43 (m, 2H), 2.50 (q, 1H), 2.78 (q, 1H), 2.93 (m, 1H). $^{13}$C NMR ($CDCl_3$): δ 119.8, 51.6, 47.0, 31.5, 22.6, 17.3. IR (KBr): 3056, 2994, 2942, 2874, 2246, 1596, 1560, 1438, 1458, 1429, 1389, 1262, 928, 910, 853, 828, 760, 739 $cm^{-1}$. MS (EI): 112.1 [$M^{+}$+1].

**Glycidy *tert*-butyldimethylsilyl ether**

Glycidol (0.5 g, 6.75 mL) was added to a mixture of imidazole (0.46 g, 6.75 mmol) in 10 mL of $CH_2Cl_2$. The mixture was stirred for 5 min. after which 1.02 g of *tert*-butyldimethylsilyl chloride (6.75 mmol) was added portionwise. The mixture was then stirred for 1 hour followed by concentration of the mixture. The addition of 30 mL ether resulted in the precipitation of the imidazolium salt. The salt was then filtered and washed with ether. The ether solution was then washed three times with water and dried ($MgSO_4$). Filtration followed by evaporation afforded the product that was further purified by column chromatography on basic alumina. Yield: 0.46 g (2.4 mmol, 36%). $^1$H NMR ($CDCl_3$): δ 3.85 (dd, *J*=3.29, 11.94, 1H), 3.65 (dd, *J*= 4.8, 11.94, 1H), 3.08 (m, 1H), 2.76 (dd, *J*=3.98, 5.21, 1H), 2.63 (dd, *J*=2.74, 5.21, 1H), 0.90 (s, 9H), 0.07 (d, 6H). IR (KBr): 2957, 2930, 2896, 2859, 1473, 1256, 1162, 1138, 1099, 918, 838, 779, 669 $cm^{-1}$.

## 6.5 Computations

Computational modeling was performed using the commercially available Jaguar package.[143] The LACVP basis set, incorporating Hay-Wadt effective core

potential[144] for rhenium and the 6-31G basis set for all other atoms, was used throughout. All geometry optimizations of the ground state structures and location of transition states were first optimized without polarization or diffuse functions, but were then reoptimized with the added functions (LACVP*+). This encompasses the use of d-type polarization functions and diffuse functions for all heavy atoms. Diffuse functions were included since bonding in the transition state involves elongated bonds. A Pulay 6-31G* scaled[145] vibrational analysis was used to show that calculated ground state structures (no imaginary frequencies) were true minima and that transition state structures (one imaginary frequency) were saddle points. Vibrational analysis utilized the final Hessian; frequencies were scaled by a factor of 0.9614[146], and zero point energies were calculated for all compounds. Transition states were generally located by QST methods, using reactant and product structures as boundaries for defining the initial transition state structure guess.

## Bibliography

1. *Cytochrome P-450: Stucture, Mechanism, and Biochemistry*; Ortez de Montellano, P.R., Ed.; Plenum: New York, 1985.

2. *Molybdenum Enzymes*; Spiro, T. G., Ed.; Wiley: New York, 1985.

3. *Multiple-Ligand Multiple Bonds*; Nugent, W. A., Mayer, J. M., Ed.; Wiley: New York, 1988.

4. Schröder, M. *Chem. Rev.* **1980**, *80*, 187.

5. (a) Sharpless, B. K.; Lauer, R. F. *J. Am. Chem. Soc.* **1972**, *94*, 7154. (b) Umbreit, M. A.; Sharpless, B. K. *J. Am. Chem. Soc.* **1977**, *99*, 5526.

6. Djerassi, C.; Engle, R. R. *J. Am. Chem. Soc.* **1953**, *75*, 3838.

7. (a) Wolfe, S.; Ingold, C. F.; Lemieux, R. U. *J. Am. Chem. Soc.* **1981**, *103*, 938. (b) Lee, D. G.; Chen, T. *J. Am. Chem. Soc.* **1989**, *111*, 7534.

8. Sharpless, K. B.; Teranishi, A. Y.; Backvall, J. -E. *J. Am. Chem. Soc.* **1977**, *99*, 3120.

9. Brown, S. N.; Mayer, J. M. *J. Am. Chem. Soc.* **1996**, *118*, 12119.

10. (a) Newcomb, M.; Le Tadic, M. -H.; Putt, D. A.; Hollenburg, P. F *J. Am. Chem. Soc.* **1995**, *117*, 3312. (b) Newcomb, M.; Le Tadic-Biadatti, M. -H.; Chestrey, D. L.; Roberts, E. S.; Hollenberg, P. F. *J. Am. Chem. Soc.* **1995**, *117*, 10121.

11. (a) Stultz, L. K.; Binstead, R. A.; Reynolds, M. S.; Meyer, T.J. *J. Am. Chem. Soc.* **1995**, *117*, 2520. (b) Traylor, T. G.; Kim, C.; Richards, J. L.; Xu, F.; Perrin, C. L. *J. Am. Chem. Soc.* **1995**, *117*, 3468.

12. (a) Hentges, S. G.; Sharpless, K. B. *J. Am. Chem. Soc.* **1980**, *102*, 4263. (b) Jacobsen, E. N.; Marko, I.; Mungall, W. S.; Schroder, G.; Sharpless, K. B. *J. Am. Chem. Soc.* **1988**, *110*, 1968. (c) Kolb, H. C.; VanNieuwenhze, M. S.; Sharpless, K. B. *Chem. Rev.* **1994**, *94*, 2483.

13. Jacobsen, E. N. In *Catalytic Asymmetric Synthesis*, Ojima, I., Ed.; VCH Publishers: New York, 1993 and references cited therein.

14. Kolb, H. C.; VanNieuwenhze, M. S.; Sharpless, K. B. *Chem. Rev.* **1994**, *94*, 2483.

15. Kolb, H. C.; Andersson, P. G.; Sharpless, K. B. *J. Am. Chem. Soc.* **1994**, *116*, 1278.

16. Kwong, H.-L.; Sorato, C.; Ogino, Y.; Chen, H.; Sharpless, K. B. *Tetrahedron Lett.* **1990**, *31*, 2999.

17. Döbler, C.; Mehltretter, G.; Beller, M. *Angew. Chem. Int. Ed. Engl.* **1999**, *38*, 3026.

18. Zhang, W.; Jacobsen, E. N. *J. Org. Chem.* **1991**, *56*, 2296.

19. Zhang, W.; Loebach, J. L.; Wilson, S. R.; Jacobsen, E. N. *J. Am. Chem. Soc.* **1990**, *112*, 2801.

20. Palucki, M.; Pospisil, P. J.; Zhang, W.; Jacobsen, E. N. *J. Am. Chem. Soc.* **1994**, *116*, 9333.

21. (a) Cook, G. K.; Andrews, M. A. *J. Am. Chem. Soc.* **1996**, *118*, 9448. (b) Andrews, M. A.; Klaeren, S. A.; Gould, G. L. In *Carbohydrates as Organic Raw Materials II*, Descotes, G., Ed; VCH: New York, 1993.

22. Gable, K.P.; Phan, T.N. *J. Am. Chem. Soc.* **1994**, *116*, 833.

23. (a) Pfenninger, A. *Synthesis* **1986**, 89. (b) Johnson, R. A.; Sharpless, K. B. In *Catalytic Asymmetric Synthesis*, Ojima, I., Ed; VCH: New York, 1993.

24. Mimoun, H.; Mignard, M.; Brechot, P.; Saussine, L. *J. Am. Chem. Soc.* **1986**, *108*, 3711.

25. Sharpless, K. B.; Teranishi, A. Y.; Bäckvall, J. E. *J. Am. Chem. Soc.* **1977**, *99*, 3120.

26. Stewart, R. In *Oxidation in Organic Chemistry*, Part A; Wilberg, K. B., Ed.; Academic Press: New York, 1971, Chapter 1.

27. Lee, D. G.; Van den Engh, M. In *Oxidation in Organic Chemistry*, Part B; Trahanovsky, W. S., Ed.: Academic Press, New York, 1973, Chapter 4.

28. (a) Herrmann, W. A.; Fischer, W.; Marz, D. W. *Angew. Chem., Int. Ed. Engl.* **1991**, *30*, 1638. (b) Espenson, J. H.; Al-Ajlouni, A. *J. Am. Chem. Soc.* **1995**, *117*, 9243.

29. Herrmann, W. A.; Marz, D.; Herdtweck, E.; Schäfer, A.; Wagner, W.; Kneuper, H. J. *Angew. Chem., Int. Ed. Engl.* **1987**, *26*, 462.

30. Espenson, J.H.; Zhu, Z. *J. Org. Chem.* **1995**, *60*. 7728.

31. Espenson, J.H.; Abu-Omar, M.M. *J. Am. Chem. Soc.* **1995**, *117*, 272.

32. Espenson, J.H.; Vassell, K.A. *Inorg. Chem.* **1994**, *33*, 5491.

33. Espenson, J.H.; Pestovsky, O.; Huston, P.; Staudt. S. *J. Am. Chem. Soc.* **1994**, *116*, 2869.

34. Yamazaki, S.; Espenson, J.H.; Huston, P. *Inorg. Chem.* **1993**, *32*, 4683.

35. Herrmann, W. A.; Fischer, R. W.; Scherer, W.; Rauch, M. U. *Angew. Chem., Int. Ed. Engl.* **1993**, *32*, 1157.

36. Gable, K .P. *Adv. Organomet. Chem.* **1997**, *41*, 127.

37. Vassell, K. A.; Espenson, J.H. *Inorg. Chem.* **1994**, *33*, 5491.

38. Herrmann, W.A.; Watzlowik, P.; Kiprof, P. *Chem. Ber.* **1991**, *124*, 1101.

39. Zhu, Z.; Al-Ajlouni, A. M.; Espenson, J. H. *Inorg. Chem.* **1996**, *35*, 1408.

40. Zhu, Z.; Espenson, J. H. *J. Mol. Catal.* **1995**, *103*, 87.

41. Gable, K. P.; Phan, T. N. *J. Am. Chem. Soc.* **1993**, *115*, 3036.

42. Allinger, N. L.; Sprague, J. T. *J. Am. Chem. Soc.* **1972**, *94*, 5734.

43. Gordon, A. J.; Ford, R. A. In *The Chemist's Companion*; J. Wiley & Sons: New York, 1972; p. 113.

44. Pietsch, M. A.; Russo, T. V.; Murphy, R. B.; Martin, R. L.; Rappé, A. K. *Organometallics* **1998**, *17*, 2716.

45. Gable, K. P. *Organometallics* **1994**, *13*, 2486.

46. Gable, K. P.; Juliette, J. J. J. *J. Am. Chem. Soc.* **1996**, *118*, 2625.

47. Gable, K.P.; Juliette, J.J.J. *J. Am. Chem. Soc.* **1995**, *117*, 955.

48. (a)Shea, K. J.; Kim, J.-S. *J. Am. Chem. Soc.* **1992**, *114*, 3044. (b) Shea, K. J.; Kim, J.-S. *J. Am. Chem. Soc.* **1992**, *114*, 4846.

49. Deubel, E.V.; Frenking, G. *J. Am. Chem. Soc.* **1999**, *121*, 2021.

50. (a) Criegee, R. *Justus Liebigs Ann. Chem.* **1936**, *522*, 75. (b) Criegee, R.; Marchand, B.; Wannowius, H. *Justus Liebigs Ann. Chem* **1942**, *550*, 99.

51. (a) Beno, B. R.; Houk, K. N.; Singleton, D. A. *J. Am. Chem. Soc.* **1996**, *118*, 9984. (b) Singleton, D. A.; Merrigan, S. R.; Liu, J.; Houk, K. N. *J. Am. Chem. Soc.* **1997**, *119*, 3385.

52. DelMonte, A. J.; Haller, J.; Houk, K. N.; Sharpless, K. B.; Singleton, D. A.; Strassner, T.; Thomas, A. A. *J. Am. Chem. Soc.* **1997**, *119*, 9907.

53. Singleton, D. A.; Thomas, A. A. *J. Am. Chem. Soc.* **1995**, *117*, 9357.

54. Gable, K. P.; Zhuravlev, F. A. *J. Am. Chem. Soc.* **2002**, *124*, 3970.

55. Herrmann, W. A.; Serrano, R.; Küsthardt, U.; Ziegler, M. L.; Guggolz, E.; Zahn, T. *Angew. Chem., Int. Ed. Engl.* **1984**, *23*, 515.

56. Gable, K. P.; Juliette, J. J. J.; Gartman, M.A. *Organometallics* **1995**, *14*, 3138.

57. Gable, K. P.; Juliette, J. J. J. *Organometallics* **1996**, *15*, 5250.

58. Gisdakis, P.; Antonczak, S.; Rösch, N. *Organometallics* **1999**, *18*, 5044.

59. Gable, K. P.; Zhurzvlev, F. A.; Yokochi, A. F. T. *Chem. Commun.* **1998**, 799.

60. Holm, R. H.; Donahue, J. P. *Polyhedron* **1993**, *12*, 571.

61. Jørgensen, K. A. *Chem. Rev.* **1989**, *89*, 431.

62. (a) Sono, M.; Roach, M. P.; Coulter, E. D.; Dawson, J. H. *Chem. Rev.* **1996**, *96*, 2841. (b) Wallar, B. J.; Lipscomb, J. D. *Chem. Rev.* **1996**, *96*, 2625. (c) Que, L., Jr.; Ho, R. Y. N. *Chem. Rev.* **1996**, *96*, 2607. (d) Gibson, D. T. In *Microbial Degradation of Organic Compounds*; Marcel Dekker: New York, 1984.

63. Ittel, S. D.; Parshall, G. W. In *Homogeneous Catalysis*, 2nd Ed.; John Wiley & Sons: New York, 1992; p. 150.

64. Groves, J. T.; Quinn, R. *J. Am. Chem. Soc.* **1985**, *107*, 5790.

65. Lai, T.; Cheung, K.; Kwong, H.; Che, C. *Chem. Commun.* **1998**, 1583.

66. Sunay, U.; Mootoo, D.; Molino, B.; Fraser-Reid, B. *Tetrahedron Lett.* **1986**, *27*, 4697.

67. Jacobsen, E. N. *Acc. Chem. Res.* **2000**, *33*, 421.

68. Deslongchams, P. *Pure and Appl. Chem.* **1977**, *49*, 1329.

69. Johnson, W.S.; Plummer, M.S.; Reddy, S.P.; Bartlett, W.R. *J. Am. Chem. Soc.* **1993**, *115*, 515.

70. Kraus, G.A.; Thomas, P.J. *J. Org. Chem.* **1988**, *53*, 1395.

71. (a) Hayasi, Y.; Schwartz, J. *Inorg. Chem.* **1981**, *20*, 3473. (b) Martin, M. G.; Ganem, B. *Tetrahedron Lett.* **1984**, *25*, 251. (c) Moloy, K. G. *Inorg. Chem.* **1988**, *27*, 677. (d) Whinnery, L. L.; Henling, L. M., Jr.; Bercaw, J. E. *J. Am. Chem. Soc.* **1991**, *113*, 7575. (e) Isobe, H.; Branchaud, B. P. *Tetrahedron Lett.* **1999**, *40*, 8747.

72. (a) Bryan, J. C.; Mayer, J. M. *J. Am. Chem. Soc.* **1990**, *112*, 2298. (b) Bryan, J. C.; Mayer, J. M. *J. Am. Chem. Soc.* **1987**, *109*, 7213.

73. Bryan, J. C.; Geib, S. J.; Rheingold, A. L.; Mayer, J. M. *J. Am. Chem. Soc.* **1987**, *109*, 2826.

74. Brock, S. L.; Mayer, J. M. *Inorg. Chem.* **1991**, *30*, 2138.

75. Sharpless, K. B.; Umbreit, M. A.; Nieh, M. T.; Flood, T. C. *J. Am. Chem. Soc.* **1972**, *94*, 6538.

76. Sanderson, R. T. *Inorg. Chem.* **1986**, *25*, 3518.

77. Tellers, D. M.; Skoog, S. J.; Bergman, R.G. *Organometallics* **2000**, *19*, 2432.

78. Kitajima, N.; Tolman, W. B. *Prog. Inorg. Chem.* **1995**, *43*, 419.

79. Masui, C. S.; Mayer, J. M. *Inorganica Chimica Acta* **1996**, *251*, 325.

80. (a) Domingos, Â.; Marcalo, J.; Paulo, A.; Pires de Matos, A.; Santos, I. *Inorg. Chem.* **1993**, *32*, 5114. (b) Paulo, A.; Domingos, Â.; Marcalo, J.; Pires de Matos, A.; Santos, I. *Inorg. Chem.* **1995**, *34*, 2113.

81. Degnan, I.A.; Herrmann, W.A.; Herdtweck, E. *Chem. Ber.* **1990**, *123*, 1347.

82. Zhuravlev, F. Ph.D. Thesis, Oregon State University, Corvallis, OR, 2001, Chapter 3.

83. Gable, K.P.; AbuBaker, A.; Zientara, K.; Wainwright, A.M. *Organometallics* **1999**, *18*, 173.

84. Trofimenko, S. *J. Am. Chem. Soc.* **1967**, *89*, 3170.

85. Gable, K.P.; Brown, E.C. *Organometallics* **2000**, *19*, 944.

86. Espenson, J.H. *Chem. Commun.* **1999**, 479.

87. Wittig, G.; Haag, W. *Chem. Ber.* **1955**, *88*, 1654.

88. Mutano, Y.; Northcutt, T. O.; Brugman, J.; Bennett, B. K.; Lovell, S.; Mayer, J. M. *Organometallics* **2000**, *19*, 2781.

89. Coe, B. J. *Polyhedron* **1992**, *11*, 1085.

90. Lahti, D. W.; Espenson, J. H. *Inorg. Chem.* **1999**, *38*, 5230.

91. DuMez, D. D.; Mayer, J. M. *Inorg. Chem.* **1995**, *34*, 6396

92. Canali, L.; Sherrington, D. C. *Chem. Soc. Rev.* **1999**, *28*, 85.

93. Hughes, D. L.; Smith, G. B.; Liu, J.; Dezeny, G. C.; Senanayake, C. H.; Larsen, R. D.; Verhoeven, T. R.; Reider, P. J. *J. Org. Chem.* **1997**, *62*, 2222.

94. Srinivasan, K.; Michaud, P.; Kochi, J. K. *J. Am. Chem. Soc.* **1986**, *108*, 2309.

95. (a) Finney, N. S.; Pospilil, P. J.; Chang, S.; Palucki, M.; Konsler, R. G.; Hansen, K. B.; Jacobsen, E. N. *Angew. Chem. Int. Ed. Engl.* **1997**, *36*, 1720. (b) Palucki, M.; Finney, N. S.; Pospisil, P. J.; Güler, M. L.; Ishida, T.; Jacobsen, E. N. *J. Am. Chem. Soc.* **1998**, *120*, 948.

96. Hamada, T.; Fukuda, T.; Imanishi, H.; Katsuki, T. *Tetrahedron* **1996**, *52*, 515.

97. Buschmann, H.; Scharf, H.-D.; Hoffmann, N.; Esser, P. *Angew. Chem. Int. Ed. Engl.* **1991**, *30*, 477.

98. Norrby, P.; Linde, C.; Åkermark, B. *J. Am. Chem. Soc.* **1995**, *117*, 11035.

99. Linde, C.; Arnold, M.; Norrby, P.; Åkermark, B. *Angew. Chem. Int. Ed. Engl.* **1997**, *36*, 1723.

100. (a) Cristol, S. J.; Eilar, K. R. *J. Am. Chem. Soc.* **1950**, *72*, 4353. (b) Stairs, R. A.; Diaper, D. G. M.; Gatzke, A. L. *Can. J. Chem.* **1963**, *41*,1059.

101. (a) Ráppe, A. K.; Goddard, W. A. *J. Am. Chem. Soc.* **1980**, *102*, 5114. (b) Ráppe, A. K.; Goddard, W. A. *J. Am. Chem. Soc.* **1982**, *104*, 3287.

102. Torrent, M.; Deng, L.; Duran, M.; Solà, M.; Ziegler, T. *Can. J. Chem.* **1999**, *77*, 1476.

103. Atagi, L. M.; Over, D. E.; McAlister, D. R.; Mayer, J. M. *J. Am. Chem. Soc.* **1991**, *113*, 870.

104. Schiøtt, B.; Jørgensen, K. A. *J. Chem. Soc., Dalton Trans.* **1989**, 2099.

105. Traylor, T. G.; Xu, F. *J. Am. Chem. Soc.* **1988**, *110*, 1953.

106. (a) Collman, J. P.; Kodadek, T.; Raybuck, S. A.; Brauman, J. I.; Papazian, L. M. *J. Am. Chem. Soc.* **1985**, *107*, 4343. (b) Groves, J. T.; Nemo, T. E.; Myers, R. S. *J. Am. Chem. Soc.* **1979**, *101*, 1032.

107. Michaelis, L.; Menton, M. L. *Biochem. Z.* **1913**, *49*, 333.

108. Hansch, C.; Leo, A.; Taft, R. W. *Chem. Rev.* **1991**, *91*, 165.

109. Jaffé, H. H. *Chem. Rev.* **1953**, *53*, 191.

110. Breno, K. L.; Tyler, D. R. *Organometallics* **2001**, *20*, 3864.

111. Herrmann, W. A.; Roesky, P. W.; Wang, M.; Scherer, W. *Organometallics* **1994**, *13*, 4531.

112. Paulo, A.; Domingos, A.; Pires de Matos, A.; Santos, I.; Carvalho, M. F. N. N.; Pombeiro, A. J. *Inorg. Chem.* **1994**, *33*, 4729.

113. *Physical Organic Chemistry* Issacs, N.; Longman Scientific & Technical: Essex, 1995.

114. *Advanced Organic Chemistry* Carey, F. A.; Sunberg, R. J.; Kluwer Academic / Plenum Publishers: New York, 2000, p. 203.

115. Gable, K. P.; Brown, E. C. Submitted to *J. Am. Chem. Soc.*

116. Chuawong, P., M.S. Thesis, Oregon State University, Corvallis, OR, 2001, Chapter 2.

117. Gable, K. P.; Chuawong, P.; Yokochi, A. F. T. *Organometallics* **2002**, *21*, 929.

118. *Metal-catalyzed Oxidations of Organic Compounds* Sheldon, R.A.; Kochi, J. K. Academic: New York, 1981, Ch. 6.

119. Bader, A.; Lindner, E. *Coord. Chem. Rev.* **1991**, *108*, 27.

120. Galakhov, M. V.; Heinz, G.; Royo, P. *Chem. Commun.* **1998**, 17.

121. Hampton, K. G.; Harris, T. M.; Hauser, C. R. *J. Org. Chem.* **1965**, *30*, 61.

122. (a) Chisholm, M. H.; Eilerts, N. W.; Huffman, J. C.; Iyer, S. S.; Pacold, M.; Phomphrai, K. *J. Am. Chem. Soc.* **2000**, *122*, 11845, (b) Chisholm, M. H.; Iyer, S. S.; Streib, W. E. *New. J. Chem.* **2000**, *24*, 393.

123. Okuda, J.; du Plooy, K. E.; Toscano, P. J. *J. Organomet. Chem.* **1995**, *495*, 195.

124. Patton, A. T.; Strouse, C. E.; Knobler, C. B.; Gladysz, J. A. *J. Am. Chem. Soc.* **1983**, *105*, 5804.

125. King, R. B.; Bisnette, M. B. *J. Organomet. Chem.*. **1967**, *8*, 267.

126. King, R. B.; Iqbal, M. Z.; King, A. D., Jr. *J. Organomet. Chem.* **1979**, *171*, 53.

127. (a) Kühn, F. E.; Herrmann, W. A.; Hahn, R.; Elison, M.; Blümel, J.; Herdtweck, E. *Organometallics* **1994**, *13*, 1601. (b) Romão, C. C.; Kühn, F. E.; Herrmann, W. A. *Chem. Rev.* **1997**, *97*, 3197.

128. Okuda, J.; Herdtweck, E.; Herrmann, W. A. *Inorg. Chem.* **1988**, *27*, 1254.

129. Fischer, E. O.; Fellmann, W. *J. Organomet. Chem.* **1963**, *1*, 191.

130. Zhang, J.; Sutton, D. *Organometallics* **1991**, *10*, 1516.

131. Thiel, W. R.; Fischer, R. W.; Herrmann, W. A. *J. Organomet. Chem.* **1993**, *459*, C9.

132. Herrmann, W.A. ; Kiprof, P.; Rypdal, K.; Tremmel, J.; Blom, R.; Alberto, R.; Behm, J.; Albach, R. W.; Bock, H.; Solouki, B.; Mink, J.; Lichtenberger, D.; Gruhn, N. E. *J. Am. Chem. Soc.* **1991**, *113*, 6527.

133. Gable, K. P.; Phan, T. N. *J. Organomet. Chem.* **1994**, *466*, C5.

134. Herrman, W. A.; Voss, E.; Flöel, M. *J. Organomet. Chem.* **1985**, *297*, C5.

135. Wallis, J. M.; Kochi, J. K. *Inorg. Chim. Acta* **1989**, *160*, 217.

136. Yudin, A. K.; Sharpless, B. K. *J. Am. Chem. Soc.* **1997**, *119*, 11536.

137. *Spartan*, v. 5.0; Wavefunction, Inc.: 18401 Von Karman Ave., Irvine CA 92715.

138. Halgren, T. A. *J. Computational Chem.* **1996**, *17*, 490.

139. *Spectroscopic Methods in Organic Chemistry* Hesse, M.; Meier, H.; Zeeh, B., Georg Thieme Verlag: Stuggart, 1997.

140. *The Manipulation of Air-Sensitive Compounds* Shriver, D. F.; Drezdon, M. A., Wiley: New York, 1986.

141. Curci, R.; Fiorentino, M.; Troisi, L. *J. Org. Chem.* **1980**, *45*, 4758.

142. de Raadt, A.; Klempier, N.; Faber, K.; Griengl, H. *J. Chem. Soc.Perkin Trans.*1 **1992,** 137.

143. Jaguar, v. 4.1. Schrödinger, Inc., Portland, OR.

144. Hay, P. J.; Wadt, W. R. *J. Chem. Phys.* **1985**, *82*, 299.

145. Baker, J.; Jarzecki, A. A.; Pulay, P. *J. Phys. Chem. A* **1998**, *102*, 1412.

146. Scott, A. P.; Radom, L. *J. Phys. Chem.* **1996**, *100*, 16502.

# Appendix

# Appendix I. Kinetic Data

Table A1.1 Dependence of reaction rate on initial rhenium concentration (plotted in Figure 3.2).

| Mol % | Rhenium Conc. (M) | $k_{obs}$ (M/s) |
|---|---|---|
| 2.5 | 4.52E-03 | 5.52E-07 |
| 5.0 | 9.03E-03 | 1.38E-06 |
| 7.5 | 1.35E-02 | 2.71E-06 |
| 10.0 | 1.81E-02 | 2.83E-06 |
| 12.5 | 2.26E-02 | 4.07E-06 |

Table A1.2 Dependence of reaction rate on initial phosphine concentration (plotted in Figure 3.3).

| Equiv. | Phosphine Conc. (M) | $k_{obs}$ (M/s) |
|---|---|---|
| 1 | 1.99E-01 | 1.33E-06 |
| 2 | 3.61E-01 | 1.53E-06 |
| 3 | 5.42E-01 | 1.39E-06 |
| 4 | 7.23E-01 | 1.41E-06 |
| 5 | 9.03E-01 | 1.16E-06 |

Table A1.3 Dependence of reaction rate on initial epoxide concentration (plotted in Figure 3.4).

| Equiv. | Epoxide Conc. (M) | $k_{obs}$ (M/s) |
|---|---|---|
| 0.25 | 4.38E-02 | 9.43E-07 |
| 0.5 | 8.80E-02 | 1.22E-06 |
| 1.0 | 3.51E-01 | 1.41E-06 |
| 2.0 | 5.26E-01 | 1.66E-06 |
| 3.0 | 7.01E-01 | 1.85E-06 |
| 5.0 | 8.76E-01 | 2.00E-06 |

Table A1.4 Hammett kinetic data (plotted in Figure 3.5).

| Styrene Oxide | $\sigma_p$ | $k_{obs}$ (M/s) | $\log(k_i/k_h)$ |
|---|---|---|---|
| *p* - OMe | -0.27 | 8.66e-8 | 0.346 |
| *p* - Me | -0.17 | 6.32e-8 | 0.209652 |
| *p* - H | 0.0 | 3.90e-8 | 0 |
| *p* - F | 0.06 | 4.24e-8 | 0.036301 |
| *p* - Br | 0.23 | 5.11e-8 | 0.117356 |
| *p* - $CF_3$ | 0.54 | 7.50e-8 | 0.283997 |

Table A1.5 Dependence of reaction rate on temperature for *cis*-stilbene oxide deoxygenations under catalytic conditions (data used in Figure 3.13).

| Temp (K) | $k_{obs}$ (M/s) |
|---|---|
| 338.15 | 4.63E-07 |
| 348.45 | 1.43E-06 |
| 358.55 | 4.81E-06 |
| 363.05 | 8.09E-06 |
| 367.95 | 1.45E-05 |

Table A1.6 Dependence of reaction rate on temperature for cycloreversion of *syn*-monophenyldiolate **3-3** (data used in Figure 3.14).

| Temp(K) | $k_{obs}$(M/s) |
|---|---|
| 348 | 6.51E-07 |
| 358 | 2.71E-06 |
| 368 | 7.88E-06 |
| 378 | 2.39E-05 |

# Appendix II. NMR Spectra

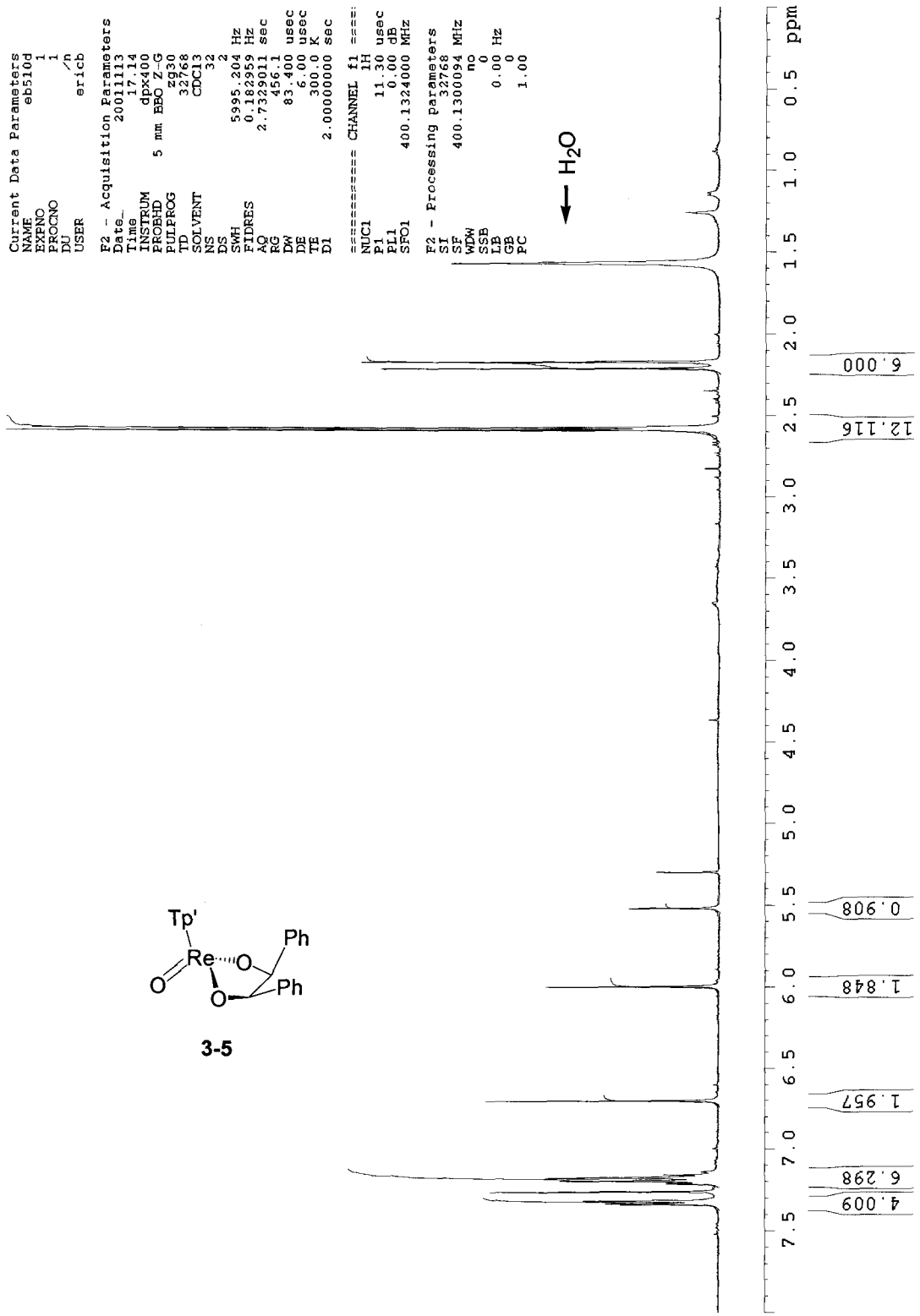





**3-5**

```
Current Data Parameters
NAME                  eb577c
EXPNO                      1
PROCNO                     2
DU                        /n
USER                  ericb

F2 - Acquisition Parameters
Date_              20020326
Time                   7.47
INSTRUM              dpx400
PROBHD     5 mm BBO Z-G
PULPROG             zgpg30
TD                   65536
SOLVENT              CDCl3
NS                   30000
DS                       4
SWH              25125.629 Hz
FIDRES               0.383387 Hz
AQ                1.3042164 sec
RG                    1024
DW                   19.900 usec
DE                    6.00 usec
TE                   300.0 K
D1              0.00300000 sec
D11             0.03000000 sec
D12             0.00002000 sec

============ CHANNEL f1 ==============
NUC1                   13C
P1                    7.50 usec
PL1                  -3.00 dB
SFO1           100.5936186 MHz

============ CHANNEL f2 ==============
CPDPRG2            waltz16
NUC2                   1H
PCPD2                80.00 usec
PL2                   0.00 dB
PL12                 17.40 dB
PL13                 18.00 dB
SFO2           400.0116000 MHz

F2 - Processing parameters
SI                    32768
SF             100.5825550 MHz
WDW                      EM
SSB                       0
LB                     3.00 Hz
GB                        0
PC                     1.40
```

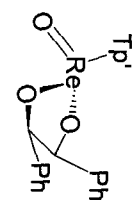


3-5

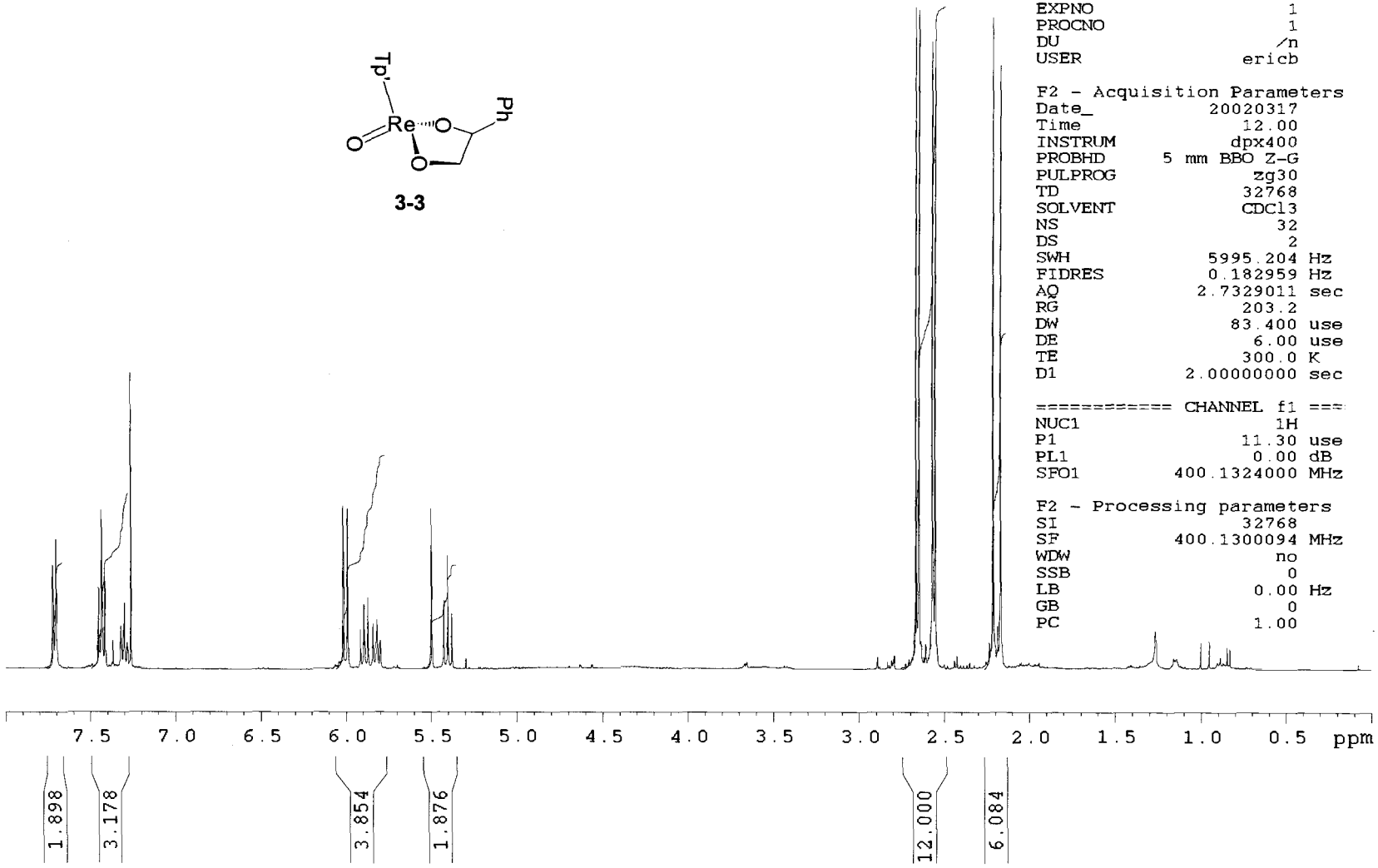
Tp'
Re
O
O
O
Ph
3-3
Current Data Parameters
NAME eb568a
EXPNO 1
PROCNO 1
DU /n
USER ericb
F2 - Acquisition Parameters
Date_ 20020317
Time 12.00
INSTRUM dpx400
PROBHD 5 mm BBO Z-G
PULPROG zg30
TD 32768
SOLVENT CDCl3
NS 32
DS 2
SWH 5995.204 Hz
FIDRES 0.182959 Hz
AQ 2.7329011 sec
RG 203.2
DW 83.400 use
DE 6.00 use
TE 300.0 K
D1 2.00000000 sec
========== CHANNEL f1 ===
NUC1 1H
P1 11.30 use
PL1 0.00 dB
SFO1 400.1324000 MHz
F2 - Processing parameters
SI 32768
SF 400.1300094 MHz
WDW no
SSB 0
LB 0.00 Hz
GB 0
PC 1.00
7.5 7.0 6.5 6.0 5.5 5.0 4.5 4.0 3.5 3.0 2.5 2.0 1.5 1.0 0.5 ppm
1.898
3.178
3.854
1.876
12.000
6.084

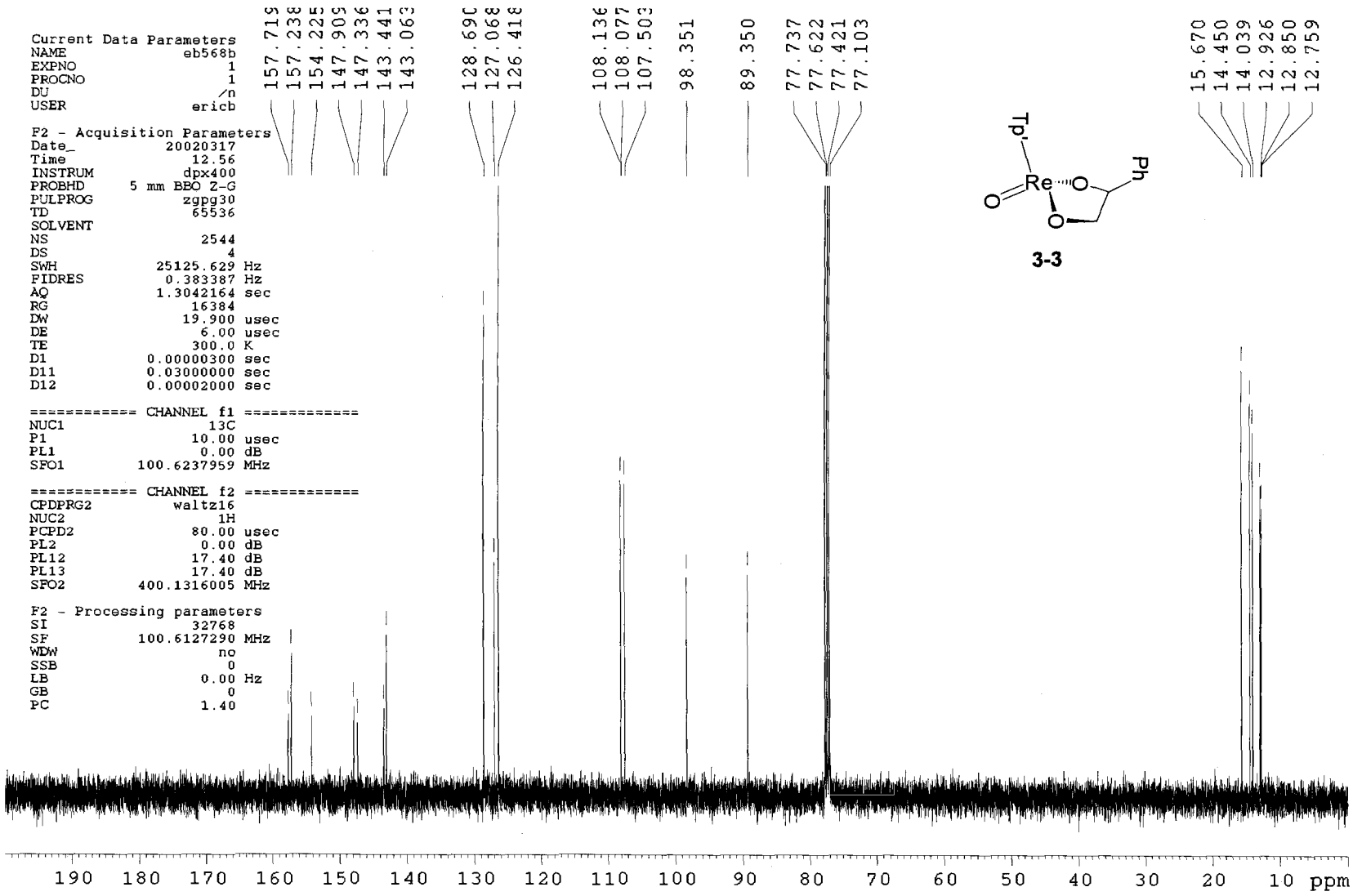
Current Data Parameters
NAME eb568b
EXPNO 1
PROCNO 1
DU /n
USER ericb
F2 - Acquisition Parameters
Date_ 20020317
Time 12.56
INSTRUM dpx400
PROBHD 5 mm BBO Z-G
PULPROG zgpg30
TD 65536
SOLVENT
NS 2544
DS 4
SWH 25125.629 Hz
FIDRES 0.383387 Hz
AQ 1.3042164 sec
RG 16384
DW 19.900 usec
DE 6.00 usec
TE 300.0 K
D1 0.00000300 sec
D11 0.03000000 sec
D12 0.00002000 sec
========== CHANNEL f1 ==========
NUC1 13C
P1 10.00 usec
PL1 0.00 dB
SFO1 100.6237959 MHz
========== CHANNEL f2 ==========
CPDPRG2 waltz16
NUC2 1H
PCPD2 80.00 usec
PL2 0.00 dB
PL12 17.40 dB
PL13 17.40 dB
SFO2 400.1316005 MHz
F2 - Processing parameters
SI 32768
SF 100.6127290 MHz
WDW no
SSB 0
LB 0.00 Hz
GB 0
PC 1.40
157.719
157.238
154.225
147.905
147.336
143.441
143.063
128.690
127.068
126.418
108.136
108.077
107.503
98.351
89.350
77.737
77.622
77.421
77.103
15.670
14.450
14.039
12.926
12.850
12.759
Tp'
Re
O
O
O
Ph
3-3
190 180 170 160 150 140 130 120 110 100 90 80 70 60 50 40 30 20 10 ppm

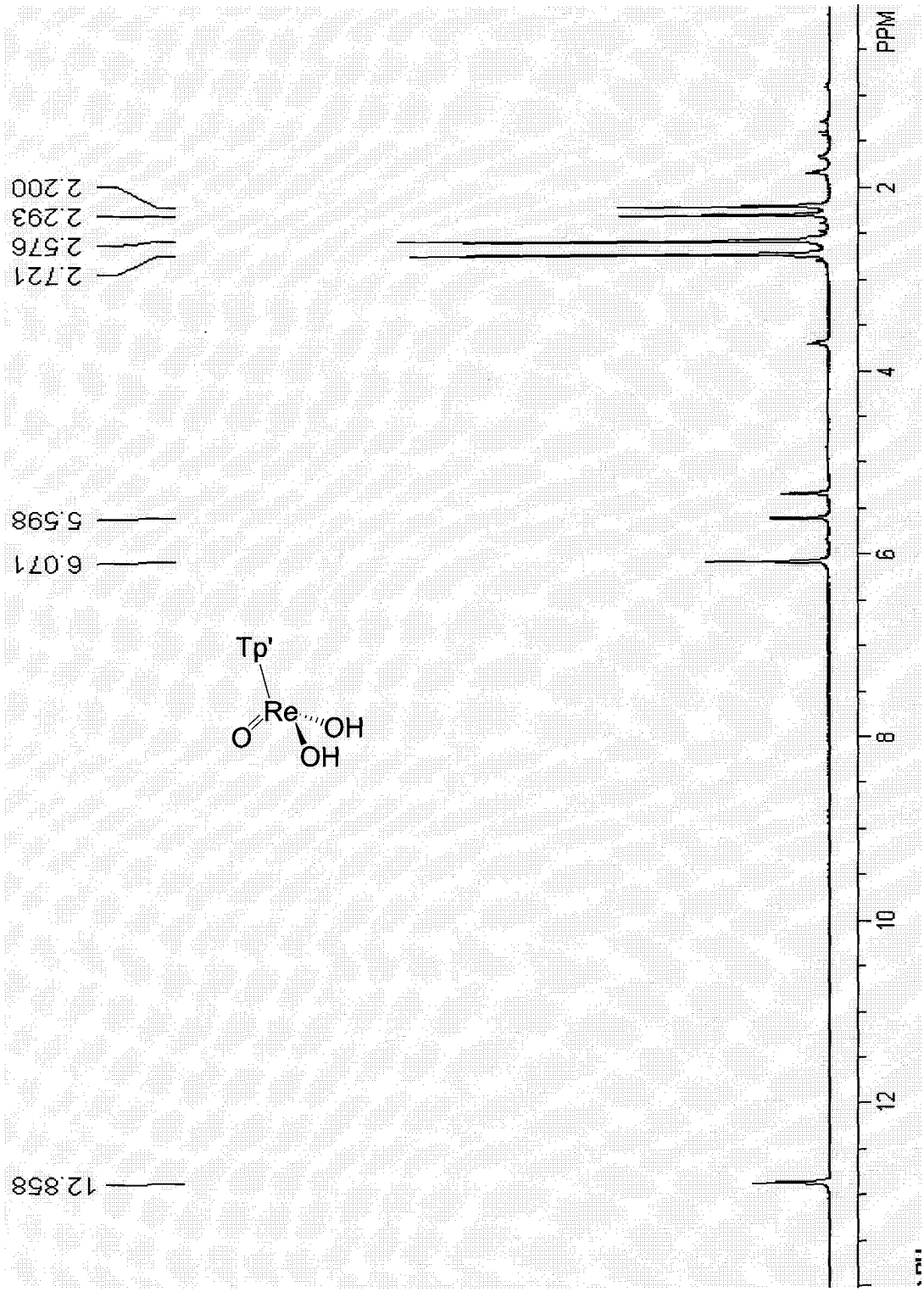
2.200
2.293
2.576
2.721
5.598
6.071
12.858
Tp'
Re
O
OH
OH
PPM
2
4
6
8
10
12

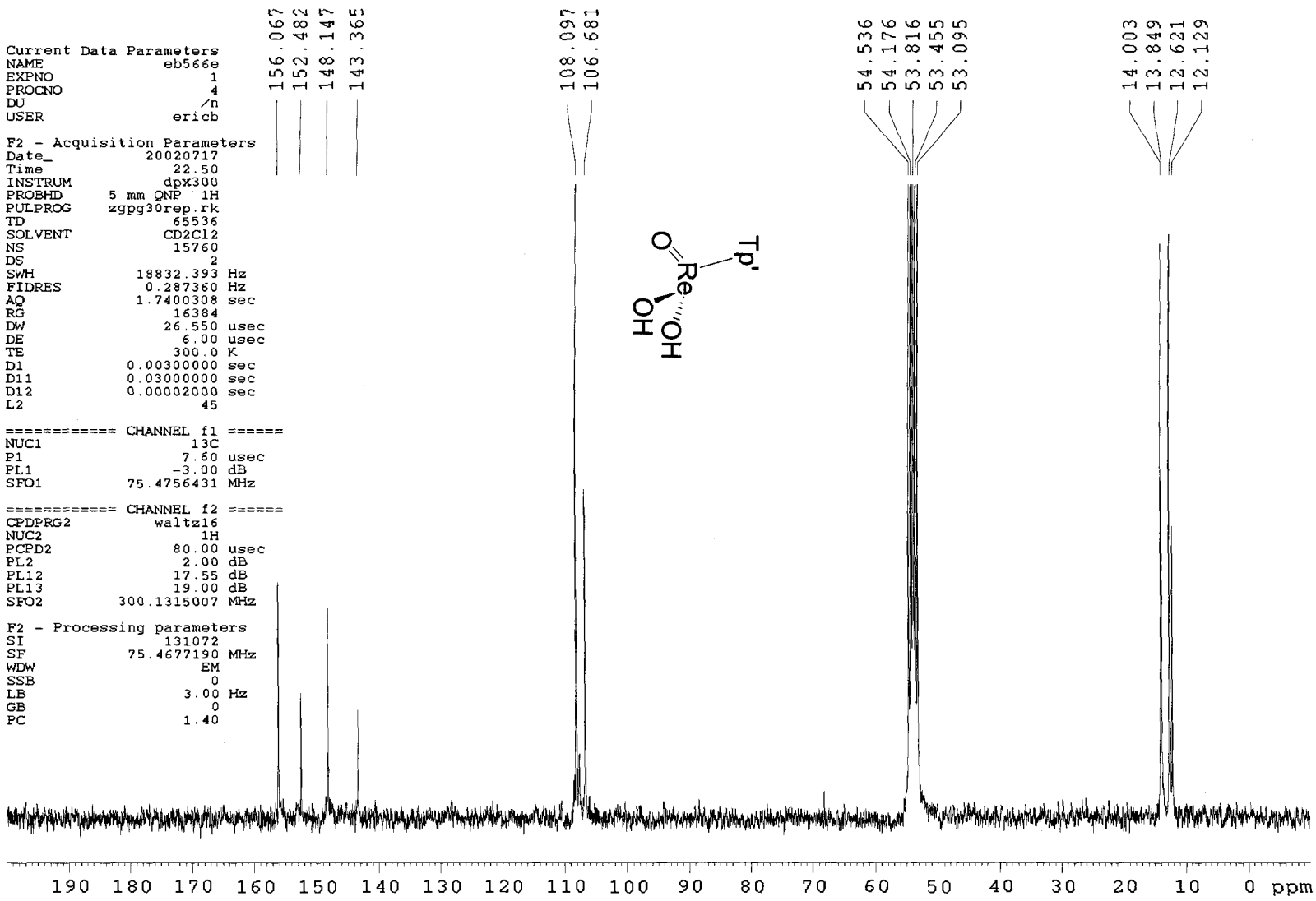
Current Data Parameters
NAME eb566e
EXPNO 1
PROCNO 4
DU /n
USER ericb
F2 - Acquisition Parameters
Date_ 20020717
Time 22.50
INSTRUM dpx300
PROBHD 5 mm QNP 1H
PULPROG zgpg30rep.rk
TD 65536
SOLVENT CD2Cl2
NS 15760
DS 2
SWH 18832.393 Hz
FIDRES 0.287360 Hz
AQ 1.7400308 sec
RG 16384
DW 26.550 usec
DE 6.00 usec
TE 300.0 K
D1 0.00300000 sec
D11 0.03000000 sec
D12 0.00002000 sec
L2 45
CHANNEL f1
NUC1 13C
P1 7.60 usec
PL1 -3.00 dB
SFO1 75.4756431 MHz
CHANNEL f2
CPDPRG2 waltz16
NUC2 1H
PCPD2 80.00 usec
PL2 2.00 dB
PL12 17.55 dB
PL13 19.00 dB
SFO2 300.1315007 MHz
F2 - Processing parameters
SI 131072
SF 75.4677190 MHz
WDW EM
SSB 0
LB 3.00 Hz
GB 0
PC 1.40
156.067
152.482
148.147
143.365
108.097
106.681
54.536
54.176
53.816
53.455
53.095
14.003
13.849
12.621
12.129
Tp'
Re
O
OH
OH
190 180 170 160 150 140 130 120 110 100 90 80 70 60 50 40 30 20 10 0 ppm

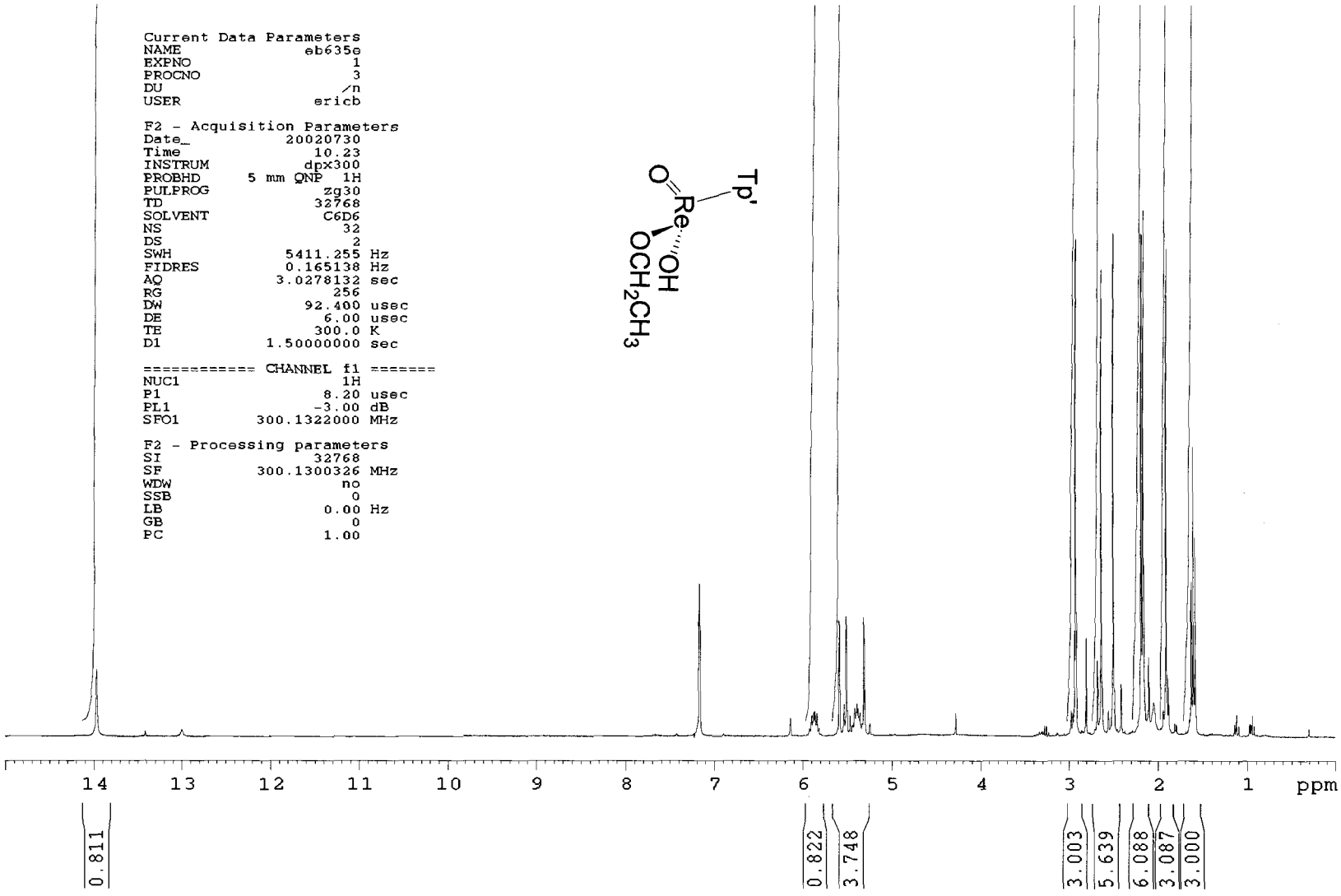
Current Data Parameters
NAME eb635e
EXPNO 1
PROCNO 3
DU /n
USER ericb
F2 - Acquisition Parameters
Date_ 20020730
Time 10.23
INSTRUM dpx300
PROBHD 5 mm QNP 1H
PULPROG zg30
TD 32768
SOLVENT C6D6
NS 32
DS 2
SWH 5411.255 Hz
FIDRES 0.165138 Hz
AQ 3.0278132 sec
RG 256
DW 92.400 usec
DE 6.00 usec
TE 300.0 K
D1 1.50000000 sec
CHANNEL f1
NUC1 1H
P1 8.20 usec
PL1 -3.00 dB
SFO1 300.1322000 MHz
F2 - Processing parameters
SI 32768
SF 300.1300326 MHz
WDW no
SSB 0
LB 0.00 Hz
GB 0
PC 1.00
Tp'
O
Re
OH
OCH2CH3
14
13
12
11
10
9
8
7
6
5
4
3
2
1
ppm
0.811
0.822
3.748
3.003
5.639
6.088
3.087
3.000

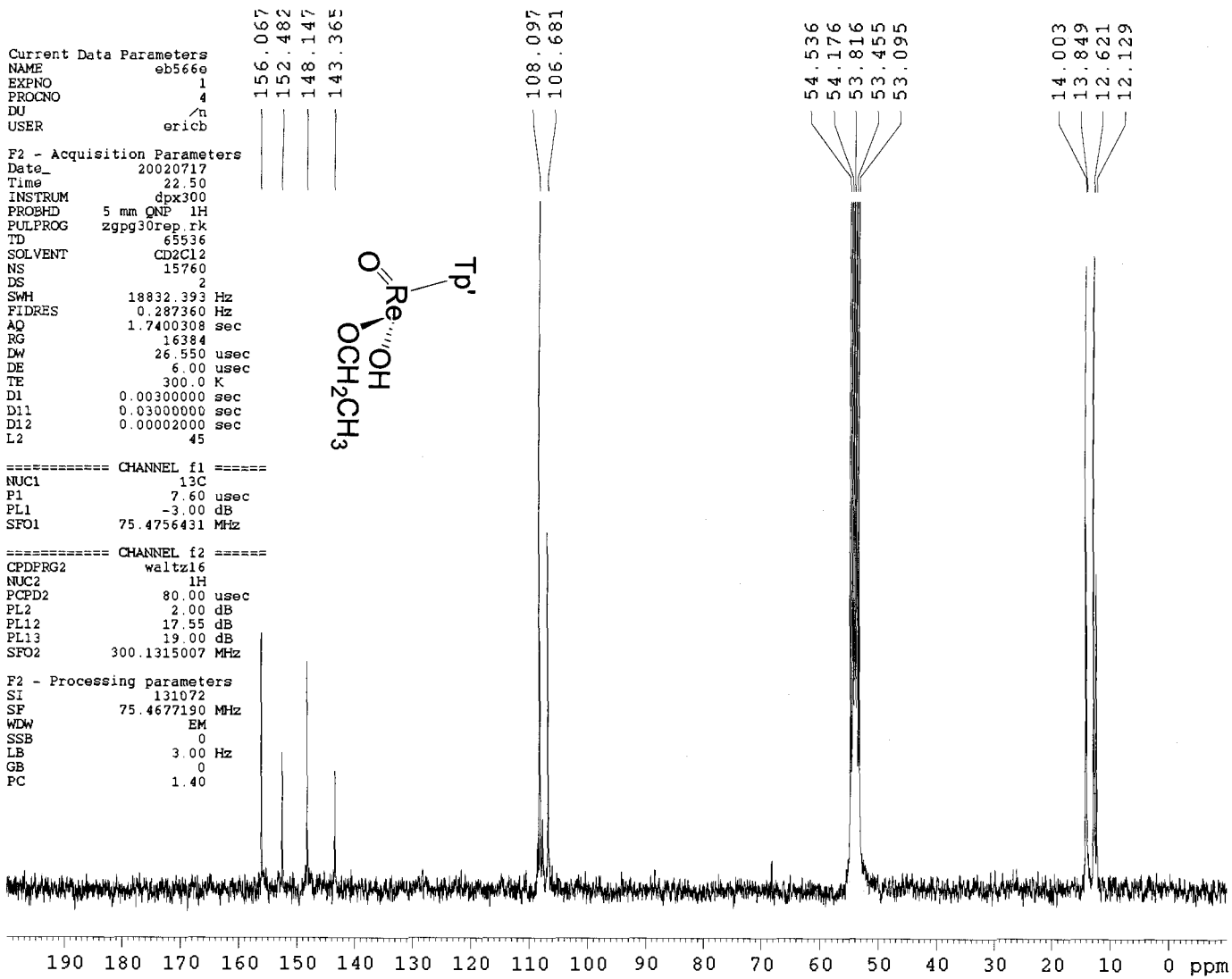
Current Data Parameters
NAME eb566e
EXPNO 1
PROCNO 4
DU /n
USER ericb
F2 - Acquisition Parameters
Date_ 20020717
Time 22.50
INSTRUM dpx300
PROBHD 5 mm QNP 1H
PULPROG zgpg30rep.rk
TD 65536
SOLVENT CD2Cl2
NS 15760
DS 2
SWH 18832.393 Hz
FIDRES 0.287360 Hz
AQ 1.7400308 sec
RG 16384
DW 26.550 usec
DE 6.00 usec
TE 300.0 K
D1 0.00300000 sec
D11 0.03000000 sec
D12 0.00002000 sec
L2 45
CHANNEL f1
NUC1 13C
P1 7.60 usec
PL1 -3.00 dB
SFO1 75.4756431 MHz
CHANNEL f2
CPDPRG2 waltz16
NUC2 1H
PCPD2 80.00 usec
PL2 2.00 dB
PL12 17.55 dB
PL13 19.00 dB
SFO2 300.1315007 MHz
F2 - Processing parameters
SI 131072
SF 75.4677190 MHz
WDW EM
SSB 0
LB 3.00 Hz
GB 0
PC 1.40
156.067
152.482
148.147
143.365
108.097
106.681
54.536
54.176
53.816
53.455
53.095
14.003
13.849
12.621
12.129
Tp'
O
Re
OH
OCH2CH3
190 180 170 160 150 140 130 120 110 100 90 80 70 60 50 40 30 20 10 0 ppm

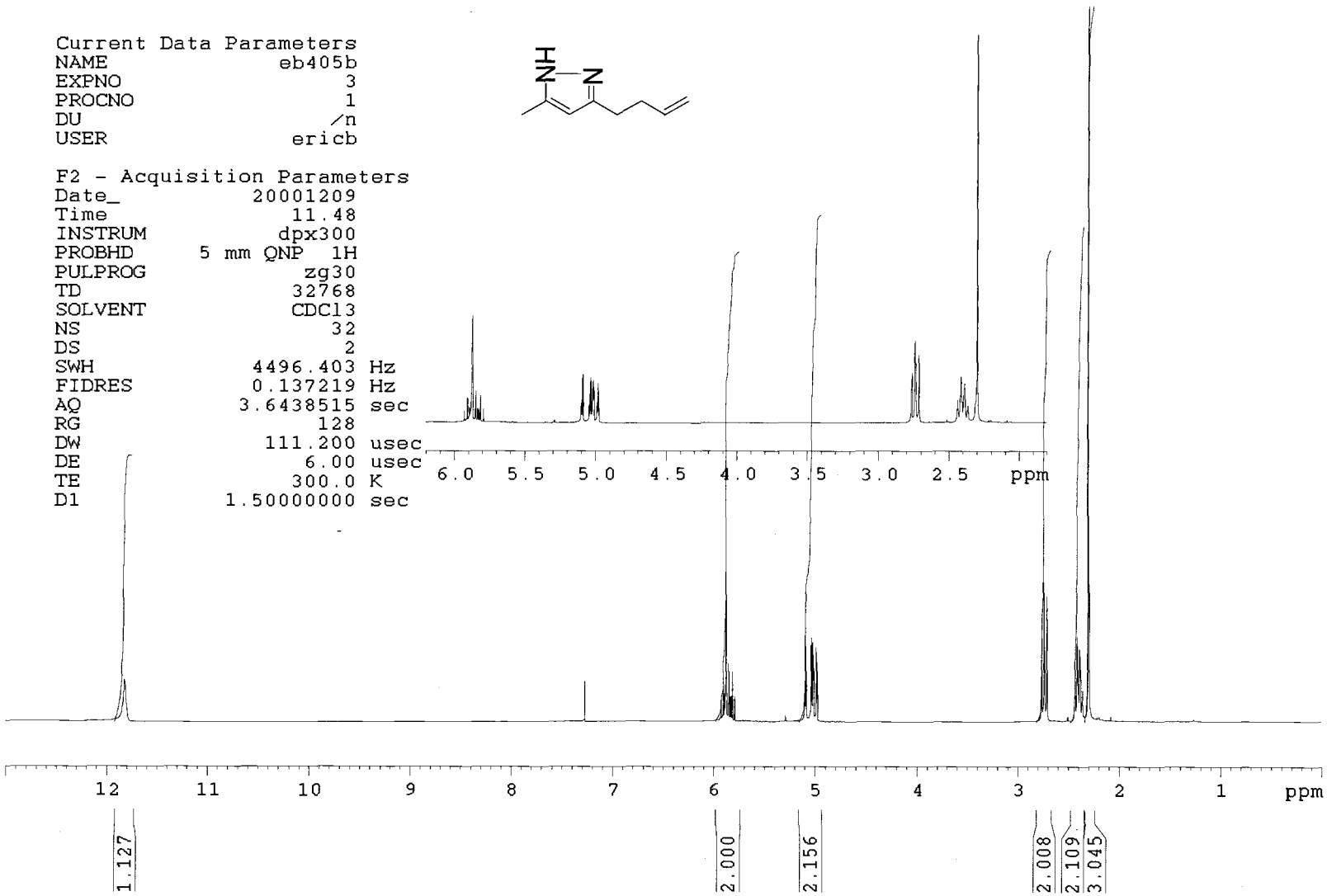
Current Data Parameters
NAME eb405b
EXPNO 3
PROCNO 1
DU /n
USER ericb
F2 - Acquisition Parameters
Date_ 20001209
Time 11.48
INSTRUM dpx300
PROBHD 5 mm QNP 1H
PULPROG zg30
TD 32768
SOLVENT CDCl3
NS 32
DS 2
SWH 4496.403 Hz
FIDRES 0.137219 Hz
AQ 3.6438515 sec
RG 128
DW 111.200 usec
DE 6.00 usec
TE 300.0 K
D1 1.50000000 sec
NH
N
6.0 5.5 5.0 4.5 4.0 3.5 3.0 2.5 ppm
12 11 10 9 8 7 6 5 4 3 2 1 ppm
1.127
2.000
2.156
2.008
2.109
3.045

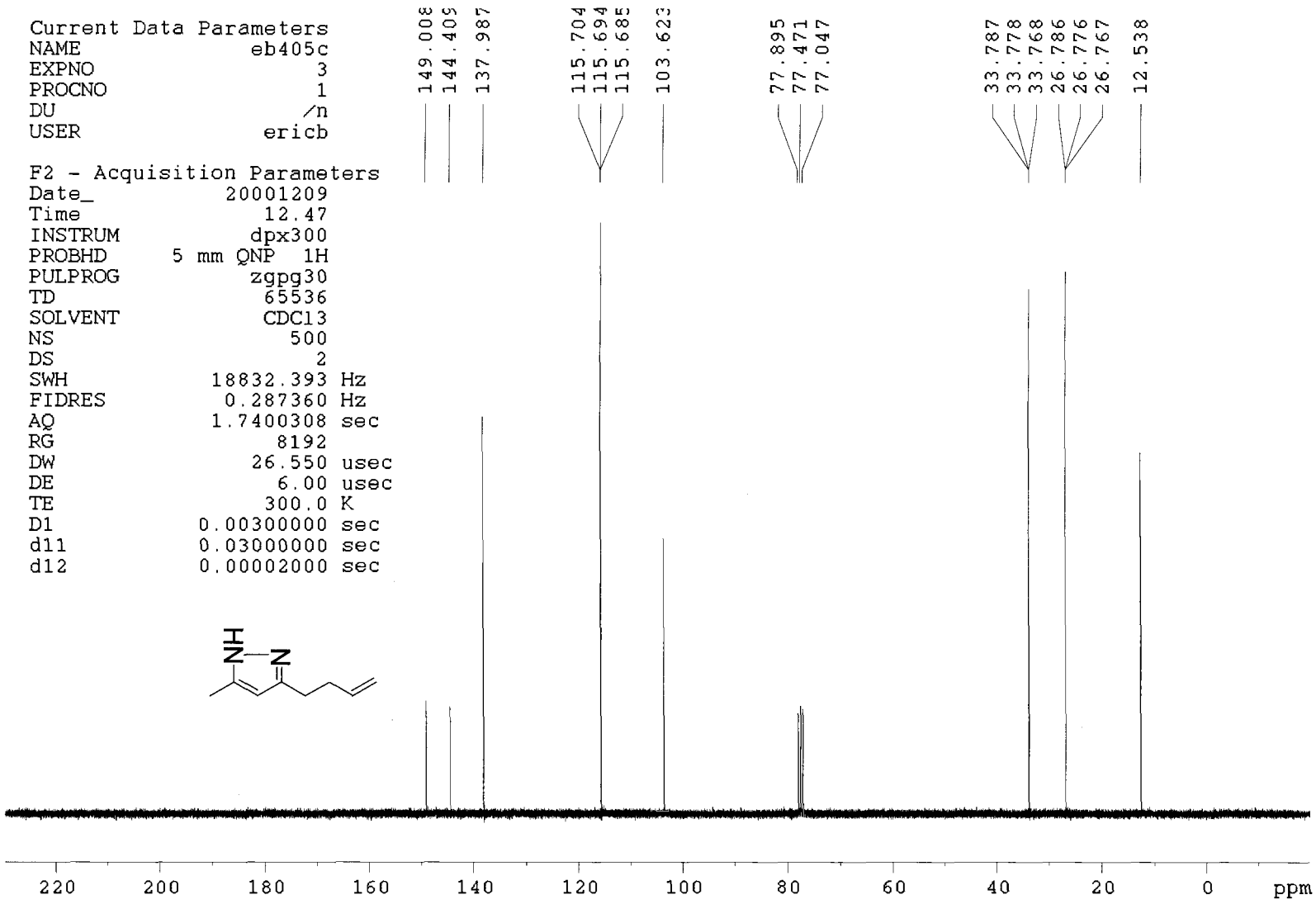
Current Data Parameters
NAME eb405c
EXPNO 3
PROCNO 1
DU /n
USER ericb
F2 - Acquisition Parameters
Date_ 20001209
Time 12.47
INSTRUM dpx300
PROBHD 5 mm QNP 1H
PULPROG zgpg30
TD 65536
SOLVENT CDCl3
NS 500
DS 2
SWH 18832.393 Hz
FIDRES 0.287360 Hz
AQ 1.7400308 sec
RG 8192
DW 26.550 usec
DE 6.00 usec
TE 300.0 K
D1 0.00300000 sec
d11 0.03000000 sec
d12 0.00002000 sec
149.008
144.409
137.987
115.704
115.694
115.685
103.623
77.895
77.471
77.047
33.787
33.778
33.768
26.786
26.776
26.767
12.538
NH
N
220
200
180
160
140
120
100
80
60
40
20
0
ppm

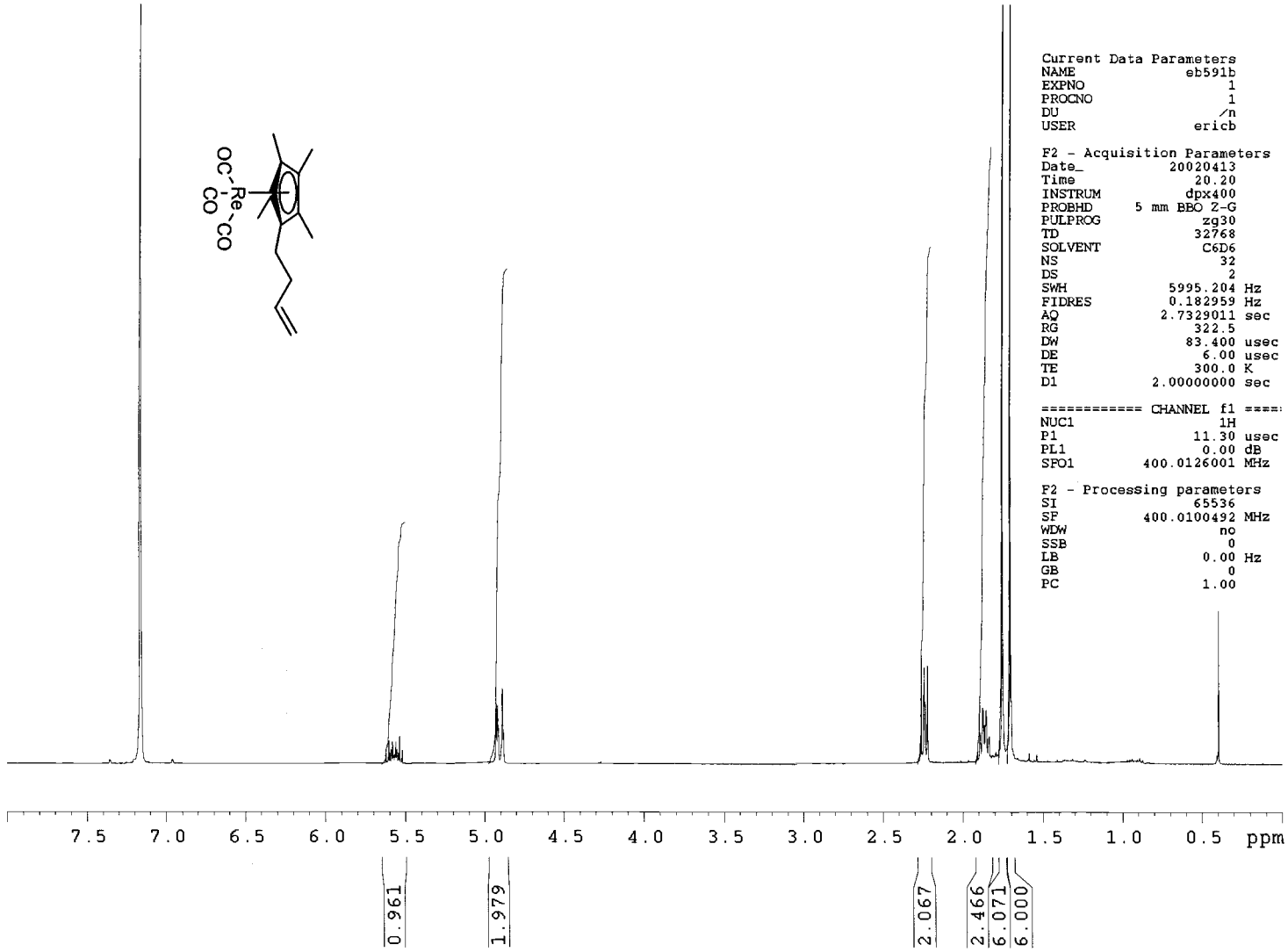
OC
Re
CO
CO
Current Data Parameters
NAME eb591b
EXPNO 1
PROCNO 1
DU /n
USER ericb
F2 - Acquisition Parameters
Date_ 20020413
Time 20.20
INSTRUM dpx400
PROBHD 5 mm BBO Z-G
PULPROG zg30
TD 32768
SOLVENT C6D6
NS 32
DS 2
SWH 5995.204 Hz
FIDRES 0.182959 Hz
AQ 2.7329011 sec
RG 322.5
DW 83.400 usec
DE 6.00 usec
TE 300.0 K
D1 2.00000000 sec
CHANNEL f1
NUC1 1H
P1 11.30 usec
PL1 0.00 dB
SFO1 400.0126001 MHz
F2 - Processing parameters
SI 65536
SF 400.0100492 MHz
WDW no
SSB 0
LB 0.00 Hz
GB 0
PC 1.00
7.5 7.0 6.5 6.0 5.5 5.0 4.5 4.0 3.5 3.0 2.5 2.0 1.5 1.0 0.5 ppm
1.961
1.979
2.067
2.466
6.071
6.000

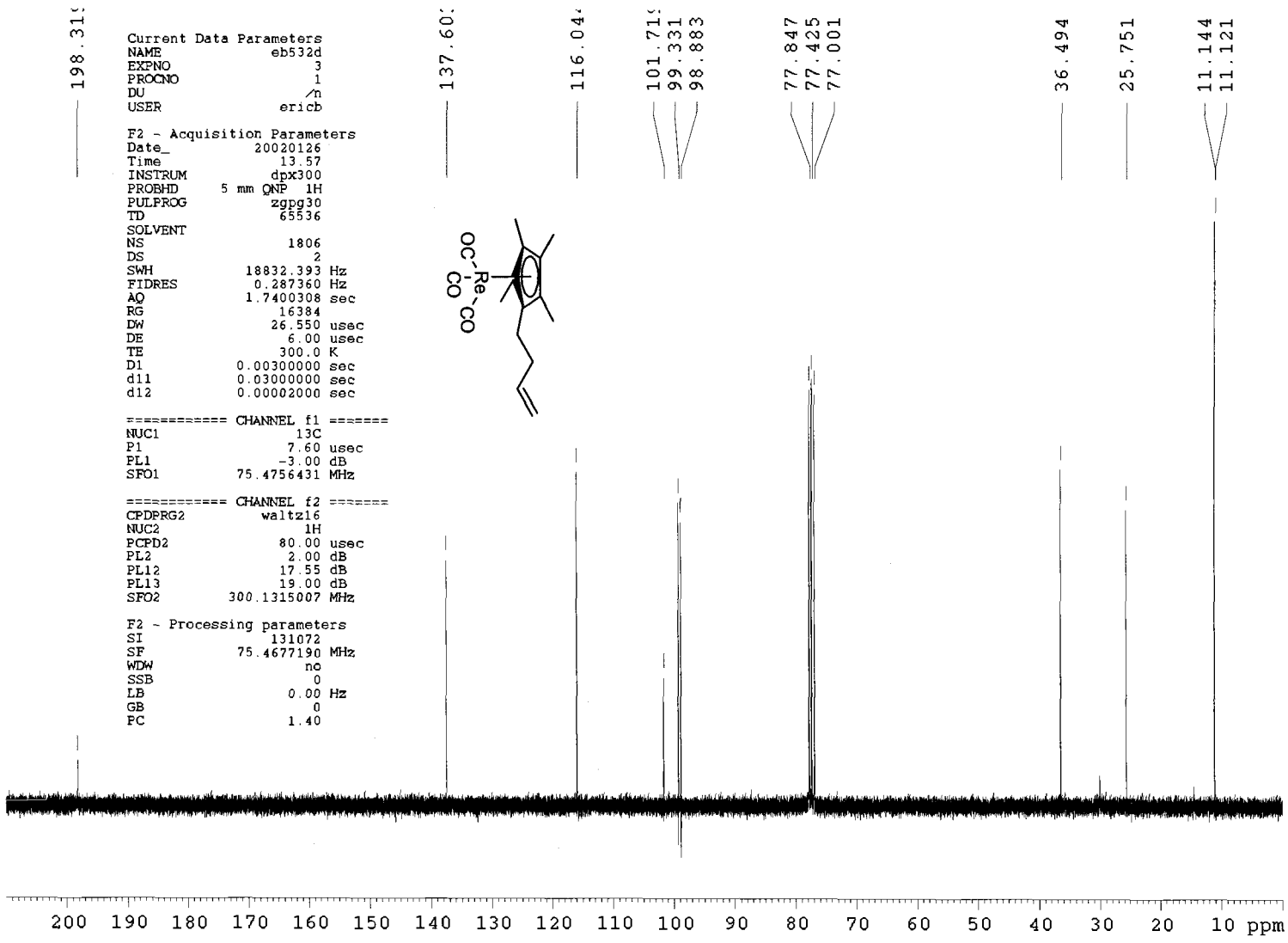
198.31
137.60
116.04
101.71
99.331
98.883
77.847
77.425
77.001
36.494
25.751
11.144
11.121
Current Data Parameters
NAME eb532d
EXPNO 3
PROCNO 1
DU /n
USER ericb
F2 - Acquisition Parameters
Date_ 20020126
Time 13.57
INSTRUM dpx300
PROBHD 5 mm QNP 1H
PULPROG zgpg30
TD 65536
SOLVENT
NS 1806
DS 2
SWH 18832.393 Hz
FIDRES 0.287360 Hz
AQ 1.7400308 sec
RG 16384
DW 26.550 usec
DE 6.00 usec
TE 300.0 K
D1 0.00300000 sec
d11 0.03000000 sec
d12 0.00002000 sec
========== CHANNEL f1 =======
NUC1 13C
P1 7.60 usec
PL1 -3.00 dB
SFO1 75.4756431 MHz
========== CHANNEL f2 =======
CPDPRG2 waltz16
NUC2 1H
PCPD2 80.00 usec
PL2 2.00 dB
PL12 17.55 dB
PL13 19.00 dB
SFO2 300.1315007 MHz
F2 - Processing parameters
SI 131072
SF 75.4677190 MHz
WDW no
SSB 0
LB 0.00 Hz
GB 0
PC 1.40
OC
Re
CO
CO
200 190 180 170 160 150 140 130 120 110 100 90 80 70 60 50 40 30 20 10 ppm

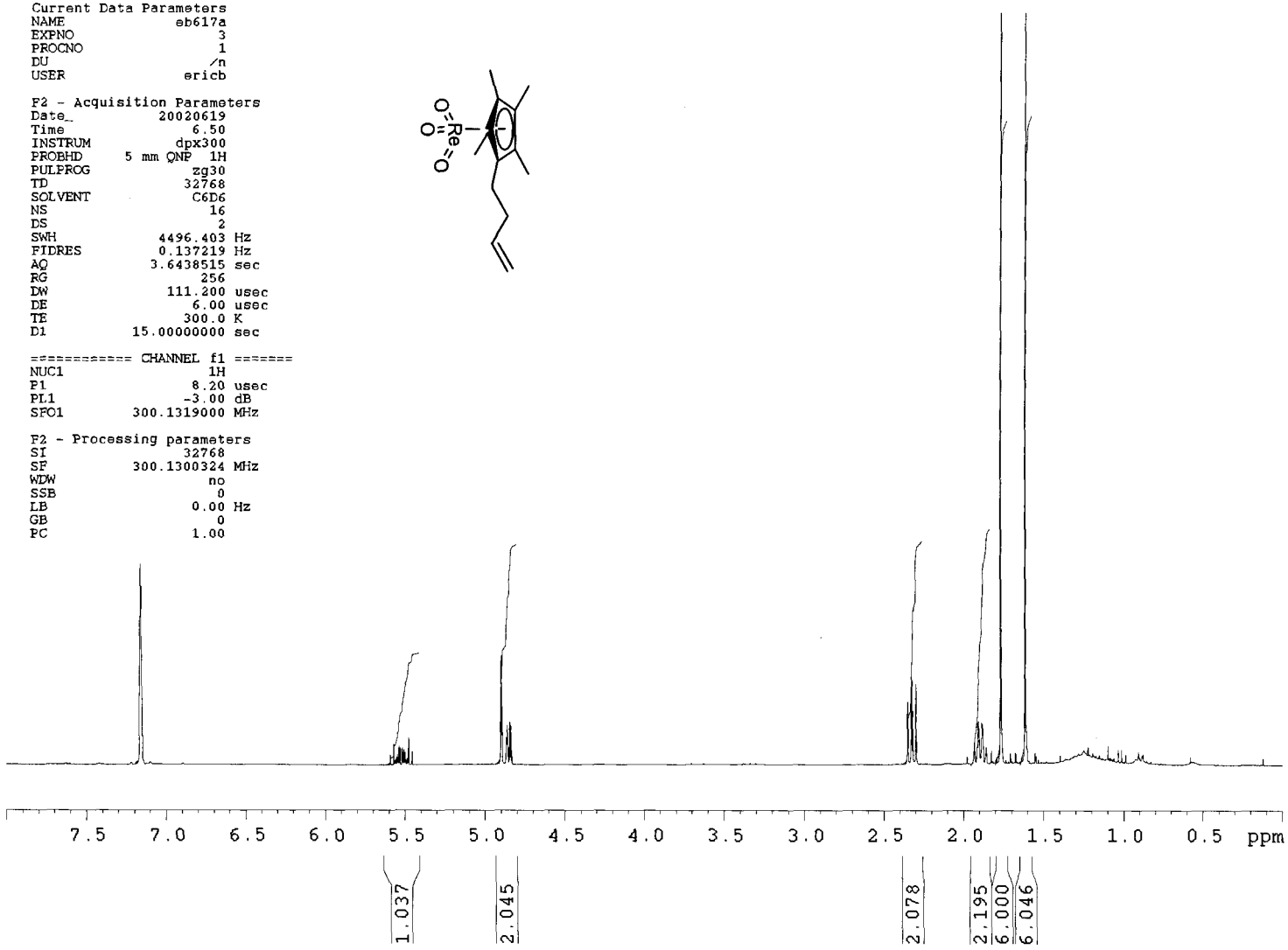
Current Data Parameters
NAME eb617a
EXPNO 3
PROCNO 1
DU /n
USER ericb
F2 - Acquisition Parameters
Date_ 20020619
Time 6.50
INSTRUM dpx300
PROBHD 5 mm QNP 1H
PULPROG zg30
TD 32768
SOLVENT C6D6
NS 16
DS 2
SWH 4496.403 Hz
FIDRES 0.137219 Hz
AQ 3.6438515 sec
RG 256
DW 111.200 usec
DE 6.00 usec
TE 300.0 K
D1 15.00000000 sec
============ CHANNEL f1 =======
NUC1 1H
P1 8.20 usec
PL1 -3.00 dB
SFO1 300.1319000 MHz
F2 - Processing parameters
SI 32768
SF 300.1300324 MHz
WDW no
SSB 0
LB 0.00 Hz
GB 0
PC 1.00
O=Re=O
7.5
7.0
6.5
6.0
5.5
5.0
4.5
4.0
3.5
3.0
2.5
2.0
1.5
1.0
0.5
ppm
1.037
2.045
2.078
2.195
6.000
6.046

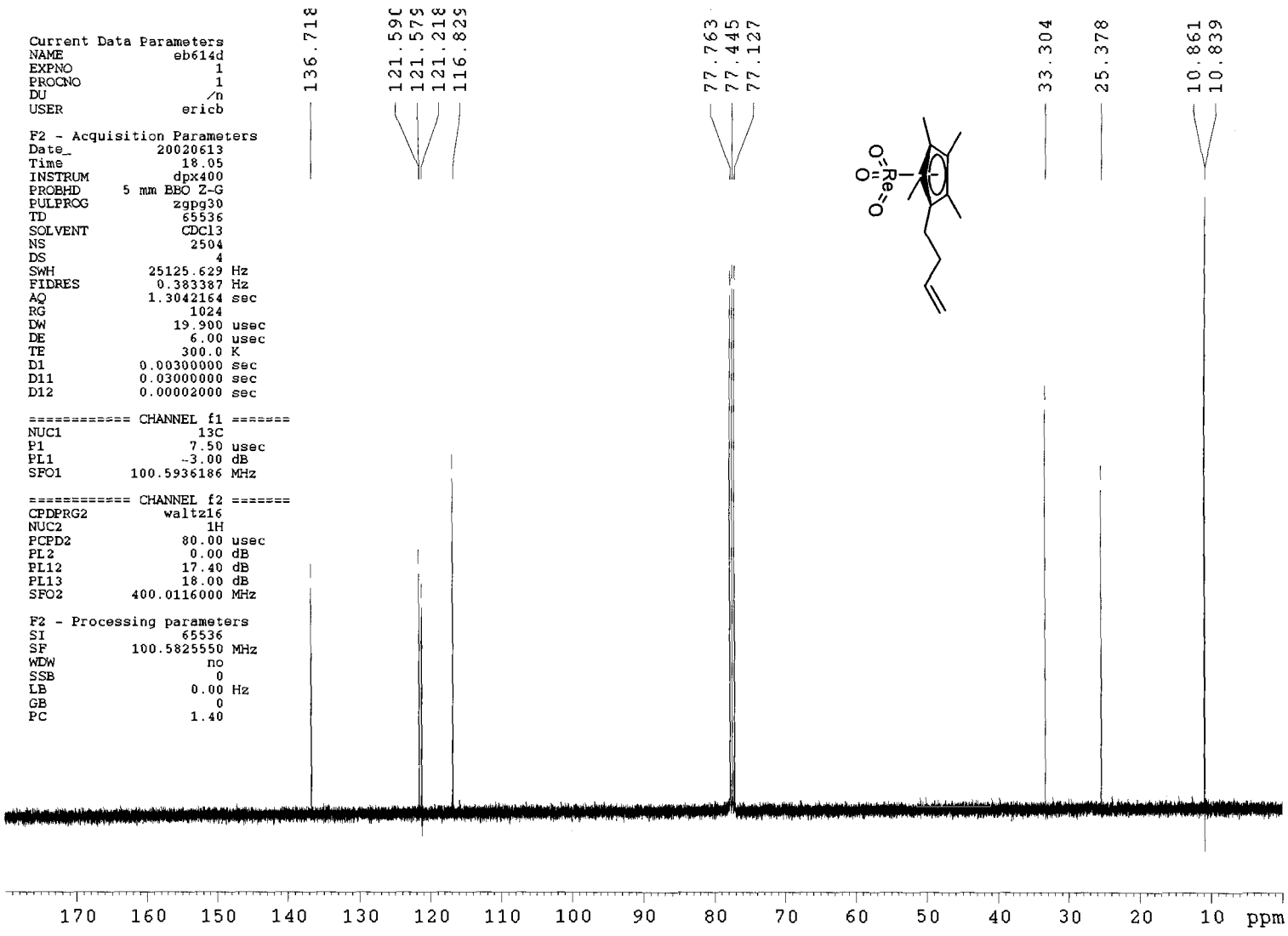
Current Data Parameters
NAME eb614d
EXPNO 1
PROCNO 1
DU /n
USER ericb
F2 - Acquisition Parameters
Date_ 20020613
Time 18.05
INSTRUM dpx400
PROBHD 5 mm BBO Z-G
PULPROG zgpg30
TD 65536
SOLVENT CDCl3
NS 2504
DS 4
SWH 25125.629 Hz
FIDRES 0.383387 Hz
AQ 1.3042164 sec
RG 1024
DW 19.900 usec
DE 6.00 usec
TE 300.0 K
D1 0.00300000 sec
D11 0.03000000 sec
D12 0.00002000 sec
============ CHANNEL f1 =======
NUC1 13C
P1 7.50 usec
PL1 -3.00 dB
SFO1 100.5936186 MHz
============ CHANNEL f2 =======
CPDPRG2 waltz16
NUC2 1H
PCPD2 80.00 usec
PL2 0.00 dB
PL12 17.40 dB
PL13 18.00 dB
SFO2 400.0116000 MHz
F2 - Processing parameters
SI 65536
SF 100.5825550 MHz
WDW no
SSB 0
LB 0.00 Hz
GB 0
PC 1.40
136.718
121.590
121.579
121.218
116.829
77.763
77.445
77.127
33.304
25.378
10.861
10.839
O=Re=O
170 160 150 140 130 120 110 100 90 80 70 60 50 40 30 20 10 ppm

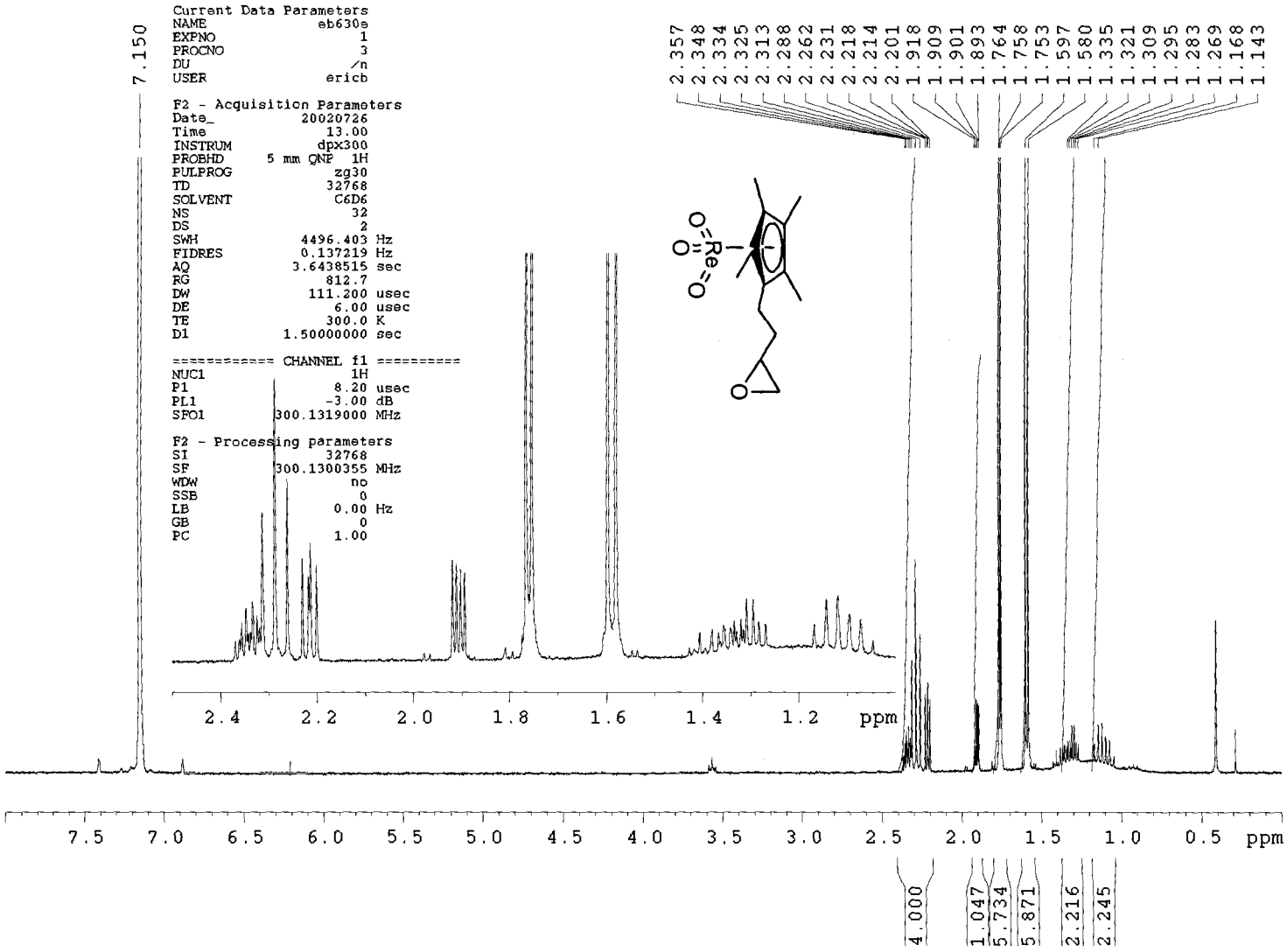
Current Data Parameters
NAME eb630e
EXPNO 1
PROCNO 3
DU /n
USER ericb
F2 - Acquisition Parameters
Date_ 20020726
Time 13.00
INSTRUM dpx300
PROBHD 5 mm QNP 1H
PULPROG zg30
TD 32768
SOLVENT C6D6
NS 32
DS 2
SWH 4496.403 Hz
FIDRES 0.137219 Hz
AQ 3.6438515 sec
RG 812.7
DW 111.200 usec
DE 6.00 usec
TE 300.0 K
D1 1.50000000 sec
========== CHANNEL f1 ==========
NUC1 1H
P1 8.20 usec
PL1 -3.00 dB
SFO1 300.1319000 MHz
F2 - Processing parameters
SI 32768
SF 300.1300355 MHz
WDW no
SSB 0
LB 0.00 Hz
GB 0
PC 1.00
7.150
2.357
2.348
2.334
2.325
2.313
2.288
2.262
2.231
2.218
2.214
2.201
1.918
1.909
1.901
1.893
1.764
1.758
1.753
1.597
1.580
1.335
1.321
1.309
1.295
1.283
1.269
1.168
1.143
O=Re=O
2.4
2.2
2.0
1.8
1.6
1.4
1.2
ppm
7.5
7.0
6.5
6.0
5.5
5.0
4.5
4.0
3.5
3.0
2.5
2.0
1.5
1.0
0.5
ppm
4.000
1.047
5.734
5.871
2.216
2.245

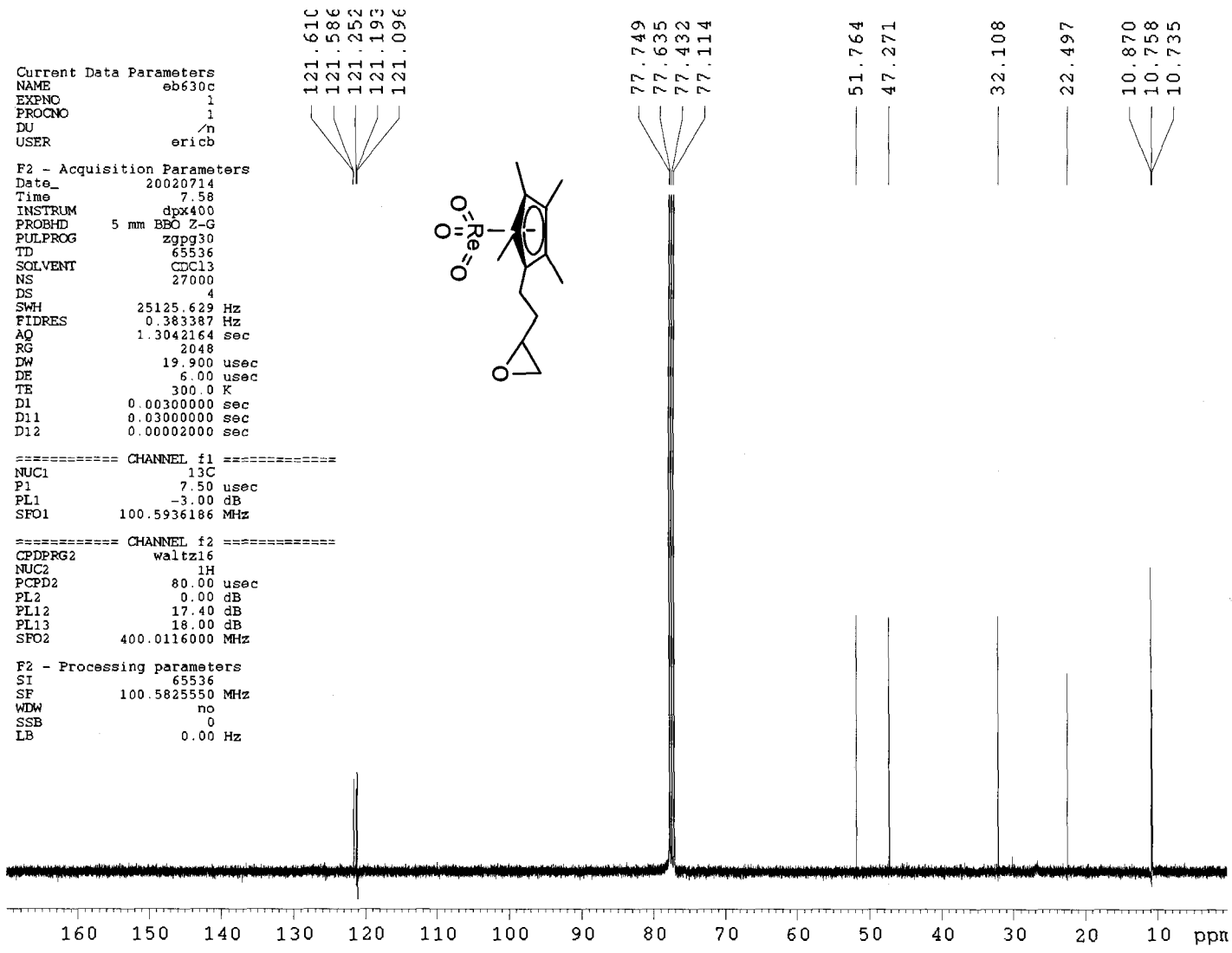
121.610
121.586
121.252
121.193
121.096
77.749
77.635
77.432
77.114
51.764
47.271
32.108
22.497
10.870
10.758
10.735
Re
O
O
O
Current Data Parameters
NAME eb630c
EXPNO 1
PROCNO 1
DU /n
USER ericb
F2 - Acquisition Parameters
Date_ 20020714
Time 7.58
INSTRUM dpx400
PROBHD 5 mm BBO Z-G
PULPROG zgpg30
TD 65536
SOLVENT CDCl3
NS 27000
DS 4
SWH 25125.629 Hz
FIDRES 0.383387 Hz
AQ 1.3042164 sec
RG 2048
DW 19.900 usec
DE 6.00 usec
TE 300.0 K
D1 0.00300000 sec
D11 0.03000000 sec
D12 0.00002000 sec
========== CHANNEL f1 ==========
NUC1 13C
P1 7.50 usec
PL1 -3.00 dB
SFO1 100.5936186 MHz
========== CHANNEL f2 ==========
CPDPRG2 waltz16
NUC2 1H
PCPD2 80.00 usec
PL2 0.00 dB
PL12 17.40 dB
PL13 18.00 dB
SFO2 400.0116000 MHz
F2 - Processing parameters
SI 65536
SF 100.5825550 MHz
WDW no
SSB 0
LB 0.00 Hz
160 150 140 130 120 110 100 90 80 70 60 50 40 30 20 10 ppm

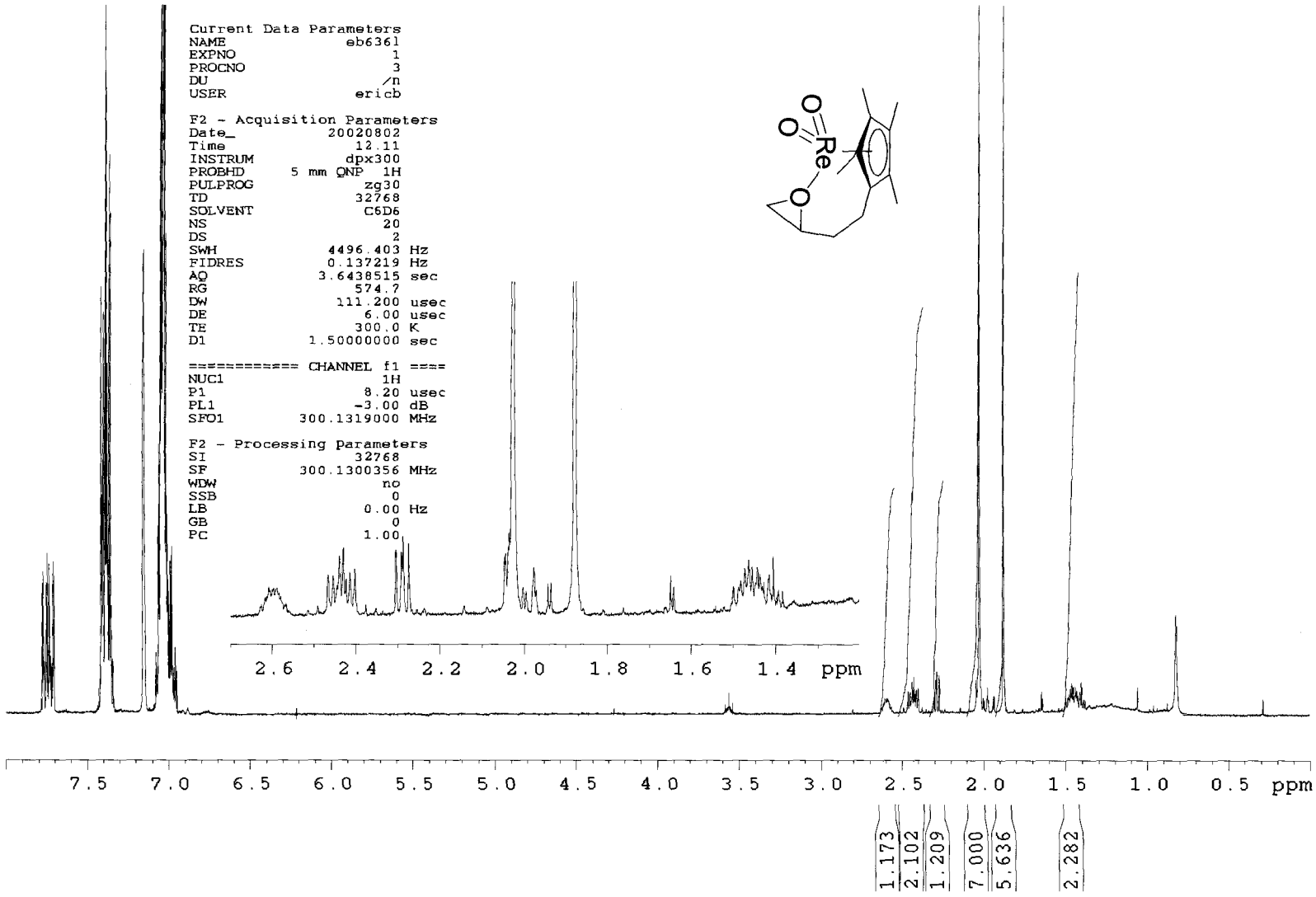
Current Data Parameters
NAME eb6361
EXPNO 1
PROCNO 3
DU /n
USER ericb
F2 - Acquisition Parameters
Date_ 20020802
Time 12.11
INSTRUM dpx300
PROBHD 5 mm QNP 1H
PULPROG zg30
TD 32768
SOLVENT C6D6
NS 20
DS 2
SWH 4496.403 Hz
FIDRES 0.137219 Hz
AQ 3.6438515 sec
RG 574.7
DW 111.200 usec
DE 6.00 usec
TE 300.0 K
D1 1.50000000 sec
========== CHANNEL f1 ====
NUC1 1H
P1 8.20 usec
PL1 -3.00 dB
SFO1 300.1319000 MHz
F2 - Processing Parameters
SI 32768
SF 300.1300356 MHz
WDW no
SSB 0
LB 0.00 Hz
GB 0
PC 1.00
O
O
Re
O
2.6 2.4 2.2 2.0 1.8 1.6 1.4 ppm
7.5 7.0 6.5 6.0 5.5 5.0 4.5 4.0 3.5 3.0 2.5 2.0 1.5 1.0 0.5 ppm
1.173
2.102
1.209
7.000
5.636
2.282